Stars of Low Luminosity

Iain Neill Reid

Ph. D.

Edinburgh University

1982

Declaration

This thesis is an account of work carried out at Edinburgh University between September, 1979 and November, 1982. While I have benefitted from discussions with many others, both in the University and at R.O.E., unless specifically stated, the work described here is my own.

Chapter 3 has appeared as a paper in Monthly Notices of the Royal Astronomical Society (M.N. 201, 54 (1982)), while both chapter 4 and the Appendix have also been published (M.N. 201, 73 and M.N. 196, 15P respectively) under joint authorship with G. Gilmore.

I. Neill Reid

Abstract

The mass density of stars in the Solar Neighbourhood is
a fundamental parameter in Galactic Structure studies. We have
applied the method of photometric parallaxes (the M_V, (V-I))
relation) to two complete samples of late-type dwarfs; one
selected from an objective prism survey, the other from COSMOS
photographic photometry of BVI UK Schmidt Telescope plates. The
resultant kinematically unbiased luminosity function shows that
the stellar number density peaks at M_V = +13 locally, falling off
very steeply thereafter. This result excludes hydrogen burning
stars brighter than M_V = +19 as significant contributors to any
local missing mass. We have also examined the kinematic selection
effects inherent in proper-motion based determinations of the
luminosity function, and show that high velocity halo stars
significantly affect results derived by this method. These effects
are substantial enough to permit an investigation of the local
subdwarf number density, which we find to be $\sim$0.4 percent that
of disk dwarfs. Finally, using UBVRIJHK photometry, we have applied
a blackbody fitting technique to derive temperatures and luminosities
for low luminosity dwarfs, and conclude that even the least luminous
are consistent with their interpretation as main sequence dwarfs.

Contents   .

Introduction

The study of Galactic Structure in general and of the stellar content of the Solar Neighbourhood in particular has long been a crucial area of astronomical research. One of the most important aspects in this work is the derivation of the run of stellar number density with absolute magnitude - the stellar luminosity function. Taken together with the mass-luminosity relation, this parameter is of fundamental importance not only in determining the distribution of stellar mass locally within the Disk, but also, through the establishment of the main sequence present-day mass function, as a significant constraint on theories of star formation. Over the years a wide range of different techniques have been employed in studying this problem, and as a result the space densities at bright absolute magnitudes ($M_v < {\sim}7$) are well known. However, the intrinsically faint nature of the late K and M dwarf stars, compounded by the use of blue-sensitive detectors in searches for these very red stars, has severely limited the resolution of most previous surveys fainter than $M_v \sim +10$, while widely discrepant space densities, ranging over several orders of magnitude, have been inferred from those studies which have had the capability of detecting statistically significant numbers of these stars.

Studies of low luminosity main sequence stars are of particular importance in several fields - statistically, through the luminosity function, in the determination of the Galactic mass distribution and in studies of star formation, and, individually, in studies of stellar structure. All previous studies of the luminosity function (chapter 2) have shown that most of the mass that has formed stars resides in the form of K and M dwarfs, with individual masses between 0.1 and 0.4 $M_\odot$. Thus

determining the shape of the luminosity function at faint magnitudes is of paramount importance for studies of the overall distribution of mass in the Galaxy. In particular, there is the question of the local "missing mass" — the apparent discrepancy between the total mass density attributable to observed objects and the dynamical mass density calculated from the motions of stars at large distances above the Plane. With conventional main sequence luminosity functions (i.e. functions which peak in number density at $M_y \sim +13$), the stellar mass density is $\sim 0.048\ M_\odot$ per cubic parsec, with an additional contribution from white dwarfs, dust and gas — giving a final value of between $0.09 - 0.11\ M_\odot\ /pc^3$. (Hill, Hilditch and Barnes, 1979).

Estimates of the dynamical mass density, however, range from 0.11 to $0.18\ M_\odot\ /pc^3$ (Oort, 1960, 1965; Jones, 1962; Woolley and Stewart, 1967; Turon Lacarrieu, 1971; Hill et al., 1979) with a most likely value of $0.14\ M_\odot\ /pc^3$ (Jones, 1972). These values are derived by using luminous stars — generally A stars or K giants — as tracers of the Galactic gravitational force law perpendicular to the Plane (K_z). The consequent mass density can be inferred using methods described by Oort (1932, 1960) and Camm (1950, 1952). While this difference can be interpreted as implying that up to 50 percent of the local mass is 'invisible', it should be noted that there are significant assumptions implicit to the dynamical method — notably that the stellar populations are well mixed, and that the stars used as tracers of K_z accurately reflect the overall mass distribution. With this in mind, various authors have argued that the discrepancy is not significant (eg. Joeveer and Einasto, 1977; Krisciunas, 1977; Miller and Scalo, 1979; House and Kilkenny, 1980).

Nonetheless, interpreting the mass discrepancy as a real effect

implies the presence of a substantial population of objects with high mass
to light ratios — which therefore escape detection in direct observational
surveys. Low luminosity M dwarfs (M/L (bol.) of 10 to 100) or the even
lower mass black dwarfs (M/L $>$ 500) which are unable to ignite the hydrogen
nuclear reactions, are obvious candidates for the missing mass. To supply
the deficit, the number density must be substantial — 0.5 stars per cubic
parsec for individual masses of $0.1M_\odot$. Hence it may be feasible, with the
correct technique, to attempt to set useful observational limits.

Large numbers of low mass stars have also been proposed as the
dark matter in the halo missing mass, but so few stars are required locally
that they are practically indetectable. However, if star formation
processes were sufficiently well understood, the likelihood of this
proposition could be assessed indirectly — as could the hypothesis that the
halo dark matter is formed of the burnt out remnants of massive Population
III stars (Rees, 1976). Many star formation mechanisms have been proposed
based on fragmentation, coalescence, aggregation and other processes. As is
discussed further below, while most of these acceptably represent the data
at high masses, virtually all predict power law (Log N = c Log (Mass))
relations extending to very low masses (M $<$ $0.1M_\odot$). Initial mass
functions of this form are at variance with those derived from conventional
stellar luminosity functions and the standard mass—luminosity relation
(Lacy, 1977a). An improved observational definition of the disk luminosity
function to fainter absolute magnitudes is therefore of considerable
importance in determining whether any of these theories are in any sense
realistic. These practical constraints can be further enhanced if
observations can be extended to cover the luminosity functions of other
stellar populations.

Finally there is the question of the evolutionary status of very
low luminosity stars ($M_v > +15$). The standard mass-luminosity relation
shows that these objects have masses close to the theoretical hydrogen
burning limit ($0.085M_\odot$) if they lie on the main sequence. Alternatively,
it has been suggested that there may be black dwarfs with masses below this
limit. If the few such stars known are on the main sequence, an explanation
must be found for the dispersion of approximately four magnitudes in the
(M_v, log (mass)) relation fainter than $M_v \sim +14$. On the other hand, if the
alternative picture is correct, the short luminous lifetimes characteristic
of these "stars" imply that the any observed are merely the tip of a much
larger iceberg. As is discussed further in Chapter 2, the few available
candidates do not possess motions consistent with such youthful objects,
but observational determinations of effective temperatures, luminosities
and radii for many such objects are required before conclusions can be
drawn with any degree of confidence.

The primary aim of this research has been the observational
derivation of the stellar luminosity function for M dwarfs and its
interpretation in terms of the resultant local mass density. In the
following chapters, previous studies are reviewed (ch. 2); the stellar
luminosity function is derived by applying the method of photometric
parallaxes to samples of bright apparent magnitude (ch. 3) and faint
apparent magnitude (ch. 4) red dwarfs; using these results, a simple
numerical modelling technique is used to investigate the overall population
structure in the Solar Neighbourhood, particularly the proportion of
different kinematic populations detected by proper motion surveys. This
also allows an estimate of the local halo star number density (ch. 5).
Finally, we briefly consider the nature of the red dwarf stars of very low

luminosity (ch. 6) using a combination of visual and infrared broadband colours and near-infrared spectrophotometry. Chapters 3,4 and 5 form the bases of a series of papers published in Monthly Notices of the R.A.S., Appendix A and ch. 4 being written in collaboration with gerard Gilmore (R.O.E.) . All of the observations, with the exception of the UBVRI photometry carried out at SAAO in May/June 1981, were also mad in collaboration with Gerry Gilmore.

Chapter 2

The use of star counts as a probe of Galactic Structure has a long and successful history. It was through "star gauging" a number of areas covering a range of galactic latitude and longitude that Herschel (1785) discovered, and Kapteyn (1914) confirmed, the flattened nature of our stellar system. Subsequent investigations of the stellar luminosity function ($\Phi(M)$) - the number of stars per unit absolute magnitude per unit volume (usually cubic parsec) - and the density laws (D(r)) - the run of stellar density either in the Plane, radially from the Galactic Centre, or with height, z, above the disk - have relied on minor modificatins of the same basic technique. These quantities are combined in the classical star counts formula, initially developed by von Seeliger (1898),

$$A(m) = \omega \int \Phi (m + 5 + 5\log r - a(r)) D(r) r^2 dr \qquad (1)$$

where A(m) is the observed number of stars per unit apparent magnitude within solid angle ω, D(r) the density law and a(r) the variation of absorption with distance. In the main, studies of the luminosity function have been confined to the Solar Neighbourhood - the volume of space centred on the Sun and with radius ~50-100 parsecs - within which the effects of both absorption and density variation are small and, by and large, well known.

The first half of this century saw considerable effort devoted to

the study of the stellar luminosity function - given the rapid growth in photographic expertise and the consequent burgeoning of data on trigonometric parallaxes and proper motions, a classic case of an idea whose time had come (Jenkins, 1980). Both the methods applied and the resultant functions have been extensively reviewed by Trumpler & Weaver (1953) and by McCuskey (1966), and for this reason we only briefly consider the earliest studies . However, no review should omit mention of van Rhijn's (1925, 1936) classic work in the field, nor the major contributions made by Luyten (1938a,b, 1968) and McCuskey (1956).

The principal requirement for any space density study is that the sample of stars being analysed be either complete or be incomplete in a known, understood fashion. van Rhijn's luminosity function was derived using a variety of methods to analyse stellar number counts between 3rd and 14th visual magnitude within three Galactic latitude zones (0 to ±20, ±20 to ±40 and ±40 to the Poles) in the light of known proper motion and parallax distributions. Given the comparatively small extent of direct distance information, the analysis was of necessity predominantly statistical, resting heavily on the more easily observed parameters - spectral type and tangential motion. For example, the method developed by Kapteyn takes the mean parallax for stars of a given apparent magnitude - principally derived from the parallactic motions - and computes the probable distribution of parallax with m and μ , constrained to agree with the known form for high proper motion objects. Hence the luminosity function follows from dividing the observed counts into (m, μ) cells, and applying the predicted distribution to each cell.

Similarly the method of trigonometric parallaxes bins the stellar

number counts by m and μ and uses the observed distribution amongst stars of known parallax within each bin to infer the overall distribution, applying corrections for incompleteness in both parallax and proper motion surveys, and for errors in the respective observed parameters. The statistical corrections necessitated by this type of method are usually large - introducing significant uncertainties into the final conclusions. Such considerations are not so significant in the other methods outlined here - both of which were included by van Rhijn in his final analysis. These are the method of mean absolute magnitudes, used extensively by Luyten, and the method of spectroscopic parallaxes, widely applied by McCuskey.

The method of mean absolute magnitudes (Trumpler & Weaver, 1953; Wanner, 1972; chapter 5) adopts a statistical approach to the calibration of absolute magnitude, analysing proper motion star number magnitude counts. For each (m, μ) cell, the distribution in absolute magnitude can be represented by

$$F(m, \mu , M) = N(m, \mu) \, \Phi(M \mid m, \mu) \qquad (2)$$

where $\Phi (M \mid m, \mu)$ is the relative frequency of M in the given cell - i.e. the "luminosity function". Luyten demonstrated (1925) that under certain circumstances, this function could be replaced by $\Psi (M \mid H)$, where H is the reduced proper motion,

$$H = m + 5 + 5 \log \mu \qquad (3)$$

an easily observable quantity. Using stars of known trigonometric parallax, Luyten derived the relation

$$\langle M \rangle = a + bH \qquad (4)$$

with a dispersion of approximately one magnitude in absolute magnitude. Hence, $\Psi(M \mid H)$ can be calculated, and, replacing $\Phi(M \mid m, \mu)$, F can be derived. As is described in more detail in chapter 5, this analysis is strongly dependent on the kinematics of the observational sample and breaks down if the programme stars have a velocity distribution substantially different from that of the bright parallax stars used in the calibration of (4).

The above methods all derive the general luminosity function, which describes the variation of stellar number density with absolute magnitude without regard to luminosity class. Thus the space density at $M_v = 0$ includes both A0 dwarfs and K giants. This is not the case for the specific luminosity function derived by McCuskey from spectroscopic parallaxes of stars within ten areas distributed in longitude around the Galactic Plane. These data were obtained from objective prism surveys — the first widespread application of the technique to this subject — and, as a result, were limited to bright absolute magnitudes ($M_v < +7$). Furthermore, since the surveyed regions are comparatively small (~ 15 square degrees), to acquire statistically significant samples at bright absolute magnitudes where the absolute space density is less than 0.001 stars per cubic parsec ($M_v < +2$), stars up to a kiloparsec in distance had to be included. The analysis thus requires knowledge of and correction for the effects of absorption and intrinsic density variation with distance (although since the areas lie very near the Plane, the latter effects are expected to be small). Furthermore, variations in the shape of the luminosity function from place to place in the Plane might be expected — although McCuskey's results indicated that these were comparatively small.

Table 2.1 and Figure 2.1 show the mean luminosity function derived by McCuskey together with those of the other two classical analyses. Generally, the agreement is good, save for the dip between $M_v = +7$ and $+11$ which is present in the van Rhijn function, but not in Luyten's. As is discussed in chapters 3 and 5, this dip is a real feature of the local disk luminosity function, and has probably been removed from Luyten's data by excessive smoothing. Of the three functions, however, only Luyten's goes fainter than $M_{pg} = +13$ ($M_v \sim 11.5$), and the number density of stars at these very faint absolute magnitudes has been a subject of substantial contention in recent years.

The main argument has centred round the importance of the kinematical bias present in Luyten's sampling technique. Not only is absolute magnitude calibrated through the observed motion, but the sample itself is selected on the basis of a proper motion (i.e. tangential velocity) limit. As is discussed in more detail in chapter 5, this is unimportant if all stars come from the same kinematic population. However, if there were a sizeable population with velocity dispersions lower than those of the disk, their smaller contribution to proper motion surveys would lead to Luyten's function underestimating the true space density. There are theoretical problems implicit in the existence of many such stars (Schmidt, 1975a) - both with regard to their age if the Spitzer-Schwarzschild scattering mechanism is correct (Spitzer and Schwarzschild, 1951) and for the surface mass density, and hence stability of the disk (Toomre, 1964). Nonetheless suggestions of the existence of such a population were prompted by the results from the initial kinematically unbiased surveys (Biermann, 1975; Schmidt, 1975a).

Table 2.1
Log (number density)

M(pg)	McCuskey	van Rhijn	Luyten
-2.00	-5.30	-5.25	-5.05
-1.00	-4.65	-4.93	-4.52
0.00	-4.12	-4.32	-4.00
1.00	-3.60	-3.66	-3.52
2.00	-3.23	-3.23	-3.21
3.00	-2.99	-3.14	-2.89
4.00	-2.84	-2.81	-2.51
5.00	-2.80	-2.65	-2.54
6.00	-2.55	-2.51	-2.46
7.00	-2.33	-2.47	-2.38
8.00	-	-2.55	-2.35
9.00	-	-2.54	-2.28
10.00	-	-2.36	-2.20
11.00	-	-2.16	-2.12
12.00	-	-2.05	-2.05
13.00	-	-	-2.02
14.00	-	-	-2.00
15.00	-	-	-2.04
16.00	-	-	-2.10

Figure 2.1   The luminosity functions derived by van Rhijn ($\triangledown$),
McCuskey   ($\triangle$) and Luyten.(+)

Figure 2.2   The luminosity function derived by Sanduleak.

LOG (SPACE DENSITY) - STARS/CUBIC PARSEC

ABSOLUTE PHOTOGRAPHIC MAGNITUDE

LOG (SPACE DENSITY) - STARS/CUBIC PARSEC

ABSOLUTE PHOTOGRAPHIC MAGNITUDE
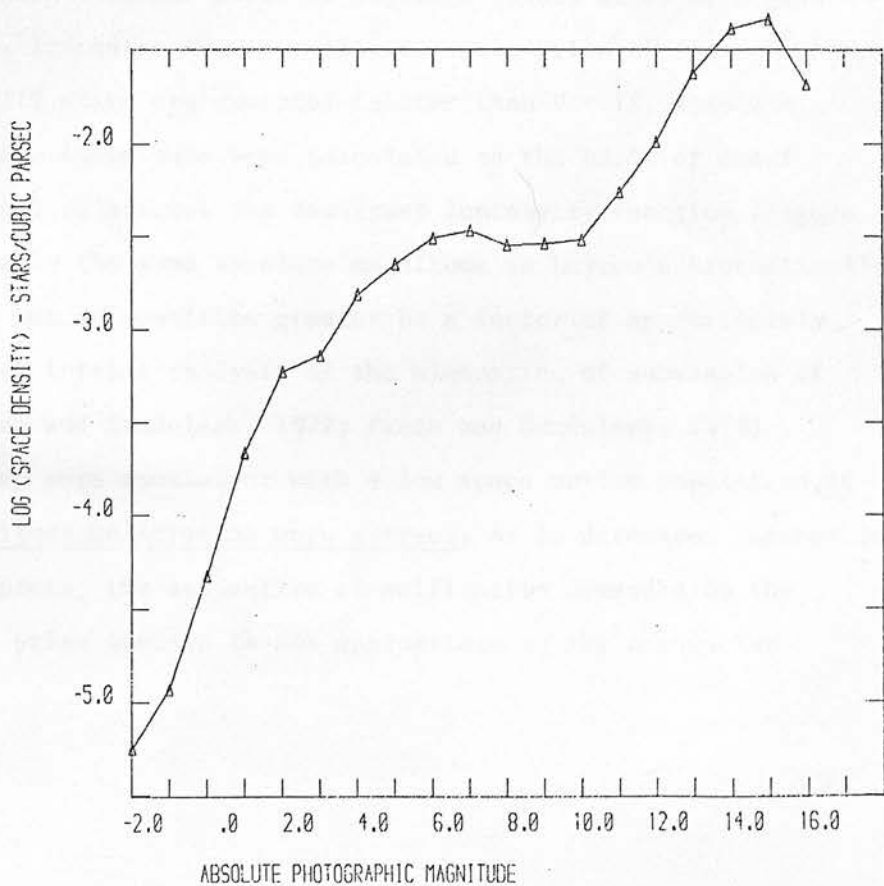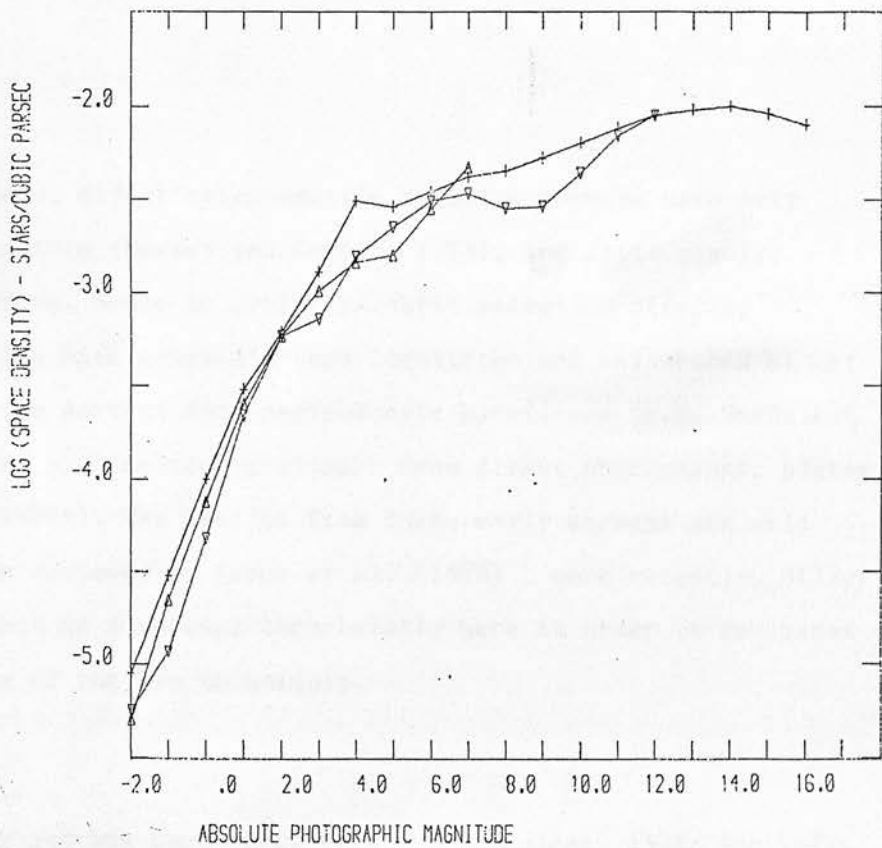
Large scale, direct trigonometric parallax surveys have only recently become feasible (Murray and Corben, 1979), and still require extensive plate series. Hence to avoid kinematic selection effects, observational samples have generally been identified and calibrated either using objective prism surveys and spectroscopic parallaxes (e.g. Sanduleak 1965; 1976) or using photometric parallaxes from direct photographic plates (Weistrop, 1972a; 1972b). The results from these early surveys are well known and have been reviewed by Faber et al. (1976) , more recently, Miller and Scalo (1979), but we summarise them briefly here in order to re-assess the relative merits of the two techniques.

Sanduleak and his co-workers (Pesch & Sanduleak, 1978; Smethells, 1974) have carried out a number of objective prism surveys to varying limiting magnitudes and presented catalogues of M-type stars in the Northern and Southern Galactic Caps. As Upgren's (1962) study of M-giants towards the N.G.P. indicates that a negligible proportion of disk luminosity class III stars are expected fainter than V = 12, absolute magnitudes for these stars have been calculated on the basis of dwarf (M_V , spectral type) relations. The resultant luminosity function (figure 2.2) peaks at roughly the same absolute magnitude as Luyten's kinematically derived function, but at densities greater by a factor of approximately three. Furthermore, initial analysis of the kinematics of subsamples of these stars (Murray and Sanduleak, 1972; Pesch and Sanduleak, 1978) indicated that they were consistent with a low space motion population,if the absolute magnitude calibration were correct. As is discussed further in the following chapters, the subjective classification demanded by the complex nature of prism spectra is not appropriate to the accuracies

required for space density analysis - at least for late type stars. In particular there is no guarantee that an internally self-consistent system coincides with the standard system used to calibrate the H-R diagram.

Although it is only recently that these problems have become fully apparent (this work; Pesch and Dahn, 1982), earlier quantitative calibration of stars from these surveys did reveal the presence of scale errors. Higher dispersion spectroscopy by Pesch (1972) of 27 of Sanduleak's N.G.P. sample showed that while the absolute magnitude calibration of the brighter, early-type M-stars was secure, those classed as M5 or later (which were also fainter in apparent magnitude) were systematically typed too late by ~3 subclasses - corresponding to more than 2 magnitudes in M_v. Similarly photometry by Koo and Kron (1975) and Weistrop (1977) of the Murray and Sanduleak sample indicated that the lateness of the later type stars had been exaggerated by a comparable amount.

Photometric parallaxes, on the other hand, are derived from an absolute magnitude - colour index relation, where the colour index can be determined from the measurement of direct plates taken in different passbands. The simple structure of the stellar images makes this a method much more tractable to automatic analysis techniques and especially powerful in view of the availibility of high quality, wide field Schmidt plates from the UK Schmidt telescope and of high-speed automatic measuring machines for subsequent data extraction . However, previous studies strike a cautionary note on too casual an application of this method.

Apart from Weistrop's celebrated red dwarf excess, both Gliese

(1972a), analysing the Lowell Proper Motion survey of the S.G.P. (Giclas, Burnham and Thomas, 1972), and Staller, The and Bochem-Becks (1982) have carried out surveys of this type, using colour class estimated by visual comparison of red and blue plates as an absolute magnitude indicator. As is discussed in more detail in chapter 4, both of these analyses can be shown to have overestimated the local number density of late type M dwarfs.

These erroneous results do not invalidate the technique of photometric parallax itself. The source of the error in all cases lies with inadequate matching of the photometric systems of the absolute magnitude calibrators with those of the programme stars. Warren (1976) has shown that the Giclas' colour classes are not uniformly defined over the area of the S.G.P. - given the low altitude from Lowell, probably a result of differential atmospheric reddening. Similarly Weistrop's photographic B and V magnitudes were defined on a self consistent system - but one which had systematic scale errors both with magnitude and colour relative to the photoelectric calibrators (Weistrop, 1976). These were compounded by errors in the photoelectric calibrators themselves (Faber et al, 1976). The systematic errors were small (~0.1 to 0.2 magnitudes), but because of the small dynamic range of the (B-V) colour index for red ((B-V)>1.2; M_V >+9) dwarfs even such small errors underestimate the stellar luminosity by two to three magnitudes. This same problem of low resolution afflicts spectral classification of late type stars, which are therefore susceptible to the same systematic errors (see Chapter 3). As we shall show there are colour indices eminently more suitable than (B-V). We merely note here that (V-I) as defined on a Kron-type system (eg the Kron-Cousins system of SAAO (Cousins, 1980) or the Kron-Mayall system of the U.S. Naval Observatory (Strand et al, 1976)) combines the advantages of a long, well calibrated colour baseline with the high solid angle coverage of photographic

detectors. Further discussion is postponed until the following chapter.

By no means all studies of the luminosity function have produced results in disagreement with those of Luyten. Starikova (1960) analysed the Yale Bright Star Catalogue (Schlesinger and Jenkins, 1940) and Gliese's (1956) original Nearby Star Catalogue using the method of trigonometric parallaxes and deriving densities close to Luyten's values. Wielen (1974) essentially repeated and extended this analysis using the second Nearby Star Catalogue (Gliese, 1969), applying varying distance limits to define complete samples at different absolute magnitudes. The resultant function is closely in agreement with Luyten's (apart from the K dwarf deficit) giving the same overall mass density (0.048 M $_\odot$/ pc^3) and peaking near M_V= +13 - although the function becomes increasingly incomplete fainter than M_V = +14. However it should be noted that this derivation is not completely free of kinematic bias, since the majority of nearby stars have been detected through their having relatively high proper motions. The same bias obviously resides in Eggen's (1979b) sample of M-dwarfs with annual proper motions greater than 1" arc. Eggen calibrated absolute magnitudes using (R-I) photometric parallaxes, but again numbers limit this analysis to stars brighter than M_V ~+13 - there are only 36 stars in the total sample fainter than M_V = +12.

Essentially all these surveys (apart from the Palomar proper motion survey) suffer from a lack of very low luminosity stars. Recently a specific attempt was made to look for such low mass (M < 0.1 $M_\odot$) objects through infrared (JHK) photometry of white dwarfs in a search for red dwarf companions (Probst and O'Connell, 1981). Of the 121 white dwarfs observed only three proved to have infrared excesses, with the faintest companion

detected only $M_V \sim +14.7$. While this is a very sensitive technique in terms of the detection of such stars, it is not obvious that it is relevant to the overall problem. First, it requires identification of a volume complete sample of white dwarfs which, while comparatively easy for hot, ultraviolet excess objects, is more difficult for the more numerous, redder degenerates. Second, there is no guarantee that the luminosity function of secondaries in evolved binary systems of this type accurately reflects that of field main sequence stars. Finally, the survey was restricted to companions within 15" arc of the white dwarf − yet the existence of wide binary systems amongst late type stars is well established, even if their survival is little understood. For example, both VB 8 ($M_V = +17.5$) and VB 10 ($M_V = +18.5$) (van Biesbroeck, 1944, 1966), two of the lowest luminosity stars known, lie at substantial distances from their primaries − 1800 and 400 A.U. respectively. Even at 25 parsecs neither would fall within the photometer's aperture.

With the discrediting of the early kinematically independent surveys, most studies requiring the disk luminosity function have used functional forms similar to Luyten's results − despite the fact that there is still no independent confirmation of their accuracy at very low luminosities. Furthermore, the "observed" function is generally smoothed through the K dwarf deficit and held flat in log(number density) at the faint end. As Upgren and Armandroff (1981) have pointed out, since this smoothing is carried out in logarithmic number density, it corresponds to substantial alterations in number density. In particular, the present day mass function derived by Miller and Scalo (1979) assumes a radically different shape if the Wielen function is adopted (see chapter 7, fig. 1) and this alteration could substantially affect their conclusions regarding the initial mass function of star formation (IMF). The derivation of the

IMF requires knowledge not only of the present day mass function (in Miller and Scalo's notation the PDMF), but also of what is termed the creation function - the number of stars born per unit area in the Disk, per unit log (Mass) and per unit time. The variation of the latter function with time is the birthrate. Obviously, for stars with main sequence lifetimes longer than the age of the Disk, the PDMF represents the time integration of the creation function and the IMF, while for shorter lived stars only a proportion of the total population are still unevolved.

In order to deconvolve the IMF from the observed PDMF several simplifying assumptions have to be made, notably concerning its variation with time and space. Of these, the simplest are that the IMF is time invariant, and that the locally observed PDMF can be taken as representing the averaged quantity for the Solar Neighbourhood. In this case the low mass (M $<$ 1-2M$_\odot$) IMF has the same shape as the PDMF, while at higher masses it depends on the birthrate adopted. Miller and Scalo adopt these assumptions, justifying this on indirect theoretical grounds - that most fragmentation mechanisms of star formation are metallicity independent, i.e. will not vary with disk enrichment - and observationally - with reference to Dixon's (1970) failure to detect significant differences in the luminosity function of two groups of K dwarfs selected by age; by the apparent constancy of the planetary nebula - white dwarf formation rate; and the (model-dependent) constancy of the yield of nucleosynthesis from high mass (M $>$ 10M$_\odot$) stars (Arnett, 1978).

Against this it should be pointed out that none of the fragmentation mechanisms actually produces an IMF remotely resembling the inferred observed function at low masses. Their insensitivity to opacity

cannot therefore be counted as a particularly strong argument either way. Furthermore, there are significant differences amongst the observed mass functions (and hence IMFs) of different star clusters - particularly for low mass stars (Scalo, 1979). Miller and Scalo adjudge that this probably reflects a dependence on initial conditions, or between the IMF in star clusters and in stellar asociations, in which most field stars are formed. If so, since a high proportion of the stars at present in the Solar Neighbourhood are sufficiently old to have survived several Galactic orbits (Woolley, 1962), they may have migrated from substantially different original environments - introducing the influence of both temporal and spatial variations. In this context it should be noted that recent work by Garmany, Conti and Chiosi (preprint) strongly suggests that more high mass O stars are born within than outwith the solar radius - i.e. the PDMF of O stars steepens with increasing Galactocentric radius. Furthermore, Larson (1982) has presented arguments that the shape of the IMF for low mass stars (less than a solar mass) is strongly dependent on the mass spectrum and spatial distribution of molecular clouds. Thus the time invariance of the IMF cannot be considered to be more than weakly supported. However, there is not, as yet, any obvious alternative to this constraint that is not even more ad hoc and even more difficult to justify.

The second major assumption fundamental to Miller and Scalo's IMF is the assumption of continuity. This requires that the birthrate be such that the IMF for high mass stars fits smoothly onto that for the low mass stars. Essentially this implies that a single star formation process is dominant over the full mass range, and to some extent this prejudice must be influenced by the apparently regular shape of their low mass PDMF. Miller and Scalo argue that it is unreasonable to expect two star formation processes to cut on and off at the same mass, resulting in a discontinuity.

On the other hand, there could be several processes with substantially
different efficiencies acting within different mass ranges, overlapping to
some degree, and producing, if not a discontinuity, certainly a significant
change in slope. The irregular shape of the PDMF with the K dwarf deficit
included suggests that this may, indeed, be the case. However, it is
unlikely that such a break occurs at the mass exactly corresponding with
the old disk main sequence turnoff. Hence the limits that Miller and Scalo
set in the creation function, and their preference for a constant birthrate
are probably reasonable.

One point on which Miller and Scalo lay particular emphasis is
the substantial difference between their derived IMF and a Salpeter-type
function, and the inability of star formation mechanisms to reproduce this
shape - especially below one solar mass. Fragmentation mechanisms (e.g.
Fowler and Hoyle, 1963; Silk, 1977) predict steep (index -1 to -2) power
law distributions extending to 0.1 $M_\odot$, while Miller and Scalo's IMF has a
power law index varying from -2.3 at $10M_\odot$, through -0.5 at $1M_\odot$ to 0 at
$0.1M_\odot$. (Note this is the slope of the differential counts). On the other
hand, models involving coalescence of gas clouds after fragmentation
(Pumphrey and Scalo, preprint) can produce flatter mass spectra by merging
large numbers of small fragments - although it is possible that these move
too far to the other extreme. Since the luminosity function found in this
work turns over where Miller and Scalo's stays flat, these arguments apply
with even more force.

Miller and Scalo truncate their IMF at $0.1M_\odot$ (M_V = +16),
although Luyten's luminosity function purports to extend to even lower
masses. (Luyten quotes number densities to M_{pg} = +22, but notes that his

sample may be incomplete (i.e. underestimating the space density) fainter than M_{pg} ~+17.) As mentioned above, the theoretical mass limit for the main sequence, determined by when electron degeneracy prevents the temperature rising high enough to permit H-burning, is 0.085 $M_{\odot}$ (Graboske and Grossman, 1971). Kumar (1969) and Staller (1975) have suggested that lower mass, black dwarfs could supply a large fraction of the local mass density. Grossman, Hays and Graboske (1974) have shown that, these "stars" are luminous for periods of up to 7.5 x 10^7 years, either through energy produced by gravitational contraction or by the deuterium burning process. If there were large numbers of such objects it might be expected that examples could be found amongst known low luminosity dwarfs - such as VB 8, VB 10 and GJ1002. All of these stars have old disk motions (the G1 752 (VB 10) system is classed as young disk, but has a space motion of ~60 km/sec) - but , since most such stars are identified by high proper motion, this could be another selection effect biased against young, low space motion objects.

Staller and de Jong (1980) have calculated luminosity functions in various passbands under the assumptions that these objects radiate as black bodies (which is unlikely to be the case, given the prominence of molecular bands in low luminosity M dwarfs); that they are completely convective with time independent effective temperatures; and follow the degenerate cooling tracks given by Tarter (1975) and Stevenson (1978). Finally, the initial mass function adopted is of the Salpeter power law type with indices ranging from -2.0 to -2.7, normalised to Luyten's space density for M_B = +11 dwarfs. The resultant function predicts a factor three more stars at M_V = +13 than found by Luyten (1968), Wielen (1974) and by this work. Furthermore, if the function has a power law index so much steeper than the disk IMF (even at M=1.0$M_{\odot}$), then it also seems reasonable

to assume that a different formation process is at work. Renormalising Staller and de Jong's function our observed density at M_v = +15 (Ch. 4) and retaining the steep mass spectrum would reduce the predicted number densities by virtually a factor of ten.

Finally, while Staller and de Jong discuss the detection of these objects with either IRAS or the Space Telescope, the photographic programme outlined here presents a substantially more efficient method for their detection. IRAS is limited to apparent magnitudes brighter than ~6.6 at 11.8 microns (an effective distance limit of ~0.5 parsecs for these objects) while even the combination of Staller & de Jong's IMF and a constant birthrate function predicts only 70 black dwarfs per square degree at V=26 — equivalent to 1.4 per wide field camera frame. They calculate that at this magnitude there are ~1900 disk objects per square degree. More sophisticated Galaxy models (Gilmore, 1981) predict ~7500 disk, halo or intermediate population stars per square degree at or brighter than this limit — and this takes no account of extragalactic objects, which dominate number counts fainter than V ~ 22. Thus the separation of a few black dwarfs from these other contaminants would require numerous multicolour, deep exposures of several different fields — expensive in time and unlikely to be productive.

On the other hand, with a limiting magnitude of I ~ 19, U.K.S.T. plates can provide a complete sample of stars with M_I < +14 within 100 parsecs. Furthermore, one Schmidt field covers the same solid angle as 1800 wide field camera frames and therefore, since the effective distance limit is similar, has a substantial multiplexing advantage. As will be discussed further in chapter 4, practical considerations limit samples to I < +17 and

$M_I < +12$. However, within these limits all black dwarfs (and any other
very red objects, such as extreme quasars or high redshift galaxies) can be
identified by isolating all objects visible on I plates, but indetectable
on SRC J survey plates ($B_J > 23$) (Hewett, Gilmore & Reid, in preparation).

In summary, previous studies of the luminosity function of
M-dwarf stars have produced conflicting estimates of their local space
density. While the available corroborative evidence suggests that the
higher space densities found from analysis of objective prism surveys is
due to inadequate absolute magnitude calibration, it is nevertheless valid
to question the kinematic biases that enter into the Luyten luminosity
function. Indeed, as chapter 5 shows, these effects are significant -
although not in the sense hypothesised by Sanduleak. In the following
chapters the method of photometric parallaxes is used to investigate two
samples of late type stars : photoelectric photometry of Smethells' sample
of bright southern M dwarfs, and photographic photometry using COSMOS of a
complete sample of very red objects towards the South Galactic Pole.

Chapter 3

One of the investigations of the red dwarf luminosity function which was based on an objective prism survey and claimed to find a substantial excess of late type M dwarfs was that carried out by Smethells (1974). This survey covers ~1720 square degrees of the southern sky to a visual apparent magnitude limit of ~12, providing a kinematically unbiased sample of bright, nearby late type dwarfs. As such it perfectly complements the deeper photographic survey described in the following chapter, which, although extending to fainter than V=19 and I=17, covers only 18 square degrees.

Furthermore, Sanduleak hypothesises a population of M stars with low velocity dispersion relative to the local standard of rest, implying that the stars are highly concentrated towards the Plane. Thus the low velocity population would be under-represented in the polar survey. Since Smethells original study claimed to find an excess of this type amongst the bright, nearby stars in his sample, re-analysis directly tests the Sanduleak hypothesis.

Smethells calibrated the absolute magnitudes from the observed spectral types using the (M_v, spectral type) relation quoted by Gliese (1971), while apparent magnitudes were estimated from the prism plates

themselves. Photoelectric photometry by Weistrop (1980) of a subset of the complete sample has shown that serious scale errors distort both magnitude scales. Using these observations, Gliese (1981) has computed the appropriate corrections for the 95 stars not observed by Weistrop, but only with the intention of deciding which of the latter sample most probably lie within 25 parsecs. Gliese also extensively analysed Weistrop's photometry — in particular comparing the various absolute magnitudes derived from colour indices or spectral types — but did not attempt to derive density information since over half the sample lacked accurate photometry.

In this paper photometry is presented for all previous unobserved stars and a magnitude-limited complete sample defined. Deriving absolute magnitudes from photometric parallaxes, the space density and kinematics of this complete sample are examined for any evidence of an extra low-velocity population. Section II describes the observations and calibration techniques adopted; Section III presents the programme star observations in detail, while the re-analysis is discussed in Section IV.

II   i)   Observations

The photoelectric photometry described here had two aims:— first, to obtain accurate photometry for all Smethells' stars not observed by Weistrop; second, to provide magnitudes and colours for stars of known trigonometric parallax, which act as calibrators in the absolute magnitude relations described further below. All the photometry was obtained during two observing runs in 1980, August/September (2 weeks) and 1981, May/June (3 weeks) at the Sutherland station of the South African Astronomical

Observatory. Both the Radcliffe Peoples Photometer on the 40" reflector and the Peoples Photometer on the 20" Boller and Chivens reflector were used in 1980, when only parallax calibrators were observed, while all of the programme stars, together with additional Gliese stars were observed on the 20" during the second run. Both photometers are single-channel, twin-tube devices, using an EMI extended S20 photomultiplier tube as a red channel (BVRI) and an S13 for the blue (UBV). (B-V) measures were made on the red channel, save where a (U-B) is quoted, when the colour is the mean of "blue" and "red" values. All of the latter measurements were made on the 20", and there is no relative colour term evident from the residuals from the two tubes.

Both sets of observations have been reduced at SAAO, Cape Town using the standard programmes available there. However the stars considered here cover a large range in colour and for the method of photometric parallaxes to be applied it is essential that all observations - both of programme stars and calibrators - are on the same system. For this reason a number of stars from the Gliese Nearby Star Catalogue (Gliese, 1969) which have photometry by Cousins (1980) were included with the E-region standards (Menzies, Banfield & Laing, 1980) to ensure an accurate transformation to to the Kron-Cousins (kc) system. The photometry for these stars is presented in Table 3.1. All save two of the (B-V) colours quoted were derived from the present series of observations, and thus have not been subjected to the same rigorous scrutiny as Cousins's own photometry. The rms scatter of the new (B-V) determinations is listed. As emphasised above, all of the parallax star photometric standards are used in the definition of the $(M_V, (V-I))$ relation described below, and thus the derivation of photometric parallaxes does not require the additional uncertainties of further colour transformations.

Table 3.1

Gliese	V	V-R	V-R'	V-I	B-V	rms	n(obs)	n(nights)
393	9.66	1.014	1.030	2.248	1.492	0.014	12	6
551	11.11	1.671	1.853	3.668	1.878	0.028	24	13
628	10.09	1.164	1.290	2.680	1.54	0.02	2	1
654	10.09	0.960	0.979	2.126	1.422	0.015	4	3
674	9.390	1.018	1.086	2.398	1.547 (*)		31	12
699	9.565	1.226	1.343	2.788	1.703	0.006	6	4
784	7.970	0.910	0.910	1.831	1.426 (*)		16	7
832	8.66	1.010	1.020	2.18	1.777	0.003	3	2

Very red standards used. (*) denotes Cousins's (B-V) values.

For consistency Cousins's photometry of Gl 551 (Proxima) is adopted rather than that by Bessell (1980, preprint). Cousins (priv. comm.) has commented that with such an extremely red star it is not adviseable to be dogmatic in the matter of photometric transformations. The large scatter in (B-V) for this star should be noted. The range (1.83 to 1.93) is much larger than photon statistics would lead one to expect and may be indicative of intrinsic night to night variations.

The only significant non-linearity in the transformation between the instrumental and standard systems occurs for (V-R). There is a large colour term for stars redder than (V-I) = 2.0, reaching a value of -0.18 (in the sense R(observed) - R(kc)) for the reddest standard (Proxima Centauri). This effect arises from an anomaly in the Sutherland reduction programme in the implementation of the non-linear corrections for very red stars (Menzies, private communication). Since this affects very few stars - either programme or parallax - no attempt has been made to estimate corrections. Small amplitude (0.04 magnitude maximum) linear colour terms were detected in V and (V-I) (but not in (B-V)) and these have been corrected for. Hence while all V, (B-V) and (V-I) values quoted are on the Kron-Cousins system, the few stars redder than (V-I) = 2.0 have (V-R) colours on a non-standard system (denoted (V-R')). Beyond (V-I) = 3.67 (Proxima Centauri) the (V-I) index is outside the range of calibration, and cannot be guaranteed to agree with any other system. Since there are no Smethells' stars redder than 2.8 in (V-I) neither of these uncertainties affects the conclusions of this paper.

On average 30 standards were observed during a complete nights photometry on the 20", while about 20 were observed with the 40". An individual observation consisted of the filter sequence VBRIIRBV followed by VBRI sky measurements. Zero point drift had to be allowed for on a few nights, but even before correction none of the nights from 1981 has standard star residuals greater than 0.015 rms in V. The 1981 photometry is discussed in more detail in Section III, and the parallax star photometry tabulated in Appendix ii, but it is noted here that the overall internal accuracy is not significantly different from 0.01 in all passbands.

The same is not true for the 1980 observations, when poor weather permitted observations of only a few stars on more than one night. Thus the internal accuracy of the August runs can be estimated only by considering the consistency of the standard observations. With due allowance for drifts in zero point these give standard deviations of 0.02 in V and 0.015 in the colours. As the parallax stars observed are considerably fainter it is probable that their errors are larger, but even if these are as large as 0.05 (which is the uncertainty in V, from three nights observations, of VB 8 - the faintest star observed), they are still unimportant in comparison with the probable errors in the trigonometric parallaxes. There are seven stars which have V and (B-V) photometry by the U.S. Naval Observatory (Harrington and Dahn, 1980) and these give residuals of -0.01 ± 0.04 (standard deviation) in V and -0.05 ± 0.04 in (B-V). There is no evidence of systematic errors and, although unsatisfactory, the observational accuracy is adequate for the present purposes.

ii) The Absolute Magnitude - Colour Relations

The method of photometric parallaxes stems from the fact that stars follow well-defined sequences on the H-R diagram. Hence the effective temperature-luminosity correlation for main sequence stars leads to the observed relations between absolute magnitude and colour index. In defining any such relation, three criteria must first be applied. First, reliable trigonometric parallaxes must be available. Lutz and Kelker (1973) and Upgren et al. (1978) have shown that a systematic bias in derived

absolute magnitude is introduced when a upper limit in percentage accuracy of parallax is used to select calibrators. The correction factors amount to -0.11 magnitudes in derived absolute magnitude for a 10% (σ_π / π) accuracy in measured parallax and increase to -0.43 at 17% accuracy. Because of this rapid increase, the uncertainty in estimating the true accuracy of a parallax becomes itself a significant source of uncertainty in the correction.

The other criteria are photometric. The colour index chosen must be well suited to the type of stars that are to be calibrated, and all photometry of the calibrators (and, subsequently, of the programme stars) must be on the same system to avoid systematic errors introduced by erroneous transformations. None of the published calibrations satisfies all these criteria. Gliese (1971) has tabulated relations between M_V and the indices (B-V) and (U-B) on the Johnson system, $(U-B)_c$ on the Cape system and the Kron (R-I) index. The ultraviolet indices are only acceptable for G and early K stars, while, although most of the (R-I) data is from Kron et al. (1957), some values have been linearly transformed from $(R-I)_J$. Bessell (1979) has shown that this transformation is non-linear and furthermore, few modern photometers mimic the original Kron system. Finally, as his paper predates that of Lutz and Kelker, Gliese selected his calibrators to have probable errors in parallax less than 10% (standard error < 15%) - so the published relations require correction.

Cousins (1980) has recently published photometry of a large number of stars from the Gliese Catalogue (Gliese 1969) and its more recent supplement (Gliese and Jahreiss, 1979). This provides a homogeneous set of calibrators on a precisely defined and readily accessible photometric
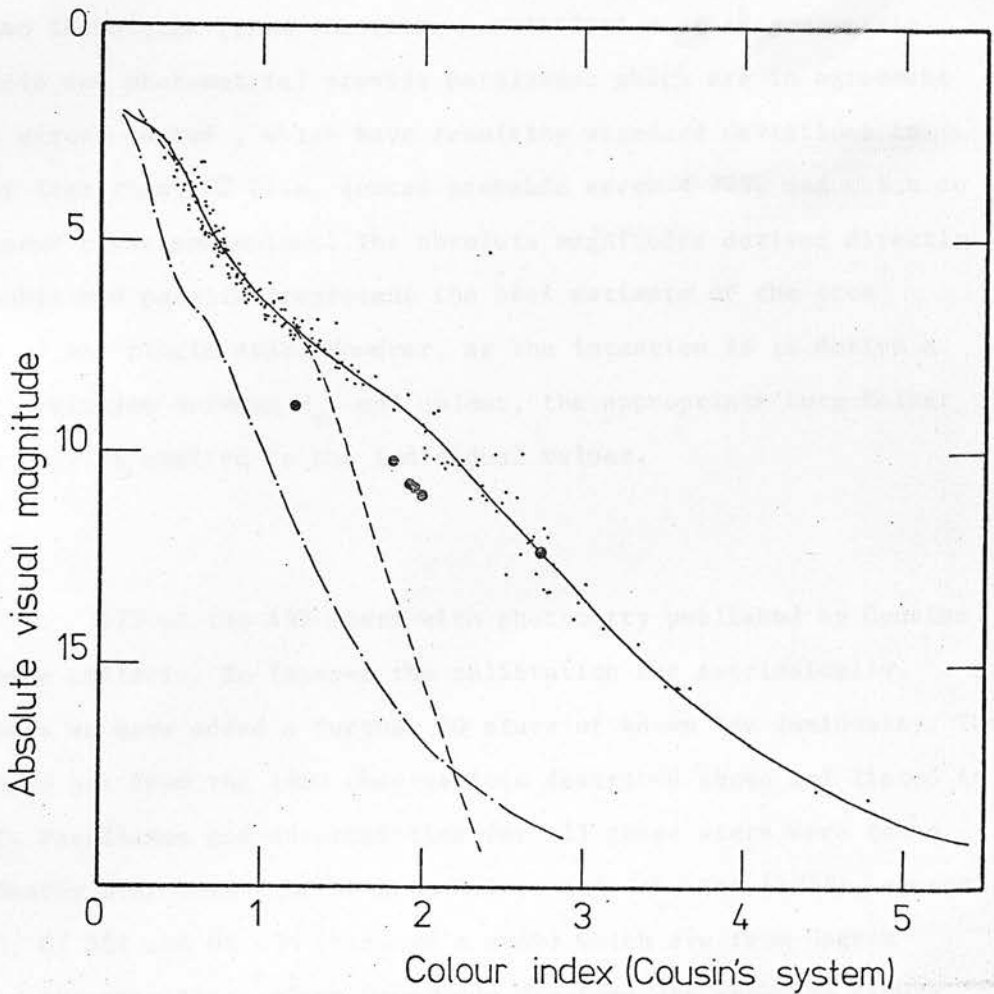
Figure 3.1 – Absolute Visual magnitude – colour
relations. a) (dashed line) for (B-V) , b) (dot-dash line) for (V-R)kc
and c) (solid line) for (V-I)kc. The individual observations of parallax
main sequence (dots) and subdwarf (filled circles) stars are plotted for
the last case.

system - moreover, the same system as the programme star observations. To avoid the uncertainties introduced by the Lutz-Kelker effect we have restricted our sample of calibrating stars to include only those for which at least two techniques (from the three possibilities of trigonometric, spectroscopic and photometric) provide parallaxes which are in agreement within the errors quoted , which have resulting standard deviations in parallax of less than 10% (i.e. quoted probable error < 7%), and which do not have known close companions. The absolute magnitudes derived directly from the published parallax represent the best estimate of the true luminosity of any single star. However, as the intention is to derive a statistical relation between M_V and colour, the appropriate Lutz-Kelker correction must be applied to the individual values.

173 of the 493 stars with photometry published by Cousins satisfy these criteria. To improve the calibration for intrinsically fainter stars we have added a further 30 stars of known low luminosity. The bulk of these are from the 1980 observations described above and listed in Appendix i. Parallaxes and uncertainties for all these stars were taken from the Nearby Star catalogue or from Gliese and Jahreiss (1979), except for Gl 273, Gl 551 and Gl 699 (Barnard's star) which are from Upgren (1977), and the resultant colour magnitude diagrams are shown in Figure 3.1. The continuous curves are third order spline functions, and the total scatter about each is listed in Table 3.2, together with σ_{12} , the dispersion in absolute magnitude at $M_V = 12$ for an uncertainty of 0.1 in colour index. As the calibrators have trigonometric parallax errors less than 10%, the tabulated dispersions are essentially the cosmic scatter for each relation. The steep gradient in (B-V) at faint absolute magnitudes accounts for the drastic effect of small systematic errors (Weistrop, 1976; Faber et al., 1976), while (V-R) is significantly worse than (B-V) for

Table 3.2

Absolute Magnitude - Colour Relations

Colour	r.m.s. scatter	σ_{12}
(B-V)	0.42	1.25
(V-R)kc	0.40	0.90
(V-I)kc	0.35	0.40

stars brighter than M_V ~8 (although it is better than (R-I) throughout). (V-I)kc is manifestly the most suitable for faint stars, while it has the added advantage that it has the same resolution as (B-V) for even late A stars (M_V ~ +2).

 The colour magnitude relations derived here are valid only for disk main sequence stars. It has long been known that subdwarfs describe a separate sequence lying approximately 1 magnitude below disk stars in the (M_I,(R-I)k) plane (Eggen, 1973), and much the same can be expected to be true of the (M_V,(V-I)kc) relation. The exact definition of this sequence is difficult, however, since very few halo dwarfs have well determined parallaxes (using the criteria described above) and, as a result, absolute magnitudes are not well known. In view of this we have relaxed our error limits in selecting subdwarfs from the photometry of Rodgers and Eggen (1974) and Hartwick (1977), and used these stars to roughly define the subluminous star domain in Figure 3.1. As can be seen, metal poor stars do form a low luminosity sequence, at least between (V-I) = 1.0 and 2.0. However, the two reddest subdwarfs in our sample (LHS 61 and Gl 699) both lie amongst the disk stars. Model atmosphere calculations by Bessell and Wickramasinghe (1979) found that no extreme metal poor stars ([z] < -2) could be expected to have colours redder than 1.0 in (R-I) (or 2.0 in (V-I)). Thus it may be that there is a single (M_V,(V-I)) sequence for stars redder than 2.25 in (V-I).

 Any bluer ((V-I) < 2.25) subdwarfs in the sample will be calibrated 1 to 1.5 magnitudes too bright by this technique, leading to an underestimate of the local stellar number density. However since the local disk/halo number ratio is of order 0.005 (Chiu, 1980a), it is extremely

unlikely that subdwarfs provide a significant contribution to the nearby late type star population sampled here. The high velocity programme stars are discussed individually in Section IV.

III Observations of Programme Stars

123 stars of the 186 listed by Smethells were observed from Sutherland and the new data are tabulated in Table 3.3. Besides wideband photometry the table includes the equatorial co-ordinates (equinox 1950.0) and the magnitude and direction of poper motions given by Smethells for these stars. The latter values are taken mainly from the Bruce Proper Motion Survey (BPM ; Luyten, 1938a, 1963a). Stars from the Luyten Half Second Catalogue (LHS ; Luyten,1980) and from the Catalogue of Nearby Stars and its Supplement are identified, and absolute magnitudes derived from the photometric (V-I) parallaxes are tabulated for all stars. As the latter has a dispersion of 0.35 magnitudes, M_v is given only to the nearest tenth of a magnitude. All programme stars except those marked with colons in Table 3.3 were observed through at least two filter sequences. Lack of time forced expediency for the latter set and for similar reasons it proved possible to measure only 30 stars on more than one night. However, taken together with 35 Gliese stars in the same magnitude range, night to night comparisons show the internal consistency in Table 3.4.

Two stars are excluded from the above comparison. Sm 20 was

Table 3.3

Photometric Observations of stars from Smethells' Survey

Sm	RA	Dec.	V	B-V	V-R	V-I	M	μ	θ	Comments
1	16 44.8	-64 58	10.33	1.33	0.82	1.56	7.8	0.134	142	W
2	16 50.6	-65 10	11.38	1.35	0.84	1.63	8.0	0.252	188	
3	17 42.4	-57 17	10.76	1.60	1.14	2.54	1.5	1.713	220	W,Gl 693,LHS 454,CE
4	17 50.1	-44 16	11.15	1.36	0.84	1.61	8.0	0.210	223	
5	17 53.7	-41 59	11.36	1.51	1.02	2.16	9.9	0.392	194	
6	17 56.6	-48 22	12.26	1.45	0.98	2.12	9.8	0.061	156	W
7	17 57.7	-62 59	10.39	1.28	0.78	1.45	7.5	0.243	157	W,
8	17 59.0	-64 30	11.54	1.47	0.94	1.91	9.0	0.192	20	
9	18 1.7	-55 7	11.58	1.33	0.81	1.54	7.8	0.161	176	
10	18 2.0	-48 30	11.31	1.36	0.90	1.85	8.8			W,
11	18 8.7	-43 27	8.37	1.28	0.78	1.47	7.6	0.448	159	W,Gl 707,CE
12	18 13.5	-49 28	11.28	1.36	0.87	1.75	8.4	0.188	196	W,
13	18 23.3	-57 45	11.35	1.33	0.85	1.65	8.1			
14	18 25.8	-58 18	9.84	1.45	0.93	1.91	9.0	0.430	182	W,Gl 714,C
15	18 29.4	-62 47	9.54	1.43	0.74	1.40	7.4			W, Giant ?
16	18 31.4	-61 16	9.32	1.16	0.70	1.31	7.2	0.364	181	W,
17	18 36.7	-60 28	11.24	1.42	0.88	1.73	8.4			
18	18 37.0	-56 55	10.49	1.21	0.76	1.43	7.5			
19	18 41.5	-51 28	11.54	1.39	0.93	1.95	9.1			
20	18 42.2	-62 12	12.00	1.42	0.95	2.00	9.3			VARIABLE ?
21	18 44.7	-62 5	10.70	1.44	0.97	2.02	9.4			
22	18 45.8	-62 7	10.74	1.48	0.97	2.02	9.4	0.141	48	
23	18 48.7	-57 12	12.11	1.48	1.05	2.30	0.5	0.800	198	LHS 3421
24	18 53.3	-56 3	9.59	1.44	0.94	1.92	9.0	0.445	180	Gl 737A
25	18 53.3	-56 3	9.59	1.44	0.94	1.92	9.0	0.445	180	Gl 737B
26	18 55.2	-48 17	11.14	1.43	1.05	2.35	0.7	0.498	165	W,Gl 739,LHS3423
27	18 56.6	-52 26	12.10	1.37	0.87	1.69	8.2	0.135	151	
28	18 59.2	-42 50	11.19	1.24	0.78	1.50	7.7	0.104	138	DBLE, Primary
29	19 7.2	-47 14	9.36	1.32	0.81	1.55	7.8	0.626	184	W,Gl 747.3, LHS 3439
30	19 8.4	-52 19	9.96	1.49	0.79	1.49	7.6			W, Giant?
31	19 8.4	-55 57	11.31	1.42	0.94	1.95	9.1	0.329	238	Gl 747.4,C
32	19 10.8	-47 0	12.91	1.50	1.01	2.20	0.1			
34	19 13.0	-45 59	9.38	1.43	0.93	1.88	8.9	0.428	154	W,Gl 750AB, DBLE
36	19 15.8	-53 48	10.82	1.58	1.02	2.24	0.2	0.102	164	
37	19 18.3	-46 15	11.70	1.38	0.87	1.72	8.3	0.165	139	
38	19 26.2	-55 3	11.33	1.37	0.86	1.69	8.2	0.312	179	
39	19 30.2	-52 33	12.80	1.55	1.20	2.50	1.3	0.255	181	VARIABLE ?
43	19 41.4	-51 32	12.06	1.47	0.93	1.91	9.0	0.250	185	DBLE?
46	19 52.9	-59 25	10.90	1.31	0.80	1.53	7.7	0.168	146	W,
47	19 53.0	-59 25	10.32	1.20	0.74	1.37	7.3	0.168	146	W,
48	19 59.4	-65 43	11.33	1.46	1.03	2.26	0.3	0.855	174	W,Gl 774A,LHS 3513 DBLE,E
50	20 10.3	-45 19	7.97	1.42	0.91	1.84	8.7	0.812	106	W,Gl 784,LHS 3531,C
51	20 16.2	-46 35	8.72	1.17	0.71	1.31	7.2	0.349	259	W, Gl 787,CE
54	20 18.6	-58 27	10.58	1.42	0.89	1.77	8.5	0.827	120	W,Gl 788.1,LHS 3542
55	20 23.1	-44 55	11.58	1.26	0.76	1.40	7.4			
57	20 30.3	-46 23	11.88	1.40	0.85	1.70	8.3	0.047	329	
58	20 31.5	-51 20	12.14	1.44	0.93	1.95	9.1	0.117	100	DBLE
59	20 34.5	-55 47	11.36	1.42	0.89	1.77	8.5	0.070	172	
60	20 35.8	-43 55	12.26	1.44	0.96	2.01	9.3	0.132	163	W,
61	20 35.8	-43 55	12.72	1.48	1.03	2.25	0.3	0.132	163	W,
63	20 38.6	-52 52	8.82	1.33	0.83	1.59	7.9	1.054	176	W,Gl 798,LHS 49
64	20 44.7	-54 42	11.90	1.36	0.86	1.73	8.4	0.175	163	
65	20 50.5	-53 42	12.07	1.49	0.98	2.08	9.6	0.173	199	DBLE
70	20 59.5	-57 9	12.83	1.60	1.29	2.68	2.1	0.507	318	GJ 2151, NOT LHS 536
71	21 3.4	-41 17	11.09	1.26	0.77	1.43	7.5			

72	21	6.5	−53 16	11.65	1.29	0.82	1.53	7.7	0.202	152	
73	21	8.5	−45 32	11.95	1.40	0.92	1.86	8.8	0.319	62	
74	21	8.5	−43 48	12.01	1.56	1.05	2.27	0.4	0.717	164	W,LHS 3639
75	21	14.0	−60 2	11.17	1.18	0.72	1.33	7.2			
76	21	15.2	−42 37	11.42	1.18	0.72	1.33	7.2	0.096	232	DBLE ?
78	21	20.9	−46 55	12.45	1.52	1.04	2.24	0.2	0.728	96	Gl 826.2,LHS 3666
79	21	23.0	−42 39	12.67	1.53	1.13	2.52	1.4	0.087	340	
81	21	25.5	−47 29	12.20	1.42	0.93	1.92	9.0			
82	21	26.3	−55 15	11.56	1.38	0.88	1.73	8.4			
83	21	30.2	−39 13	8.68	1.46	1.02	2.18	0.0	0.793	185	W,Gl 832,LHS 3685,C
84	21	31.1	−49 46	11.13	1.30	0.80	1.50	7.7	0.232	111	
85	21	34.0	−63 57	10.63	1.42	0.95	2.00	9.3	0.157	261	W,
86	21	40.7	−61 13	11.72	1.40	0.91	1.84	8.7	0.046	132	
87	21	42.8	−54 33	11.25	1.31	0.81	1.55	7.8	0.186	50	
88	21	43.0	−57 55	8.77	1.33	0.83	1.58	7.9	0.864	174	W,Gl 836.9AB, LHS 3707, DBLE
89	21	46.1	−41 48	11.52	1.57	1.12	2.48	1.2	0.342	121	W, DBLE
93	21	51.6	−47 13	11.96	1.55	1.05	2.30	0.5	0.497	222	Gl 838.6
96	21	56.0	−59 59	9.73	1.45	0.95	1.99	9.3	0.876	96	W,Gl 842,LHS 3741,C
98	21	56.3	−62 19	11.97	1.42	0.91	1.84	8.7			
99	21	57.9	−52 0	10.78	1.27	0.79	1.51	7.7			DBLE
100	22	0.2	−50 53	12.09	1.57	1.02	2.23	0.2	0.574	148	LHS 3748
101	22	5.0	−51 28	10.51	1.20	0.71	1.30	7.2	0.345	112	W,Gl 848.1A, DBLE
103	22	12.6	−57 33	11.56	1.41	0.89	1.76	8.5			
104	22	16.8	−49 18	10.92	1.30	0.81	1.53	7.7	0.294	124	
107	22	20.2	−57 29	10.74	1.44	0.96	2.01	9.3	0.699	119	W,Gl 855,LHS 3802,E
109	22	24.6	−58 21	11.51	1.30	0.79	1.49	7.6	0.237	75	
111	22	34.3	−44 25	10.26	1.35	0.71	1.33	7.2			W, Giant?
113	22	34.9	−65 37	11.49	1.58	1.31	2.73	2.3	0.832	102	W,Gl 865,LHS 3839,E
117	22	48.0	−59 53	11.77	1.23	0.76	1.43	7.5	0.136	107	
118	22	48.2	−47 28	11.61	1.39	0.88	1.75	8.4	0.184	123	
123	23	1.7	−43 45	11.57	1.20	0.71	1.30	7.2			
124	23	2.1	−50 16	11.84	1.34	0.85	1.67	8.2	0.375	174	
125	23	3.5	−66 18	10.96	1.25	0.78	1.50	7.7			DBLE
126	23	7.5	−63 56	11.39	1.36	0.86	1.67	8.2	0.496	94	
127	23	10.3	−49 4	10.78	1.34	0.84	1.59	7.9			
128	23	11.4	−57 6	11.99	1.48	0.97	2.00	9.3	0.485	238	
129	23	11.6	−60 32	11.50	1.25	0.72	1.34	7.2			
131	23	14.9	−42 28	10.42	1.31	0.82	1.55	7.8	0.282	97	W, Gl 894,CE
135	23	23.0	−45 53	11.28	1.43	0.94	1.93	9.0	0.466	96	Gl 895.1
136	23	26.6	−45 54	11.15	1.29	0.79	1.50	7.7	0.206	134	
137	23	26.8	−47 19	10.21	1.30	0.79	1.50	7.7	0.186	100	Gl 895.3,C
138	23	33.3	−46 25	9.73	1.19	0.72	1.34	7.2	0.385	214	
139	23	33.7	−48 52	10.09	1.37	0.85	1.68	8.2	0.127	272	
140	23	33.8	−52 43	11.53	1.09	0.68	1.23	7.0			
141	23	35.4	−41 50	12.76	1.35	0.87	1.75	8.4	0.093	37	
142	23	45.6	−41 47	11.93	1.46	1.05	2.30	0.5	0.303	129	
143	23	39.2	−43 1	10.93	1.38	0.85	1.68	8.2	0.377	212	
144	23	40.4	−65 4	10.33	1.20	0.74	1.35	7.3	0.230	112	E
145	23	48.2	−53 1	10.79	1.19	0.71	1.32	7.2			E
147	23	55.7	−54 5	10.75	1.35	0.82	1.58	7.9	0.167	46	
148	23	57.2	−44 21	12.82	1.64	1.15	2.57	1.6	0.276	356	
149	23	59.9	−46 17	12.43	1.49	0.98	2.08	9.6	0.220	90	
150	0	1.4	−42 50	11.55	1.26	0.75	1.42	7.4	0.087	76	
153	0	3.7	−66 7	12.17	1.55	1.08	2.38	0.8	0.577	161	LHS 1019
157	0	13.8	−47 0	11.05	1.26	0.78	1.47	7.6	0.198	80	
158	0	14.1	−50 33	12.39	1.51	1.02	2.22	0.2	0.446	50	
159	0	14.9	−47 43	11.36	1.22	0.73	1.40	7.4	0.182	106	
161	0	15.1	−64 40	11.30	1.31	0.78	1.47	7.6	0.171	127	
165	0	21.7	−62 28	11.33	1.39	0.89	1.84	8.7	0.086	124	
171	0	40.0	−57 9	10.45	1.16	0.71	1.30	7.2			
172	0	40.0	−44 40	11.17	1.24	0.74	1.37	7.3	0.262	253	DBLE
173	0	43.2	−51 54	11.91	1.48	1.01	2.18	0.0	0.094	124	
174	0	46.7	−50 26	10.75	1.43	0.93	1.89	8.9	0.288	134	

175		0	47.1	-54	52	9.49	1.19	0.70	1.28	7.1			
176		0	47.3	-61	18	12.13	1.46	1.01	2.23	0.2	1.106	94	GJ 1022,LHS 124,E
177		0	50.1	-41	31	11.92	1.49	1.00	2.15	9.9			
178	:	0	53.2	-52	7	12.38	1.47	1.03	2.20	0.1	0.470	41	Gl 43
179	:	0	53.7	-47	25	11.06	1.30	0.85	1.67	8.2			
180	:	0	55.0	-51	52	10.77	1.30	0.83	1.63	8.0	0.150	143	
181	:	0	55.2	-62	31	9.49	1.30	0.80	1.51	7.7	1.063	81	Gl 45,LHS 128,E
182	:	1	2.3	-57	55	11.45	1.31	0.81	1.59	7.9	0.229	85	
183	:	1	5.3	-63	41	11.43	1.54	0.89	1.74	8.4	0.193	77	Subdwarf?
184	:	1	12.6	-54	12	11.09	1.48	0.98	2.09	9.7	0.320	21	
185	:	1	15.8	-48	25	11.56	1.43	0.88	1.80	8.6	0.254	64	Gl 56.2

Notes to Table 3.3

:		Single observation
DBLE		Double star
C		Photometry by Cousins and Stoy (1963), Cousins, Lake and Stoy (1966) or Cousins (1980)
W		Photometry by Weistrop (1980)
E		Photometry by Eggen (1974) or Rodgers and Eggen (1974)

The quoted absolute magnitudes are derived directly from the absolute magnitude colour relation shown in Figure 1. No Malmquist corrections have been applied.

Sm 15	Probable giant, (U-B) = 1.73
Sm 24/25	Joint photometry - equal luminosities assumed
Sm 28	Faint companion
	Joint photometry gives V=10.92 B-V=1.28 V-R=0.81 V-I=1.55
Sm 30	Probable giant, (U-B) = 1.85
Sm 34	Double, joint photometry
Sm 43	Faint companion V=13.7 V-R=0.4 V-I=0.8
Sm 48	Gl 774B V=12.82 B-V=1.53 V-R=1.15 V-I=2.58
Sm 65	Nearby star (sep. 20′) has V=12.42 B-V=0.59 U-B=0.06 V-R=0.36 V-I=0.72
Sm 70	The quoted position is the same as that of LHS 5363 but the measured colours are completely inconsistent. The nearest candidate for the latter has
	V=12.23 B-V=0.70 U-B=0.23
	and is +1.0 m. distant in R.A. and +0.′5 in Dec.
Sm 76	Close double - sep. 10″ , position angle 150 degrees (N. through E.)
	companion V=12.57 B-V=0.40 U-B=0.07 V-R=0.20 V-I=0.48
Sm 88	Double, joint photometry
Sm 89	Double, joint photometry
Sm 99	Double - separation 30″, p.a. 170 degrees
	companion V=14.1 B-V=1.5 V-R=1.1 V-I=2.5
Sm 111	Probable giant, (U-B) = 1.62
Sm 125	Double, separation 25″, p.a. 150 degrees
	companion V=14.7 B-V=0.8 U-B=-0.15 V-R=0.45 V-I=0.75
Sm 139	Double, separation 25″, p.a. 150 degrees
	companion V=12.37 B-V=1.44 V-R=1.32 V-I=2.71
Sm 172	Double, separation 1′, p.a. 90 degrees
	companion V=11.88 B-V=1.38 V-R=0.87 V-I=1.75
Sm 183	Probable giant

Table 3.4

Intercomparison of photoelectric photometry

Source	N	V	B-V	V-R	V-I
Internal	63	0.012 ± 0.010	0.015 ± 0.019	0.009 ± 0.008	0.014 ± 0.015
Weistrop	34	0.02 ± 0.02	0.00 ± 0.02	0.05 ± 0.02	0.04 ± 0.02
Cape	19	0.007 ± 0.016	0.020 ± 0.025	0.002 ± 0.008	0.004 ± 0.005
Rodgers & Eggen	18	-0.055 ± 0.026	-0.010 ± 0.026	-	-

The internal accuracy is assessed by comparison of stars observed
on more than one night. The external comparisons are all made in the
sense (Reid) - (other) and are as follows :
    Weistrop - Weistrop (1980)
    Cape - 18 stars in common in V from Cousins and Stoy (1963),
           Cousins, Lake & Stoy (1966) and Cousins (1980)
          14 stars in (B-V) (Cousins and Stoy,Cousins, Lake and Stoy)
          5 stars in (V-R) and (V-I) (Cousins)
    Rodgers and Eggen - Eggen (1974), Rodgers and Eggen (1974)

It should be noted that eleven stars in common between Cape and Rodgers
and Eggen give mean residuals (in the sense Cape - RE) of -0.05 ± 0.05 in V

observed on June 2/3 (standards give rms scatter of 0.007 in V after
taking out 0.025 zero point drift) and again on June 12/13 (rms scatter
0.007 - no drift). On both occasions the two sets of integrations give
better than 0.01 agreement and the night was clear and stable. The two sets
of colours are completely consistent, but the V magnitudes are respectively
12.03 and 11.94.

Observations of the other star, Sm 39, are listed in Table
3.5. The individual observations from the first night are listed separately
in view of the large discrepancy (photon statistics 0.016 in V). Again
there were no indications of cloud or unstable atmospheric conditions at
the time of observation, nor any similar irregularities in any stars
observed before and after. Fifteen other stars with V > 12 have photometry
on more than one night, either from this run or by Weistrop (1980), and for
none of these does the difference exceed 0.03 in V. Thus photometric error
is unlikely, and Sm 20 and 39 are suggested as candidate variables. For the
purpose of this study they are assumed to be dwarfs, (Sm 20 certainly is)
and the mean magnitudes quoted in Table 3.3 adopted.

All stars in Smethells' survey not observed at Sutherland
have BVRI photometry by Weistrop. 34 stars have observations on both
systems and the resultant comparison is given in Table 3.4. Again two stars
show sizeable discrepancies - Weistrop makes Sm 10 and Sm 16 fainter in V
by 0.15 and 0.19 magnitudes respectively. The latter has colours quoted
which place it well off the VRI two colour diagram, and the published
values are assumed to be in error. The former, although observed on only
one night during the present run, is very bright and misidentification is
unlikely - especially since the discrepancy was noted from the on-line

Table 3.5

Observations of Sm 39

HJD 24447	V	B-V	V-R′	V-I	n(obs)
64.502	13.04	1.62	1.35	2.77	1
64.505	12.95	1.67	1.35	2.72	1
68.500	12.87	1.54	1.28	2.65	2
69.477	12.80	1.58	1.14	2.57	1
71.447	12.82			2.56	2
71.502	12.81			2.66	2
71.578	12.84			2.62	2

reductions and the few possible candidates within about 15 arc minutes checked and excluded. Magnitudes and colours from the Sutherland observations have been adopted for both stars.

The other 32 stars give transformations from Weistrop's system to Kron-Cousins that are colour dependent in (V-R) and (V-I) . The composite relation for the latter is

$$(V-I)kc = (V-I)w + 0.03 \quad , \quad (V-I)w < 2.0$$

$$(V-I)kc = 1.08(V-I)w - 0.13 \quad , \quad (V-I)w > 2.0$$

A comparison with the other available photometry is also given in Table 3.4. As noted by Weistrop, Eggen's V magnitudes (Eggen 1974; Rodgers and Eggen, 1974) are systematically fainter by 0.06 magnitudes, while the R and I passbands are on a significantly different system. Approximate transformations are

$$(V-I)kc = 0.99 (V-I)e + 0.17 \quad , \quad \text{rms scatter} = 0.05$$

$$(V-R)kc = 0.70 (V-R)e + 0.23 \quad , \quad \qquad\quad = 0.06$$

As the large rms scatter indicates, the two systems are not particularly well matched.

IV Analysis   a: The Two Colour Diagram

With the exception of four stars, all of the Smethells'
sample are in the region of the (B-V)-(V-I) plane occupied by late type
dwarfs (Figure 3.2). The relation between these indices shows considerably
increased scatter beyond (V-I)=2.4, presumably due to the increasing
influence of differential blanketting. Similarly, the dispersion increases
with increasing (V-I) in the (V-I)-(V-R) diagram, but to a lesser extent.
The four discrepant stars lie substantially above the main sequence in the
BVI plane, in the region populated by late K/early M giants and metal poor
dwarfs. Three (Sm 15, $3\frac{1}{4}$ and 111) were also observed by Weistrop and
suggested as possible subdwarfs. However they are not identified as proper
motion stars in the Bruce Proper Motion survey (Luyten, 1963a), and the
(U-B) colours are consistent with normal giants. We have assumed that they
are misclassified K giants, and they are excluded from further
considerations.

The fourth star, Sm 183, does have a measured
proper motion and the observed colours are very similar to Kapteyn's star
((B-V)==.53, (V-I)=1.83 ; Rodgers and Eggen, 1974). No (U-B) measurement
exists of this object, but if it were a K giant the proper motions imply a
tangential velocity of more than 800 km/sec . Alternatively, is the star is
subluminous by 1. 5 magnitudes, the the distance is $2\frac{1}{4}$ parsecs and the
transverse velocity only 18 km/sec. The latter interpretation is more
reasonable, so Sm 183 has been omitted from further discussion as a
probable subdwarf and further studies will be carried out at a later date.
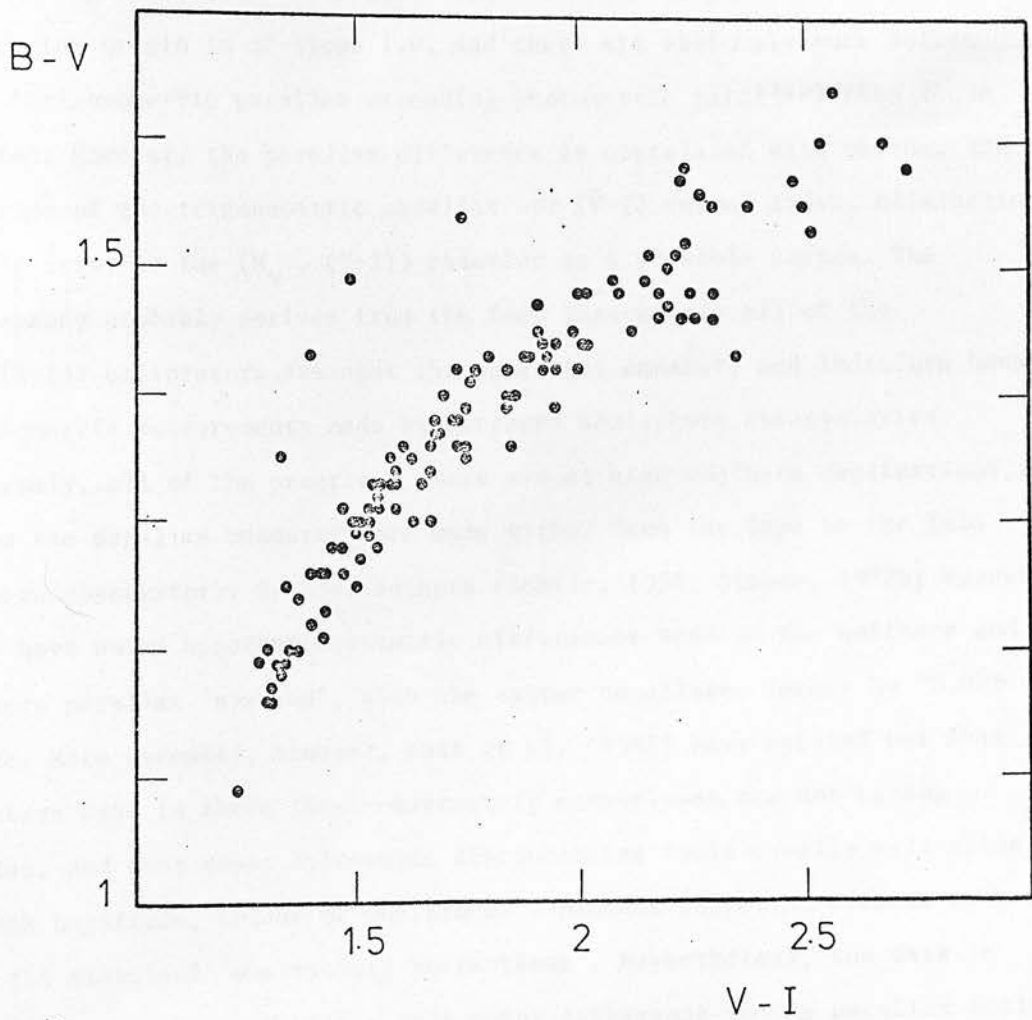
Figure 3.2 - The (B-V)-(V-I) two-colour diagram for the dwarfs from Smethells' sample

Trigonometric parallaxes have been measured for 32 of Smethells' sample (Gliese, 1969; Gliese and Jahreiss, 1979), and Figure 3.3 shows a comparison with the photometric determinations. The solid line through the origin is of slope 1.0, and there are obviously more points below (trigonometric parallax exceeding photometric parallax) than above the line. However, the parallax difference is correlated with neither the magnitude of the trigonometric parallax nor (V-I) colour index, eliminating a scale error in the $(M_V, (V-I))$ relation as a possible source. The discrepancy probably derives from the fact that nearly all of the $(M_V, (V-I))$ calibrators are near the celestial equator, and therefore have trigonometric measurements made by northern hemisphere observatories. Conversely, all of the programme stars are at high southern declinations, and so the parallax measures were made either from the Cape or the Yale southern observatory. Several authors (Schilt, 1954; Gliese, 1972b; Upgren, 1977) have noted apparent systematic differences between the northern and southern parallax 'systems', with the latter parallaxes larger by ~0.005 arcsec. More recently, however, Lutz et al. (1981) have pointed out that the stars used in these inter-observatory comparisons are not random samples, and that these systematic discrepancies could equally well arise through magnitude, colour or positional dependent selection effects rather than the classical 'observatory corrections'. Nevertheless, the data in Fig. 3.3 are consistent with a zero point difference in the parallax scales of approximately 0.005 arcsec, whatever the source, with over 60 percent of the sample lying within one sigma of the one-to-one relation if this offset is included in the trigonometric parallax data.

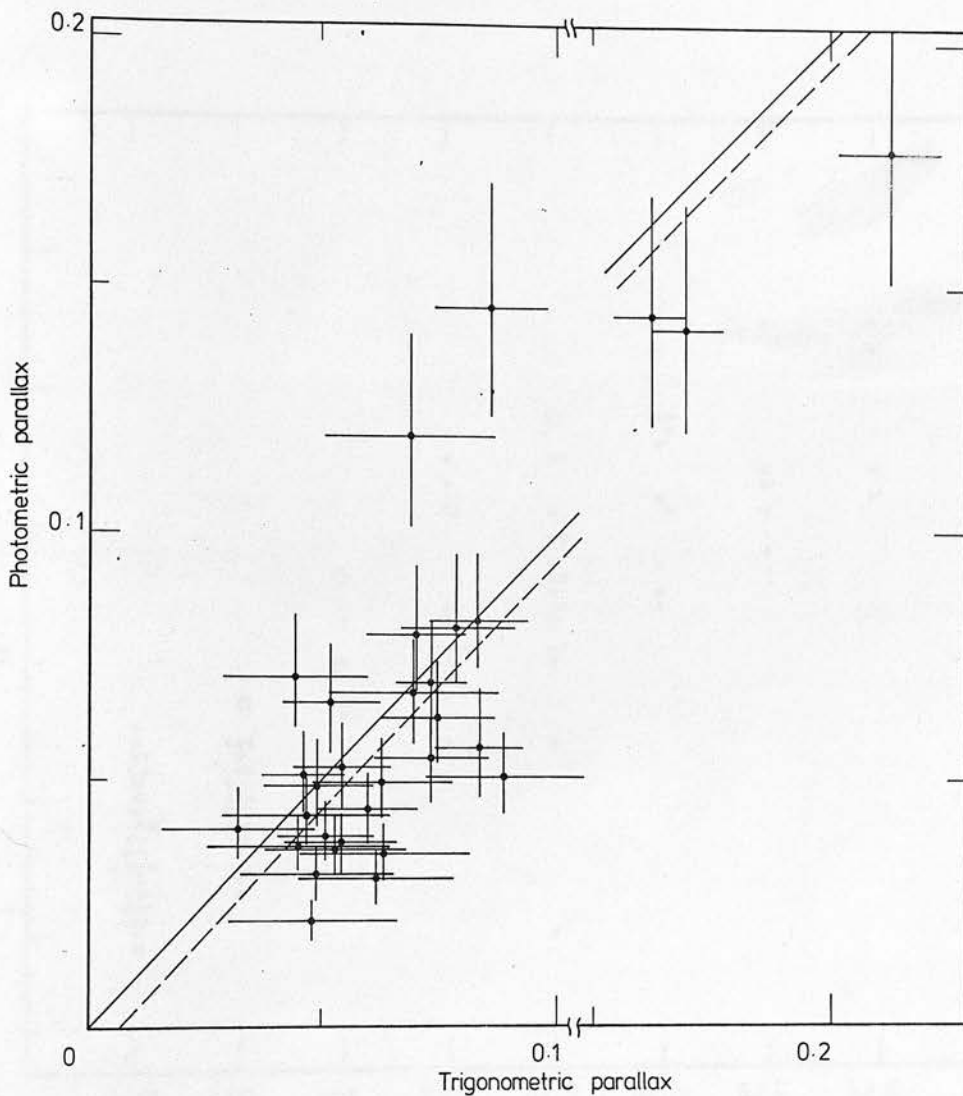Figure 3.4 shows a comparison of the photometric absolute

Figure 3.3 - The relation between trigonometric and
photometric parallax for those of Smethells' stars listed in the Nearby
Star Catalogue and it's Supplement. One sigma error bars are shown and both
lines are of slope 1.0 . The dashed line is offset by 0".005 in
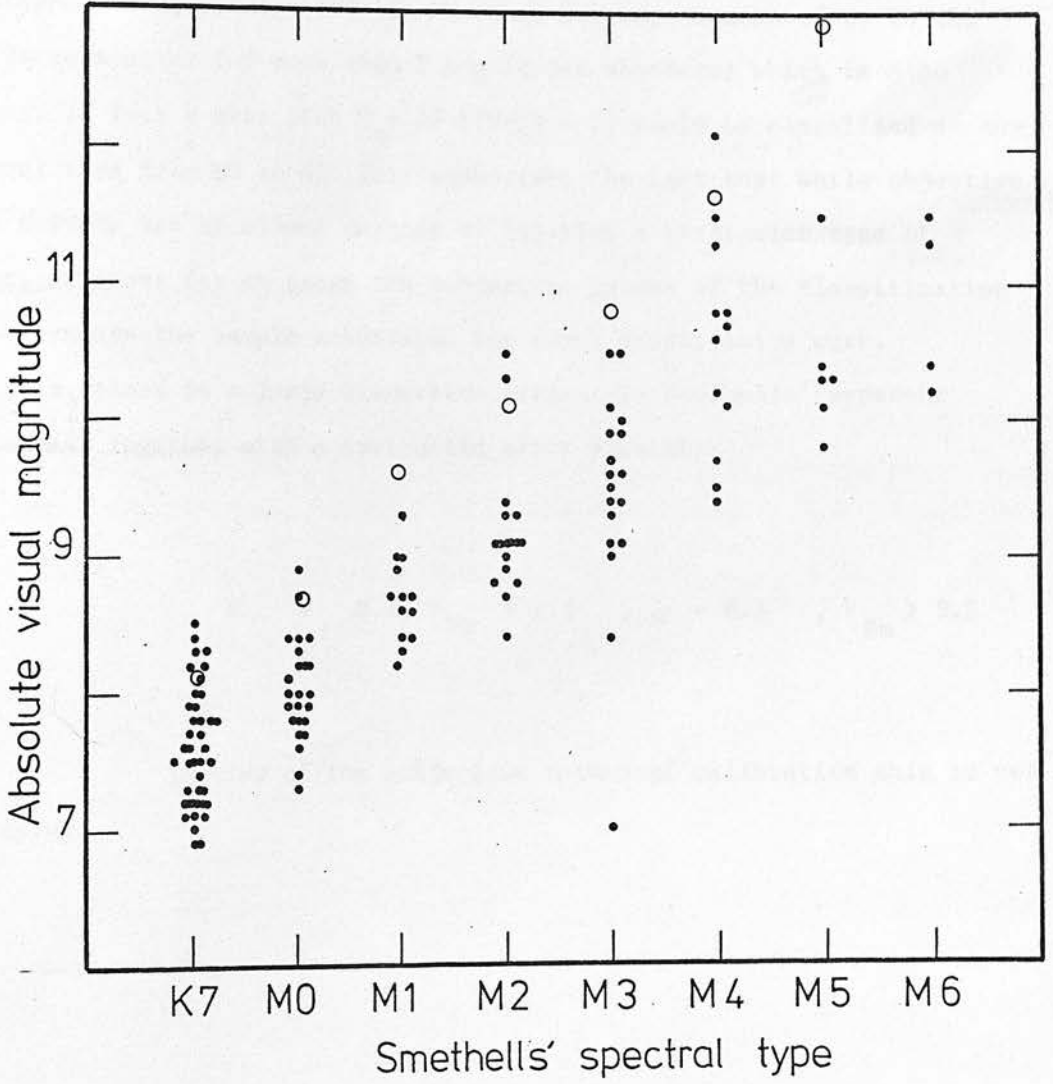trigonometric parallax.

Figure 3.4 - The (Smethells') spectral type - visual absolute magnitude relation for all 182 stars retained in the final sample. The circles mark the (M_v, Spectral Type) relation originally adopted by Smethells.

magnitudes with the spectral types quoted by Smethells. That the scale of the (M_v, Spectral Type) relation used was wrong has already been noted (Weistrop (1980), Gliese (1981)). What has not been commented on is the very large scatter (of more than 2 magnitudes absolute) which is also present. In fact a star with $M_v = 10$ (($V-I$) = 2) could be classified as any spectral type from M0 to M5. This emphasises the fact that while objective prism surveys are excellent methods of locating a particular type of object, at least for dM stars the subjective nature of the classification scheme renders the sample unsuitable for exact quantitative work. Similarly, there is a large dispersion evident in Smethells' apparent magnitudes, together with a systematic error such that

$$ V = 0.80\ V_{Sm} + 1.9 \quad , \quad \sigma = 0.3 \quad , \quad V_{Sm} > 9.5 $$

In view of the subjective method of calibration this is not surprising.

b: The luminosity function

Table 3.6 gives the $N(M_v, V)$ distribution for the complete Smethell' sample. In binning the ($V-I$) derived absolute magnitudes, Malmquist corrections must be applied since the ($V-I$) calibration is appropriate to a distance-limited, rather than apparent magnitude limited, sample. These corrections are of the form (Malmquist, 1936)

$$M(vol.) = M_{(V-I)} - \sigma^2 / \log e \quad . \quad d\log(A(m))/dm$$

where σ is the total dispersion in absolute magnitude from all sources, and $d\log(A(M))/dm$ is the slope of the apparent magnitude number counts (0.6 for uniform density). Thus the effect is that the corrected magnitudes are all brighter by 0.17 magnitudes. This argument applies to all magnitude limited samples, including those calibrated by $(M_V,$ Spectral Type) relations, where the corrections can exceed a magnitude. In the latter case it is particularly difficult to quantify the bias introduced by the non-Gaussian digitised uncertainty in spectral typing.

If the stars are uniformly distributed, the number counts should increase by a factor of 2 for each increase in V of 0.5. This is clearly the case at bright apparent magnitudes, and this criterion can be used to set apparent magnitude limits for each absolute magnitude interval. The most distant stars in this magnitude limited sample are then 50 parsecs from the Sun and 40 parsecs different in Z . Stars brighter than $M_V = 7$ are (intentionally) scarce in the sample, while the increase in limiting magnitude with absolute magnitude merely reflects the increasing TiO strength, and thus more easily recognisable spectra (Smethells, 1974).

A number of Smethells' stars have nearby, fainter companions, and photometry of these stars (see notes to Table 3.3) indicates that, including previously known doubles, 16 are probably genuine binary or multiple systems. Of these four have blue ((V-I)<0.8) companions (i.e. candidate degenerate secondaries), while the others are associated

- 50 -

Table 3.6

Number (Absolute magnitude, Apparent magnitude)

M_V	6.5	7.5	8.5	9.5	10.5	11.5	12.5
7.75			1				
8.25		1					
8.75		4		1			
9.25	1	3	1				
9.75		3	5	1			
10.25	4	11	4		1		
10.75		23	5	4	1	1	
11.25	1	18	15	9	2		1
11.75	1	9	13	5	6	1	
12.25			3	7	7	2	
12.75			1	1	1	4	1
Multiples		+2	+3	+2	+3	+1	
Sm		88,108	34,56,121	101	48,89,99	139	

Magnitudes refer to the central value of each bin
i.e. 6.5 is equivalent to $6 < M_V \leqslant 7$

with fainter main sequence red dwarfs. As this study is concerned with the main sequence luminosity function, the degenerates are excluded from further discussion. However M-stars which are companions of stars within the range of completeness defined above (Table 3.6) are included in the number density calculations. Several of the secondary components included do not have direct photometry. With the exception of Sm 121 and 101, these binaries were assumed to consist of two equal components. In the case of Sm 121, Weistrop's suggested magnitude difference of 2 magnitudes has been adopted, while the three magnitude differential between Sm 101A and it's two proper motion companions has been taken from the Gliese Catalogue.

As Table 3.7 and figure 3.5 show, the resultant densities and their logarithmic equivalents, far from indicating a substantial excess over Luyten's function, are in remarkably close agreement. The number densities of the two brightest absolute magnitude intervals are 35% of those quoted in the Palomar Survey and it is possible that this reflects an incompleteness in the objective prism data. Smethells records 37 additional stars detected in his survey as ' Possible dM stars and probable giants with strong Na I D'. Unfortunately it was not possible to observe any from Sutherland, but as twelve were detected in the BPM this group must include a reasonable proportion of misclassified M dwarfs. If we assume that all are dwarfs, we can correct Smethells' apparent magnitudes using the relation derived above and take the mean absolute magnitude - spectral type relation from figure 3.4. This places 22 of this subset and 11 of the proper motion stars beyond the limits of completeness. (It should be emphasised that the inclusion of the additional stars in no way affects these limits). Adding the sole remaining BPM star ($M_V = 8$) to the number counts produces no significant changes. Were all non-BPM stars in this additional sample dwarfs, then the revised number densities (bracketted

Table 3.7   The Number Density

M_V	No		limit of completeness in V	density x E-03		log density + 10.0		Luyten
7.5	45		11.0	2.05		7.31		7.76
8.5	34	(39)	11.5	3.08	(3.31)	7.49	(7.55)	7.87
9.5	18	(24)	11.5	6.50	(8.67)	7.81	(7.94)	7.95
10.5	12	(18)	12.0	8.65	(12.98)	7.94	(8.11)	8.02
11.5	7		12.5	10.06		8.00		8.08
12.5	2		12.5	11.46		8.06		8.17

The number densities computed here include the contribution from the secondary components listed in Table 3.6. Bracketed values from M_V= 8.5 to 10.5 show the effect of including additional stars from Smethells' supplementary list.
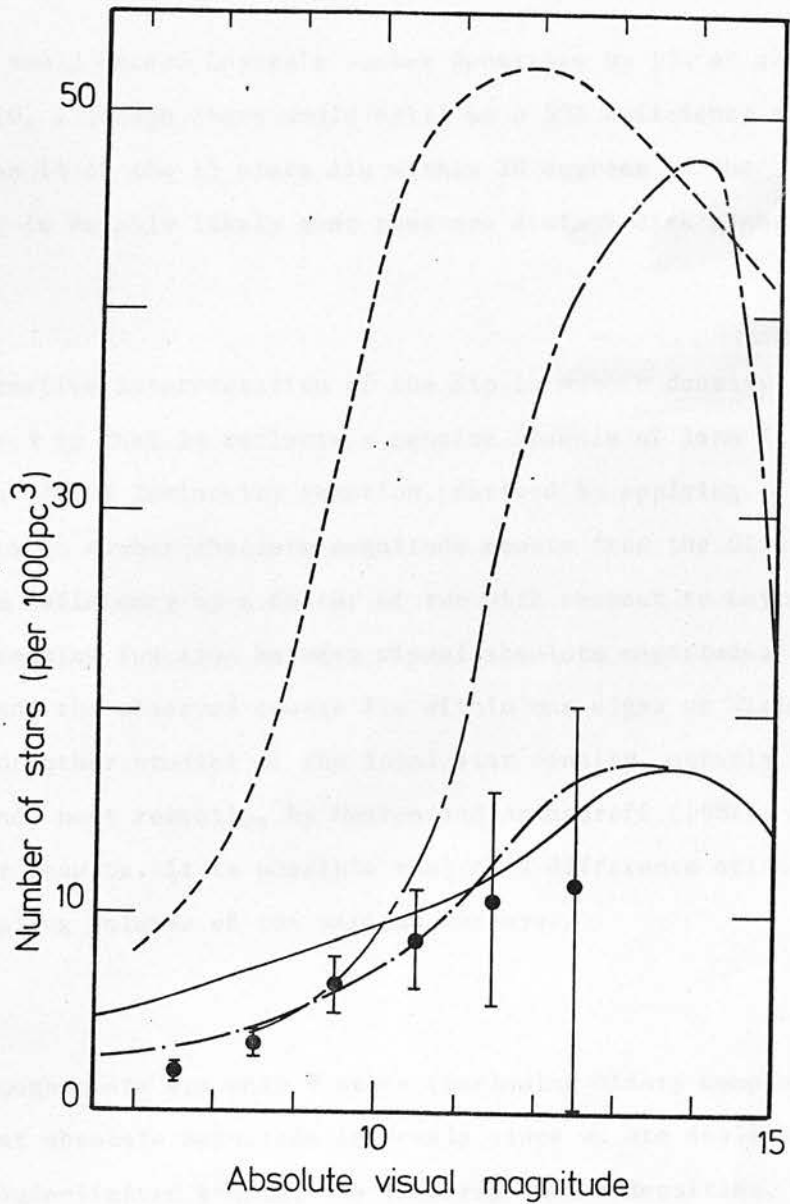
Figure 3.5 - The Main Sequence luminosity function derived from analysis of the magnitude limited complete sample (solid points plotted with one sigma Poisson error bars). Also shown are the functions derived by Smethells (1974 ; short dashes), Sanduleak (1976 ; long dashed line), Wielen (1974 ; dot-dash line) and Luyten (1968 ; solid line). The upper limit from the Wielen function for $M_v = 14$ is indicated.

values-Table 3.7) would exceed Luyten's number densities by 15% at absolute magnitudes 9 and 10, although there would still be a 50% deficiency at $M_v = 8$. However, as 14 of the 15 stars lie within 20 degrees of the Galactic Plane, it is equally likely that they are distant disk giants.

An alternative interpretation of the dip in number density brighter than $M_v = 9$ is that it reflects a genuine absence of late K dwarfs. The Wielen (1974) luminosity function, derived by applying completeness limits to number-absolute magnitude counts from the Gliese Catalogue, shows a deficiency by a factor of two with respect to Luyten's monotonically increasing function between visual absolute magnitudes 7 and 11 (figure 3.5), and the observed counts lie within one sigma of Wielen's values. A number of other studies of the local star density, notably by McCuskey (1966) and, most recently, by Upgren and Armandroff (1981), have arrived at similar results. It is possible that this difference arises from the different sampling volumes of the various surveys.

Although there are only 9 stars (including binary companions) in the two faintest absolute magnitude intervals since we are dealing with a complete, magnitude-limited sample, the inferred number densities, with the appropriately large Poissonian uncertainties shown in figure 3.5, accurately reflect the space densities of these late M dwarfs. Thus the fact that Sanduleak's proposed luminosity function (from stars of $14 < V < 16$) lies more than three standard deviations above our result is significant - even at $M_v = +13$ - and if we accept his result we are forced to conclude that the Sun is in a localised region of abnormally low space density.

It is also worth noting that four of seven stars fainter
than absolute magnitude 11 are members of double or multiple systems.
Despite a considerable number of statistical studies, there is still
considerable uncertainty in the figure quoted for duplicity and
multiplicity amongst faint main sequence stars. Woolley et al. (1971)
estimate from the nearby stars that at least 30% of all dM stars and 60% of
dMe stars are visual or spectroscopic binaries, while 10 out of 25 of the
nearest stellar systems (and therefore presumably the most complete sample)
are non-single (van de Kamp, 1971). Other estimates put the ratio of the
number of stars to the number of systems as 1.7 (Batten, 1973) or even 2.0
(Heintz 1969). Taking 40% duplicity as a conservative estimate, this
implies that approximately 60 of Smethells' stars are unresolved binaries.
However, as the majority of comites can be expected to be fainter than
$M_V = 12$ (again based on the nearest stellar systems), these stars are only
relevant to this study insofar as they affect the photometry of the primary
star and hence the inferred absolute magnitude.

Consider photometry of an apparently single stellar object.
If this is in reality a binary star, the presence of the secondary
component will increase the total observed flux through both the V and the
I passbands. If the two components are equal both V and I are brighter by
0.75 magnitudes, but if the secondary is fainter then it will increase the
flux in I more than in V, increasing the (V-I) colour and leading to too
faint an absolute magnitude being assigned from the photometric parallax.
The latter effect is maximum (+0.4 magnitudes in M_V) for a magnitude
difference of 1.5 in the two components. Both effects (brighter V and
fainter M_V) will lead to the distance to the system being underestimated –
but since the number of objects is also underestimated, there is no

Table 3.8

Magnitude difference	0	1	2	3	4
% of binaries	30	20	25	15	10

The mean primary/secondary magnitude differences adopted in the computation of the photometric influence of unrecognised duplicity.

straightforward overestimate of the number density.

In order to model the extent to which unrecognised duplicity affects number counts an averaged version of the distribution of primary-secondary magnitudes given by Weistrop (1974) has been adopted (Table 3.8). It is assumed that 40% of all stars are members of binary systems. (Since 7% of the Smethells' sample are known or suspected to be non-single, this implies that a further 33% of the apparently single stars are really members of stellar systems). Two further assumptions are made - that stars are uniformly distributed in space, and that the single stars luminosity function is given by the Luyten Function, which is approximated by a power law (index 0.1) from $5 < M_V < 13$.

This model allows the calculation of the actual relative numbers in each absolute magnitude-apparent magnitude interval - the distribution $N'(M_V, V)$. The proportion of stars displaced - either through having brighter observed magnitudes or redder colours (i.e. fainter deduced M_V) - can then be compared with the relative numbers added from those stars which are really fainter in V or intrinsically brighter in M_V. Finally, allowance is made for the stars which cannot be counted as they are the secondary components in unrecognised binaries. The "true" distribution $N'(M_V, V)$ increases with both fainter M_V and fainter V, so the two magnitude effects described here tend to act in opposition. By increasing V the binary is moved to a sparser populated apparent magnitude interval, but if the absolute magnitude is affected then it is transferred to fainter M_V bins, with higher number densities. For the parameters outlined above, and quoting percentages relative to the original numbers in the $N'(M_V, V)$ distribution, 55% extra stars are added to a given bin, while

33% are lost to neighbouring bins and a further 16% "hidden" as faint binary secondaries. Thus the net excess is only about 10%, and is heavily outweighed by counting error in small samples such as this.

<div align="center">c :   Kinematics of the Sample</div>

The number densities derived in the preceeding section show no evidence for an overall M-star excess. Analysis of the kinematics of the sample directly tests the reality of the proposed low velocity population. If a significant number of M-dwarfs have velocities clustered around the local standard of rest this will be reflected in a reduction of the overall velocity dispersion derived from any volume-complete sample. No radial velocity measurements are available, but, using the BPM proper motions, Smethells derived a mean tangential motion of 20 km/sec, with an overall dispersion (i.e. the quadratic mean of the dispersions in Right Ascension and Declination) of 18 km/sec. Allowing for uncertainties in the proper motions (σ_μ = 0".03, interpreted as σ_μ / μ = 9%) the computed intrinsic value is only 13 km/sec. In comparison Dyer (1954) obtained a dispersion of 28 km/sec for the McCormick dwarfs and, from the same stars, Wielen has derived dispersions of 39, 23 and 20 km/sec along the galactic U, V and W axes respectively.

Smethells' result is paradoxical, however, since both his and the McCormick samples were compiled using the same kinematically unbiased method. In fact the discrepancy arises mainly because the original

distance scale placed stars too near the Sun, and hence with
correspondingly reduced velocities. Furthermore Smethells did not define a
complete sample by volume but analysed all 186 stars (divided into four
subgroups by R.A.). Thus even with the correct distance scale, the
calculated mean velocity and dispersion are heavily weighted by the 43
stars not included in the BPM (and therefore accorded zero motions).
Alternatively, if these stars are arbitrarily excluded, the sample is
artificially biased towards higher velocities by the distant stars which do
possess measureable motions.

We have repeated the analysis using only the 101 systems
from the volume-complete sample defined in IV b). Of these, 19 are not
included in the BPM and their treatment here is complicated by
incompleteness in the proper motion survey. It has been stated (Luyten and
La Bonte, 1973) that "the Bruce Survey is woefully incomplete for stars
brighter than 13.0 pg [B ~ 13.4 - Gliese and Jahreiss (1980)] with
motions smaller than 0".3 annually". In fact analysis of the results for
the South Polar Cap area showed that stars with 10.5 < m(pg) < 14.5 and
with motions between 0".1 and 0".2 were only 50% to 67% complete, while
even those with motions between 0".2 and 0".4 were between 74% and 96%
complete (Luyten, 1938b). It is therefore probable that at least some of
the non-BPM stars have motions exceeding 0".05 annually (the nominal BPM
limit).

Bearing this uncertainty in mind, the volume-complete
sample has been subdivided in a manner similar to that employed by
Smethells, and Table 3.9 shows the velocity parameters derived if the
non-BPM stars are assigned zero motions. The overall dispersion in

tangential motion is (25 ±3)km/sec, and the distribution (excluding non-BPM stars) is shown in Figure 3.6. The three stars with V(tangential) greater than 100 km/sec are Sm 54, 126 and 181, all of which have normal main sequence colours, implying that they are unlikely to be significantly metal-poor. Excluding these objects as possible halo subdwarfs reduces the velocity dispersion by ~2 km/sec, and allowing for proper motion uncertainties the lower limit to the dispersion then becomes (23 ±3) km/sec. Proper motions amongst the non-BPM stars will only reduce this value further if they are aligned with the solar motion, but even for motions as large as 0".15 the reduction is only 0.5 km/sec. Thus the observations indicate a dispersion of at least 22.5 km/sec (or 24.5 km/sec if the high velocity stars are included).

This result is substantially larger than the figure quoted by Smethells and can be compared with a recent analysis of the space motions of 145 McCormick K and M dwarfs (Upgren, 1978). Table 3.10 shows the projected velocity dispersion predicted from two of Upgren's solutions for the motions of the complete sample - one weighted by the square of the parallax (solution (i)) and the other by the errors in the U, V and W motions (ii) . The close agreement between the predictions of the higher dispersion solution (i) and the observational figures from Table 3.9 shows is especially striking. Comparing Figure 3.6 with the distribution predicted using the kinematics from this solution indicates two points of dissimilarity. Firstly, there is the apparent bimodality of the observed distribution. However, a quantitative comparison with the Upgren distribution using the Kolmogorov-Smirnov test shows that the second peak to be significant at only the 2.5 σ level, and there is no evidence for any corresponding preferred direction of motion amongst stars with tangential velocities near 65 km/sec.

Table 3.9

Kinematics of Smethells' Stars

Area	n	⟨RA⟩	⟨Dec⟩	$⟨V_\alpha⟩$	σ_α	$⟨V_\delta⟩$	σ_δ	σ_{tot}
A	28	18 50	−54	3.4	17.2	−29.8	21.3	19.4
B	20	21 10	−54	9.7	33.7	−18.5	26.7	30.4
C	29	22 45	−54	15.2	30.1	−11.8	19.1	25.2
D	24	00 30	−54	19.9	33.5	−12.9	22.5	28.5
Mean values					28.0		22.0	25.4 ± 2

The mean tangential velocities and velocity dispersions in Right
Ascension and Declination from the volume-complete sample. The four
subgroups are –   A   Smethells Nos. 3 – 48
                     B   49 – 94
                     C   95 –140
                     D   141 –186
The approximate centroid (in equatorial co-ordinates) is shown for each.
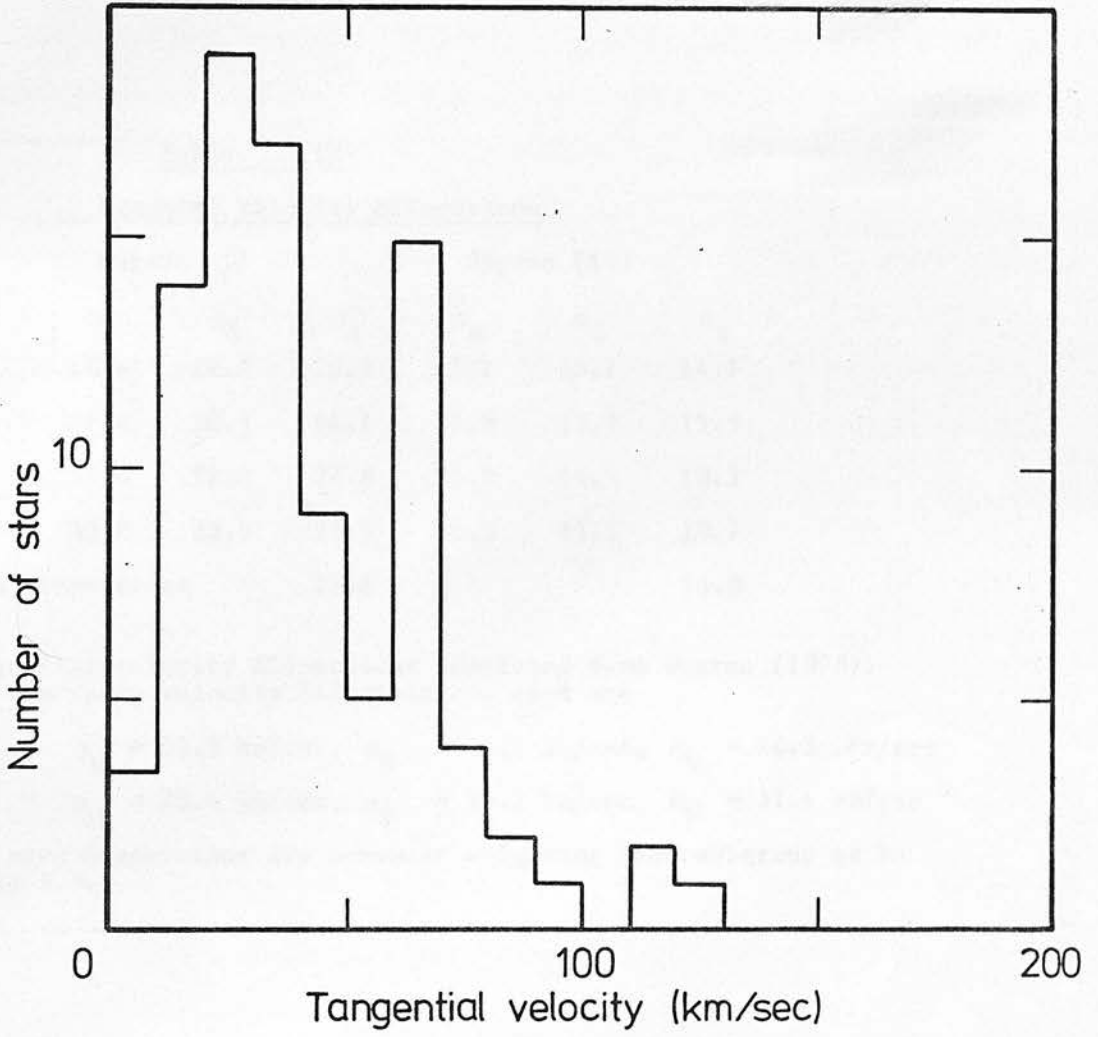
Figure 3.6 - Distribution of tangential velocities for the 82 stars with known proper motions from the magnitude limited complete sample discussed in the text.

Table 3.10

Expected Velocity Dispersions

	Upgren (i)			Upgren (ii)		
Area	σ_α	σ_δ	σ_t	σ_α	σ_δ	σ_t
A	18.4	22.9	20.8	13.1	15.1	14.1
B	27.0	20.8	24.1	17.8	13.7	15.9
C	32.6	22.0	27.8	21.7	14.1	18.3
D	32.8	23.5	28.5	21.5	15.3	18.7
Mean dispersions		25.4			16.8	

Tangential velocity dispersions predicted from Upgren (1978). The two space velocity distributions used are

(i) - σ_U = 35.3 km/sec, σ_V = 21.1 km/sec, σ_W = 16.3 km/sec

(ii) - σ_U = 23.4 km/sec, σ_V = 13.2 km/sec, σ_W = 11.4 km/sec

The mean dispersions are computed weighting each subgroup as in Table 3.9.

Secondly, the solution (i) kinematics predict that only ~8 stars of the volume-complete sample should have heliocentric tangential motions less than 10 km/sec, whereas there are 20 stars in the observed sample. However, this includes the non-BPM stars, and we can use the BPM completeness limits given above together with the distribution of stars with total proper motion to estimate that between 8 and 31 stars with motions less than 0".4 are likely to have remained undetected. As the sample includes 19 stars with unknown motions, the observations are consistent with this incompleteness estimate, and, as mentioned above, the redistribution produces little effect on the overall velocity dispersion. Thus this analysis provides no evidence of the existence of an extensive low-velocity population locally.

V   Conclusions

Objective prism surveys represent a very effective method of detecting complete samples of late type stars over a large area. However, as the large scatter in Figure 3.4 dramatically emphasises, the types estimated from the low dispersion spectra are extremely sensitive to subjective error, usually tending to overestimate the lateness of type, and hence the absolute magnitude. This effect is compounded by the steep variation of mean absolute magnitude with spectral type for these very red stars, with correspondingly severe systematic errors. Thus these surveys must proceed in two stages, with the initial detection being followed up by

exact quantitative measurements. In that context the usefulness of (V-I)kc
in determining photometric parallaxes should be emphasised.

Re-evaluation of Smethells' objective prism survey of
bright M-dwarfs confirms that the original analysis overestimated both the
apparent and absolute magnitudes of the stars detected. If the sample is
re-analysed using photoelectrically determined photometric parallaxes, the
resultant luminosity function - and hence space density - is shown to be in
good agreement with the densities derived from Luyten's analysis of the
Palomar Proper Motion Survey. Furthermore, the kinematics from a complete
magnitude limited sample are largely consistent with the normal disk
motions, and certainly provide no evidence for a low space motion
population. Thus the results of this study give little support to the
suggestion that spectroscopically located samples of dwarf M stars have
mean properties radically different from the late type dwarfs identified in
proper motion surveys.

Appendix   Observations of Parallax Stars

i)   August/September 1980 Observations

Star	N	V	(B-V)	(U-B)	(V-R)	(V-I)	π	σ_π / π	M(π)	M(V-I)	
Gl 54.1	1	12.05	1.77		1.60	3.13	0.1450	0.0986	12.86	13.97	*
Gl 118.1	1	8.21	0.94		0.54	1.02	0.0480	0.2083	6.62	6.42	
Gl 190	1	10.30	1.49		1.17	2.64	0.0910	0.2198	10.10	11.93	
Gl 595	1	11.85	1.63		1.01	2.52	0.1110	0.1288	12.08	11.42	
Gl 611.3	1	11.59	1.48		0.98	2.07	0.0520	0.2750	10.17	9.59	
Gl 618.4	1	11.81	1.47		1.00	2.16	0.0490	0.1755	10.26	9.94	*
Gl 634	1	11.58	1.59		1.07	2.24	0.0570	0.1754	10.36	10.26	*
Gl 643	2	11.78	1.67		1.32	2.75	0.1610	0.0354	12.81	12.44	*
Gl 644AB	1	9.02	1.54		1.10	2.45	0.1610	0.0354	10.05	11.13	*
Gl 644C	3	16.78	1.85		2.41	4.47	0.1610	0.0354	17.81	17.86	*
Gl 708.3	1	12.56	1.67		1.19	2.46	0.0660	0.1515	11.66	11.17	*
Gl 708.4	1	12.59	1.45		0.82	1.71	0.0470	0.1511	10.95	8.30	*
Gl 729	1	10.47	1.70		1.34	2.77	0.3450	0.0330	13.16	12.48	*
Gl 739	1	11.20	1.49		1.04	2.37	0.0830	0.1205	10.80	10.79	*
Gl 748	1	11.11	1.47		1.26	2.60	0.0980	0.0878	11.07	11.76	*
Gl 752	1	9.13	1.43		1.17	2.35	0.1730	0.0329	10.32	10.71	*
Gl 754	1	12.22	1.66		1.44	2.97	0.1750	0.0651	13.42	13.32	*
Gl 769	1	12.51	1.54		1.02	2.24	0.0350	0.2857	10.23	10.26	
Gl 791.2	1	13.01	1.61		1.31	2.83	0.1060	0.3236	13.14	12.73	
Gl 810A	1	12.43	1.59		1.33	2.81	0.0800	0.1962	11.52	12.65	
Gl 810B	1	14.56	1.65		1.34	3.16	0.0800	0.1962	13.65	14.16	
Gl 811.1	1	11.51	1.47		1.17	2.37	0.0560	0.2554	10.25	10.79	
Gl 816	1	11.18	1.45		1.18	2.37	0.0500	0.2580	9.67	10.79	
Gl 817	1	11.40	1.43		1.04	2.03	0.0550	0.1818	9.67	9.44	
Gl 821	3	10.86	1.49		0.96	2.03	0.0930	0.1075	10.70	9.44	*
Gl 876	1	10.17	1.53		1.37	2.74	0.2090	0.0340	11.77	12.35	*
Gl 899	1	11.23	1.41		1.13	2.23	0.0800	0.1425	10.75	10.22	*
GJ 1002	1	13.80	1.89		1.77	3.59	0.2140	0.0234	15.47	15.67	*
GJ 1005	1	11.45	1.71		1.39	2.77	0.117			12.48	*
GJ 1018	1	12.56	1.52		1.23	2.50	0.050			11.34	*
GJ 1218	1	12.60	1.43		1.35	2.68	0.079			12.10	
GJ 1251	1	13.84	1.77		1.41	2.95	0.098			13.27	
USNO 72	1	12.88	1.55		1.04	2.30	0.0418	0.0622	10.99	10.51	*
USNO 172	1	12.28	1.45		1.07	2.37	0.0558	0.0681	11.01	10.79	*
USNO 176	2	13.10	1.15		0.69	1.33	0.0094	0.3191	7.97	7.30	
USNO 187	1	12.81	1.40		1.05	2.01	0.0242	0.1322	9.73	9.36	
USNO 190	1	13.70	0.85		0.50	1.10	0.0096	0.4896	8.61	6.76	

ii) May/June 1981 Observations

Star	N	V	(B-V)	(U-B)	(V-R)	(V-I)	π	σ_{π} / π	M(π)	M(V-I)	
Gl 298	2	11.76	1.47		1.10	2.44	0.0390	0.512	9.72	11.09	
Gl 308.3	2	10.78	1.22		0.76	1.41	0.0540	0.344	9.44	7.46	
Gl 341	2	9.48	1.47	1.22	0.95	1.96	0.1040	0.223	9.57	9.12	
Gl 345	1	10.12	0.57	-0.19	0.35	0.73	0.0570	0.350	8.90		
Gl 385	1	10.18	0.34		0.20	0.39	0.0570	0.326	8.96		
Gl 389AB	2	10.56	1.40		0.95	2.03	0.0520	0.136	9.14	9.44	
Gl 389A	1	10.74	1.39		0.93	1.94	0.0520	0.136	9.32	9.10	
Gl 422	2	11.59	1.44		1.08	2.43	0.0770	0.111	11.02	11.04	
Gl 429.3	1	7.38	0.40	-0.07	0.25	0.49	0.0520	0.301	5.96	3.20	
Gl 429.4	2	8.33	1.06		0.60	1.11	0.0500	0.142	6.72	6.71	
Gl 437	1	6.47	0.52	0.05	0.30	0.57	0.0390	0.220	4.43	3.72	
Gl 438	2	10.36	1.50	1.18	0.98	2.07	0.1200	0.130	10.76	9.61	
Gl 440	2	11.50	0.18	-0.65	0.16	0.30	0.2060	0.055	13.05		
Gl 455.1	2	9.96	1.32	1.20	0.83	1.60	0.0460	0.310	8.27	7.96	
Gl 465	2	11.30	1.56	1.17	1.06	2.31	0.1100	0.078	11.51	10.55	*
Gl 467A	1	13.65	1.55		1.09	2.48	0.0610	1.218	12.58	11.28	
Gl 467B	1	15.44			1.39	2.90	0.0610	1.218	14.37	13.14	
Gl 472	1	7.13	0.84	0.47	0.48	0.90	0.0680	0.126	6.29	5.89	
Gl 477	2	11.11	1.45	1.14	1.02	2.20	0.0760	0.225	10.51	10.10	
Gl 478	2	10.97	1.29	1.14	0.83	1.62	0.0550	0.310	9.67	8.02	
Gl 479	2	10.66	1.51	1.18	1.10	2.44	0.1210	0.082	11.07	11.07	*
Gl 480.1	2	12.26	1.71	1.19	1.29	2.65	0.0480	0.297	10.67	11.97	
Gl 496.1	2	9.06	1.36	1.28	0.85	1.65	0.0500	0.142	7.55	8.11	
Gl 508.3	2	11.79	1.40	1.08	0.91	1.90	0.0460	0.280	10.10	8.95	
Gl 510	2	11.02	1.49		1.00	2.15	0.0570	0.752	9.80	9.90	
Gl 524	2	12.67	1.52		1.07	2.34	0.0650	0.153	11.56	10.50	
Gl 524.1	2	10.53	1.33	1.17	0.83	1.57	0.0480	0.179	8.94	7.87	
Gl 531	2	7.39	0.89	0.55	0.52	0.99	0.0650	0.153	6.45	6.31	
Gl 534.1	1	6.00	0.78	0.27	0.43	0.84	0.0800	0.161	5.52	5.55	
Gl 536	2	9.72	1.45	1.17	0.97	2.05	0.0920	0.123	9.54	9.51	
Gl 539.1	1	6.01	0.58	0.06	0.32	0.64	0.0450	0.157	4.28	4.21	
Gl 539.2	1	11.81	1.43		0.94	1.94	0.049	0.163	10.26	9.26	
Gl 540.2	1	13.8			1.45	2.9	0.072	0.236	13.08	13.22	
Gl 542	1	6.66	1.03	0.94	0.57	1.04	0.1040	0.096	6.75	6.49	
Gl 545.1	1	9.02	1.10	1.04	0.64	1.16	0.0450	0.222	7.29	6.84	
Gl 550	2	7.85	0.68	0.19	0.38	0.72	0.0330	0.172	5.44	4.76	
Gl 552.1	2	11.63	1.48	1.12	1.04	2.29	0.0540	0.316	10.46	10.29	
Gl 563.2	1	11.66	1.43		0.98	2.08	0.045	0.267	9.93	9.79	
Gl 563.2	1	12.05	1.47		1.01	2.18	0.045	0.267	10.32	10.19	
Gl 588	1	9.32	1.49	1.17	1.08	2.38	0.1690	0.042	10.47	10.84	*
Gl 599.1	2	9.94	1.02	0.59	0.58	1.12	0.0510	0.307	8.48	6.74	
Gl 606.1	2	7.71	0.77	0.41	0.41	0.78	0.0440	0.161	5.93	5.17	
Gl 606.1	2	11.03	1.36	1.19	0.88	1.76	0.0440	0.161	9.25	8.47	
Gl 611.1	2	7.24	0.73	0.29	0.39	0.75	0.0450	0.157	5.51	4.97	
Gl 613	2	7.12	0.85	0.48	0.49	0.92	0.0700	0.142	6.35	5.99	
Gl 615	1	7.54	0.82	0.30	0.50	0.95	0.0660	0.107	6.64	6.14	
Gl 616	1	10.61	1.51		1.10	2.43	0.1310	0.076	11.20	11.04	
Gl 616.1	1	6.41	0.79	0.31	0.44	0.86	0.0490	0.204	4.86	5.67	
Gl 618AB	1	10.58	1.52	1.17	1.17	2.48	0.1310	0.076	11.11	11.25	
Gl 637	3	11.31	1.51	1.16	0.99	2.08	0.0680	0.167	10.47	9.63	
Gl 639.2	1	10.91	0.71	0.03	0.41	0.83	0.0520	0.328	9.49	5.52	

Gl 676A	1	9.59	1.42		0.89	1.82	0.0850	0.184	9.24	8.67
Gl 676B	1	13.31	1.51		1.36	2.83	0.0850	0.184	12.96	12.73
Gl 693	2	10.76	1.60		1.14	2.54	0.1700	0.041	11.91	11.51 *
Gl 698.1	2	9.63	0.93	0.71	0.53	0.98	0.0470	0.395	7.99	6.27
Gl 700A	2	6.88	0.62		0.33	0.65	0.0200	1.430	3.39	4.28
Gl 700B	2	12.52	1.35		1.05	2.26	0.0200	1.430	9.03	10.34
Gl 714	2	9.85	1.45		0.93	1.91	0.0700	0.244	9.08	8.99
Gl 724.1	2	9.32	0.68	0.14	0.38	0.74	0.0200	1.430	5.83	4.90
Gl 724.2	1	6.39	0.57	0.12	0.33	0.63	0.0450	0.157	4.66	4.14
Gl 725.3	1	8.70	0.64	0.12	0.35	0.69	0.0240	1.429	5.60	4.56
Gl 756.1	1	8.38	1.03	1.00	0.57	1.02	0.0500	0.142	6.87	6.42
Gl 773.6	1	8.66	1.12	1.09	0.68	1.23	0.0550	0.207	7.36	7.01
GJ 1123	2	13.15			1.49	3.05				13.81
GJ 1128	2	12.71			1.51	3.08				13.92
GJ 1244	1	8.39	1.04		0.60	1.08				6.62
LHS 61	1	11.47	1.42		0.96	2.03	0.0500	0.200	9.53	9.44
LHS 336	2	11.10	0.80		0.44	0.84	0.1160	0.155	11.14	

Notes to Appendix

(*) indicates stars that were used in the definition of the
  $(M, (V-I))$ relation.

Gl 345	White dwarf
Gl 385	Uncertain identification
Gl 440	L145-141 DC white dwarf
Gl 540.2	Photometry accurate to only 0.05
Gl 639.2	This star has a finding chart in the LHS Atlas (LHS 3248). Thus the large discrepancy between the trigonometric and photometric absolute magnitudes is not due to misidentification
Gl 429.3	As with Gl 639.2, the absolute magnitude discrepancy is real.
Gl 644C	Van Biesbroeck 8
LHS 336	White dwarf

Chapter 4

The last few years have seen a considerable revival of interest in various applications of star counts, with the use of large and/or wide field reflectors and automatic measuring machines. Recent projects have consisted mainly of very deep studies of small fields, using large reflectors (e.g. Chiu, 1980a), or wide field searches for specific classes of stars using Schmidt telescopes and objective prisms (e.g. Pesch and Sanduleak, 1978). The only successful attempt to combine the merits of a faint limiting magnitude and a wide field is that by the Basel group (Becker, 1980 and refs. therein), and even here the total area searched in 8 fields is only 10 square degrees, with the largest single field being ~2 square degrees.

In addition, all the deep surveys published to date have involved the use of blue sensitive plates, as the primary aim was either a study of faint galaxies where the stellar foreground is a contaminant (e.g. Kron (1980), Jarvis and Tyson (1981)), or a study of the Galactic halo, where blue colours allow a deeper survey to be achieved, as well as disk/halo segregation in the two-colour diagram (Becker, 1980). The principal aim of most of the objective prism searches was the determination of the intrinsically faint luminosity function, and the local mass density of M dwarfs. The use of blue sensitive plates is manifestly unsuitable for this project, as M dwarfs are extremely red objects.

The availability of good quality red sensitive emulsions (IV-N), a red corrected achromat on a large Schmidt telescope (the U.K. Schmidt) and an automatic measuring machine capable of reliably detecting and estimating a magnitude for every image on a Schmidt plate (COSMOS) now allows us to optimise studies based on deep star counts. We are able to sample large areas of sky in passbands maximising both disk/halo discrimination and the derivation of reliable absolute magnitudes for low luminosity stars, to usefully faint apparent magnitudes.

We present here the first results of such a survey, which involves the determination of reliable absolute magnitudes for the complete sample of stars in 18.24 square degrees towards the South Galactic Pole brighter than I=17.0. We have therefore a complete sample of all stars brighter than M_v =+19 within 25 parsecs of the Sun, and brighter than M_v =+15.5 within 100 parsecs, in our field, and can derive a kinematically unbiased estimate of the main sequence luminosity function to substantially fainter absolute magnitudes than the currently estimated maximum (near M_v ~ +14).

Similarly we are able to derive density laws as a function of absolute magnitude to an interesting distance from the Galactic Plane. These results are discussed in Paper III of this series (Gilmore & Reid, 1982).

II   STANDARD STARS

II.1   Comparison of Existing Data

The magnitude scales adopted in this work have been derived by empirical
calibration of COSMOS measurement of UKSTU plates using over 1800
photometric standard stars collected from several sources.   The majority
are photographic standards calibrated by Eriksson (1978), but there are
also over 250 photoelectric standards due to Corben (1980, priv.comm.),
Cannon (1974), Jennens (1975), Graham (1980, priv.comm.) and ourselves
(Appendix 1).   With different data-sets predominant at different
magnitudes it is essential to ensure that all of the standard magnitudes
are defined on the same photometric system and that there are no systematic
errors being introduced into the calibration.   We have thus devoted
considerable effort to an extensive intercomparison of the data.

Most of the photoelectric photometry is due to Corben, Jennens, Gilmore
and Reid, and is defined with reference to the Cousins E-region standards.
From the stars in common we derive

$$V_{RG} - V_C = 0.006 \pm 0.025$$

29 points

$$(B-V)_{RG} - (B-V)_C = 0.002 \pm 0.027$$

and

$$V_{RG} - V_J = -0.01 \pm 0.03$$

6 points

$$(B-V)_{RG} - (B-V)_J = 0.03 \pm 0.03$$

with the quoted errors being sample standard deviations.

Our photoelectric observations of two stars in Cannon's NGC 288 sequence
and of two stars in Graham's SGP sequence show no indications of systematic
discrepancies. Thus as far as it is possible to test them, the photo-
electric systems are well matched. Taking these stars as a homogeneous
group we have identified all photoelectric standards within Eriksson's
photographic lists and carried out a similar intercomparison.

Eriksson's photometry is derived from iris diaphragm measures of the
central (1° radius) regions of Uppsala Schmidt plates, with each magnitude
and colour based on measurements of between five and ten individual
plates in each colour, and the original calibration given by a grid of
176 photoelectric standards, measured in the Cousins system and spatially
distributed over the entire region. The preliminary results from this
work represent B and V photometry of all stars brighter than V = 15 in
the declination band -29° to -30° over a range in Right Ascension that
completely embraces the UKST SGP field. A considerable number of
fainter stars (to V = 17) are also included in certain regions, and of
the 1481 stars that were identified in COSMOS measures, fifty have also
been measured photoelectrically giving

$$V_U - V_{p/e} = -0.02 \pm 0.04$$

$$(B-V)_U - (B-V)_{p/e} = 0.04 \pm 0.08$$

with the errors being sample standard deviations.

II.2 Photographic extension of the standards

In view of the paucity of faint standards we have also obtained photo-
graphic B,V and I magnitudes for 160 stars by iris photometer measurement
of 5 UK Schmidt Telescope plates exposed with the use of a Pickering
sub-beam prism (Pickering 1891), originally designed for the Isaac
Newton Telescope at RGO.   This is a small, very low dispersion prism
which is placed in front of the corrector plate of the telescope.   It
produces secondary images slightly displaced from the primary images and
fainter by a fixed number of magnitudes.   The difference in magnitudes
(the prism step) is determined by the relative areas of the prism and
the telescope achromat, their optical transmission properties, the
differing vignetting suffered by the light path through each, and the
different image structure between primary and secondary images.   The
effects and causes of the differing image structure are briefly discussed
by Carney (1979c),and Couch and Newell (1980), who also illustrate the
sensitivity of the observed prism step to the seeing during exposure.
They also emphasise the necessity of determining the value of the step
for each combination of plate plus measuring machine, and the error in
assuming a constant value.

The most reliable way in which the prism step may be determined is by
use of standard stars on the plate of interest which have a significantly
greater range in magnitudes than the prism step.   We are fortunate in
the case of the SGP that reliable standards are available for the range
$10 < m < 16.3$.   As the predicted prism step, derived from the geometry
of telescope and prism, is near $3^m.25$ (R. Martin, 1980 priv. comm.), we
are able both to derive the appropriate value of this step, and to test

its independence of apparent magnitude.

The plates measured consisted of 2B and 2V plates with a common centre, and one I plate with a different centre. Because of obstructions inside the telescope, primarily by the plate holder, only a relatively small part of the plate has both primary and secondary images unvignetted (Fig. 4.1). It was not therefore possible to derive I magnitudes for the same faint stars for which B and V magnitudes were derived. The B and V magnitudes were derived independently for each plate measured and there was no significant difference in either zero-point or magnitude scale between the different plates. The details of the measurement are given in Table 4.1. The mean prism step for the B plates, 3.36 ± 0.04, is in agreement with that derived from measurement of other blue plates (R. Martin 1980, priv. comm.). For the V plates, however, very discordant values are derived. The mean prism step in V found at ROE from UKST plates measured with an iris photometer is 3.32 ± 0.03, in agreement with plate V6218. A very much lower value for V5511 does, however, produce magnitudes for faint stars in agreement with those from V6218, the mean difference for all stars in common being

$$V_{5511} - V_{6218} = +0.03 \pm 0.04$$

This difference in derived prism step illustrates again the dangers in assuming a mean value derived from other plates.

Besides the five UKST plates, one deep B-band Pickering prism plate from the CTIO 4-metre telescope was kindly made available by Dr. John Graham.

TABLE 4.1

Plate	No. of standards	No. of stars	Δm
B 6219	52	93	3.36 ± 0.05
B 6332	52	93	3.36 ± 0.04
V 5511	51	89	3.12 ± 0.04
V 6218	51	89	3.35 ± 0.04
I 6178	12	52	3.30 ± 0.10

Sub beam prism plates measured to extend the magnitude calibration. Δm is the magnitude offset derived from iris photometry of the number of standards listed.
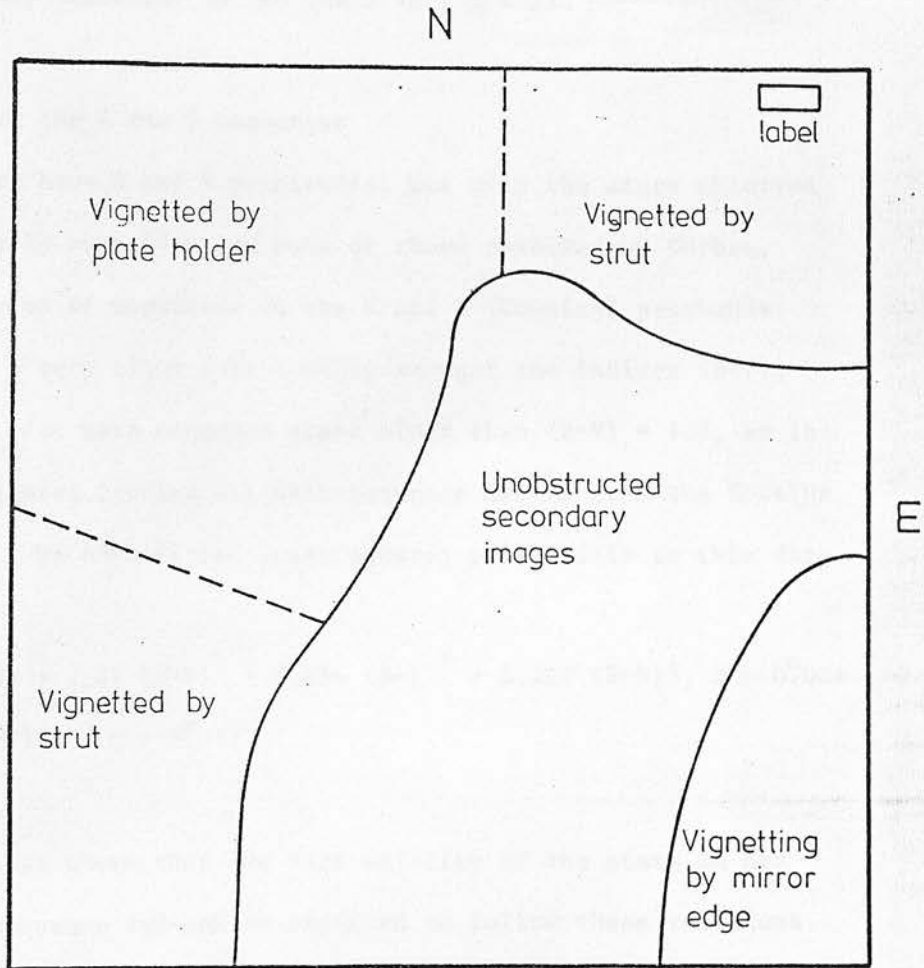
Figure 4.1

The vignetting profile of a UK Schmidt telescope plate with the Pickering
sub-beam prism mounted, showing the usable area. This profile was
kindly provided by Dr. Ann Savage of the UK Schmidt Telescope Unit.

This was measured with the ROE iris photometer and calibrated primarily
using a photoelectric sequence established by Graham (1980, priv.
comm.). The measured magnitude offset is found to be 6.80 ± 0.05
magnitudes, in agreement with determinations quoted by Couch and Newell
(1980). These measurements allowed reliable magnitude calibration, by
use of 47 secondary standards in the range 18 < B < 21.

II.3 Extension of the R and I sequences

All of these stars have B and V magnitudes, but only the stars observed
photoelectrically by ourselves and some of those observed by Corben,
have direct measures of magnitude in the R and I (Cousins) passbands.
However there is a very tight relationship amongst the indices (B-V),
$(V-R)_C$ and $(V-I)_C$ for main sequence stars bluer than (B-V) = 1.0, as is
illustrated in figure4.2(using all main sequence dwarfs from the Cousins
E-region lists). We have fitted least squares polynomials to this data
giving

$$(V-I) = 0.70 \ (B-V) + 2.87 \ (B-V)^2 - 5.636 \ (B-V)^3 + 3.220 \ (B-V)^4, \quad \sigma = 0\overset{m}{.}021$$

$$(V-R) = 0.565 \ (B-V) \qquad \sigma = 0\overset{m}{.}012$$

Eriksson's study has shown that the vast majority of the stars in his
sample are main sequence and can be expected to follow these relations.
Even at fainter magnitudes with increasing numbers of halo subdwarfs, it
is only extremely metal poor stars (such as LHS 489 and 453 (Ake and
Greenstein, 1981)) which follow significantly different colour-colour
relations, and such stars are very rare. We have thus computed R and I
magnitudes for all of our standards with only B and V magnitudes and
with (B-V) < 1.0. As an empirical check on the resultant calibrations
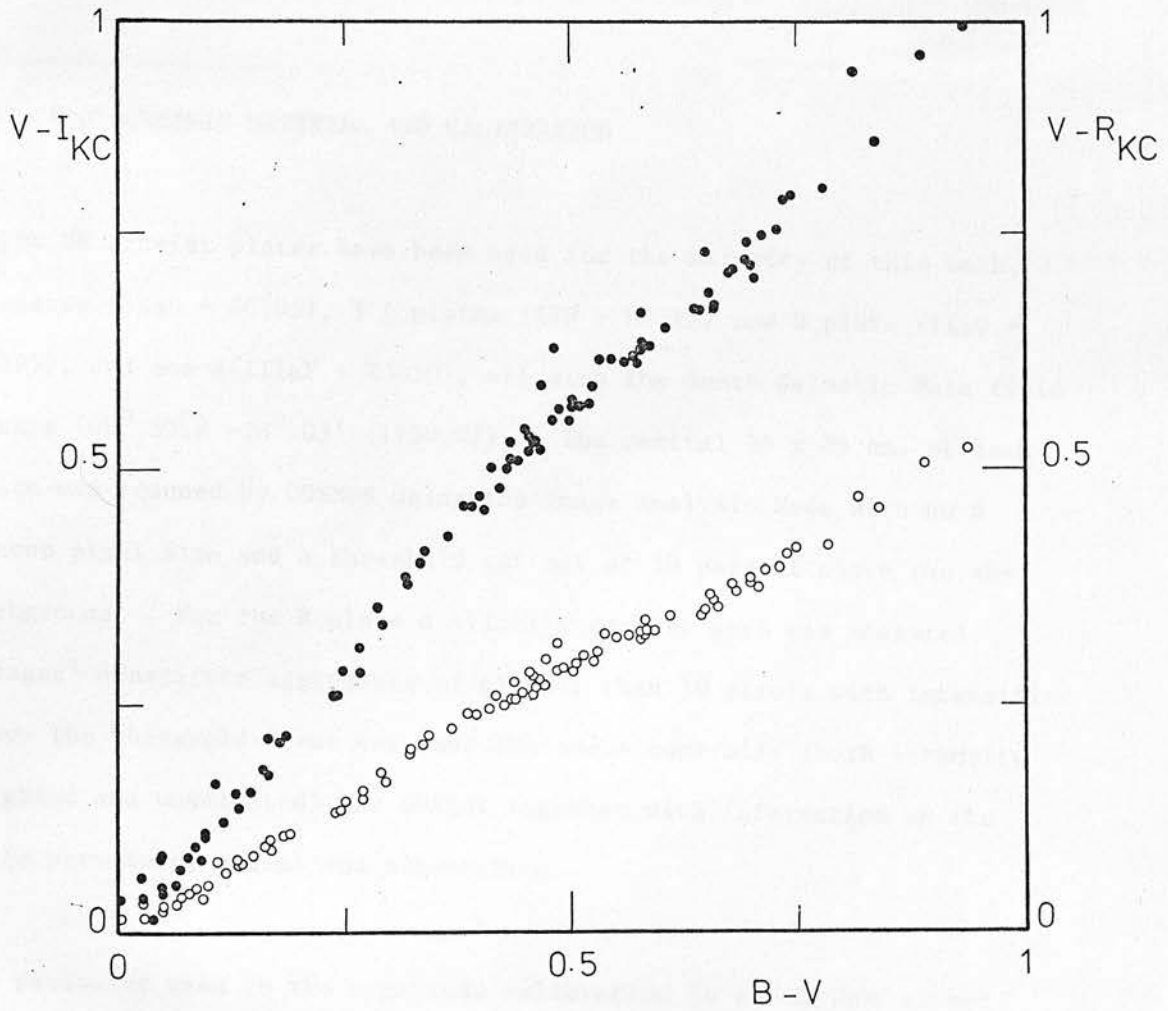
Figure 4.2

The B-V/V-R (open circles) and B-V/V-I (solid points) relations for all

main sequence stars in the E-region photometric standards list.

we have used the COSMOS calibrations derived from these stars only to compare COSMOS photographic and photoelectric I magnitudes for the 152 available photoelectric standards.   On all three I plates the mean residual is not significantly different from zero and the standard deviations of the standards about the mean curve are ± 0.03 magnitudes.

III   PHOTOGRAPHIC MATERIAL AND CALIBRATION

Eight UK Schmidt plates have been used for the majority of this work, 3 V plates (IIaD + GG495), 3 I plates (IVN + RG715) one B plate (IIaO + GG395), and one R(IIIaF + RG630), all with the South Galactic Pole field centre ($00^h 53^m.8 -28^{\circ} 03'$ (1950.0)).   The central 25 x 25 cm. of each plate was scanned by COSMOS using the Image Analysis Mode with an 8 micron pixel size and a threshold cut set at 10 percent above the sky background.   For the R plate a slightly smaller area was measured. 'Images' constitute aggregates of greater than 10 pixels with intensities above the threshold level set, and the image centroids (both intensity weighted and unweighted) are output together with information on the image structure, extent and orientation.

The parameter used in the magnitude calibration is the COSMOS summed intensity,

$$\Sigma I = -250 \times Log \left(\sum_{i} (I_i - I_{sky}) \right) \tag{1}$$

where I_i is the computed intensity for the ith pixel in the image in question.   Since COSMOS actually measures in 128 steps of transmission

TABLE 4.2

Plate	No. of stars	r.m.s.	order of poly	limit
V3475	1518	0.10	5	19.4
V6608	1524	0.10	5	19.4
V6619	1489	0.10	5	19.4
I4338	1234	0.19	5	18.5
I6427	1246	0.14	5	18.5
I6523	1231	0.14	5	18.5
R4676	1180	0.12	5	18.0
B3499	1506	0.12	8	20.7

Calibration details for the plates used in this study. The number of
standards, and the magnitude limits below which a straight line fit were
used are indicated.

the intensity calibration is derived from measures of the Schmidt step-wedges or sensitometer spots. From these measures Log (Intensity) is calibrated in terms of Baker Density in the form

$$\text{Log (I)} = \gamma \text{ Log } \left(\frac{T_c - T_b}{T - T_b} - 1 \right) + \text{constant} \qquad (2)$$

with T_c the transmission of clear plate, T_b a machine zero point, and T the measured value, and a lookup table computed for each digital transmission step.

The resulting calibration of COSMOS ΣI parameter against standard magnitude shows two major changes of slope in the well calibrated regions. At about 4 magnitudes above sky (V $\sim$ 16) the COSMOS image becomes completely saturated and the slope of the relation changes from near 1.0 to

$$\Delta \Sigma I \sim 0.5 \ \Delta \text{ (magnitude)}$$

The second break occurs at bright magnitudes (V $\sim$ 10), where the slope steepens again as the Schmidt plate halo rises above the level of the threshold cut, and contributes to the measured magnitude.

The entire calibrated range in magnitude has been fitted for each plate using a Chebyshev least squares polynomial, usually of order 5. However at very faint magnitudes the polynomial is no longer constrained, and a linear relation has been adopted as a magnitude estimator until such time as there are sufficient good photometric standards in all colours. A typical calibration curve is shown in Figure 4.3.

During the course of these calibrations it became apparent that certain plates exhibited systematic trends in the (standard - COSMOS) residuals from the polynomial which were correlated with position on the plate. To examine these effects for each plate we set up a 5 x 5 matrix in X and Y (the size being limited by the number of standards) and, excluding the fainter standards and those calibrated by sub-beam prism, used the individual residuals to compute a mean value for each position. The resultant array was then smoothed and used to plot a contour map which was examined for evidence of large scale gradients. Of the plates studied so far, none with IIaD emulsion show signs of anything save random noise, but systematic trends are evident in B3499 ($\pm$ 0.1 mag.) and on the hypersensitised IV-N (typically $\pm$ 0.15) with no two plates exactly alike. Similar results have been obtained from U, B, V and I plates of the Morton-Tritton field (22 hours 03 minutes, -18 degrees 54 minutes).

Amongst the plates studied which show these effects are three short exposure unfiltered blue plates taken as part of the Royal Greenwich Observatory proper motion survey of the SGP (Murray & Corben, 1979), and we have used the COSMOS measures of these plates to compare the relative effects in the saturated and unsaturated (COSMOS) regimes. The results indicate no significant magnitude dependence of the field effects, and as the effects are small we have adopted the simple expedient of a zeropoint correction to the COSMOS magnitude equivalent to that given by the smoothed residual at the given position.
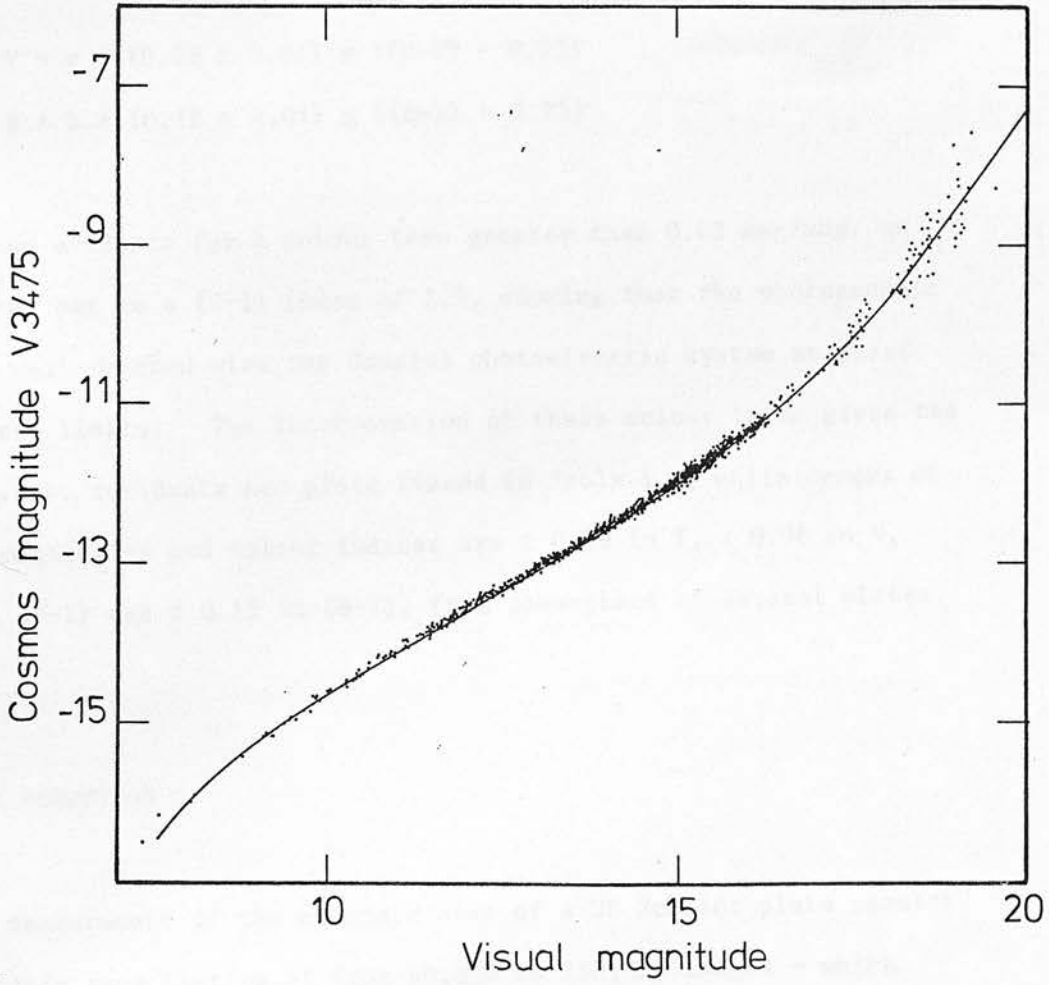
Figure 4.3
Calibration curve for the 30-minute A grade plate V3475.

Finally, once positional effects are corrected for, the colour terms of each emulsion/filter combination relative to the photoelectric passbands were derived using the (standard-COSMOS) magnitude residuals. These are:

$$V = v + (0.08 \pm 0.01) \times ((B-V) - 0.75)$$

$$B = b + (0.12 \pm 0.01) \times ((B-V) - 0.75)$$

There was no evidence for a colour term greater than 0.03 mag/mag. on the I plates out to a (V-I) index of 2.9, showing that the photographic system is well matched with the Cousins photoelectric system at least within these limits. The incorporation of these colour terms gives the overall r.m.s. residuals per plate listed in Table 4.2, while errors of the mean magnitudes and colour indices are $\pm$ 0.09 in I, $\pm$ 0.06 in V, $\pm$ 0.11 in (V-I) and $\pm$ 0.13 in (B-V), from comparison of several plates.

IV   DATA REDUCTION

A COSMOS measurement of the standard area of a UK Schmidt plate results in a magnetic tape listing of from 60,000 to 250,000 images - which include apart from genuine stellar and non-stellar objects, dust, emulsion flaws, sputtering around bright stars, and satellite and meteor trails. Thus one of the chief problems in a machine-based multi-plate survey is selecting the real data on any plate and then correlating the individual datasets. This has been tackled here by inverting the process. Using a plate pairing programme (written by

B.V. McNally), all plates are transformed onto a standard co-ordinate
system defined by one master plate, and then each dataset mapped onto
the master set.   The resultant mean residuals between transformed and
master co-ordinates of the paired images are usually ~4 microns, for
plates with the same field centre.

Usually the paired dataset has only 65-70 percent of the number of
images on a single plate measure, with most of the unpaired images
contributed by spurious images (as mentioned above), by images merged
into one by COSMOS on one plate and not the other, and by threshold
detections.   We have tested the efficiency of the pairing using five
4cm^2 areas from plates V3475 and V6608, and the results are tabulated in
Table III.   Of the ten images matched by eye but not by the pairing,
all are very faint (V > 20) and elliptical, with correspondingly uncertain
centroids.   For such faint images a search radius of 25 microns upper
limit is employed in the pairing and nine of the ten have positional
residual (between master and transformed co-ordinates) greater than this
limit.   As 1375 images were successfully paired, the one elusive image
gives an estimate of 0.07 percent as the incompleteness of the pairing.
The efficiency of pairing in removing spurious images is discussed
further below.

Once all measures have been mapped onto the standard co-ordinate system
adopted, one pairing is chosen as the master image set (plates 1 & 2).
The depth of this master list is obviously defined by the brighter
limiting magnitude, and in merging further plates (using a second
programme written by B.V. McNally) only the images within the area

TABLE 4.3

| Area | Total no. of images | | | Unpaired images | |
	V3475	V6608	paired data	Matched by eye	position residual < 25μm
1	435	302	279	6	0
2	545	326	277	1	0
3	461	315	280	3	1
4	371	268	240	0	0
5	388	324	299	0	0
All areas	2200	1535	1375		

Tests of the completeness achieved in pairing COSMOS measures of
different plates.   All the unpaired images which were matched by eye
are fainter than V = 20.

common to all measures are retained.   All objects in the master list
within this area are kept, with fields of zeros used to represent the
COSMOS parameters from plates where the image is unmatched, but any
extra images only on subsequently added pairings (plates 1+3, 1+4, etc.)
are discarded.

This modus operandus has the advantage that an initial list can be
defined by pairing the two best plates in a suitable passband and there
is no loss of the extreme coloured objects in subsequent pairings.   In
the present study we are primarily interested in red stars, and thus the
initial dataset is defined by a mapping of I6427 onto I6523 - the two
deepest I plates.   Differential number counts show that the final
seven-plate merge is complete (without regard to colour) to a limiting
magnitude of I = 18, while from a similar process, the V plates are
complete to V = 19.5.

As noted above, data from a COSMOS measure of one Schmidt plate results
in many spurious images around bright stars, the vast majority of which
are eliminated through failing to pair from plate to plate.   There is a
small percentage, however, of the sputtering around the brightest stars
which does pair and appears on the master list.   In addition the
presence of a bright star gives an artificially enhanced local sky
background, especially on the unbacked I-plates, and correspondingly
inaccurate photometry.   For these two reasons we have 'drilled' (in
software) areas of avoidance of 2 x 2cm around the seven brightest stars
in the field, and of 4 x 4cm around the globular cluster NGC 288
which appears in our field.   The larger area is adopted in the last

case not only because the globular is physically larger on the plate, but also because it is obviously important to minimise as far as possible contamination by cluster stars of the number-magnitude-colour counts. Removing these eight regions reduces the total area of sky from 19.91 to 18.24 square degrees.

The next step was the separation of this dataset into stars and galaxies. This process is undertaken by eye classification of an initial sub-sample, examination of the relations between various machine parameters for the two species and, on the basis of this examination, the definition of global, automated separation criteria. For this work a one square degree region and three 1/4 square degree regions (one in the extreme corner of the COSMOS measured area) on V3475 were selected for eye classification and a total of 2000 images were classified. A second V plate (V6608) together with glass copies of the relevant SRC IIIaJ survey plates (limited at $B_J \sim 23$ magnitude) served as checks on the classification for all the areas, while for two of the smaller regions a high quality, deep AAT IIIaF plate ($R_{lim} \sim 24$) provided final confirmation. All the images classified were at least two magnitudes above the limits of the IIIa-J survey plates and the separation is subject to practically no error.

For the automated separation, two methods were examined - central intensity versus ΣI (an extension of the T_{min} vs. Area method (McGillivray et al, (1976)), and Log (Area) versus ΣI. Over the range $15 < V < 20$ both techniques give very similar performances, but for brighter magnitudes the central intensity discriminant tends to break

down due to saturation effects in COSMOS. For this reason the Log
(Area) vs. ΣI was employed for the whole magnitude range. This technique
does not work at the brightest magnitudes on sky limited IIIaF and IIIaJ
plates through the presence of very strong diffraction spikes, adding a
large, low surface brightness component to stellar images. On IIaD
plates, however, diffraction spikes are much weaker, and eye classification
of the 100 brightest images from V3475 showed that all images are correctly
classified.

Eye classification places an image into one of seven categories - single
stars, double stars, star + galaxy with the stars dominant, galaxy
+ star with the galaxy dominant, single galaxies, multiple galaxies and
spurious images. Approximately 100 objects fell under the last heading
and all could be identified with features visible on V3475. None of
these had been paired, however, and so contamination from spurious
images is practically non-existent in the final master image set.

Taking images from all four regions, we have plotted Log (Area) versus
ΣI for stellar dominated images (Figure 4.4a) and galaxy-dominated images
(Figure 4.4b) together with the discrimination line adopted for star
galaxy separation. The tight stellar sequence shows that there are no
systematic displacements in the Log (Area) - ΣI plane despite the fact
that the regions sampled effectively cover the plate, and we can therefore
use a global relation to classify the images. Objects that lie above
this line in the stellar sample are either multiple images or single
stars close by emulsion fluctuations, which have contributed proportionately
more to image area than to COSMOS magnitude. Both cases should lead to

the loss of samples which are random with regard to magnitude and colour.   Counting double stars as two images then ≈ 4 percent of the total stellar sample is lost and we have adopted this as an appropriate correction throughout the remainder of the paper.

Brighter than 17th magnitude in V, the contamination of the stellar sample by galaxies is < 1 percent.   Fainter than this limit, the galaxy sequence starts to merge with the stars, giving a contamination of 2 percent at V = 19, and rising steeply at fainter magnitudes.   The discrimination line was chosen so that the stellar sample was maximised, and thus 96 percent of all stars are included even at these fainter magnitudes.   The extent of the galaxy contamination with regard to colour and magnitude has been reliably determined owing to the large number of eye classified objects, and correspondingly precise corrections to the number-magnitude-colour diagrams have been made.   These corrections did not exceed 1 percent in any colour bin, and were usually much less. They are discussed in detail in Section VII.

Thus the final step in the data reduction is to construct the working dataset, comprising the master plate X,Y co-ordinates together with magnitudes and eccentricities from each plate and the star/galaxy label. This dataset forms the basis for the number-magnitude-colour counts, which are given in Table 4.4 .

V   ABSOLUTE MAGNITUDE - COLOUR RELATIONS

The crucial step in analysis of our data is the conversion of our measured

TABLE 4.4

I \ V-I	-0.38	-0.13	0.13	0.38	0.63	0.88	1.13	1.38	1.63	1.88	2.13	2.38	2.63	2.88	3.13	3.38	3.63	3.88	4.13
7.25																			
7.75																			
8.25																			
8.75					1														
9.25					1	2													
9.75				1															
10.25				1	2	5	5	4	4	1									
10.75			1	2	5	9	8	10	7	4	2								
11.25		3		1	6	7	3	2	1		1								
11.75		1		2	9	8	7	3	2			2							
12.25		1		4	8	5	2	1	4	1	2								
12.75			3	9	16	29	22	12	10	8	3	1	1						
13.25			11	16	81	59	23	7	7	2	1			1					
13.75			9	130	132	81	29	12	4	3	3	1							
14.25			8	150	165	62	32	21	10	8	7	3	2						
14.75	1	2	11	195	188	79	47	26	12	10	12	16	3	1					
15.25		1	2	213	236	105	74	34	22	15	16	19	4	3	1				
15.75		2	4	244	290	124	84	53	40	22	30	16	3	2	1	1			
16.25	1	2	25	329	268	149	89	98	53	47	22	25	5	5	1		1		
16.75		2	50	408	281	141	121	130	115	75	69	53	29	14	12	6		1	
16.75	1	4	61	481	305	190	178	165	148	98	79	200	109	53	14	7	1	1	
16.75	3		104	504	380	223	219	240	233	245	209	119	45	26	11	3	2		

Number-magnitude-colour distribution for all objects classified as stellar in 18.24 square degrees towards the South Galactic Pole. The listed magnitudes and colours refer to the centres of the respective bins.
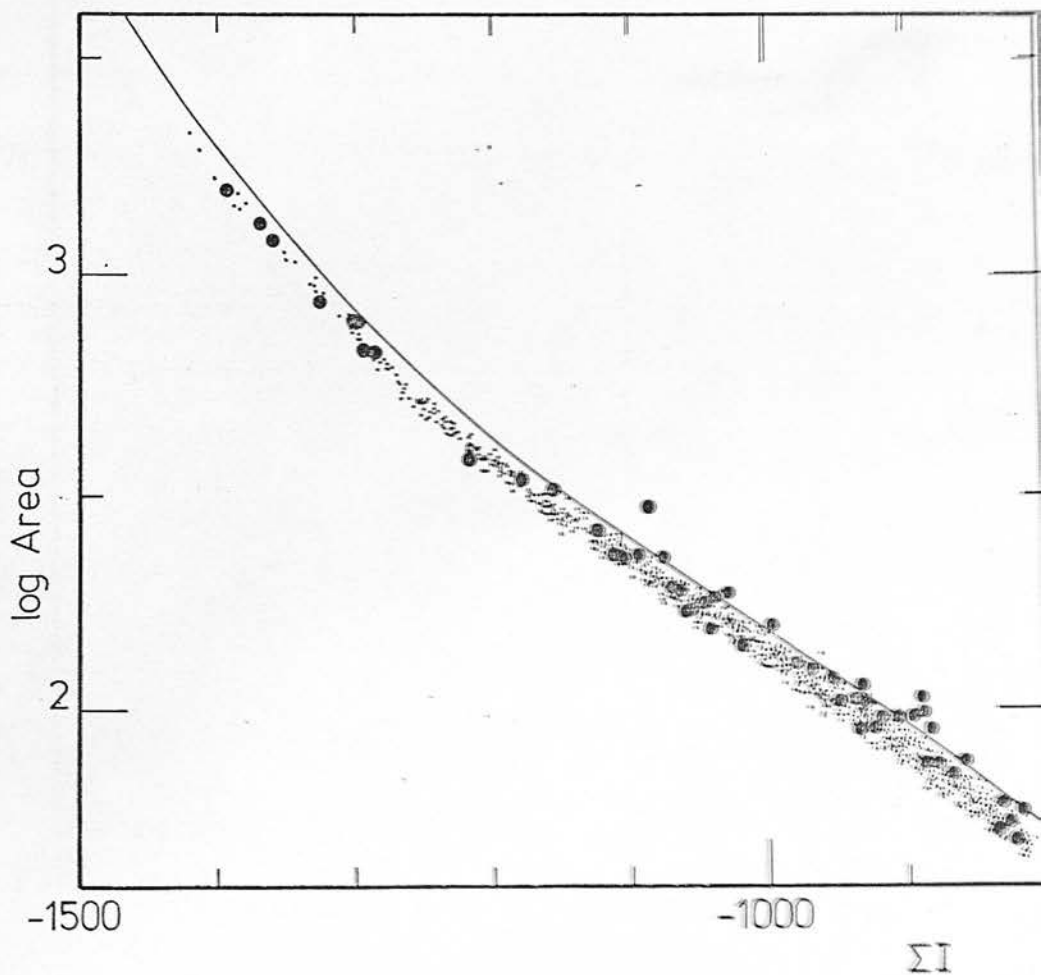
Figure 4.4a

Definition of the star-galaxy separation line (solid curve) in COSMOS

parameter space.   The dots show the positions of ˜1500 stars.   The

solid points are multiple images merged into one, with a star image

dominant.   The smooth curve has been chosen to optimise star

identification.   98% of stellar images lie below the curve.
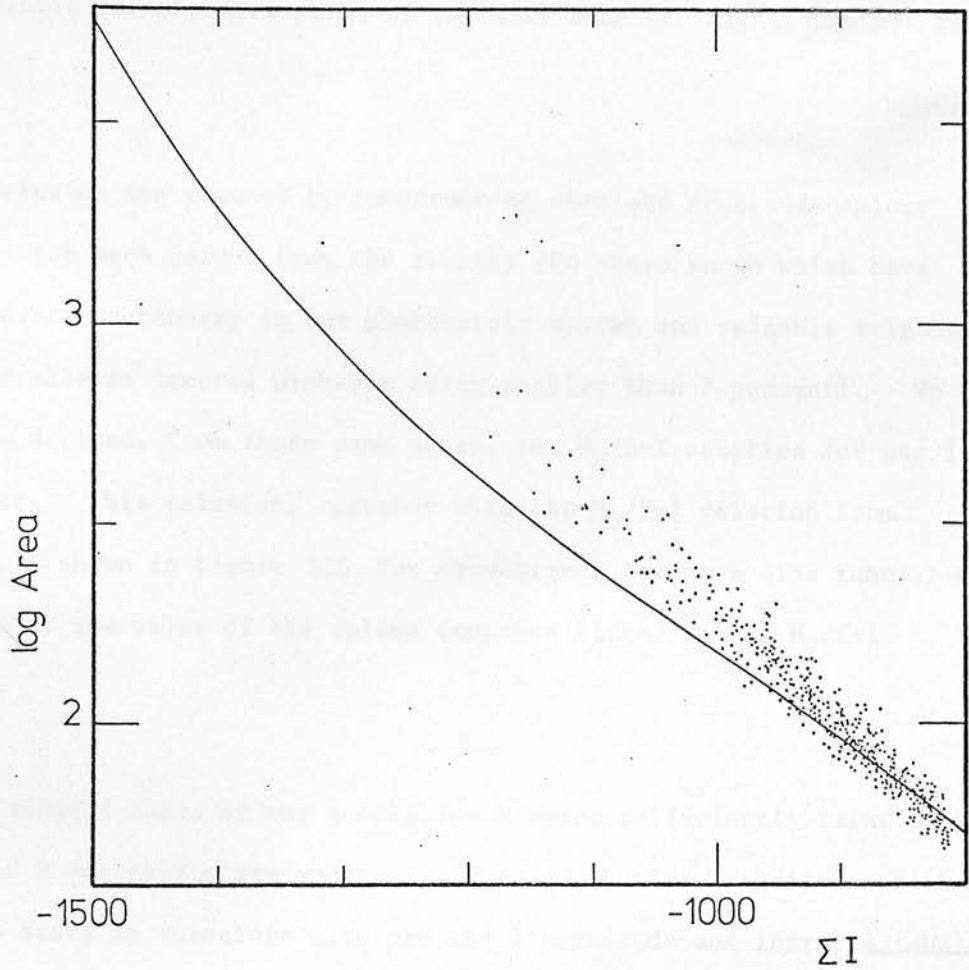
Figure 4.4b

As for Figure 4a, with the same smooth curve, and ~500 galaxy images

represented.   For ΣI<-900, 2% of galaxies are misclassified, with this

percentage rising rapidly at fainter magnitudes.

colour for each star into the corresponding absolute magnitude.   In
Paper I (Reid, 1981) we briefly discussed the three available relations
$M_V/B-V$, $M_V/V-R$, and $M_V/V-I$, and noted that the $M_V/V-I$ relation is the
most suitable for the derivation of reliable absolute magnitudes for red
stars.

This conclusion was reached by constructing absolute magnitude-colour
relations for each colour from the roughly 200 stars known which have
both accurate photometry in our photometric system and reliable trigono-
metric parallaxes (quoted probable error smaller than 7 percent).   We
have also derived, from these same stars, the $M_V/R-I$ relation for use in
this paper.   This relation, together with the $M_V/V-I$ relation from
Paper I, is shown in figure 4.5. For convenience, we have also tabulated
(Appendix 2) the value of the spline function fitted to the $M_V/V-I$
relation.

The very reddest stars of our sample are however sufficiently faint that
even their R magnitudes are uncertain.   As an absolute magnitude calibrator
for these stars we therefore also use the I magnitude and infrared (JHK)
photometry.   We wish therefore to derive the $M_V/I-K$ relations to
supplement the visual colour calibrations available.

Visual and infrared data for parallax stars in our system are available
only for a very few objects.   We are therefore forced to transform
published data to our photometric system for use as calibrators, with
all the consequent uncertainties.   The set of VIJHK data requiring the
smallest and best known corrections is that due to Mould and Hyland
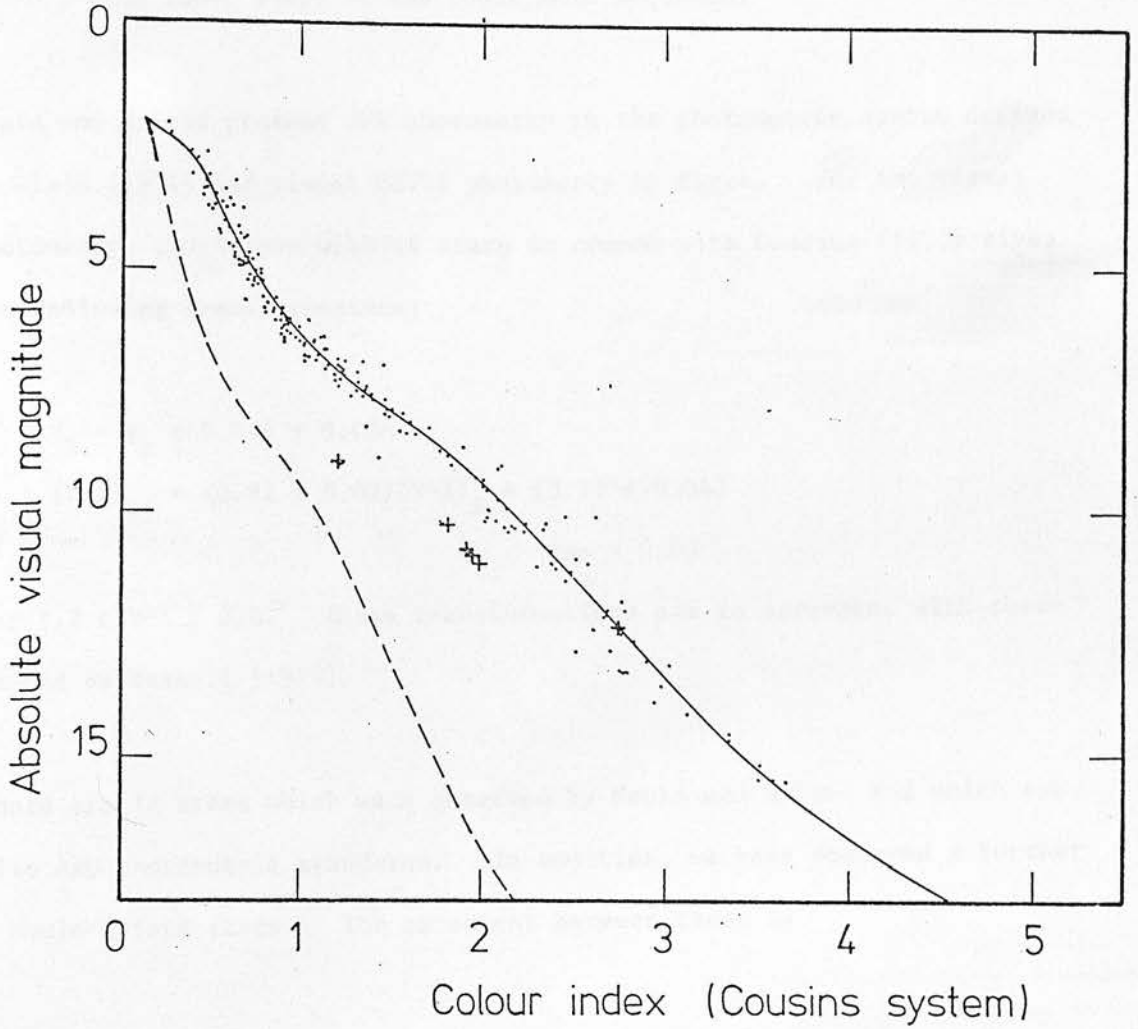
Figure 4.5

The absolute visual magnitude-colour relations derived from 202 stars of accurately known parallax. The solid line is the spline fitted $M_V/V-I$ relation derived from the dotted points and is tabulated in Appendix II. Some subdwarfs (crosses) are also shown. The broken line is the $M_V/R-I$ relation derived from the same stars.

(1976), from their study of the lower main sequence.

Mould and Hyland present JHK photometry in the photometric system defined by Glass (1974) and visual UBVRI photometry by Eggen. For the visual photometry, comparison with 16 stars in common with Cousins (1980) gives the following transformations:

$$V_E - V_c = 0.016 \pm 0.036$$
$$(V-I)_c = (0.92 \pm 0.02)(V-I)_E + (0.29 \pm 0.04)$$
$$\text{rms} = 0.03$$

for $1.2 \leqslant V-I \leqslant 3.0$. These transformations are in agreement with those quoted by Bessell (1979).

There are 12 stars which were observed by Mould and Hyland and which are also AAO photometric standards. In addition, we have observed a further 9 Mould-Hyland stars. The agreement between these is

$$\Delta K = 0.046 \pm 0.028 \qquad \text{(standard deviation, 21 points)}$$

Using the transformed visual photometry, the corrected Mould and Hyland K photometry, and our own observations, we have 52 stars with sufficiently accurate parallaxes (error less than 10 percent) so that reliable absolute magnitude corrections from Lutz and Kelker (1973) are possible. These corrections allow for the systematic error in mean absolute magnitude derived using a sample of stars selected by percentage accuracy in the trigonometric parallax, and are discussed in Paper I, and by Lutz (1978), and Upgren and Lutz (1979). The derived relation is shown in figure 4.6,
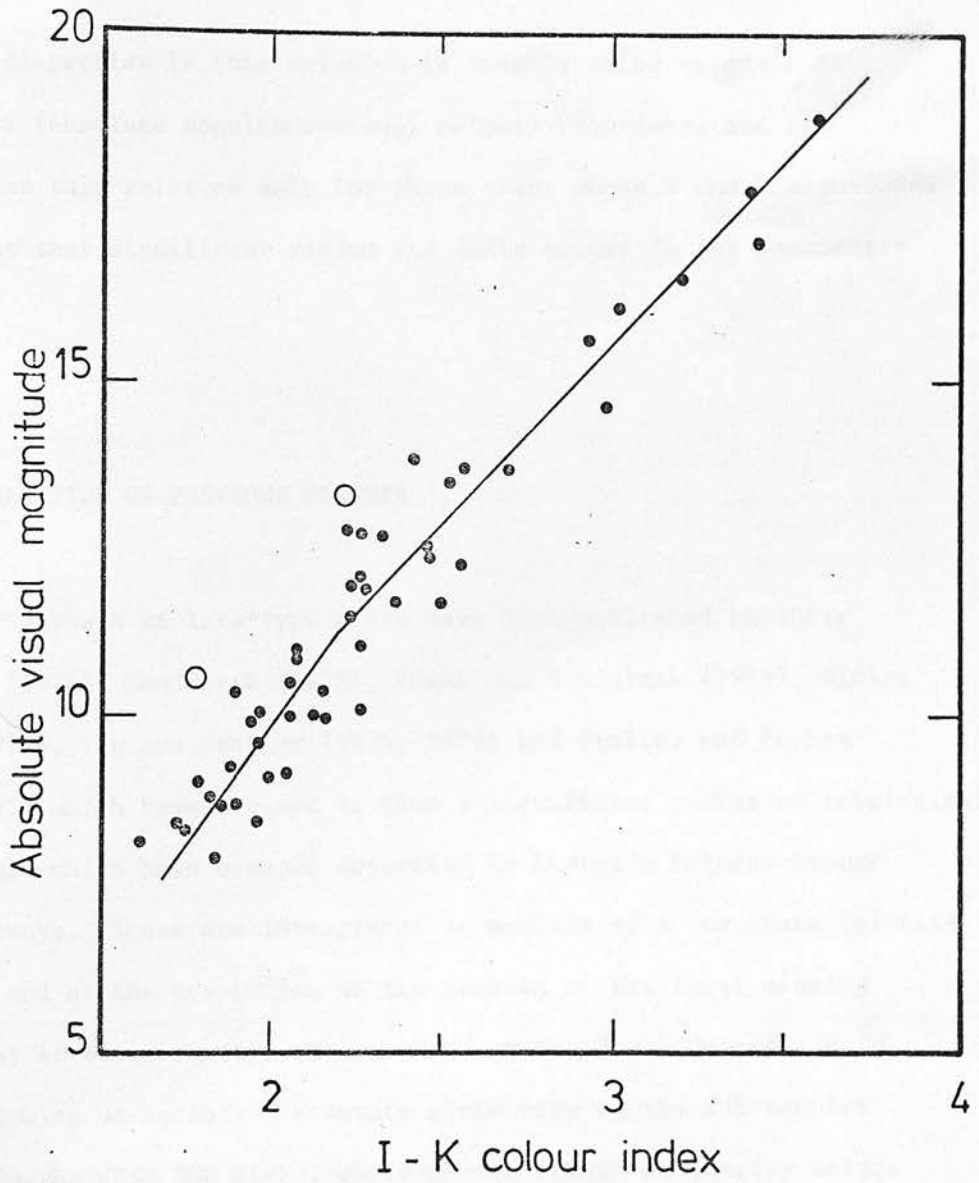
Figure 4.6

The absolute visual magnitude versus I-K relation, derived from 52
points with accurately known parallaxes.   The solid curve is the adopted
mean relation.   Two subdwarfs are marked (open circles).

together with the adopted mean relation.

The cosmic dispersion in this relation is roughly twice as great as those in the (absolute magnitude-visual colour) relations, and we therefore use this relation only for those stars whose V and R magnitudes are so faint that significant random and scale errors in our photometry may exist.

VI   RE-EVALUATION OF PREVIOUS SURVEYS

A number of surveys of late-type stars have been published recently (Smethells (1974), Sanduleak (1976), Pesch and Sanduleak (1978), Giclas et. al. (1972), The and Staller (1975, 1979) and Staller and Bochem-Becks (1979)) which have claimed to find a significant number of intrinsically faint M-stars which have escaped detection in Luyten's Palomar Proper Motions Surveys. These are interpreted as members of a low space velocity population and as the resolution of the problem of the local missing mass.   Four of these surveys were centred on the South Galactic Pole region, allowing us to obtain accurate photometry of the sub-samples lying within the UKST SGP field, while photoelectric photometry exists of the Smethells and Giclas samples.   The resultant absolute magnitude calibrations are not consistent with any local M-star excess.

The samples used by Staller and Bochem-Becks and by Giclas et al. were both selected from eye comparison of blue and red plates, with the red

TABLE 4.5

Colour class	$\langle(V-I)\rangle$	σ_{V-I}	No.
0	2.0	0.6	32
1	1.77	0.57	141
2	1.47	0.52	433
3	1.29	0.51	178
4	1.12	0.44	48
5	1.18	0.47	51

Mean colours and dispersions for the colour classes estimated for M dwarfs by Staller and Bochem-Becks (1979).

stars assigned to a colour class. The former study used the Palomar Schmidt E and O plates and covers six square degrees near NGC 288 to a limiting magnitude of R $\sim$ 18. We have identified all stars with V $\leqslant$ 18.8 lying within half of this region, as well as all of the colour class O stars in the COSMOS measured area. The resultant mean V-I colours (Table 4.5) are consistent with K-, rather than M-, dwarfs. Similarly our photometry of the two +4 and fifteen +3 colour class stars from the Lowell Proper Motion survey (Giclas et al., 1972) shows that they have colours ranging from V-I = 0.7 to V-I = 2.5 (M_V = +5 to +12), confirming the large uncertainty of the colour class system.

The other surveys are all derived from objective prism surveys, although Thé and Staller (1974, 1979) actually obtained their absolute magnitudes from photoelectric R-I colours, calibrated using Kron et al.'s (1957) RI photometry of parallax dwarfs. However it is not clear that either the agreement between the photometric systems or the absolute magnitude-colour relation adopted is reliable. A comparison with Eggen's photometry reveals random errors of up to three tenths of a magnitude in R-I ($\pm$ 1.8 in M_R). In addition there is poor agreement between the absolute magnitudes derived by Thé and Staller, and those derived by ourselves for fifteen stars within the SGP field (Table 4.6; a further three stars are merged with nearby images in the COSMOS data). This emphasises the importance of using an absolute magnitude calibration defined on the same system as that of the programme objects.

The objective prism survey by Pesch and Sanduleak (1978) covers much the same region as the above, but to a limiting magnitude of R $\sim$ 16, and

TABLE 4.6

TS	$(m-M)_{TS}$	$(V-I)$	V	$(m-M)_{cos}$	
E203	2.1	2.13	14.88	5.1	PS 18
204	4.5	2.09	14.51	4.3	PS 19
205	3.9	2.28	14.04	3.7	
216	3.1	2.51	14.92	3.5	PS 32
222	5.3	1.91	14.24	5.2	
225	2.9	2.41	15.10	4.2	PS 37
227	-	3.05	16.10	2.5	PS 42
237	6.5	1.65	13.65	5.5	
254	2.9	1.76	13.61	5.1	
255	1.9	2.31	15.11	4.6	PS 57
257	4.1	2.13	13.83	5.0	PS 59
270*	-0.1	2.65	11.81	-0.2	PS 69
275	3.2	2.13	13.54	3.7	
276**	2.3	2.50	13.91	2.6	PS 72

*   DM -28°:302

**   LP 882-169

Photometry and distance moduli for the M dwarf candidates from the
survey of Thé and Staller (1975, 1979).

[E217 is also in the UKST SGP field ($\alpha = 0^h48^m11^s$, $\delta = -28^{\circ} 32'.2$)
but there is no object with $I < 15$ redder than $V-I = 1.0$ within $5'$.   As
E217 is listed by TS as $I = 13.5$, $V > 15$, and is not marked on their
finding charts, it is possible that it is a plate flaw.]

lists 282 "probable dwarfs of type M3 and later" of which thirty three
are in the UKST SGP field.   One of these, PS 67, is too near a bright
star for accurate photometry, while positions and photometry for the
remaining stars are given in Table 4.7).   The majority have absolute
magnitudes in the range $+10 \leqslant M_V \leqslant +12$, with only three fainter than
$M_V = +13$.   As most have distance moduli greater than 4 magnitudes,
there is no necessity to postulate unusual kinematics to explain why
these stars were not detected in proper motion surveys.   Recent photo-
metry of Sanduleak's (1976) NGP sample by Pesch and Dahn (1981) is
consistent with this result, with again $\sim$ 10 percent of the sample
having $M_V > +13$.

Finally, although objective prism surveys for late type stars do provide
samples including all such objects in a given area, there is a tendency
to overestimate the lateness of type.   Upgren et al. (1972) have shown
that Vyssotsky's sample of McCormick dwarfs also suffers from this
effect, with the original classifications of K7 to M4 being revised to
K2 to M2, while Smethells' (1974) red dwarf survey has been fully
discussed in Paper I.

In general naive quantitative analysis on the basis of subjective
classification - either colour class or estimated spectral type - is
extremely susceptible to systematic errors, which often conspire to
artificially enhance the inferred dM star population.

TABLE 4.7

PS	RA (1950.0)	DEC	V	V-I	M_V
16	00 44 05.1	-29 13 15	14.81	2.14	9.85
18	44 10.6	-27 58 44	14.88	2.13	9.8
19	44 15.8	-25 54 44	14.51	2.09	9.65
26	44 58.4	-27 25 30	17.03	2.89	12.95
28	45 30.4	-26 55 03	14.68	1.94	9.1
31	46 22.9	-27 39 42	16.58	2.75	12.4
32	46 30.4	-26 21 02	14.92	2.51	11.4
33	46 54.9	-28 40 31	16.04	3.09	13.8
36	47 21.1	-28 10 51	16.07	2.51	11.4
37	47 23.7	-27 14 33	15.10	2.41	10.95
42	48 00	-26 23 33	16.10	3.05	13.65
46	49 26.6	-26 02 20	15.08	2.44	11.1
49	51 05.1	-27 32 20	16.90	3.00	13.45
57	52 45.4	-30 11 20	15.11	2.31	10.55
59	53 06.3	-26 16 33	13.83	2.13	9.8*
68	55 57.0	-26 53 28	15.38	2.27	10.4
69	56 00.8	-28 07 30	11.81	2.65	12.0*
72	56 27.5	-28 30 05	13.91	2.50	11.35*
73	56 54.2	-26 16 53	15.57	2.62	11.85
74	57 04.9	-28 36 21	16.19	2.70	12.2
80	58 39.2	-28 29 01	15.31	2.75	12.4*
82	58 52.7	-26 51 37	14.97	2.55	11.55*
87	59 23.2	-26 00 11	16.11	2.61	11.8
90	01 00 20.7	-26 40 02	15.25	2.05	9.5
92	00 39.8	-27 54 00	16.07	2.71	12.2
95	01 06.2	-26 02 14	14.74	2.26	10.3
96	01 29.8	-26 36 02	13.13	2.45	11.1*
98	01 25.8	-30 04 50	15.08	1.94	9.1
99	01 29.5	-28 21 57	16.10	3.20	14.25
101	01 52.9	-26 15 57	16.78	3.13	13.95*
102	02 34.1	-27 04 59	16.75	2.61	11.8
107	03 37.7	-27 36 59	15.31	2.16	9.95

*Luyten proper motion star

Photometry of the M dwarf candidates from the survey of Pesch and
Sanduleak (1978).

VII THE PHOTOMETRICALLY DEFINED LUMINOSITY FUNCTION

Using the number-magnitude-colour data presented in Table4.4, and our
M_V/V-I relation from section V and Paper I, we are now able to derive
absolute magnitudes, and consequently distances and space densities, for
all stars in our sample. Firstly however, the data of Table IV must be
examined for galaxy contamination, incompleteness, and Malmquist bias.

As discussed in section IV, star-galaxy separation is sufficiently
reliable that the contamination in all colour bins is less than 2 percent
of the stellar count for V brighter than 19. At fainter magnitudes,
contamination rises sharply, reaching ~25 percent near the plate limit.
Fortunately, however, examination of the colour-apparent magnitude
diagram for those objects suspected to be within 100pc of the sun,
together with our estimates of the percentage of all galaxies incorrectly
classified as a function of apparent magnitude, allows us to estimate
the contamination in our nearby star sample to the limit of our V plates.
A total of 13 galaxies have colours corresponding to stars within distance
modulus 5 magnitudes, all except 4 of which have V magnitudes at which
roughly 10 percent of galaxies are misclassified. Therefore fewer than
2 galaxies are expected in our stellar sample by error, while we have
106 stars. The contamination is therefore negligible compared to
sampling statistics.

Similarly, the correction for merged stellar images is ~4 percent, and
is also unimportant here. We will however systematically exclude
nearby visual binaries with separations in the range 1-3 arcseconds, and

apparent magnitudes differing by less than about 2 magnitudes. Simple calculations using published estimates of duplicity and separation suggest that the loss in this way will be small relative to our sampling errors.

Finally, as our goal is the derivation of a distance limited complete sample, while our data are magnitude (distance modulus) limited, it is necessary to convert our derived absolute magnitudes to the corresponding distance limited values. This is done using the well known Malmquist relation

$$M_m = M_o - \frac{\sigma^2}{\log e} \frac{d \log A(m)}{d m}$$

where M_m is magnitude limited absolute magnitude, M_o the distance limited value, $A(m)$ the differential number–magnitude counts, and σ^2 the variance of the derived absolute magnitudes. In our case this is dominated by the cosmic dispersion. In deriving the appropriate number magnitude slope, care must be taken to ensure only the population under consideration is counted. With our data, substantial contamination of the disk G-K dwarf number counts by halo giants with similar colours occurs at bright apparent magnitudes. We have therefore derived the logarithmic gradient for two ranges of V-I colour, with the division at V-I = 1.5, to minimise this contamination. Both sets of number-magnitude counts show gradients which change smoothly from 0.6 at bright magnitudes (V~10 for the blue sample, V~13.5 for the red) to 0.3 at V~18 for both samples. The derived Malmquist correction to our absolute magnitudes is then only $0\overset{m}{.}08$.

Thus, knowing the (distance limited) absolute magnitude and the apparent magnitude for each star, we are able finally to calculate the stellar space densities as a function of both absolute magnitude and distance below the Galactic plane. The stellar density gradients will be discussed in detail in Paper III of this series (Gilmore and Reid, 1982). The magnitude dependence of the solar neighbourhood space density - the luminosity function - is discussed below.

Before this is derived however, an analysis of the assumptions in our photometric parallax technique is necessary. Our implicit assumption is that all stars are main sequence dwarfs. Four common classes of star are likely to be present in our sample which do not satisfy this assumption.

1) Subdwarfs - as noted in Paper I, subdwarfs lie about 1 magnitude below the main sequence in the M_V/V-I diagram, at least for 1.0 < V-I < 2.0. Their derived magnitudes and space density will therefore be substantially in error. However, the space density of such stars is about 0.005 that of main sequence dwarfs (Chiu, 1980a). Their contamination is therefore small.

2) White dwarfs - photometric parallaxes of unrecognised degenerates are of course grossly in error. Integration of the white dwarf luminosity function predicts fewer than 6 white dwarfs per square degree brighter than V = 20, with all of these being blue (Gilmore, 1981) They will not affect our derived luminosity function, which is specifically restricted to red main sequence objects.

3) Horizontal branch stars, OB subdwarfs, etc - because these stars are blue, even our totally incorrect parallaxes will not place these stars in our sample.

4) Red Giants - these are the most common and most important contaminant, and in fact dominate the counts with $1.0 \leq V-I \leq 1.8$, and $V \leq 14$. We do not yet have luminosity classifications for all our stars in this sample, and therefore cannot reliably remove them from consideration. While statistical corrections are possible, using for example the data of Upgren (1963), in practice these are very uncertain. Jones (1976) has noted that few, if any, giants are known in the Galactic poles fainter than B ⁓ 15. We have therefore temporarily adopted the conservative policy of excluding our data on G and K stars from consideration. We cannot therefore derive a local luminosity function for stars brighter than $M_V = +8.5$. For such bright stars, several photometric studies of the local luminosity function (Paper I; Wielen, 1974; McCuskey, 1966) are available, with very much larger samples than ours. This restriction is therefore not important.

Finally, therefore, we are able to define our complete sample. As our primary aim is the space density of very low luminosity stars, we consider all stars in our 18.24 square degree area with $I \leq 17.0$. This apparent magnitude limit is chosen because it is about 2 magnitudes above our plate limit, so that completeness and photometric accuracy are both acceptable, and because we have very few fainter standard stars. The

possibility of systematic errors therefore could arise below I = 17.0.

From the images in this sample, we isolate all those whose V-I photometric parallax places them within 100pc of the sun, and which are fainter than absolute magnitude M_V = +8.5. This sample contains 97 stars. In addition, we have one star with I $\leqslant$ 17.0 which was not detected on any of our V plates, but which has M_V = +19 (RG0050-2722, Reid & Gilmore, 1981). Because most of these stars are both very faint and very red, the possibility of a systematic error in the photometry must be considered.

We have therefore observed all stars in our sample with $M_V \geqslant$ +14.5 (V-I $\geqslant$ 3.30) in the near infrared JHK bands using the 3.9m Anglo-Australian Telescope. This sample includes all the reddest objects, as well as all those with V $\geqslant$ 19.5 in the 100pc sample. (This photometry, together with its implications for the structure of the lower main sequence, will be discussed in detail elsewhere.) With these results we are then able to derive an absolute magnitude from the M_V/I-K relation for each star, as well as a probably more reliable distance limit from the M_I/I-K relation and apparent I magnitude. This then ensures that the 100pc limit is set by the most reliable photometry available, and in fact excluded a further 9 stars from the 100pc complete sample.

Our final complete sample therefore contains 89 stars with $M_V \geqslant$ +8.5 and within 100pc of the sun. Of these, 7 are fainter than M_V = +14.5, and have had absolute magnitudes and distance moduli derived from I-K photometry. The remainder have absolute magnitudes and distance moduli derived from our V-I photographic photometry.

TABLE 4.8

The Derived Luminosity Function

a) Integral Magnitude Bins

M_V (±0.5)	Number of stars*	Completeness Limit (pc)	Log Φ (stars mag^{-1} pc^{-3})	Log Φ (Wielen)
9.0	3	100	-2.67	-2.32
10.0	10	100	-2.27	-2.14
11.0	14	100	-2.12	-1.99
12.0	29	100	-1.81	-1.82
13.0	13	100	-2.15	-1.75
14.0	10	100	-2.27	> -1.99
15.0	5	100	-2.57	
16.0	1	∿ 75	-2.9	> -2.20
17.0	0	∿ 60	< -2.6	
18.0	0	∿ 50	< -2.4	>> -3.32
19.0	1	∿ 30	-1.7	

b) Half-Integral Bins

9.5	5	100	-2.57	
10.5	10	100	-2.27	
11.5	23	100	-1.91	
12.5	24	100	-1.89	
13.5	11	100	-2.23	
14.5	8	100	-2.36	
15.5	3	∿ 90	-2.65	
16.5	1	∿ 65	-2.7	
17.5	0	∿ 50	< -2.4	
18.5	1	∿ 40	-2.1	

* Number in 18.24 square degrees

Figure 4.7

The derived luminosity function (solid points, Poisson error bars).
Also shown is the luminosity function derived by Wielen (1974) from
stars within 20pc of the sun (solid curve). The points brighter than
M_V = +16 are based on the complete 100pc sample, and must be increased
by ~0.11 in log Φ (to allow for the Galactic density gradient) for
comparison with the solar neighbourhood values. The fainter points do
not require significant correction.

log Φ (stars mag⁻¹ pc⁻³)

Absolute visual magnitude
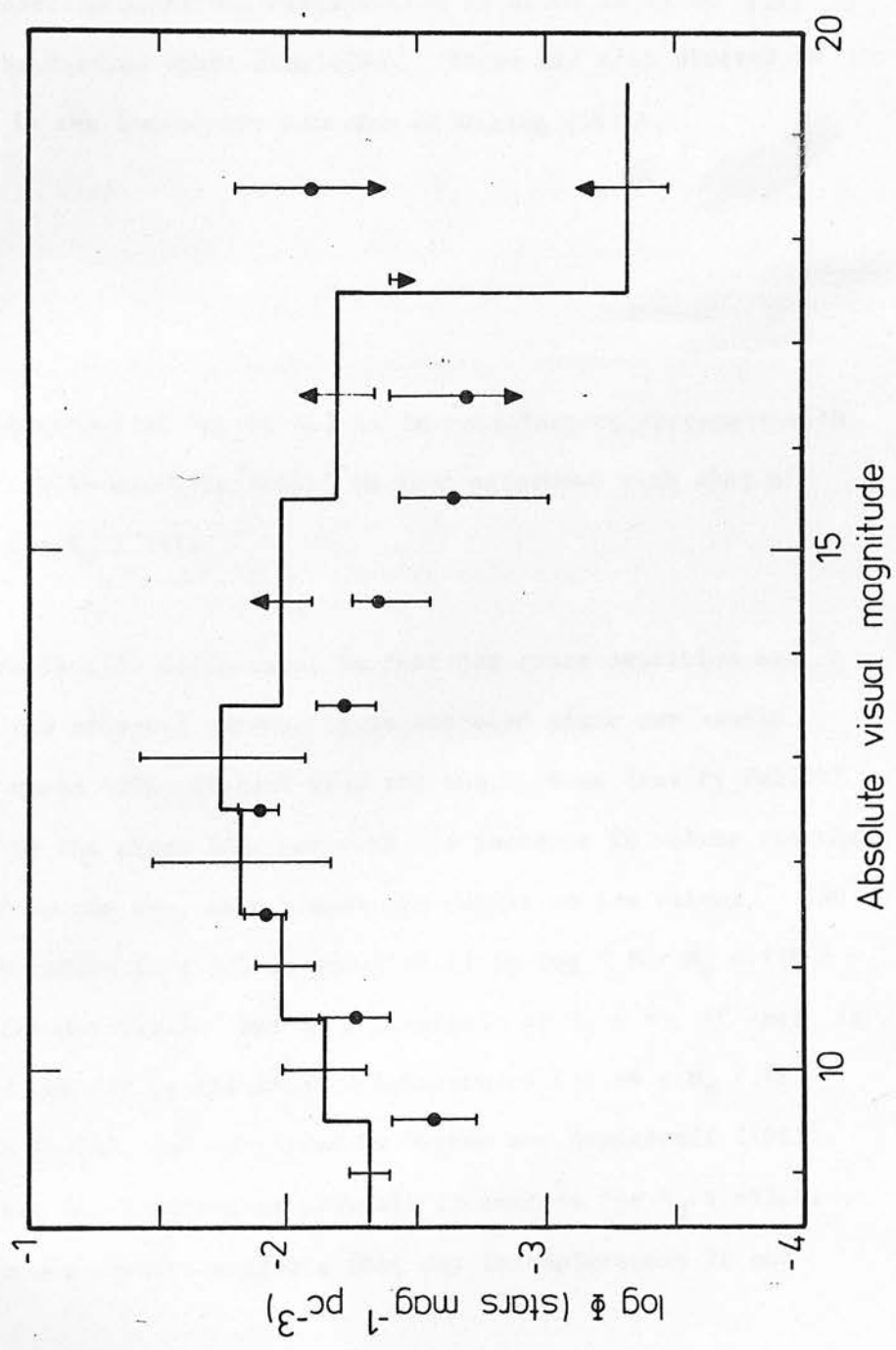
The resulting absolute magnitude distribution is shown in Table 4.8, together with the derived space densities. These are also plotted in Figure 4.7, as is the luminosity function of Wielen (1974).

VIII DISCUSSION

The luminosity function of Figure 4.7 is in satisfactory agreement with that of Wielen (1974) which is itself in good agreement with that of Luyten (1968), for $M_V \geq +11$.

The slight normalisation difference, in that our space densities are slightly below the accepted values, is as expected since our sample includes stars up to 100pc distant from the sun. Some density falloff from the value in the plane together with the increase in volume searched, with distance from the sun, then biases our result to low values. (An approximate correction to $z = 0$ is about +0.11 in log Φ for $M_V < +16$ - see paper III for details.) The slight deficit at $M_V = +9$, if real, is consistent with the dip in the solar neighbourhood for $+6 \leq M_V \leq +9$ found by Wielen (1974), and confirmed by Upgren and Armandroff (1981). Wielen notes that his function is probably incomplete for $M_V \geq +13.5$. Comparison with our results suggests that any incompleteness is not severe.

The general feature of all three functions is a broad maximum from $M_V \sim +10$ to $M_V \sim +14$, with a decrease at both brighter and fainter magnitudes. Statistical uncertainties in existing complete photometric

surveys, and in the absolute magnitude calibration for kinematic surveys, do not allow a more specific statement.

We do not, at any magnitude, find evidence for a statistically significant excess of intrinsically faint stars, relative to the numbers found in kinematic surveys. Only one star in our sample, the previously known Gl 46, lies within 20pc. As this survey reaches some 5 magnitudes deeper into the luminosity function than existing photometric studies, and as our faintest star found is comparable to the theoretical minimum mass for thermonuclear burning, we may conclude that, at least in this line of sight, there is no evidence for a significant population of low space velocity intrinsically faint stars. We are currently completing a similar study of a second field, towards $(1,b) = (30^{\circ}, -50^{\circ})$, to test the possibility that our results are atypical of all directions.

Finally, therefore, as a consequence of a careful re-evaluation of existing M dwarf surveys, and our own photometric analysis of a complete, distance-limited sample, we conclude that there is no evidence to suggest that any solar neighbourhood missing mass is in the form of main sequence stars with $M_V \leq +17$.

ACKNOWLEDGEMENTS

APPENDIX 1

Photoelectric standards in the South Galactic Cap were obtained from observations from South Africa.   These are described in section II and Paper I.   The individual stars observed are tabulated below, with those also observed by Jennens (1975) indicated.

	RA (1950.0)	DEC	V	B-V	V-R	V-I	n(obs)	
1	0 44 15.8	-25 54 42	14.44	1.50	1.01	2.24	1	
2	0 44 28.5	-25 59 22	11.97	0.54	0.32	0.61	1	
3	0 45 2.9	-29 58 34	11.42	0.66	0.34	0.68	1	
4	0 45 13.0	-29 17 27	10.52	1.34	0.71	1.40	1	JEN C36
5	0 45 36.0	-27 34 24	13.04	0.11	0.09	0.21	1	
6	0.46 1.6	-28 12 39	14.04	0.10	0.14	0.21	1	
7	0 46 10.2	-27 17 0	12.36	0.55	0.32	0.66	1	
8	0 46 20.0	-29 55 20	12.93	0.73	0.38	0.75	1	
9	0 46 29.3	-29 52 26	14.41	0.67	0.37	0.77	2	
10	0 46 38.1	-29 57 51	15.45	0.68	0.42	0.76	1	
11	0 46 43.6	-29 58 21	15.23	0.74	0.49	0.86	1	
12	0 46 44.8	-29 58 59	15.82	0.77	0.41	0.81	1	
13	0 46 48.9	-29 56 19	13.73	0.74	0.37	0.80	2	
14	0 47 55.6	-26 55 41	13.09	1.49	1.13	2.53	1	
15	0 48 8.8	-26 0 17	12.00	0.64	0.35	0.69	1	
16	0 49 19.0	-27 51 44	13.33	0.21	0.19	0.36	1	
17	0 49 37.2	-28 33 57	11.53	0.99	0.50	0.94	1	JEN C29
18	0 49 48.2	-30 7 55	14.04	0.83	0.43	0.91	1	
19	0 49 51.4	-26 40 12	8.47	0.99	0.52	1.00	1	JEN A8
20	0 50 27.8	-26 29 39	11.68	0.99	0.54	0.98	1	JEN C19
21	0 50 36.8	-30 7 54	11.80	0.68	0.36	0.67	1	
22	0 50 59.7	-29 35 24	11.61	0.72	0.40	0.78	1	
23	0 51 34.7	-28 22 28	10.38	1.17	0.58	1.09	1	JEN A6
24	0 51 53.0	-28 18 40	11.93	0.78	0.43	0.82	1	JEN C21
25	0 52 45.4	-30 11 19	15.12	1.50	1.03	2.32	1	
26	0 53 4.4	-26 9 5	11.92	1.41	1.00	1.89	1	
27	0 53 18.5	-28 9 50	9.51	1.14	0.53	1.05	1	
28	0 54 29.7	-27 54 5	13.22	0.64	0.31	0.58	1	
29	0 54 56.3	-30 8 16	12.25	0.42	0.29	0.61	2	
30	0 55 6.1	-30 16 4	14.43	1.44	0.97	2.08	1	
31	0 55 57.6	-27 56 28	12.51	1.10	0.60	1.12	1	JEN D6
32	0 56 0.8	-28 7 29	11.78	1.54	1.24	2.60	2	
33	0 56 18.7	-28 7 35	12.10	0.57	0.34	0.67	1	
34	0 56 27.3	-26 55 23	11.82	1.03	0.56	1.06	1	JEN C8
35	0 56 27.5	-28 30 53	13.89	1.50	1.24	2.56	1	
36	0 56 57.0	-27 44 24	13.23	0.77	0.42	0.81	1	
37	0 57 22.3	-26 23 35	11.89	0.58	0.34	0.67	1	
38	0 58 11.6	-26 54 24	11.10	1.17	0.62	1.12	1	JEN C2
39	0 58 16.7	-27 54 12	10.90	1.13	0.61	1.10	1	JEN C5
40	0 58 39.2	-28 29 0	15.10	(1.11):	1.21	2.59	1	
41	0 59 5.2	-27 43 9	9.20	1.50	0.88	1.74	1	
42	0 59 24.0	-26 9 17	9.75	0.35	0.18	0.35	1	
43	0 59 34.0	-25 52 37	11.61	0.77	0.41	0.77	1	
44	1 0 16.6	-28 52 36	14.89	1.44	0.91	1.83	1	
45	1 0 21.6	-27 53 8	15.40	1.42	0.94	2.00	1	
46	1 0 23.1	-27 54 57	11.58	0.47	0.28	0.59	1	
47	1 0 23.1	-28 44 17	14.16	1.44	0.92	1.88	1	
48	1 0 24.2	-27 53 54	13.59	1.16	0.73	1.35	3	
49	1 0 31.4	-27 53 10	9.86	0.77	0.42	0.79	3	
50	1 0 33.4	-27 52 7	14.35	0.66	0.39	0.75	2	
51	1 0 38.3	-27 54 9	14.48	0.72	0.43	0.84	1	
52	1 0 42.8	-27 23 44	12.34	0.61	0.31	0.67	1	
53	1 0 42.9	-25 46 25	13.46	0.31	0.19	0.36	1	
54	1 0 43.9	-27 47 33	11.52	0.52	0.31	0.63	2	
55	1 1 36.2	-28 12 38	10.02	0.98	0.52	0.99	1	
56	1 1 53.9	-27 25 21	9.63	0.29	0.17	0.34	1	
57	1 1 58.9	-25 52 18	9.77	1.21	0.73	1.35	1	
58	1 2 32.7	-29 40 33	12.54	0.63	0.36	0.70	1	
59	1 2 35.2	-27 50 9	12.85	0.54	0.32	0.65	1	
60	1 2 42.7	-30 11 57	13.18	0.61	0.33	0.65	1	
61	1 3 9.9	-28 59 46	11.75	0.85	0.49	0.94	1	
62	1 3 19.8	-29 6 36	13.73	1.50	0.99	2.18	1	

APPENDIX 2

Tabulation of (M(V), V-I) spline calibration

V-I	M(V)	V-I	M(V)	V-I	M(V)	V-I	M(V)
0.05	1.41	1.30	7.16	2.55	11.55	3.80	16.26
0.10	1.51	1.35	7.28	2.60	11.76	3.85	16.40
0.15	1.64	1.40	7.40	2.65	11.97	3.90	16.53
0.20	1.80	1.45	7.53	2.70	12.18	3.95	16.66
0.25	1.98	1.50	7.67	2.75	12.39	4.00	16.78
0.30	2.19	1.55	7.81	2.80	12.61	4.05	16.90
0.35	2.43	1.60	7.96	2.85	12.82	4.10	17.01
0.40	2.68	1.65	8.11	2.90	13.03	4.15	17.12
0.45	2.96	1.70	8.27	2.95	13.23	4.20	17.22
0.50	3.26	1.75	8.43	3.00	13.44	4.25	17.33
0.55	3.59	1.80	8.60	3.05	13.64	4.30	17.42
0.60	3.92	1.85	8.77	3.10	13.85	4.35	17.52
0.65	4.27	1.90	8.95	3.15	14.04	4.40	17.61
0.70	4.62	1.95	9.13	3.20	14.24	4.45	17.70
0.75	4.97	2.00	9.32	3.25	14.43	4.50	17.79
0.80	5.30	2.05	9.51	3.30	14.62	4.55	17.87
0.85	5.61	2.10	9.70	3.35	14.81	4.60	17.95
0.90	5.89	2.15	9.90	3.40	14.99	4.65	18.03
0.95	6.14	2.20	10.10	3.45	15.17	4.70	18.10
1.00	6.35	2.25	10.30	3.50	15.34	4.75	18.18
1.05	6.52	2.30	10.50	3.55	15.51	4.80	18.25
1.10	6.68	2.35	10.71	3.60	15.67	4.85	18.32
1.15	6.81	2.40	10.92	3.65	15.82	4.90	18.39
1.20	6.94	2.45	11.13	3.70	15.98	4.95	18.45
1.25	7.05	2.50	11.34	3.75	16.12	5.00	18.52

Chapter 5

I   Introduction

The determination of the main sequence luminosity function requires the definition of statistically complete samples of stars with well calibrated absolute magnitudes providing representative samples of the local stellar populations. The only direct method of distance determination is by trigonometric parallax. However, accurate parallax measurements are time consuming and limited to bright (V <~16) stars and, as a result, are available for a comparatively restricted number of stars. Hence studies of the luminosity function have come to rely on indirect methods of absolute magnitude determination, which are more easily applied to large stellar samples.

Two of these methods in particular have been extensively used. Proper motions can be determined with comparative ease for many objects, and Luyten has used the relation between reduced proper motion and absolute magnitude (the method of mean absolute magnitudes; Luyten, 1925) to analyse the results of several large scale surveys, notably the Palomar Schmidt automated survey (Luyten, 1963b). As described further below, distance is calibrated from mean tangential motion i.e. a statistically defined group property. More recently, automated photometry of multicolour UKST plates

described in Section 4 and discussed in Section 5.

II   The Luyten Luminosity Function

The method of mean absolute magnitudes was first outlined by
Luyten (1925) and has been described in the literature several times since
(Trumpler & Weaver, (1953), McCuskey (1966), Wanner (1972)). Thus only a
brief resume is given here. The reduced proper motion can be defined as

$$H = m + 5 + 5 \log \mu$$

or

$$H = M - 3.378 + 5 \log v_t \qquad (1)$$
$$\text{for } v_t \text{ in km/sec.}$$

Thus if the local stellar population can be characterised by a
single tangential velocity, H is linearly related to the absolute
magnitude. In a real stellar population there is a large range in v_t at any
luminosity. However, Wanner (1964) has shown that there is a most probable
value of the tangential velocity if stellar velocities follow the
Schwarzschild (1907) ellipsoidal velocity distribution. Hence H can be
empirically related to M and used as a statistical absolute magnitude
calibrator. Observational errors in μ will produce a Malmquist-type bias
due to the higher numbers of low proper motion objects. However, both this
systematic effect and the random errors introduced by measuring error
(σ_μ ~0".025) are small, since $\log \mu$ is typically ~-0.6. Thus while $\mu > \mu_{lim}$
defines the sample, the apparent magnitude is the prime factor in
determining H.

described in Section 4 and discussed in Section 5.

II The Luyten Luminosity Function

The method of mean absolute magnitudes was first outlined by Luyten (1925) and has been described in the literature several times since (Trumpler & Weaver, (1953), McCuskey (1966), Wanner (1972)). Thus only a brief resume is given here. The reduced proper motion can be defined as

$$H = m + 5 + 5\log \mu$$

or

$$H = M - 3.378 + 5\log v_t \qquad (1)$$

for v_t in km/sec.

Thus if the local stellar population can be characterised by a single tangential velocity, H is linearly related to the absolute magnitude. In a real stellar population there is a large range in v_t at any luminosity. However, Wanner (1964) has shown that there is a most probable value of the tangential velocity if stellar velocities follow the Schwarzschild (1907) ellipsoidal velocity distribution. Hence H can be empirically related to M and used as a statistical absolute magnitude calibrator. Observational errors in μ will produce a Malmquist-type bias due to the higher numbers of low proper motion objects. However, both this systematic effect and the random errors introduced by measuring error (σ_μ ~0".025) are small, since $\log \mu$ is typically ~-0.6. Thus while $\mu > \mu_{lim}$ defines the sample, the apparent magnitude is the prime factor in determining H.

The magnitude calibration is usually derived from stars of known trigonometric parallax, with the relation in the form

$$\langle M \rangle = a + bH \qquad (2)$$

Luyten (1938b) finds $\quad \langle M \rangle = -3.5 + 0.86 \, H$

This method therefore assumes that the distribution of tangential motions of the calibrators is identical with that of the programme stars. Were all stars in the Galaxy members of a single kinematic population, choosing parallax calibrators to cover the same range of m and μ as the programme stars would ensure that this were the case. However, there are at least three major kinematic stellar populations locally - the disk, the extreme halo or spheroid (hereafter referred to as the halo) and Intermediate Population II component (hereafter IP II) - while the stars calibrating the (M, H) relation are virtually all low space motion disk stars. The influence of the higher velocity constituents on deep proper motion surveys has hitherto not been fully appreciated.

Halo stars have approximately five times the space motion of disk stars (~150 km/sec as compared with ~30 km/sec). Thus if a sample is kinematically defined (by proper motion) the distance limit for detection of a halo subdwarf exceeds that of a disk dwarf by a factor of five - corresponding to a sampling volume increase of more than an hundredfold. These increased sampling volumes will compensate, at least in part, for the

overall lower absolute space densities.

This argument, however, does not apply if the proper motion survey is magnitude limited so as to exclude the distant halo stars. To estimate when halo contamination is important, consider a uniform space density population with characteristic tangential velocity V_t sampled by a proper motion survey to $\mu > \mu_{lim}$. Since the sampled volume increases with the cube of r, to first order all stars detected are at

$$r \sim r_{max} = \frac{V_t}{k \, \mu_{lim}} \quad , \quad k = 4.738$$

(r in parsecs, V_t in km/sec)

Thus stars detected have apparent magnitude

$$m = M + 5 \log r_{max} - 5 = M + f$$

and so the number of stars detected in the range $m + 1/2$ to $m - 1/2$ reflects the space density of stars of absolute magnitude $m - f$ i.e.

$$N(m) = \Phi \, (m-f) \, r_{max}^3 \qquad (3)$$

For a mix of two stellar populations, where the second population

has a characteristic velocity

$$V_2 = c\ V_1$$

and a luminosity function (LF)

$$\Phi_2 (M) = n\ \Phi_1 (M)$$

i.e. similar in shape, but with a different absolute zero point, then the population number ratio at apparent magnitude m is simply

$$\frac{N\ (m)}{N\ (m)} = \frac{\Phi_1\ (m-f)}{\Phi_1\ (m-f-5\log c)}\ \frac{1}{nc^3}$$

Taking the specific case of disk and halo as populations 1 and 2 respectively, n ~ 0.5 percent (Table 5.1), c ~ 5 so nc^3 ~ 1, and assuming similar LFs, then

$$\frac{N_H\ (m)}{N_D (m)} = \frac{\Phi_D\ (m - 6.0)}{\Phi_D\ (m - 2.5)}$$

If the halo LF can be represented by a scaled version of the disk function derived in Paper II , $N_H = N_D$ at V ~ 17. Thus proper motion surveys limited to bright apparent magnitudes (e.g. the Lowell Observatory Survey (Giclas et al., 1972)) consist largely of disk dwarfs, but the deeper (V >~20) Schmidt surveys by Luyten include substantial numbers of halo stars at faint apparent magnitudes. Taking disk dwarfs and halo subdwarfs of the same absolute magnitude (M_t), the mean value of H for these two subsets is related by

$$H_{halo}(M_t) \sim H_{disk}(M_t) + 3.5$$

Table 5.1

Source	Definition	Absolute magnitude range	halo-to-disk number ratio
Schmidt (1975)	kinematics	$4 < M_v < 12$	0.1 percent
Fenkart (1977)	uv excess	$3.5 < M_v < 7$	2 - 6 percent
Eggen (1979a)	UV kinematics	$5 < M_v < 9$	0.25 percent
Chiu (1980)	kinematics	$4.5 < M_v < 9.5$	0.5 - 0.6 percent
Bahcall, Schmidt & Soneira (1982)	star counts	$4 < M_v < 8$	0.15 percent

Determinations of the local halo star density

Applying Luyten's calibration of H against M , if M_H is the absolute magnitude derived from (2), then for stars of the same intrinsic absolute magnitude

$$M_H \text{ (halo)} = M_H \text{ (disk)} + 3$$

Apparent magnitudes fainter than V ~ 17 imply H > 18, giving M_v > +12. The net result is to enhance the inferred space density of low luminosity stars - the exact discrepancy described above.

This quantitative prediction rests on a simplified analysis which ignores a number of potentially significant factors, notably the presence of the intermediate velocity IP II. Furthermore, the extent of the halo star contribution is dependent on both the local number density and the kinematics of this population - neither of which, as Tables 5.1 and 5.2 illustrate, is unambiguously defined. A large part of this apparent uncertainty arises through the different combinations of kinematic and/or metallicity criteria that are used to define what constitutes a halo subdwarf. While Schmidt (1975b) and Chiu (1980a) select by high tangential motion, Becker (1980), Fenkart (1977, 1980) and the other members of the Basle group use solely metallicity-based criteria - ultraviolet excess in the (R-G) - (G-U) two colour diagram. Oort's (1965) estimate of the number density is also metallicity based since it used Joy's (1947) spectral classification of nearby (r < 5 parsecs) K and M dwarfs. On the other hand, Eggen (1976a, 1979b) and Sandage (1981) use a combination of both parameters, while the deep number magnitude star counts employed by Bahcall, Schmidt and Soneira (1982) essentially represent a kinematic definition. Similar problems arise in defining IP II.

Given such a wide range of possible parameters we have used

numerical simulations of the local stellar spatial and kinematic
distribution to investigate the proportion of non-disk stars included in
proper motion surveys. The results from these models, and hence the most
likely input parameters, can be assessed by comparing their predictions
with observations in a number of ways. First, through the distribution in
the (U, V) velocity plane; second, number magnitude counts of proper motion
stars ; third, the distribution in the (H, colour) or reduced proper motion
diagram (RPMD); and, finally, through using (U-B) excess to derive the
metallicity distribution. Thus the models aim to define populations
consistent with both the observed kinematic and metallicity distributions.

3 Population Models

Four components from three populations are explicitly considered
in the simulations - disk main sequence; disk white dwarfs; the IP II ; and
halo subdwarfs. In modelling each component, the luminosity function and
density law (an exponential perpendicular to the Plane for all save the
halo) are specified a priori, as are the solar motion and velocity
dispersions. It is assumed that the latter quantities are described by
Schwarzschild's (1907) equation

$$N(U,V,W) = \frac{N_o}{\pi^{3/2} \sigma_U \sigma_V \sigma_W} \exp \left\{ \frac{-(U-U_o)^2}{\sigma_U^2} - \frac{(V-V_o)^2}{\sigma_V^2} - \frac{(W-W_o)^2}{\sigma_W^2} \right\}^{\frac{1}{2}}$$

where U, V and W are the Galactic velocity axes directed towards the Galactic Centre, in the direction of Galactic rotation and perpendicular to the Galactic Plane respectively. The effects of vertex deviation are small and are not included.

While the input parameters for each population are discussed in detail below, the modelling techniques employed are identical for all. Each simulation is carried out for a specified direction (l,b). The component of solar motion (V'_Θ) is calculated and a distance limit defined where a star with tangential velocity

$$V_t = V'_\Theta + (\sigma^2_U + \sigma^2_V + \sigma^2_W)$$

has a projected motion corresponding to a pre-specified cutoff. 10,000 "stars" of a given absolute magnitude are generated within this distance, uniformly distributed within the volume. The tangential velocities are calculated from U, V and W components generated from Gaussian distributions of the requisite dispersion, and the "stars" with motions and apparent magnitudes above the sample limits are retained. Their contribution is then normalised using both the density law to allow for the non-uniform spatial distribution and the prescribed luminosity function to set all counts on the same scaling. Individual colours are taken randomly from a Gaussian distribution with dispersion 0.1 magnitude, to allow for cosmic dispersion in the H-R diagram. Finally the kinematic stellar luminosity function is calculated using equation (2) and Luyten's calibration.

Although density law variations are included, all of the models used are limited either to bright apparent magnitudes or to high proper motion limits i.e. relatively nearby stars. Thus the model uncertainties are dominated by those implicit in the LFs and kinematics of the individual

components which are discussed below.

a) The Disk

Apart from Luyten's proper motion derived functions, the most extensive determinations of the disk main sequence (DMS) LF are by McCuskey (1956, 1966) and Wielen (1974). The results of these studies are in good agreement for stars brighter than $M_v \sim +10$. Space densities of fainter stars are taken from the photometric studies in Papers I and II (normalised to z=0 following Gilmore & Reid (1982) - paper III). Main sequence stars and disk giants brighter than +1 are of negligible space density and are not specifically considered.

Each absolute magnitude range in the disk population has an associated solar motion and set of velocity dispersions in the simulation. These have been taken from Delhaye (1965), Wielen(1974) and Upgren (1978), interpolating where necessary. It is of course a considerable simplification to characterise all stars of the same luminosity by one set of motions. In particular, both Upgren and Wielen have shown that there is a substantial range of motions amongst the K and M dwarfs, with the oldest stars possessing the highest velocity dispersions. To test the importance of this, we subdivided stars fainter than $M_v = +5$ (i.e. with lifetimes greater than the age of the disk) into six velocity groups, using Wielen's Ca II HK emission classes to set the relative numbers and motions. Implicit in this are the assumptions of a single initial mass function throughout the history of disk star formation, which is reasonable (Miller and Scalo, 1979), and, less justifiably, that the relative velocity dispersions at

given M_v can be scaled relative to the overall mean following the ratios defined by the McCormick dwarfs. In the event this internal segregation produces changes at the 1 percent level in the number of disk dwarfs detected, and is consequently not a significant uncertainty.

For disk white dwarfs (DWD) the LFs derived by Sion and Liebert (1977), Liebert (1980) and Green (1980) have been combined to give a mean function covering the range $+9 < M_v < +15$. The uncertainties in this are considerable - in particular fainter than $+13$ where the separate functions differ by nearly a factor of ten. However, since the simulations show that relatively small numbers are detected, and given the characteristic position of these stars on the RPMD, this does not affect the major aims of this study. The kinematics adopted for these stars - applying to all M_v - have been calculated by taking weighted means of all the values quoted in Table I of Sion and Liebert.

As discussed above, the distance limit of the simulated sample is set kinematically. With the proper motion limit of the NLTT catalogue (Luyten 1981) and the adopted velocities, this corresponds to a distance of ~80 parsecs for both disk populations. Hence we have allowed for the decrease in number density with height above the plane by incorporating exponential density laws. For DMS stars the scale heights are taken from the empirical determinations in Paper III (300 parsecs for $M_v > +4$, 100 parsecs for intrinsically brighter, younger stars). For DWD a scale height of 400 parsecs has been adopted. The maximum density decrease is less than 25 percent for simulations towards either of the Galactic poles.

Finally, the colour magnitude relations adopted for the DMS are taken from Paper II and are based on nearby dwarfs with good trigonometric parallaxes. Hence all of the colours quoted are on the Kron-Cousins system. The DWD (M_V, (B-V)) is taken from Chiu (1980a), while (V-I) colours have been determined from the two-colour relation presented by Liebert (1980).

b) The Extreme Halo

As described above, the local density of halo subdwarfs is not unambiguously established. Similarly the shape of the luminosity function is not well defined. Globular cluster luminosity functions are steeper than the disk function brighter than $M_V \sim +4.5$ (i.e. above the turnoff in the colour magnitude diagram) and appear to flatten fainter than $M_V \sim +7$ (M92, Hartwick, 1970, van den Bergh, 1975; NGC 6397, da Costa, 1982). The steepening at bright magnitudes should also be present in the halo since it is of comparable age. On the other hand, while the luminosity function derived by Eggen (1976a) from field stars shows flattening at faint magnitudes, Chiu (1980b) finds that number densities increase monotonically to $M_V \sim +11$. Furthermore, da Costa has shown that cluster luminosity functions differ significantly in shape at fainter absolute magnitudes. Hence to cover the full range of possibilities, three types of halo LFs have been included in the computations. These comprise a function flat for $M_V > +7$ (cf. M 92 - denoted HG); Chiu's observational determination from SA 57 and SA 68 (HC); and a function identical in shape with the disk LF

i.e. including a GK dwarf deficity (HW). All functions are truncated brighter than $M_v = +4$, the absolute magnitude corresponding to the main sequence turnoff of most globular cluster colour magnitude diagrams. As with the Disk, the space densities of evolved stars are so low that their contribution is not significant.

Halo stars of all magnitudes are assumed to belong to one kinematic group. Solar motions have been derived by Notni (1956), and van Herk (1965) using the motions of RR Lyraes; by Kinman (1959) from globular cluster radial velocities ; and by Parenago (1951) and Carney (1979b) from field subdwarfs. Finally, following Chiu, the halo can be assumed to have no rotation and the solar motion calculated by combining the basic solar motion (Delhaye, 1965) with the circular rotational velocity of the local standard of rest (taken from Gunn et al, 1979). These values are shown in Table 5.2a, together with the dispersions quoted by Parenago, van Herk, Oort (1965), Notni, Wielen (1974) and Woolley (1978).

Both Parenago's and Carney's determinations use a substantial number of field subdwarfs – although it is not clear that either sample is kinematically unbiased. Even though the latter sample is defined photometrically, kinematic biases may exist in the original catalogue from which the stars were selected. Carney's higher value of V_0 is more in line with other recent kinematic studies of the halo.

The velocity dispersions fall into three broad categories. The lowest values are those determined by Wielen and Parenago from field

Table 5.2

a

	$U_\odot$	$V_\odot$	$W_\odot$	σ_U	σ_V	σ_W	
Parenago(1951)	0	136	10	100	75	50	subdwarfs
Notni (1956)	0	217	23	160	101	122	RR Lyraes
Kinman (1959)	0.2	167	12				globular clusters
van Herk (1965)	34	184	26	155	105	77	RR Lyraes
Oort (1965) a)	15	207	15	210	119	91	RR Lyraes
b)		183		172	91	66	extreme subdwarfs
Wielen (1974)				100	80	65	subdwarfs
Woolley (1978)				150	120	80	RR Lyraes
Carney (1979b)	6	176	-1				
No rotation	9	231	6				

b

	$U_\odot$	$V_\odot$	$W_\odot$	σ_U	σ_V	σ_W
(i)	6	176	-1	100	80	65
(ii)	6	176	-1	150	120	80
(iii)	15	207	15	210	119	91
(iv)	9	231	6	210	119	91

a) Solar motions and velocity dispersions of halo objects

b) Halo kinematics adopted in models (see text for details)

subdwarfs, although since the former sample consists of only eight stars
the agreement may be fortuitous. Higher dispersions ($\sigma_U \sim$ 150 km/sec)
have been derived by Notni, van Herk and Woolley from solar neighbourhood
RR Lyrae motions, and similar values were obtained by Oort from a sample of
extreme subdwarfs. However, Oort's analysis of RR Lyrae space motions
resulted in significantly larger dispersions. Schmidt (1975b) adopted the
kinematics from Oort's study as characteristic of the halo, and the
consequences of this are discussed below.

On the whole the RR Lyrae motions are statistically better
defined, but it is not obvious that this subgroup, largely consisting of
distant stars at high z, accurately reflects the overall motions of the
extreme population II locally. Thus in order to allow for the full range of
possible velocities, four basic combinations of parameters from Table 5.2
have been considered and are listed in Table 5.2 b).

The halo counts are corrected for number density variations with
distance using Gilmore's (1981) model d) density distribution - i.e. a
galactocentric power law, index -3.0, with the solar Galactic radius taken
as 8.35 kpc (Caldwell & Ostriker, 1980). This is the halo density law
derived by Oort & Plaut (1975) from the RR Lyrae distribution. However,
since the maximum cutoff distance for $\mu = 0".2$ is only ~450 parsecs, the
density variation is less than 2 percent for the Galactic directions
considered here.

The halo $(M_V , (B-V))$ relation has been constructed by combining
Chiu's SD2 sequence $(M_V < +10)$ with photometry of fainter parallax

subdwarfs by Upgren and Weis (1975). The latter observations, together with photometry by Eggen (1973, 1976b) and Rodgers and Eggen (1974) have been used to define the (B-V)-(V-I) relation, converting all of the data onto the Kron-Cousins system using the relations given by Bessell (1979). Subdwarfs redder than (V-I)=2.7 (M_V = +13) are assumed to follow the disk (V-I) relation (Bessell and Wickramasinghe, 1979).

c) Intermediate Population II

The properties of the final stellar population included in the simulations are even less well known than those of the halo. The existence of a Galactic stellar component possessing kinematics and chemical abundance characteristics intermediate between halo and disk was first suspected through Stromgren's uvby observations of F stars (Stromgren, 1964). Further studies (Stromgren, 1976; Crawford et al, 1979; Hill et al, 1979) suggest that between 7 and 10 percent of A and F stars belong to this metallicity defined ($-0.4 <$ [Fe/H] < -1.0) stellar grouping. This abundance range is consistent with that of the metal rich ($\Delta S < 5$) RR Lyraes, which are identified as intermediate population stars on kinematic grounds by Oort (1965).

More recently, surface photometry of edge-on spirals has revealed the presence of this component as a thickened disk (van der Kruit & Searle, 1981a,b), interpreted as the response of the halo to the gravitational potential of the disk. This component is very similar morphologically to the so-called "thick disk" found in S0 galaxies by Burstein (1979). In Paper III it was shown that above z ~ 1 kpc, and to at

least z = 4 kpc, the dominant stellar population follows a density law consistent with either a Galactocentric oblate spheroid of axial ratio 4:1, or an exponential disk, scale height ~1400 pc. Both models predict absolute number densities of ~2 percent of DMS at z=0, and both are consistent with an intermediate population with velocity dispersion perpendicular to the disk of ~60 km/sec. The luminosity function of this stellar component resembles an evolved population, being steeper than the DMS for M_V < +5, but similar thereafter to at least M_V ~ +7 (Paper III, figure 4b). It is not clear, however, whether the function mimics the disk GK dwarf deficit, since the observations are limited to M_V < +7.5. Thus the same three options for the shape of the halo - scaled DMS, a scaled version of the HC LF and a cluster-type LF - have been employed here.

As to the normalisation of the scaling parameter adopted, there is a direct contradiction between the projected local density of 2 percent DMS found from the SGP number counts and the observed ratio of 7-10 percent found from Stromgren photometry. However it should be emphasised that these two intermediate populations are defined by different criteria - the SGP sample by their kinematics; Stromgren's IP II by δm_1 i.e. metallicity. In fact, using Twarog's (1980) disk age-metallicity relationship Stromgren's intermediate population component amongst the later-type F stars is most plausibly interpreted as the older components of the old disk. On the other hand, given the main sequence lifetime of A stars, Stromgren's results imply significant recent metal poor star formation. In either case Stromgren's IP II represents a subset of the disk. The simulations described here deal with the kinematically defined intermediate population, which we regard as a separate Galactic entity (albeit with possibly the same origin as the halo).

While the w velocity dispersion can be inferred from the observed density laws of the kinematic IP II, identifying the correct U and V dispersions and solar motions poses more of a problem, through lack of direct observations. Blaauw and Garmany (1976) derived dispersions of 37 km/sec and 36 km/sec in U and V respectively from a sample of F stars with $0.080 > \delta m_1 > 0.040$ taken from the McCormick fields. Results described in later sections show that less than half of the more metal-poor kinematic IP II lie within this definition, and the inclusion of disk stars biases the derived values towards lower velocities.

Similarly, although Oort (1965) identifies the metal rich RR Lyraes with IP II, the w-dispersion calculated by Notni (1956) is only 23 km/sec. Furthermore, Oort's velocity analysis of the metal poor RR Lyraes ($\Delta S > 5$) indicated that a high proportion of these stars had intermediate kinematics. This implies that the kinematic IP II is significantly more metal poor than as defined by Stromgren (see Section 4.1), and that the metal rich RR Lyraes also include a substantial number of old disk stars, as suggested by Butler et al (1979) and Taam et al (1976).

The second stellar component classified as IP II by Oort is the group of long period variables with $P < 300$ days. Theoretical studies by Wood and Cahn (1977) have shown that the initial main sequence mass of these stars lies in the range ~1.0 to 1.1 solar masses, implying ages of more than 8×10^9 years (Iben, 1967). This is borne out by the kinematical studies of Osvalds and Risley (1961) and Clayton and Feast (1969), which show the variables to be confined nearer the Plane with increasing period. Both analyses use the same data. Osvalds and Risley derive a solar motion

similar to Notni's result for the solar motion of RR Lyraes. Feast (1968) has

Table 5.3

Solar Motion

	$U_\odot$	$V_\odot$	$W_\odot$	
Notni	47 km/sec	30 km/sec	5 km/sec	RR Lyraes
Osvalds & Risley	30	35	9	LPV, P < 300 days
Feast	-4	23	30	SR , P < 149 days
	33	110	-7	LPV, 149 < P < 200
	-10	51	5	LPV, 200 < P < 250
	2	23	-4	LPV, 250 < P < 300

similar to Notni's results for the short period RR Lyraes. Feast (1963) has also determined solar motions for long period variables, grouping the stars in different period intervals (Table 5.3), with the results showing an apparent discontinuity near periods of ~250 days. Support for an IP II solar motion in this region of the (U,V) plane also comes from Eggen's diagrams for high velocity stars (Eggen, 1964) and from his sample of local "halo" stars (Eggen, 1979b; figure 5), both of which show a distinct concentration of moderate ultraviolet excess objects near this point.

In order to take observational uncertainties fully into account, two sets of IP II kinematics have been used in the simulations - Notni's RR Lyrae motions (hereafter RR) and the Osvalds and Risley LPV solar motions together with weighted mean dispersions for the same stars from Clayton and Feast (σ_U = 67 km/sec, σ_V = 57 km/sec, σ_W = 48 km/sec; hereafter LPV).

Finally, the absolute magnitude colour relations adopted lie midway between those of the disk and the halo. This represents an uncertainty of less than 0.05 magnitudes throughout the complete range of (B-V), but may be in error by up to 0.2 magnitudes in (V-I) for $M_v > + 7$.

4   Results

4.1 Observational Sample

We have used observations of well defined samples of proper

motion stars to constrain the models in order to determine the best fit parameters describing the density and kinematics of the halo and IP II. A sample of bright apparent magnitude stars has been drawn from Eggen's (1976b) observations of all known proper motion stars within ten degrees of the South Galactic Pole with V < 15.0 and μ > 0".096 (the ESGC sample). Calibrating absolute magnitudes by photometric parallax (B-V), Eggen has derived U and V velocities from the observed proper motions. Eggen's subdwarf sequence differs from Chiu's in joining the main sequence over the range 0.5 < (B-V) < 0.6, so for subdwarfs with (B-V) < 0.55 we have used Chiu's SD2 sequence to calibrate absolute magnitude. The (U-B) excess relative to the Hyades main sequence, corrected for the "guillotine effect" (Sandage, 1969), $\delta(0.6)$, provides metallicity calibration. To ensure a high degree of completeness we have limited our sample to B < 14.25 and to stars within the absolute magnitude range 4.75 < M_V < 8.75 (~5.5 < M_B < 10.0). However, although the sample is complete in the sense that all stars detected in proper motion surveys are included, allowance must be made for incompleteness in the surveys themselves.

The South Galactic Cap has been surveyed for stars of relatively large motion a number of times - notably by Luyten (1938a), Luyten and La Bonte (1973) and Giclas et al. (1969). For this reason we assume that all stars with μ > 0".2 are included. However, the main source of lower proper motion stars is the Bruce survey (BPM - Luyten, 1938a) which is known to be incomplete - especially within the magnitude range considered here (Luyten, 1938b). We have therefore adjusted the observed number magnitude counts using the incompleteness estimates given by Luyten (50 percent complete brighter than m(pg) = 12.5; 67 percent complete for 12.5 < m(pg) < 14.5). Luyten does not state the accuracy of these estimates.

The measured motions are accurate to better than 0".025 (Luyten, 1977a), corresponding to maximum errors of 25% in the tangential velocity of stars in the ESGC sample. However, for most purposes the importance of the proper motion limit is in defining the sample and the random errors in the individual motions are not important. A further consideration is that the observed motions are relative, measured with respect to "stationary" fainter stars, while the simulation produces number counts based on absolute motions. The plates used in the BPM survey are typically limited at m(pg) ~ 16, at which magnitude the typical star is a K dwarf (M(pg) ~ 7). For a solar motion of ~ 20km/sec and a typical baseline of 25 to 30 years, the correction to absolute motion is ~0".015. The corresponding adjustment to the simulations produces no changes of any significance.

Deeper samples are drawn primarily from the Luyten-La Bonte Survey (1973). The SGC sample has been defined by selecting all stars from this survey within the range 22 hour to 0 hours in Right Ascension, giving ~2500 stars with μ > 0".18. Using 139 stars in common between the NLTT and LHS catalogues and the USNO parallax star lists (Harrington and Dahn, 1980), m(r) is converted to V magnitude by

$$V = 1.09 \, m(r) - 0.90, \quad \sigma_v = 0.5$$

Luyten estimates this survey to be "reasonably complete" to a photographic magnitude of 21. Thus the number counts discussed below should be complete to V ~ 19. A smaller subset of faint proper motion stars, consisting of all known proper motion stars within the UKST South Galactic Pole field (SGP sample) has also been used. As described in previous papers (II, III) we have well calibrated photographic photometry of all stars with V ~20 in this field, so all of these possess accurate BVI magnitudes, and hence

accurate reduced proper motion diagrams can be constructed.

4.2 Model Predictions

Since the kinematics of each stellar population in the model are specified a priori, the consistency with observations can be tested through both the distribution in the (U, V) plane and the metallicity range in different sections of the plane. Since the ESGC sample is relatively small, a simple statistical comparison represents the best method of assessment. One useful technique is by using Eggen's classification of stars as "disk" or "halo" - that is, stars lying respectively inside or outside the ellipse in the (U, V) diagram defined by Galactic orbits of eccentricity e=0.42 in the ELS Galactic mass model(Eggen, Lynden-Bell and Sandage (1962)). This effectively gives the number ratio between high and low velocity stars, R_{obs}. This ratio is only slightly affected by the incompleteness corrections mentioned above - which reduce R_{obs} from 0.18 to 0.16.

R can be predicted for each model. If the fraction of IP II stars classed as Eggen "disk" is 'a', while the fraction of halo stars within the ellipse is 'b', then since the disk kinematics place all disk stars within the ellipse,

$$R(pred.) = \frac{(1-b)N(halo) + (1-a) N(IP\ II)}{b\ N(halo) + a\ N(IP\ II) + N\ (disk)}$$

where N(halo), N(IP II) and N(disk) are the absolute
contributions to the sample from halo, IP II and disk respectively. In the
calculations these are all expressed as number ratios with respect to the
disk (Table 5.4). 'b' varies only slightly with the input halo kinematics -
from 0.08 with type (i) to 0.11 with type (iv) - while 'a' is ~0.95 with RR
IP II motions and ~0.85 with the LPV IP II kinematics.

With most of the intermediate population included with the
"disk", the metallicity distribution and kinematics within this subset can
be expected to be closely dependent on the density normalisation adopted.
Adopting Stromgren's (1976) value of 7 percent disk number density predicts
an IP II to disk number ratio of between 0.43 (RR Lyrae motions) and 0.51
(LPV), as opposed to the 0.12 to 0.15 expected with the SGP normalisation.
Although the IP II is probably metal poor, the exact range of abundance is
not known. However, the overall metallicity distribution expected amongst
disk K dwarfs can be determined from Wielen's (1974) analysis of the
stellar age distribution in the solar neighbourhood, together with the mean
age-metallicity relationship (Twarog, 1980). Sampling by volume, ~70
percent of the local disk dwarfs have near solar abundances (Table 5.5).
However, the data here are not from a volume-complete sample, and since the
older dwarf subgroups described by Wielen also possess substantially higher
velocity dispersions, there is a preferential selection of the older, metal
poor disk in the ESGC sample, as illustrated in column 5 of Table 5.5. As
emphasised above, the overall proportion of disk stars detected is not
affected.
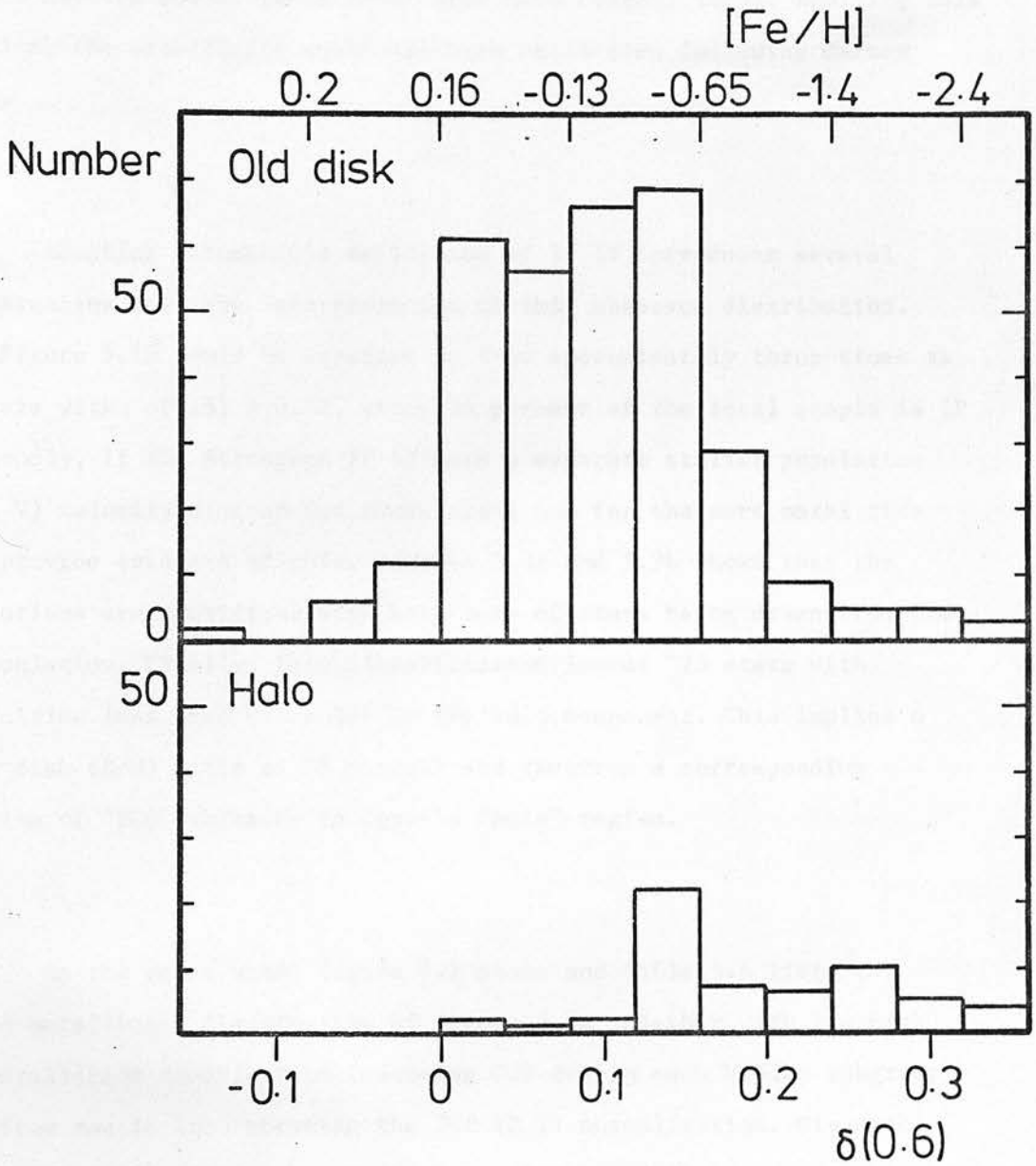
Figure 5.1 - Metallicity distribution of "disk" (figure 1a) and "halo" (figure 1b) stars from the ESGC sample.

Figure 5.1 shows the $\delta(0.6)$ distribution of both the "disk" and "halo" stellar samples. Eleven stars lacking δ (0.6) measurements have been omitted from the distribution. Eggen quotes photometric errors of less than 0.035 in (U-B), and a comparison of his system with Cousins' photometry shows that there is a systematic difference of ~0.02 in the sense C-E for the colour range considered here (Eggen, 1975). Applying this correction, the metallicity scale has been calibrated following Carney (1979a).

Adopting Stromgren's definition of IP II introduces several inconsistencies into the interpretation of this observed distribution. First, Figure 5.1a would be expected to show approximately three times as many stars with $\delta(0.6) > 0.12$, since 35 percent of the total sample is IP II. Secondly, if the Stromgren IP II were a separate stellar population, the (U, V) velocity diagram for these stars and for the more metal rich should provide evidence of this. Figures 5.3a and 5.3b shows that the distributions are consistent with both sets of stars being drawn from the same population. Finally, this classification leaves ~25 stars with metallicities less than 0.1 solar as the halo component. This implies a halo to disk (H/D) ratio of ~3 percent and requires a corresponding population of ~200 subdwarfs in Eggen's "halo" region.

On the other hand, figure 5.2 shows and Table 5.6 lists the observed metallicity distribution of figure 5.1a together with the disk dwarf metallicity distribution (assuming 0.2 dex in each Wielen subgroup) scaled from models incorporating the SGP IP II normalisation. Given the uncertainties (especially the sample incompleteness) the data are consistent with old disk stars forming the bulk of the sample (virtually
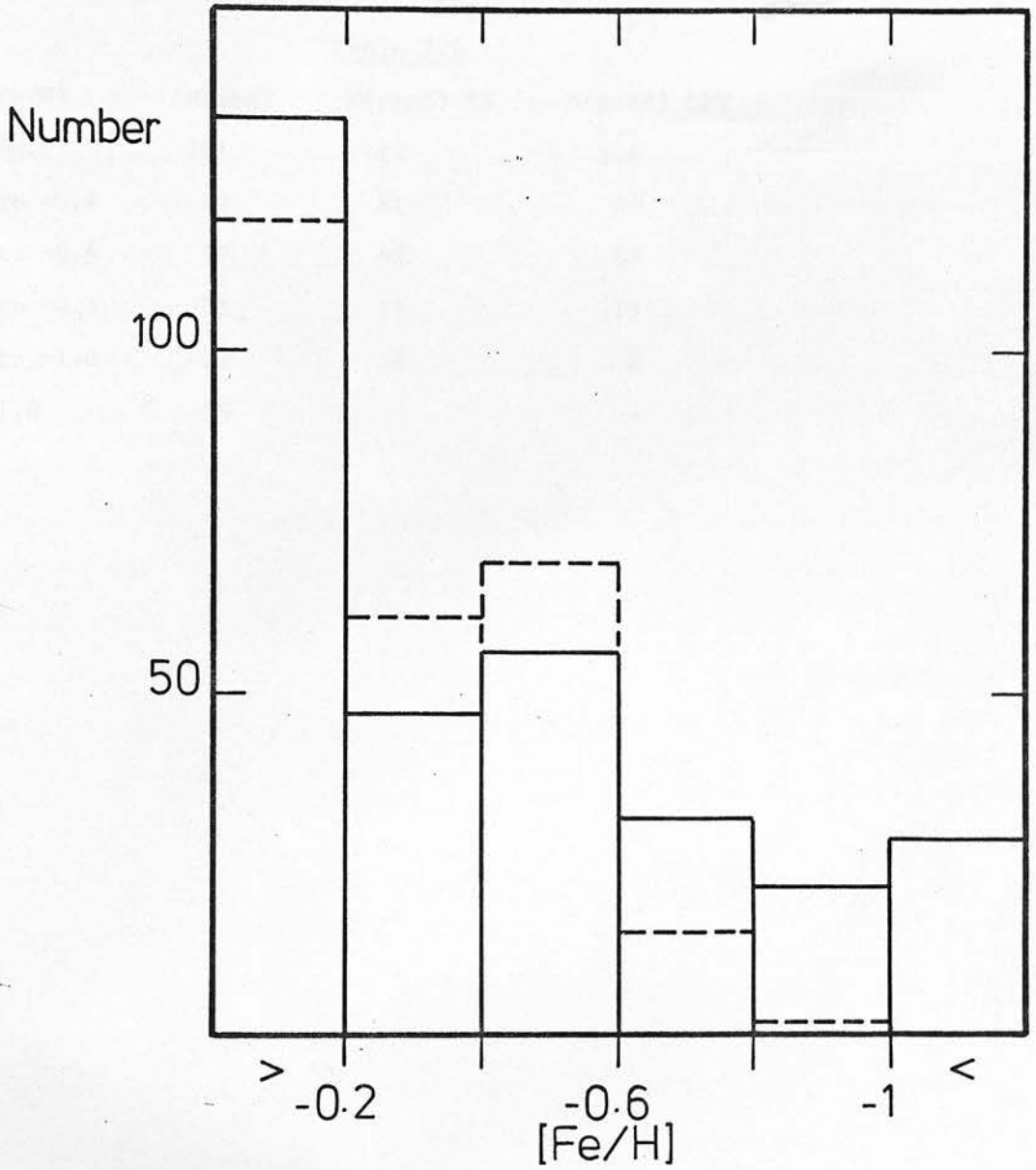
Figure 5.2 Predicted disk metallicity distribution (dashed line) and observed distribution for ESGC "disk" stars. Note that the two most extreme bins include all stars with [Fe/H] < -1.0 and [Fe/H] > -0.2 respectively.

Table 5.6

[Fe/H]	N(obs)	N(pred) RR	N(pred) LPV
> -0.2	135	119	116
-0.2 to -0.4	47	61	59
-0.4 to -0.6	57	69	67
-0.6 to -0.8	32	15	15
-0.8 to -1.0	22	2	2
< -1.0	29		

all stars with $\delta(0.6) < 0.2)$ with IP II and a few halo subdwarfs
contributing the metal poor tail. Figure 5.3c shows that the (U,V)
distribution of these metal poor stars is clumped around the the proposed
IP II solar motion.

With this normalisation for the local IP II density, the H/D
number ratio can be computed using R. However, figure 5.1b shows that a
number of these stars are only moderately metal poor, with abundances
corresponding to the old disk. In the (U, V) plane the metal rich
"subdwarfs" show the same spread in U, but less dispersion in V than the
rest of the metal poor stars - although if these dwarfs are less
subluminous than Eggen's subdwarf sequence their distances and velocities
have been underestimated. No disk dwarfs of such high velocity are expected
from Wielen's McCormick dwarf dispersions. However, given the sample size
it is possible that σ_v has been underestimated for the oldest dwarfs, and
we have adopted the assumption that the stars are old disk. Applying the
appropriate correction reduces the observed value of R by approximately a
third and could therefore lead to an underestimate of the halo number
density by the same amount.

Values of R_{pred} have been calculated for the various halo motions
described in Section 3 using either Chiu's LF (HC in Table 5.4) or a scaled
version of Wielen's disk LF (HW). The results are shown in Table 5.4. Since
the HW function is on an arbitrary scaling, the quantity tabulated is the
overall H/D ratio (with a formal accuracy of 0.02 percent) which
reproduces the observed distribution. Chiu's LF, however, is expressed in
absolute terms so that the value listed is the ratio between the required
number density and Chiu's prediction. These ratios are insensitive to
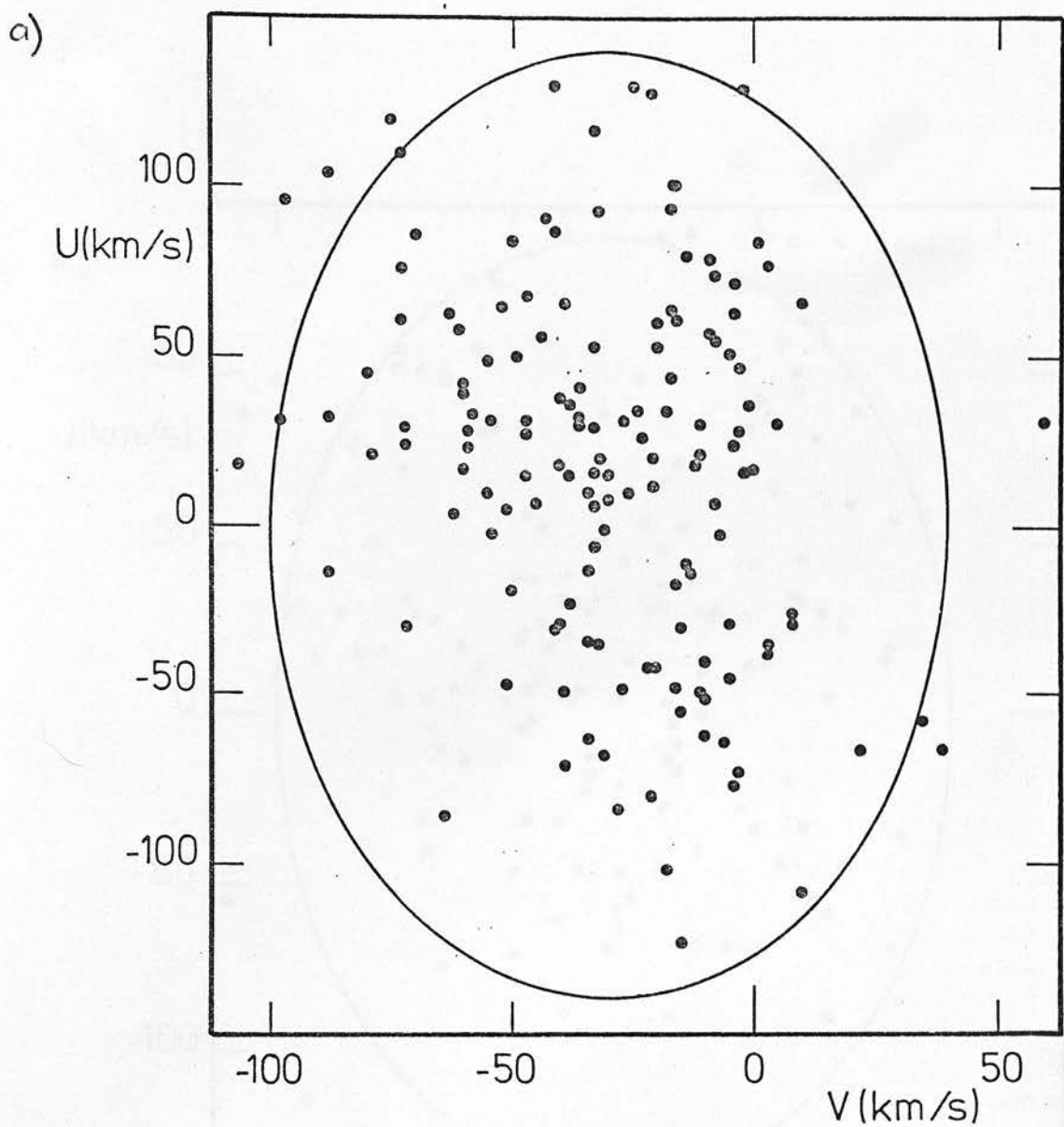
Figure 5.3 (U,V) velocity diagrams for a) metal rich ([Fe/H] > -0.1) and

b) intermediate metallicity (-0.1 < [Fe/H] < -1.0) "disk" stars, and c)

for metal poor "disk" (dots), intermediate metallicity ([Fe/H] > -1)

"halo" (crosses) and metal poor "halo" (open circlies).

b)
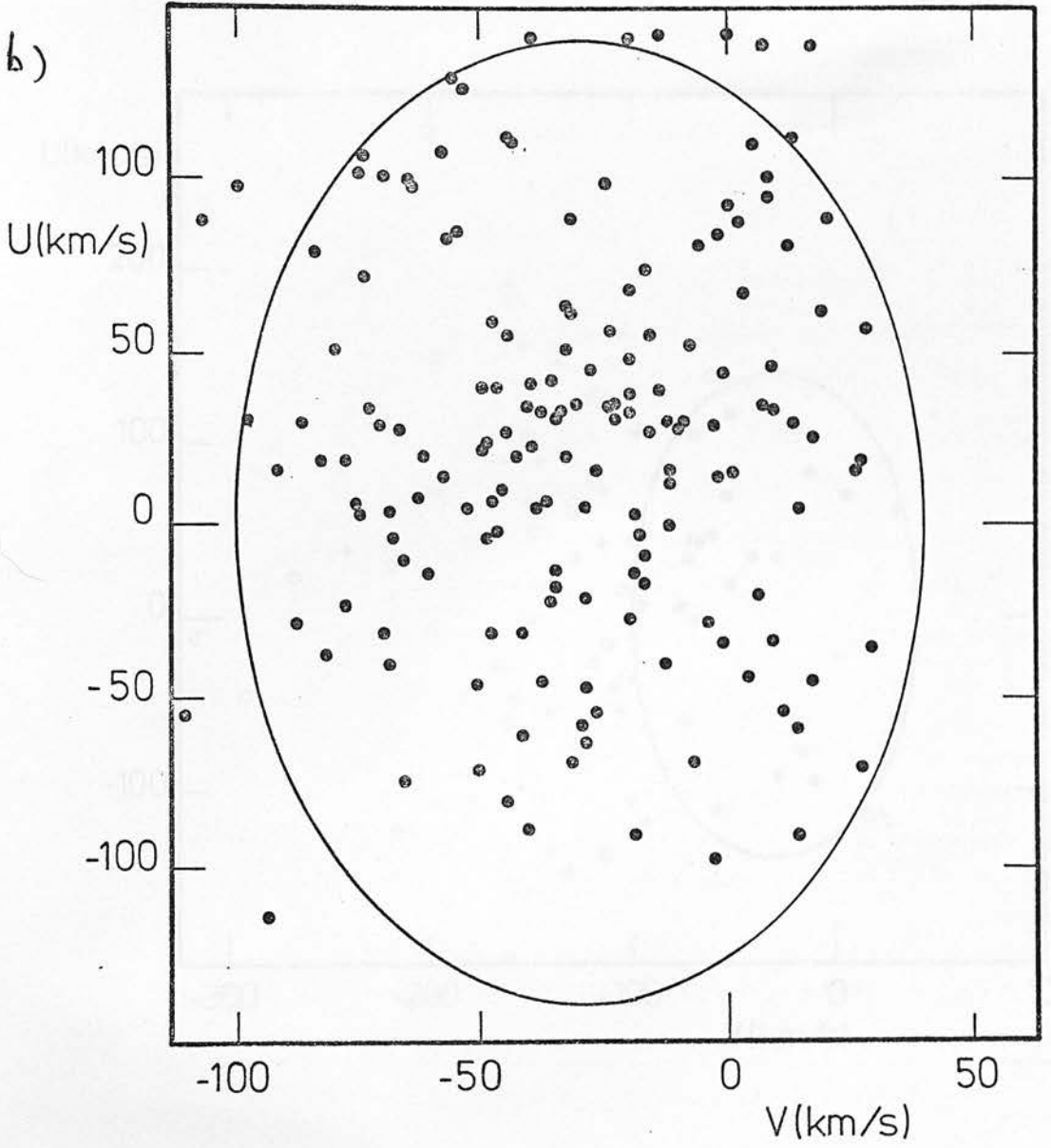
c)
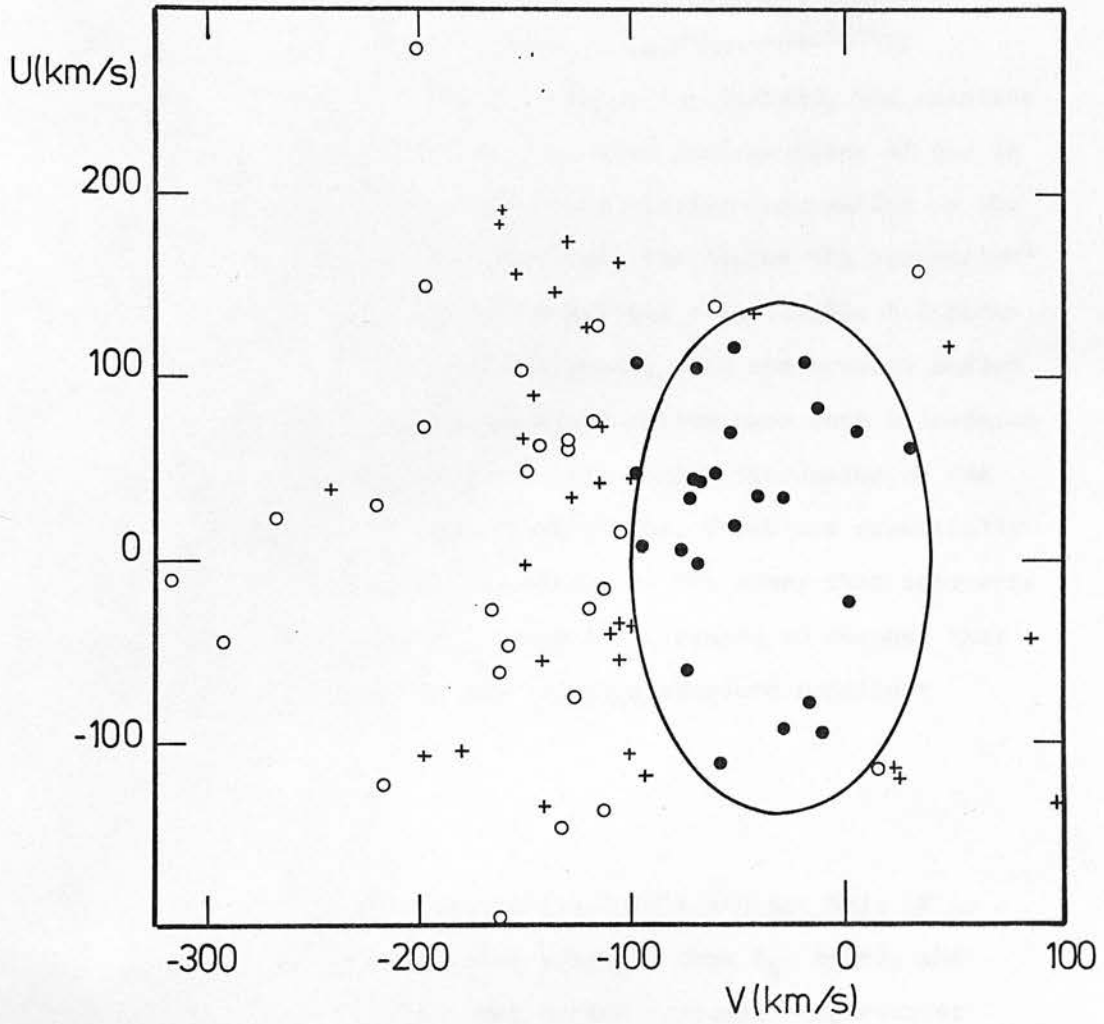
assumptions regarding the halo motions since the halo sample is magnitude, rather than proper motion, limited. Effectively all subdwarfs brighter than B = 14.25 have sufficient tangential motion to be included in the sample even with the lowest halo motions.

The deduced H/D ratio of ~0.3 percent represents the relative numbers of halo and disk main sequence stars in the magnitude range $5 < M_B < 10$. However, because the sample is magnitude limited, the relative sampling volumes decrease by a factor of four with each increase of one in M_B . Thus number counts with absolute magnitude provide information on the shape of the halo LF – the flatter the function, the higher the proportion of stars from the intrinsically brightest magnitude range. Table 5.7 shows the predicted values from the HC and HW functions, with the numbers scaled relative to the total at M_B = +7. The observed ratios have been calculated using only the metal poor stars in Eggen's halo domain (inclusion of the probable old disk stars gives the bracketted ratios, which are essentially identical). Although this sample is incomplete, in the sense that subdwarfs within the e=0.42 ellipse are omitted, there is no reason to suspect that significant systematic errors affect the relative absolute magnitude distribution.

This comparison suggests that while Chiu's steeper halo LF is a more accurate representation of the shape brighter than M_B of +7, the shallower gradient disk-type function may better represent the data at fainter magnitudes. This steepening is unlikely to be purely evolutionary, since it implies a turnoff in the colour magnitude diagram at M_B ~ 5.5 – i.e. corresponding with an age substantially greater than the Hubble time. It may reflect either a selection effect within the data or an intrinsic

property of the halo luminosity function. Assuming that the latter is the case, the H/D ratio is 0.4 percent fainter than M_B = +6.5 (with formal errors of 0.12 percent) and only 0.15 percent for M_B < +6.5 .

The SGC number counts test whether these normalisations of IP II and halo taken together with the RG disk LF plausibly reproduce the results of faint proper motion surveys. In the models shown (Figure 4a-c) the HW form of the halo LF is adapted to include the steepening noted above. Deconvolving the overall counts into the contribution from each population, it is evident that the apparent magnitude range does fall into the two regimes predicted by the qualitative discussion in Section 2. Neither white dwarfs nor IP II subdwarfs (with the SGP normalisation) contribute more than 15 percent at any magnitude. Most of the stars detected lie close to the kinematic distance limit, so going to fainter apparent magnitudes slides along the luminosity function of a given population - as the individual log N(m) curves show.

The observed number counts present a broad maximum near V = 17. Whether this is reproduced in the simulations is very sensitively dependent on both the absolute density of the halo - i.e. the luminosity function - and the adopted velocity dispersions, that is the proportion of stars detected at any absolute magnitude. Since these two parameters are strongly coupled, it is possible to construct ad hoc luminosity functions which reproduce the observed counts with any set of kinematics. With the halo input parameters described in Section 3, and using the RG luminosity function for the disk, there is a substantial range in the expected shape of the number counts fainter than V=17. None of the models with HG (cluster-type) halo LFs adequately fit the faint number counts, failing to

Table 5.7

M_B	n(obs)	Ratio relative to N (M_B = +7)		
		observed	HW	HC
+6	14 (23)	1.0 (0.92)	2.85	1.09
+7	14 (25)	1.0	1.0	1.0
+8	3 (8)	0.21 (0.32)	0.26	0.55
+9	1	0.07	0.09	0.29
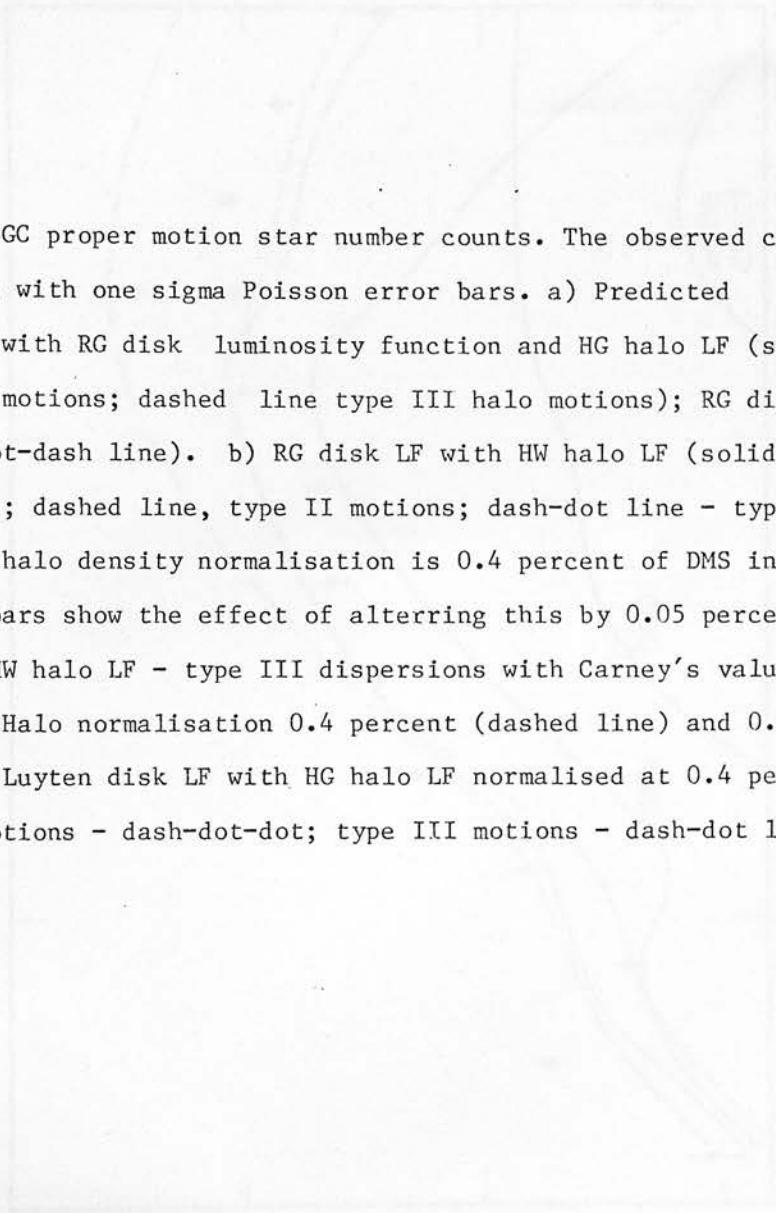
Figure 5.4 - SGC proper motion star number counts. The observed counts are shown as dots with one sigma Poisson error bars. a) Predicted distributions with RG disk luminosity function and HG halo LF (solid line - type I halo motions; dashed line type III halo motions); RG disk LF and HC halo LF (dot-dash line). b) RG disk LF with HW halo LF (solid line - type I motions; dashed line, type II motions; dash-dot line - type IV motions). The halo density normalisation is 0.4 percent of DMS in all cases. Error bars show the effect of alterring this by 0.05 percent. c)RG disk LF with HW halo LF - type III dispersions with Carney's value for the solar motion. Halo normalisation 0.4 percent (dashed line) and 0.25 percent (solid line). Luyten disk LF with HG halo LF normalised at 0.4 percent DMS.(type I motions - dash-dot-dot; type III motions - dash-dot line).

a)
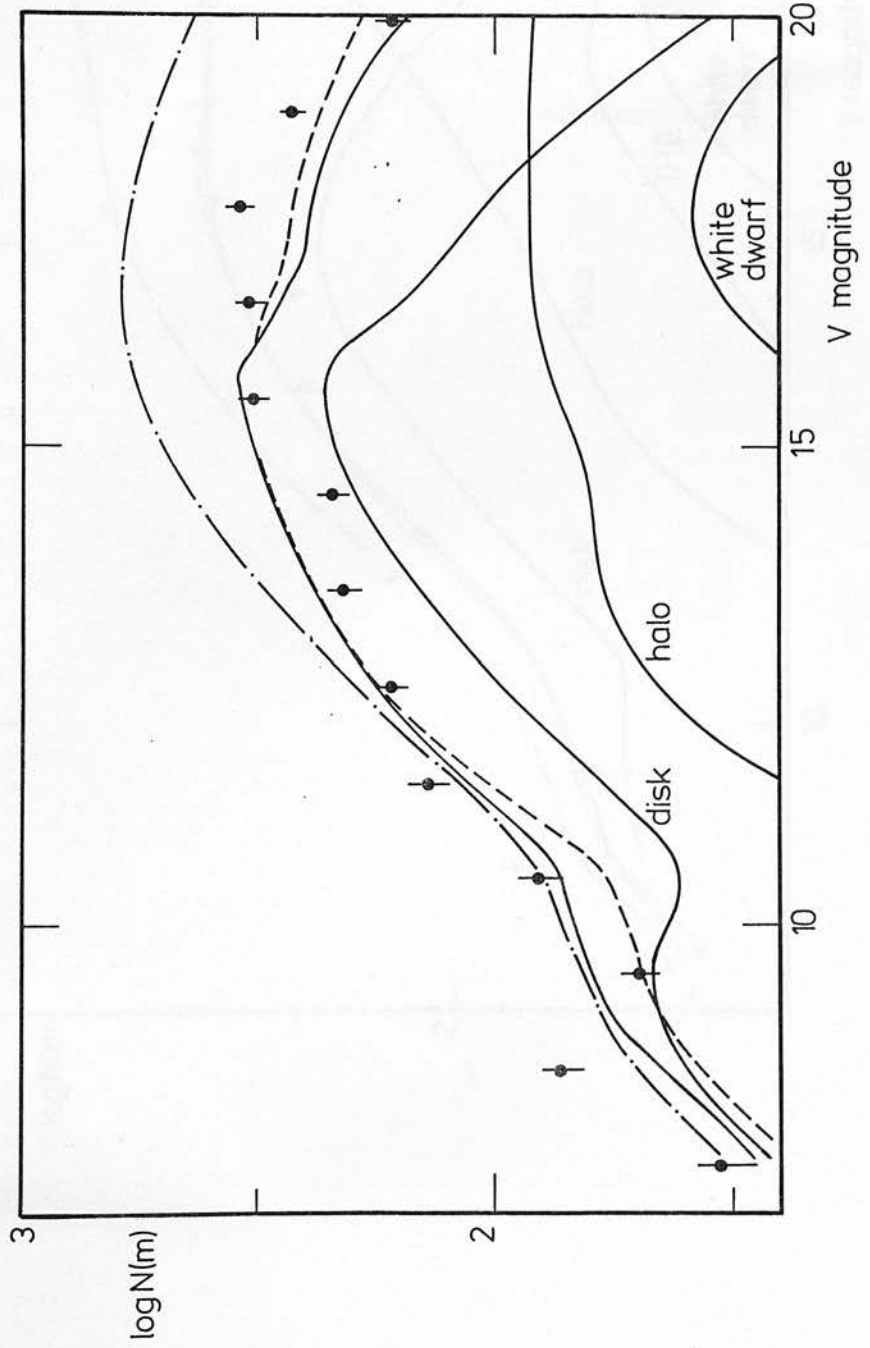
b)
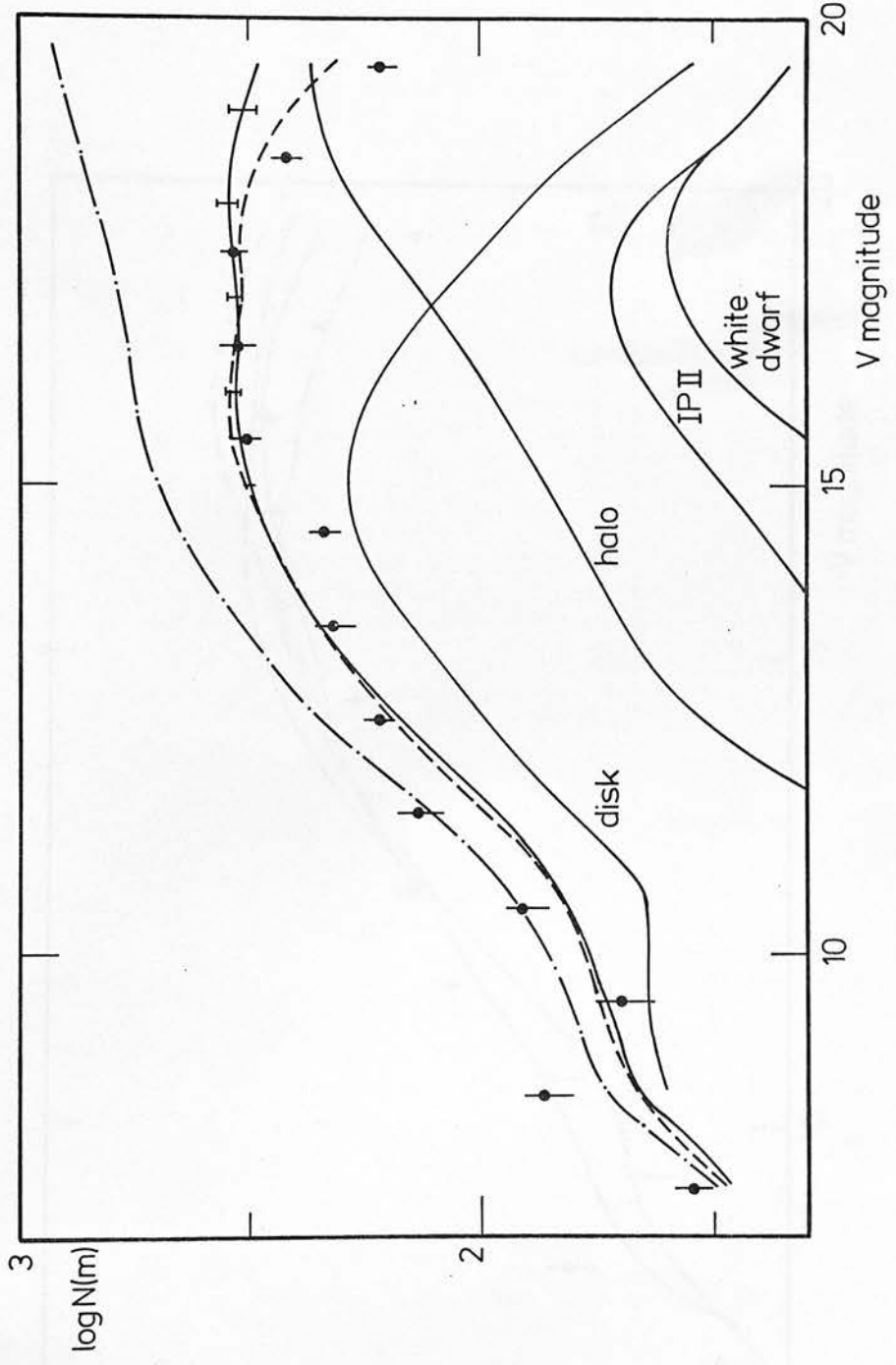
c)
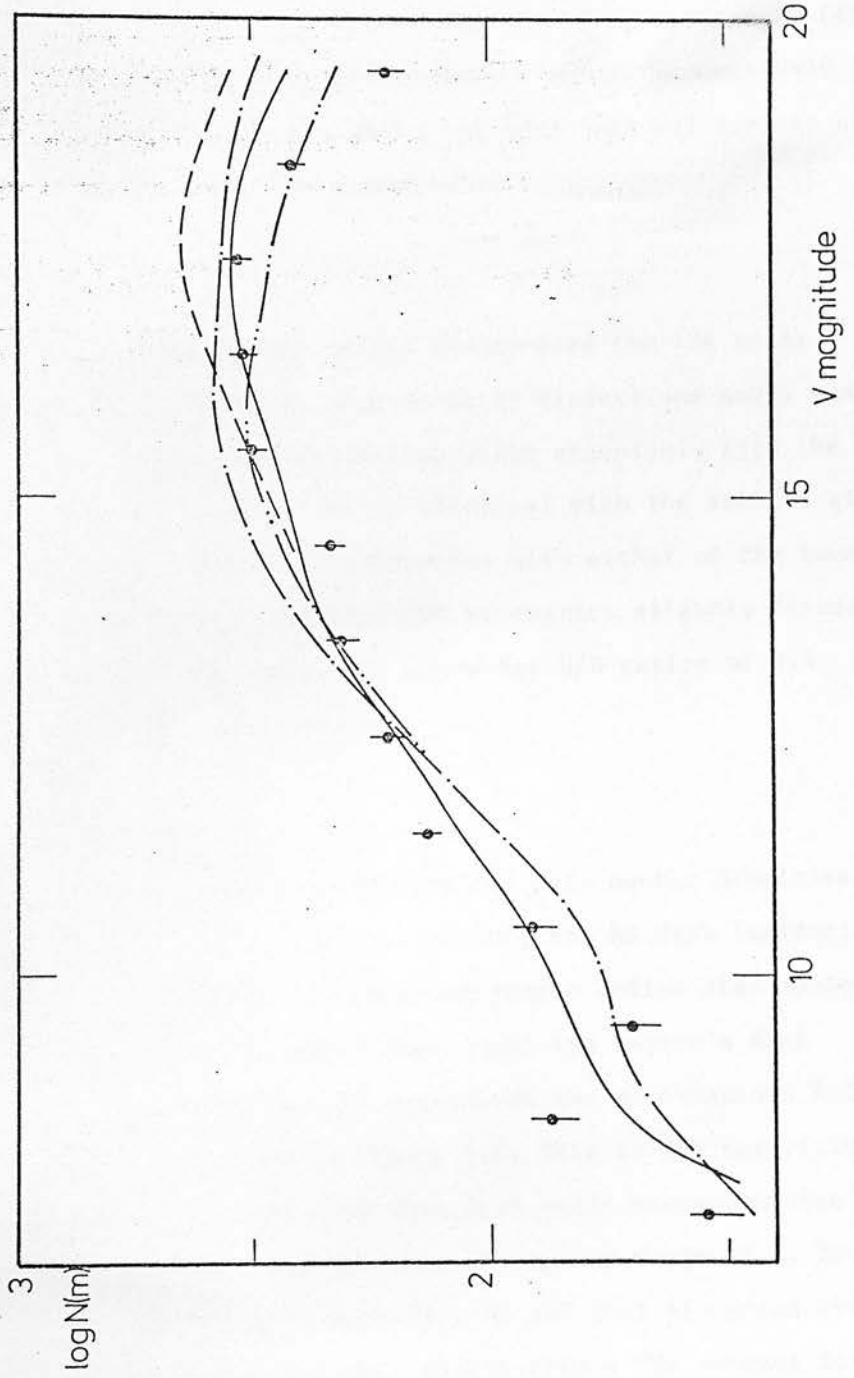
predict sufficient stars even with the highest velocity dispersions. On the other hand, the higher number densities found by Chiu produce number counts which rise too steeply with apparent magnitude (fig. 4a). Similarly, with the range of halo number ratios found above, the high dispersion type (iii) and (iv) kinematics produce a hump in the predicted counts between V=10 and 15 which is not observed. Halo-to-disk ratios of less than 0.1 percent are required before the distributions are compatible.

However, if Carney's lower values are adopted for the solar motion, a model with Oort's high RR Lyrae velocity dispersions and a number ratio of 0.25 percent produces a distribution which acceptably fits the data (figure 5.4c). In fact this is nearly identical with the results given by models incorporating the modified HW function with either of the lower dispersion halo kinematics, with the type (i) kinematics slightly favoured (figure 5.4b). The theoretical curves are drawn for H/D ratios of 0.4 percent, with error bars of 0.05 percent.

Thus, with the kinematics used here and halo number densities lying in the range 0.25 to 0.4 percent of the DMS, the RG disk luminosity function can adequately reproduce the observed proper motion star number counts. However, figure 5.4c also shows that combining Luyten's disk luminosity function with the HG halo LF reproduces the observations fully as well as any of the other curves in figure 5.4. This is not surprising, since Luyten's function is derived from this data under the assumption that one population - the disk - is dominant over the entire range in V. Thus the major difference between this interpretation and that discussed above lies in the size of the total halo stars contribution - ~20 percent for V < 19 using Luyten's disk LF, ~50 percent with the RG disk LF (Table

<center>Table 5.8</center>

halo kinematics	RG disk LF + HW halo LF		Luyten disk LF + HG halo LF
	(i)	(ii)	(iii)
disk	0.54	0.47	0.72
halo	0.26	0.35	0.15
IP II	0.14	0.13	0.08
WD	0.06	0.05	0.05

5.8). Effective discrimination between these alternatives can be achieved using the RPMD.

This technique was first applied by E.M. Jones (1972) who, from a simple 2-population model, empirically defined the locii of disk and halo. More recently, Chiu (1980a) has extensively discussed the approach, employing more refined techniques in his statistical population classification. His population ridge lines in the RPMD are defined using slightly different proceedures from those employed here - the $5\log v_t$ distribution is calculated analytically and the modal value used in equation (2), with (B-V) taken from an M_V -(B-V) distribution. Here ridge lines are determined from the simulated H_V - (V-I) distribution. If a proper motion cut is included, the $\log v_t$ distribution is biased towards higher v_t and hence large H_V see figure 5.5). However, if we adopt Chiu's preferred kinematics and a zero proper motion limit our technique closely matches Chiu's ridge lines.

Figure 5.6 shows the (V-I) SGP RPMD with population ridge lines appropriate to a proper motion limit of 0".2. The individual proper motion stars from the SGP sample are marked. Table 5.8 gives the relative proportions of each population predicted by the preferred models under the assumption that the observed sample is complete to V=19. Even without the statistical analysis carried out by Chiu it is obvious from the diagrams that there are nearly equal numbers of disk and halo stars, together with a sizeable proportion of IP II stars and at least two white dwarfs. Despite the small sample size, these ratios are substantially at variance with those predicted if Luyten's LF is adopted for the disk.
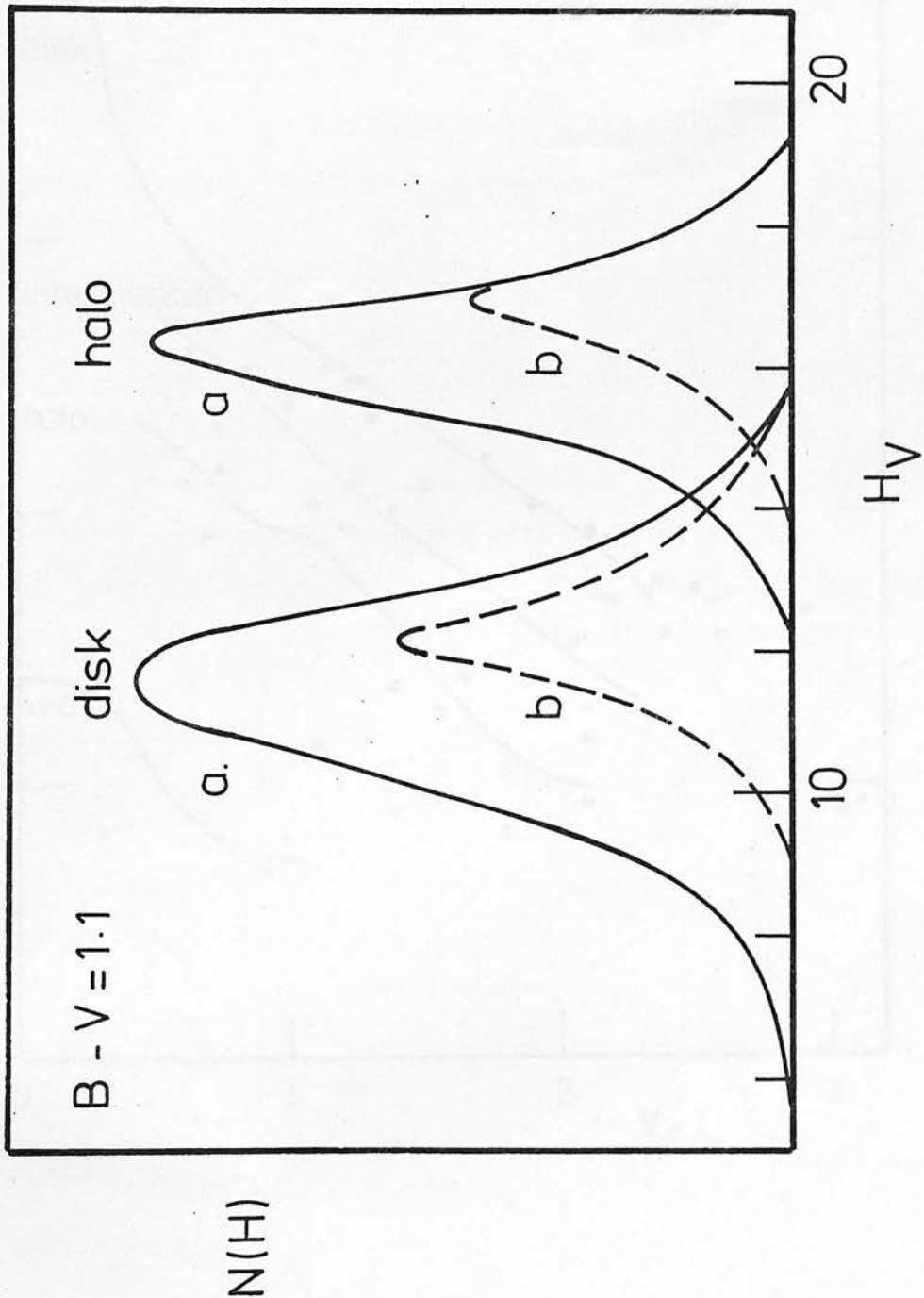
Figure 5.5 - Distribution of stars of (B-V)=1.1 with H with a) no proper
motion cut and b) proper motion limit of 0".2 .
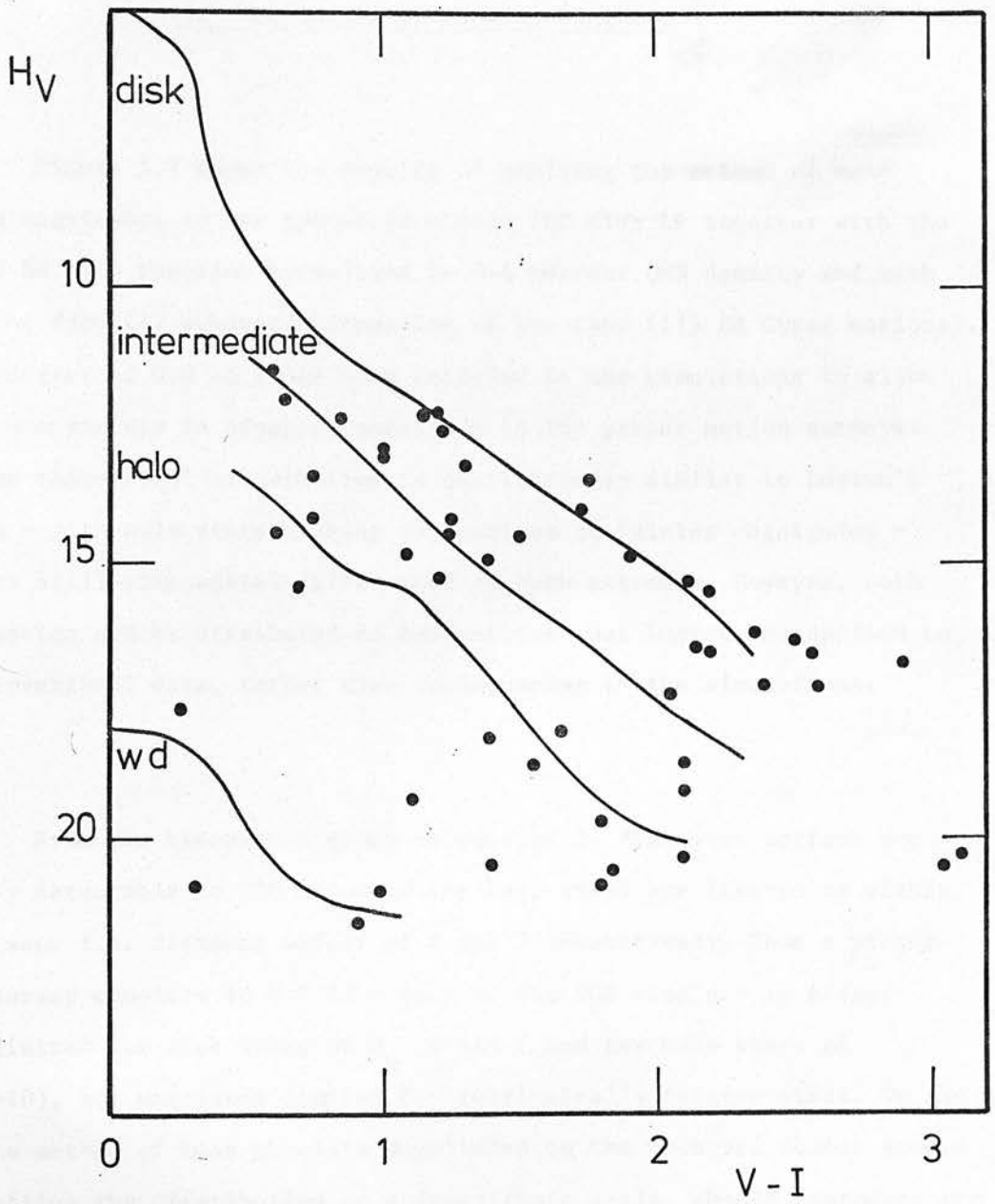
Figure 5.6 - H_V- (V-I) reduced proper motion diagram for the SGP sample
together with the theoretical ridge lines.

5 Discussion

5.1 The Luyten Luminosity Function

Figure 5.7 shows the results of applying the method of mean absolute magnitudes to the preferred models (RG disk LF together with the modified HW halo function normalised to 0.4 percent DMS density and with either the type (i) subdwarf kinematics or the type (ii) RR Lyrae motions). An rms scatter of 0.5 in V has been included in the simulations to allow for the uncertainty in apparent magnitude in the proper motion surveys. While the theoretical distribution is qualitatively similar to Luyten's function - with halo stars pushing the maximum to fainter magnitudes - there are still substantial differences at both extremes. However, both discrepancies can be attributed to corrections that Luyten has applied to his observational data, rather than inadequacies in the simulations.

From the kinematics given in section 3, disk star motions are typically detectable to ~60 parsec while halo stars are limited to within ~400 parsecs i.e. distance moduli of 4 and 7 respectively. Thus a proper motion survey complete to V ~ 19 - such as the SGC sample - is proper motion limited for disk stars of M_V < +14 (and for halo stars of M_V < ~+10), but magnitude limited for intrinsically fainter stars. We can apply the method of mean absolute magnitudes to the observed number counts and, plotting the distribution on a logarithmic scale, should reproduce the shape of the Luyten LF to M_V ~+14. Note that this does not depend on whether the results given by this method are correct in any
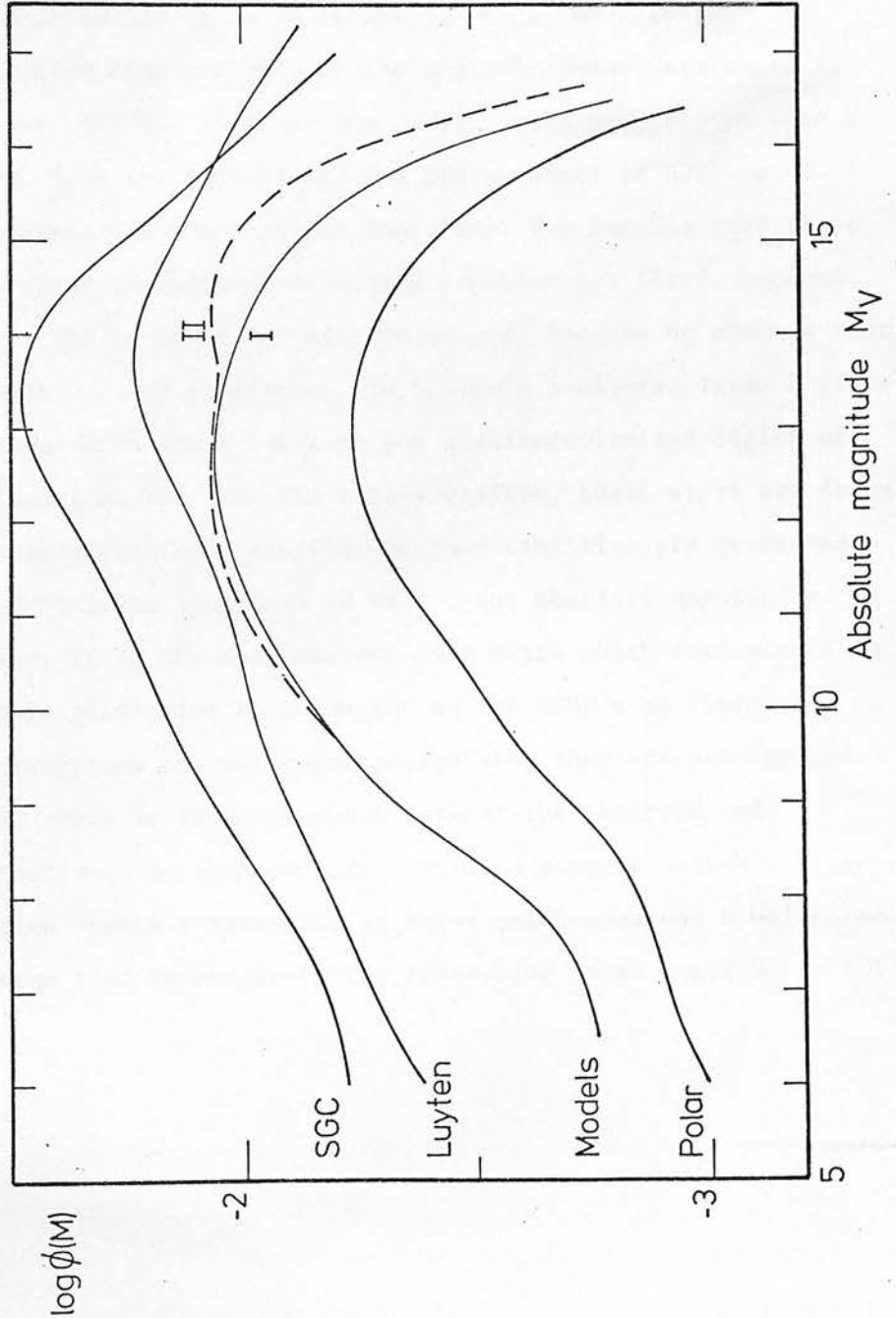
Figure 5.7 - Luyten's luminosity function together with the results from applying the method of mean absolute magnitudes to the models with HW halo LFs and type I or type II halo motions and to the number counts from Luyten's survey of the South Galactic Cap (SGC) and of both Poles combined (Polar).

sense. We are merely applying the same technique to the observed and predicted samples and comparing the results.

The comparison is shown in figure 5.7 together with the corresponding function from analysis of the complete polar catalogues as tabulated in Luyten (1977b). Although the models still predict too deep a dip near M_v = +7, both the deficit and the sharp cutoff in numbers at faint magnitudes appear in the observed functions. The reasons that these features do not appear in Luyten's tabulated function are first, because Luyten smooths out the GK dwarf deficit and second, because he assumes that he samples a single stellar population. In Luyten's analysis, large H stars are treated as faint disk stars lying in the magnitude limited region of the luminosity function. Thus in this interpretation, these stars are drawn from a smaller sampling volume, and the observed densities are corrected accordingly, producing the long tail to very faint absolute magnitudes. In our model, however, it is the more distant halo stars which predominate in the tail - and this prediction is borne out by the RPMD's as discussed above. Volume corrections are not required and when they are not applied, as in figure 5.7, there is good agreement between the observed and predicted distributions. We conclude that the data support a disk luminosity function severely truncated at faint magnitudes and a halo luminosity function that is monotonically increasing to at least M_v = +11.

5.2 The Halo Star Density in the Solar Neighbourhood

Previous studies of the local number density of halo subdwarfs
have produced substantially different results. The SGC number counts
indicate a H/D ratio of between 0.25 and 0.4 percent (dependent on the
kinematics) over the magnitude range $8 < M_v < 11$. However, while this ratio
is valid for stars of $M_v = +6.5$, brighter than this the halo luminosity
function is appears steeper than the disk, with a number ratio nearer 0.15
percent at $M_v = +5.5$. If this is the case then the overall H/D ratio is a
somewhat artificial quantity since it depend on the relative proportions of
bright ($M_v < +6$) and faint stars in the sample.

This influences the normalisation deduced by Schmidt to some
extent, since three of the seventeen subdwarfs in his complete sample lie
within this brighter absolute magnitude range. However, a more important
factor in accounting for for the lower derived density is the adoption of
250 km/sec as the median tangential velocity of the subdwarf population.
This value is based on Oort's (1965) RR Lyrae sample (i.e. the type (iii)
kinematics which fail to fit the SGC number counts). As Richstone and
Graham (1981) have pointed out, if the halo population has higher rotation
and lower velocity dispersions Schmidt's analysis underestimates the true
density by a factor of up to two. Indeed, with the type (i) or type (ii)
motions, 17 percent and 34 percent respectively of all subdwarfs (rather
than 50 percent) can be expected to have tangential motions greater than
250 km/sec, while if the Carney solar motion and the RR Lyrae dispersion
calculated by Oort are appropriate, this fraction is 40 percent. The local
number density of main sequence stars is $7 \pm 2 \times 10^{-5}$ stars/cubic parsec.
Hence applying the appropriate adjustments to Schmidt's observed number

density results in an inferred H/D ratio (for $5 < M_V < 12$) of between 0.35 and 0.8 percent - in adequate agreement with the value derived above.

Bahcall, Schmidt and Soneira (1982) have interpreted faint ($18 < V < 22$) star counts to derive a density closely similar to Schmidt's original value. They also review the various other definitions of the halo. As with the Bahcall and Soneira (1980) models, two visible stellar components (disk plus extreme halo) are considered, with no intermediate population, although Bahcall et al discuss the (not very stringent) limits that can be set on such a population using the (B-V) distributions from Kron's (1978) star counts.

The halo luminosity function is approximated by
$$\phi\,(M) \;\alpha\; 10^{\gamma}$$
and the normalisation derived from the slope of the stellar number counts after subtracting the disk contribution. However, the SGP data analysed in Paper III show that the intermediate component dominates the halo to at least $V = 18.5$, and possibly fainter. Furthermore, Bahcall et al include star counts by Peterson et al (1979) which have been shown to have severe star-galaxy classification problems (Gilmore, 1981). Retaining only the Tyson and Jarvis (1979) and Kron counts, and removing the intermediate component significantly steepens the halo number counts and substantially affects the deduced normalisation.

Another factor is the steepening of the halo luminosity function mentioned above, since the halo star density deduced from star counts is very sensitive to the functional form adopted. Between $M_V = +4$ and $+8$, the

absolute magnitude range considered by Bahcall et al, there is a significant change in slope, so a single exponential is not a good approximation. A halo luminosity function that steepens with bright absolute magnitudes leads to an underestimation of the overall H/D ratio. Finally, the flattening of the halo spheroid is not well established and is obviously a critical parameter. A full discussion of these problems using detailed models is in preparation (Gilmore, in prep.).

The unrecognised presence of the intermediate population is a significant factor in Chiu's (1980a) Bayesian analysis of the reduced proper motion diagram for SA 57 and SA 68. As described above, the derived SD2 function has a significantly different shape from the disk function, so that while the overall H/D ratio is 0.5 percent, this varies from 0.2 percent at M_v = +4.5 to ~1.6 percent at M_v = +9. Bahcall et al have proposed that in Chiu's probabilistic analysis, large numbers of disk stars with small probabilities of being halo subdwarfs could in principle lead to overestimation of the halo star density.

A more significant factor, however, is that Chiu's analysis of the RPMD is based on a two component disk-halo model of the local stellar populations. In this classification scheme stars lying well below the main sequence ridge line in the reduced proper motion diagram are classed as halo. However, the mean distance of the SD2 stars ranges from ~7 kpc for M_v =+4.5 to only 1 kpc for M_v =+9.5, and so stars fainter than M_v ~+6.5 are drawn from the regions where the intermediate population is dominant, and are more likely to represent this population. Two results in particular from Chiu's analysis support this hypothesis - first, the best fit density distribution of SD2 stars is a flattened ellipsoid, axial ratio four to

one, unlike the near spherical distribution of the RR Lyraes (Oort and
Plaut, 1975). Second, the SD2 luminosity function derived from field SA 51
- along the plane of the disk towards the Galactic Anticentre - is
substantially enhanced over the results derived from higher latitude
samples - as would be expected if contaminated by an intermediate
dispersion w-velocity component, relatively confined to the Plane.

Under this interpretation, Chiu's luminosity function actually
represents a composite of the extreme halo at bright M_v and IP II fainter.
The absolute densities at the latter magnitudes, derived on the basis of
the flattened r^{-3} halo, are 1.0 to 1.6 percent of the disk main sequence
densities at the same absolute magnitudes. If these stars are really
intermediate population, with an effectively exponential density law, the
projected local density rises to ~2.5 percent - consistent with the SGP
number counts.

Similarly the presence of the intermediate population can
account at least in part for the very much higher halo densities derived by
the Basle group (Fenkart 1977, 1980; Becker, 1980). (It should be noted
that the halo mass density derived by Fenkart ($3 - 7.7 \times 10^{-4}$ $M_\odot$ /cubic
parsecs) is based on a luminosity function flat fainter than $M_v \sim 7$.
Adopting the HW functional form increases this density by a factor of 10.)
In this work the characteristic ultraviolet excess of metal poor stars is
used to identify the halo component. However, we have argued that the IP II
is also an old stellar population, and therefore has low metal abundance.
Direct evidence is furnished by the sizeable metal poor tail evident in the
metallicity distribution of the Eggen "disk" (figure 5.1) which far exceeds
the expected number of halo stars. Indeed, Fenkart's SA 57 (NGP) "halo"

star number counts shows clear evidence for the intermediate component to
z ~ 5 kpc, with the halo detectable only beyond this point. Projecting this
halo component to z=0 for stars of M_v = +4 gives an H/D ratio of 0.15
percent - in agreement with the value found for intrinsically bright stars
from the ESGC sample.

Besides the intermediate population, the photometric
classification criteria include a significant proportion of the oldest disk
stars (as proposed by Bahcall et al). Since these comprise ~12 percent (by
volume) of the disk population (Wielen, 1974), it is not surprising that
the computed halo density is so high. As has been emphasised above, these
old disk stars contribute to the metallicity-defined Stromgren IP II, whose
local density (~7 percent) is consistent with the upper limit found by the
Basle group. Furthermore, the presence of these two 'contaminant'
populations explains why Becker's "halo" has a minimum density in the
region of the Galactic Centre. A radial metallicity gradient in both disk
and IP II will reduce the 'contamination', and hence the inferred density,
with decreasing Galactic radius.

Finally, Eggen (1979b) has quoted three criteria for identifying
subdwarfs - first, stars with e > 0.42; second, stars with e < 0.42 but
with w > 60 km/sec; and, third, stars with [Fe/H] < -0.6. Inverting these
criteria closely defines most of the disk population in our models -
although it should be emphasised that the oldest disk stars appear to be
both slightly more metal poor and of higher velocity then these limits. The
remainder, however, comprise not only extreme halo, but also the
intermediate population, overlapping in metallicity and with lower overall
motions, and this population contributes most of the metal poor

([Fe/H] < -0.8) stars with e < 0.42.

     In short, once due allowance is made for kinematic selection
effects and the influence of the metal poor, intermediate population,
previous studies of the local space density of halo subdwarfs are
consistent with the simple three component population structure proposed
here. If the disk luminosity function of Paper II normalised to 0.4 percent
of the disk density is appropriate to the halo function locally, then the
local mass density of halo main sequence stars (from Chiu's mass luminosity
relation) is $\sim 10^{-4}$ solar masses/cubic parsec. Allowing for evolved stars
(following Chiu) increases this by approximately a factor two.

6 Conclusions

     We have re-examined the kinematic selection effects in the Luyten
proper motion surveys using numerical models incorporating three separate
kinematically defined stellar populations. These models show that since
Luyten's absolute magnitude calibration technique implicitly assumes that
all stars belong to a disk population with a single set of kinematics, the
inclusion of substantial numbers of relatively bright (M_v < +11) but
distant halo subdwarfs in the proper motion surveys leads to an apparent
excess of very low luminosity dwarfs relative to a volume complete
luminosity function (Paper II).

     We have also shown that the difference between Stromgren's
estimate of the density of intermediate population stars and the value

derived from the SGP number counts arises because the former is defined solely by metallicity. Stromgren's intermediate population consists primarily of disk dwarfs, while the SGP population is a separate, more metal-poor, kinematic entity - although this does not necessarily imply a separate <u>origin</u> from the conventional halo population.

Finally, adopting a self-consistent metallicity and kinematic definition of the halo, we derive a local subdwarf to disk dwarf number ratio of 0.25 to 0.4 percent over the range $6 < M_v < 12$. Brighter than this, the halo function is steeper than that of the disk, and this, together with the presence of the intermediate population, satisfactorily accounts for the discrepancies amongst previous determinations of the local halo density. The normalisation found here corresponds to an overall mass density of $\sim 2 \times 10^{-4}$ M /pc .

Chapter 6

Late type dwarfs in the solar neighbourhood are generally
classified under three population headings - young disk, old disk and halo
- following the kinematic precepts described by Eggen (1973). While there
are specific features such as low metal abundance and subluminosity which
characterise halo subdwarfs, the segregation between the other two
populations is not so clear. Furthermore, from studies of K and early M
dwarfs Mould and Hyland (1976 - MH) have suggested that there is evidence
for a separate population of mildly superluminous stars. Although they
interpret these as still contracting to the main sequence, there is not a
one-to-one correlation between this population and Eggen's young disk. As a
further complication, theoretical models of stellar interiors of very low
mass stars ($M < 0.1M_{\odot}$) show that even objects with mass less than the
nominal H-burning limit undergo short (10^8 years) periods of luminosity,
either through deuterium burningor through gravitational collapse
(Grossman, Hays and Graboske, 1974). During deuterium burning, the these
"black dwarfs" occupy a pseudo main sequence running nearly parallel with
the true main sequence for M dwarfs, but displaced to lower temperatures.
Few stars of low enough luminosity to be candidate "black dwarfs" are
known. However, since the luminous lifetime is so short, even the detection
of one such star implies a substantial total number density - and a
significant contribution to the local mass density. For these reasons it is
important to determine the structure of the H-R diagram for low luminosity
dwarfs.

Determining the position of a star on the H-R diagram requires
knowledge of both the total luminosity (i.e. the bolometric magnitude) and

of the effective temperature. For hotter stars these parameters can be derived by a comparison of the observed spectral energy with atmosphere models. However, many molecular species are prevalent in the atmospheres of cool stars and hence model calculations are both complex and time consuming. While considerable progress has been made recently in the study of late type giants (Gustafsson, Bell, Eriksson and Nordlund, 1975), only a few attempts have been made to construct models of K and M dwarfs. The temperature structure and molecular constituents of the higher gravity dwarf atmospheres differ significantly from their giant counterparts. CO and CN dominate the opacity in the extended atmospheres of giants, while TiO and H_2O are the most important opacity sources in dwarfs (Mould, 1976) - although , as discussed later, other molecules may play a significant subsidiary role.

Because of the complex nature of the molecular band systems, careful consideration must be given to the method of opacity calculation. Straight mean opacities overestimate the overall opacity while the harmonic mean method underestimates the absorption (Carbon, 1974). Thus more sophisticated techniques - such as the use of opacity distribution functions (ODFs) or opacity sampling - are necessary. Even the most detailed models, by Mould, deal only with H_2O and TiO in a detailed manner and these models are restricted to effective tremperatures hotter than 3000K. Furthermore there are still considerable uncertainties in the laboratory determinations of fundamental quantities such as the oscillator strengths for many of the transitions considered. Finally, the treatment of convection is obviously another substantial uncertainty in these cool, almost fully convective objects. Fuller consideration of the available models is given in a later section.

As a result of the uncertainties in the theoretical models, studies of the structure of the low luminosity main sequence have been largely based on semi-empirical methods - primarily fitting black body distributions to broad band photometry (e.g. Greenstein, Neugebauer and Becklin (GNB; 1970) Petterson, 1980). Obviously there can be no question of applying this technique to UBVRI photometry, given the proliferation of molecular bands self evident in any M dwarf spectrum. It is generally assumed, however, that at infrared (> 1 micron) wavelengths line blanketting is not so severe, and the flux distribution can adequately be described by a black body curve. The effective temperature is then derived, allowing for blanketting, by ensuring that the area under the black body curve is equivalent to the total energy emitted by the star (i.e. the area outlined by the broad band photometry). However, previous investigations have not produced concordant definitions of the effective temperature scale below ~3000 K. The actual peak of an M star's spectrum occurs near a wavelength of 1.1 microns, and most of the studies noted above have been based on UBVRIHKL photometry - i.e. lacking photometry at J (1.2 microns). We have obtained not only a homogeneous set of BVRIJHK photometry of a large number of very late type dwarfs, but also have narrowband (200 Å) CVF spectrophotometry in the 1.4 to 2.5 micron range and are therefore well placed to re-examine this problem.

In the following sections the observational data and its reduction to a flux scale are discussed (section 2) and the black body fitting technique described (section 3). The resulting physical parameters are compared with interior models of low luminosity dwarfs (section 4) and finally we consider the structure of the infrared two-colour diagram (section 5).

2 Observations

Broad Band Photometry

To maintain a homogeneous sample we have, with one exception, limited the selection of late type dwarfs to a number of the parallax calibrators discussed in the previous sections together with twenty-three of the reddest stars from the SGP sample described in Chapter 4. Photoelectric BVRI photometry on the Kron-Cousins system is available for all of the former sample (except for VB 10 where we transform the photometry by Kron (1958)), while V and I magnitudes on the same system have been derived photographically for all of the latter set. Photographic B and R magnitudes have been obtained for some of the SGP stars - a number are too faint to be visible on B plates, setting a bright limit of B=22.

Near infrared JHK observations of these stars were made using the IRPS system on the AAT on October 26 and 27, 1980 and September 14 - 16, 1981. These observations are tied into the AAO system - indeed, several of the brighter (apparent magnitude) parallax stars are system defining standards - and are tabulated in Appendix A. Based on the repeatibility of the standards, the errors in the programme star magnitudes are typically 0.02. The one star for which we have no infrared photometry is Gl 406, where we use Bessell's BVRI photomtry (preprint, 1982), together with JHK measurements by Persson et al. (1977). The latter have been transformed onto the AAO system using the transformations given in Section 5. L magnitudes for several of the parallax stars have been taken from Mould &

Hyland (1976) and from Veeder (1974). It should be noted that the last mentioned magnitudes are on slightly different systems and that the observational errors are significantly higher than in JHK (~0.1 magnitude).

To reduce these magnitudes to a flux scale we have adopted the zero-magnitude calibration shown in Table 6.1. The BVRI values are those quoted by Bessell (1979) for the Kron-Cousins system, while the J and K values are those given for the AAO system by Ward, Allen, Wilson, Smith & Wright (1982). These values are consistent with the absolute measurements of Alpha Lyrae's flux by Oke and Schild (1970) and the model computations by Schild, Peterson and Oke (1971). However, the zeropoint at H of 1030 Janskys quoted by Ward et al. is slightly higher than this normalisation and more consistent with an effective wavelength of 1.63 microns. We have therefore adopted a slightly different zeropoint, as shown, although it should be emphasised that re-normalising the H photometry has very little effect on the total flux derived.

A further point is that since the Cousins R passband is very broad the effective wavelength is strongly dependent on the spectral type (Bessell, 1979). Since there is significant response up to and beyond 8000 Angstroms, in observations of M stars more than half of the flux in the R band actually comes from wavelengths within the Cousins I passband. All of the dwarfs considered are of spectral type late K or M. Hence we have adopted an effective wavelength of 7220 Angstroms for R, rather than the 6380 Angstroms characteristic of A0 stars. The flux zeropoint has been derived from the observations of Vega by Hayes and Latham (1975). Other passbands are narrower and their effective wavelengths are much less sensitive to the colour of the object observed.

Table 6.1

Passband	Effective Wavelength		Zeropoint	
B	0.44	microns	4260	Janskys
V	0.55		3640	
R	0.72		2750	
I	0.80		2550	
J	1.20		1640	
H	1.64		1000	
K	2.19		650	
L	3.4		305	(Mould/Hyland)
	3.5		280	(Veeder)

Spectrophotometry

Spectrophotometry of a few of the parallax calibrators has been obtained in two spectral regions – 5800-7500 Angstroms with the IPCS on the AAT and from 1.4 to 2.5 microns with the near-infrared CVF on UKT1 on UKIRT. The IPCS observations were made on October 31, 1980 using the 600R grating on the RGO spectrograph on the AAT and have an effective resolution of ~2 A. These data have been flux calibrated using our observations of van Maanen 2 and L745-46A, using Oke's (1973) spectrophotometric calibration. D. Hanes (SHA symposium, Sussex Univ., September 1982) has pointed out that not all of these standards are on the same system – i.e. the calibration for any one star is not necessarily absolute, with the differences between individual "standards" amounting to as much as 10 percent. (It should be noted that these stars were never intended as absolute spectrophotometric standards.) There are no obvious discrepancies between the calibrations of the two white dwarfs used here, and the resultant spectrophotometry is in relatively close agreement with the broad band fluxes. However, this uncertainty is compounded by the fact that quartz neutral density filters had to be used for most of the parallax stars observed and for these stars transmission functions taken from the AAT RGO spectrograph manual have been used to allow for the reduced intensities.

The near infrared spectrophotometry was obtained during an observing run on UKIRT in early August 1980. Owing to technical problems, cryostat UKT1 (f/9) was used with the f/35 chopping secondary. The CVF employed provides coverage of the spectral range 1.38 to 2.48 microns with a resolution of ~0.75%. Atmospheric water and CO_2 absorption bands cover the 1.7 to 2.0 micron wavelength interval. However the line of sight column

density of water vapour can be exceptionally low from Mauna Kea, and it proves possible to measure the stellar flux throughout the complete spectral range in our observations (with several important caveats, as described further below).

The observations have been reduced to a flux scale (Janskys) using observations of G stars taken from the Bright Star Catalogue (Table 6.2). If $I(\lambda)$ is the intrinsic stellar flux distribution and $f(\lambda)$ the wavelength dependence of the photometer+telescope system, including the influence of the Earth's atmosphere, then the observed spectrum is

$$S(\lambda) = I(\lambda) \ f(\lambda)$$

Late F and G stars essentially lack spectral features in the near infrared and their flux distribution can adequately be described by that of a blackbody of the appropriate effective temperature ($\sim$ 6500K). Thus observations of a programme star, $S_*(\lambda)$, can be transformed to apparent flux, $Q_*(\lambda)$, by

$$Q_*(\lambda) = S_*(\lambda) / S_s(\lambda) \quad x \ B(\lambda)$$

where $S_s(\lambda)$ is the observed G star flux distribution and $B(\lambda)$ the Planck curve. The effective temperatures used have been determined using Bessell's (1979) calibration with spectral type.

Table 6.2

Star	z	Spectral Type	Effective Temperature
BS 6775	1.09	F7 V	6300
BS 8772	1.60	G0 V	6000
BS 6093	1.09, 1.08 1.55	F0 V	7500
BS 8969	1.36	F7 V	6300
BS 7377	1.19	F0 IV	7500
BS 8665	1.55	F7 V	6300

To normalise $Q_*(\lambda)$, we use the standard star's K magnitude (effective wavelength 2.19 μ) and the blackbody flux at this wavelength, $B(\lambda_{eff})$. If,

$$S_o = 10.0^{0.4K} Z_o$$

where Z_o = 650 Jansky's (Table 6.1), then the absolute flux distribution of the programme star is given by

$$F_*(\lambda) = Q_*(\lambda)/B(\lambda_{eff}) \quad \times \quad S_o$$

This method could not be fully applied to the UKIRT observations, however. For reasons which are not at all clear the ratios between the total broadband K flux of the various stars observed were substantially different from the ratios of the flux in the CVF scans within the K passband. As the K magnitudes of both standards and programme stars are consistent with the AAT observations, this implies that the CVF scans — taken immediately after K photometry of each star - have zeropoints that are in error by up to a factor of two. Whatever the source, the indications are that this is a sensitivity variation, uncorrelated with wavelength, since the G star observations show that the ratio of intensities is constant outwith the atmospheric absorption band (Figure 6.1). Hence we have assumed that each reduced spectrum is on a flux scale, but with intensities which differ by some constant multiplicative factor from
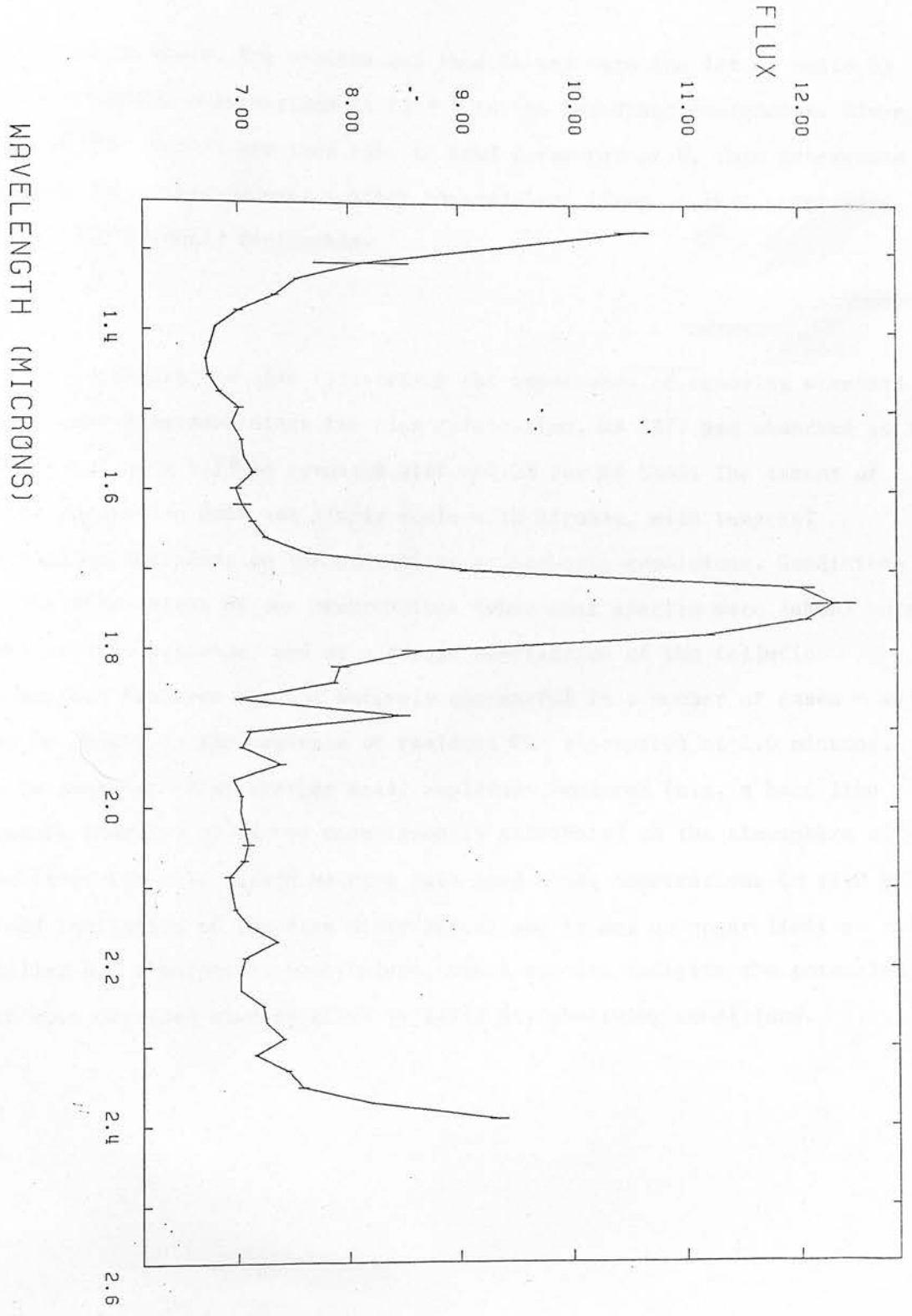
Figure 6.1   The ratio between CVF spectra of two G stars at different airmass, showing the variation in H_2O absorption.

the absolute scale. The spectra can thus be set onto the latter scale by normalising the observations at 2.19 μ to the broadband photometry. Since most of the spectra are then also in good agreement at H, this proceedure appears justified. However further observations (free of this perplexing error) are strongly desireable.

Figure 6.1 also illustrates the importance of choosing standard stars near programme stars for flux calibration. BS 7377 was observed at an airmass of only 1.19 as compared with z=1.08 for BS 8665. The extent of water absorption does not simply scale with airmass, with temporal variations dependent on the prevailing atmospheric conditions. Conditions on the final night of our observations (when most spectra were taken) were particularly variable, and as a result subtraction of the telluric absorption features was not entirely successful in a number of cases – as can be judged by the presence of residual CO_2 absorption at 2.0 microns. It is thus not clear whether small amplitude features (e.g. a band like feature near 1.8 μ) can be unambiguously attributed to the atmosphere of the star. For this reason we have only used these observations to give a broad indication of the flux distribution and to set an upper limit on the stellar H_2O absorption. Nonetheless, these spectra indicate the potential for more detailed studies given suitably dry observing conditions.

3 Luminosity Determination

The technique of fitting Planck energy distributions to broadband photometry in order to derive luminosities, effective temperatures and radii has been employed on a number of occasions. GNB used observations of two of the faintest known M dwarfs, Wolf 359 and VB 10, to determine bolometric magnitudes for these stars, as well as re-analysing Johnson's (1966) data on different spectral types to derive mean effective temperature and luminosity scales for the lower main sequence. As mentioned above, there is substantial blanketting shortward of 8000 A in M star spectra, with the absorbed radiation degraded to longer wavelengths. To allow for this GNB assume that this flux is re-emitted at a radius R_o , which is not equal to the stellar radius R, but is related to it by

$$R_o^2 \; \sigma \; T_o^4 \; = \; R \; \sigma \; T_e^4$$

Here T_e is the effective temperature and T_o the surface temperature at R_o , computed on the basis of a gray model in radiative equilibrium. Using this approximation, they calculate the variation of the expected blanketting (or backwarming) with wavelength for different effective temperatures and, maintaining the constraint that the total observed flux must equal that under the black body curve, set limits on the range of likely effective temperatures.

Less sophisticated variations of this technique - maintaining flux constancy while allowing for blanketting at shorter wavelengths - have

been used by Frogel, Kleinmann, Kunkel, Ney and Strecker (1972); Bopp, Gehrz and Hackwell (1974), Veeder (1974) and Petterson (1980).Apart from a number of stars in the last study, which includes data from a wide variety of sources, these investigations lack photometry at J which, at 1.2μ (1.25 μ for Johnson J), is close to the wavelength where maximum flux is emitted. We shall show that this leads to a significant underestimation of the total flux emitted by the stars of lowest luminosity.

The method of blackbody fitting that we have used here is to assume that there is neither significant blanketting nor backwarming at 2.19μ and thus the Planck curve can be scaled to fit at K. The effective temperature is determined by the flux constancy criterion, computing the observed total flux from the broadband photometry together with the area under the blackbody beyond K. The latter contributes between 10 and 15 percent of the total flux. To convert this apparent flux to a bolometric magnitude we adopt a solar luminosity of 3.826×10^{26} Watts (i.e. an effective temperature of 5770 K, Lang (1974)) and a solar absolute bolometric magnitude of +4.64. The latter is determined from the mean visual magnitude quoted by Harris (1961) and the bolometric correction of -0.12 derived by Buser and Kurucz (1978). Thus the apparent bolometric magnitude of a programme star is given by

$$m_{bol} = -2.5 \log f_{obs} - 19.07$$

where f_{obs} is the observed flux in Watts/m^2 .

The absolute bolometric magnitude then follows either from the known trigonometric parallax of the Gliese stars, or, for the SGP stars, from the $(M_I$, $(I-K)$) relation. In the former case the errors are ~ ± 0.2 on average, while there is a dispersion of ± 0.8 in the colour-magnitude relation. Finally, radii are derived from

$$L = 4 \pi R^2 \sigma T_e^4$$

The parameters derived for each programme star are listed in Table 6.3

There are obviously significant uncertainties in the results from this technique. All of the fits have been carried out in the $(F_\nu, \nu$) plane, where the spectrum peaks near H. In the $(F_\lambda$,λ) plane, however, the peaklies between I and J at ~ 1 micron, and this different weighting of the observed broadband photometry gives temperatures that are systematically lower by ~50K. The weighting of the data in the $(F_\nu$,ν) plane, however, is closer to the actual energy distribution and is therefore preferred. Secondly, our assumption that we measure blackbody flux at K is not in agreement with the results of GNB's blanketting computations, which indicate backwarming by ~0.13 in log(flux) at 2 microns for an effective temperature of 3500K and of 0.08 at 2750K. Inspection of their figures 2 and 3 suggests that the corresponding values at 2.2 microns are ~0.08 and 0.03 respectively. As we discuss further below, we believe that these values overestimate the extent of this effect. However, backwarming is certainly present amongst the hotter stars in the sample $(T_e > $ ~3400K) and this will lead to an underestimation of the temperatures by ~100K or more.

Indeed, it is likely that all disk stars with temperatures between ~3600K and 4000K are compressed into the range 3500-3600K by this calibration technique. Thus 3500K is effectively the useful upper limit for this method.

A further systematic bias could arise from the presence of strong spectral features between the photometric passbands. The optical regions (to 9000 Angstroms) are well covered and, indeed, there are no discrepancies of more than one percent (in inferred total flux) between the integrated IPCS flux and that derived using the VRI photomtery. However, the infrared passbands do not overlap, and strong steam bands could result in systematically too high temperatures being adopted for the coolest dwarfs. The UKIRT CVF scans cover part of these bands and show that straight line interpolation using JHK photometry adds between one (Gliese 884) and six (VB 10) percent to the final value of total flux that is deduced - equivalent to overestimating effective temperatures from 20 to 110 K (Figure 6.2). These discrepancies are relatively small and must be regarded as upper limits for two reasons. First, as we have already mentioned, residual atmospheric features are evident in several CVF spectra, including VB 10's (figure 6.4), and these will enhance the apparent discrepancy. Second, two stars (Gl 205 and 908) have scanner observatons from 5500 to 10000 Angstroms made by Cochran (1978). (In the former case .her observations at 8000 A differ by 0.05 in log F_ν from our I photometry (which exactly agrees with Cousins' (1980) magnitude) so we have scaled the scanner observations accordingly.) Both stars have more flux in the 9000 - 10000 A region than is estimated from the broadband interpolation - adding ~1 percent to the total flux. Finally, most of the available L photometry lies, within the errors, on our best-fit blackbody curve. Without complete spectral coverage it is not possible to fully
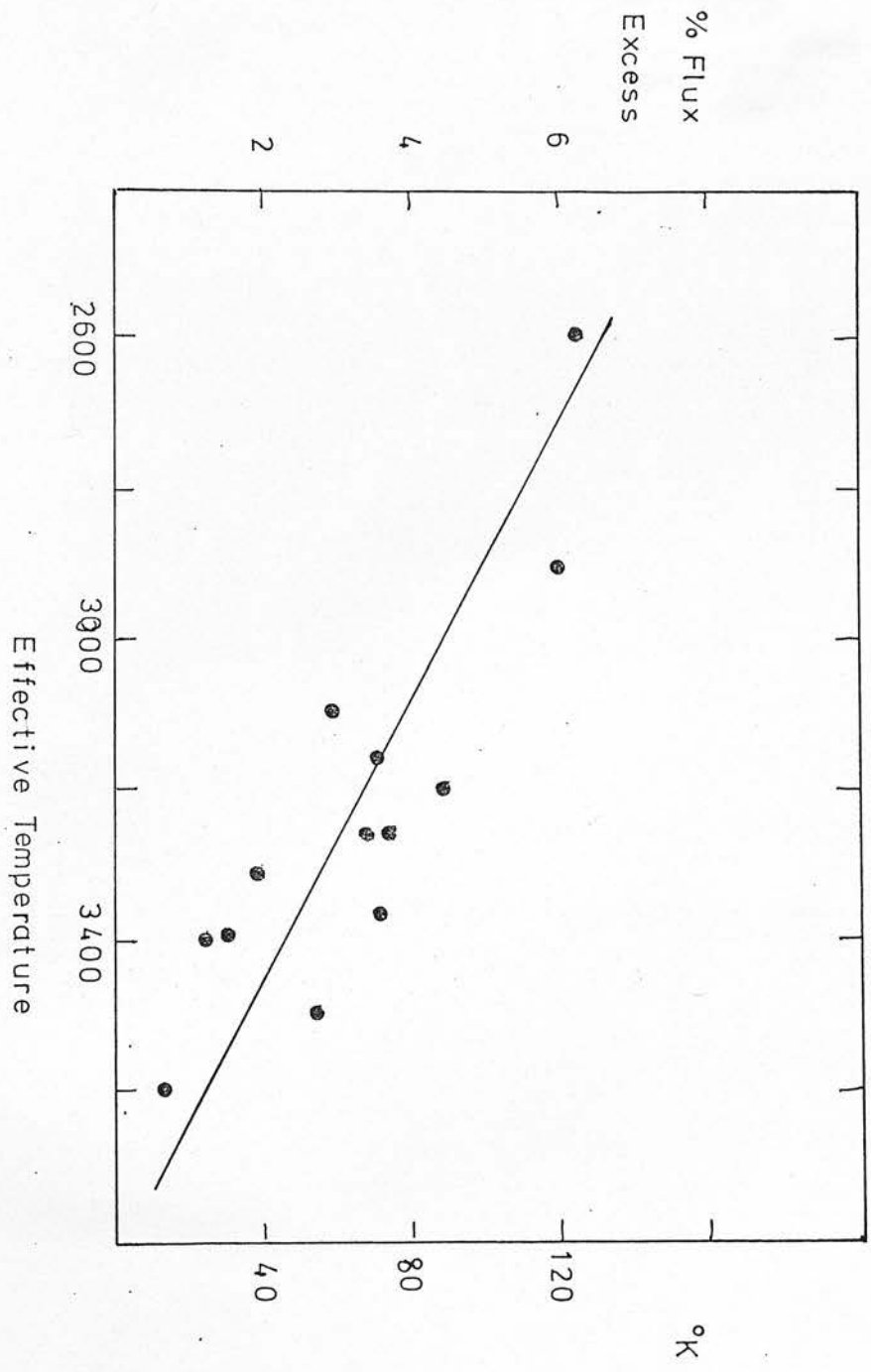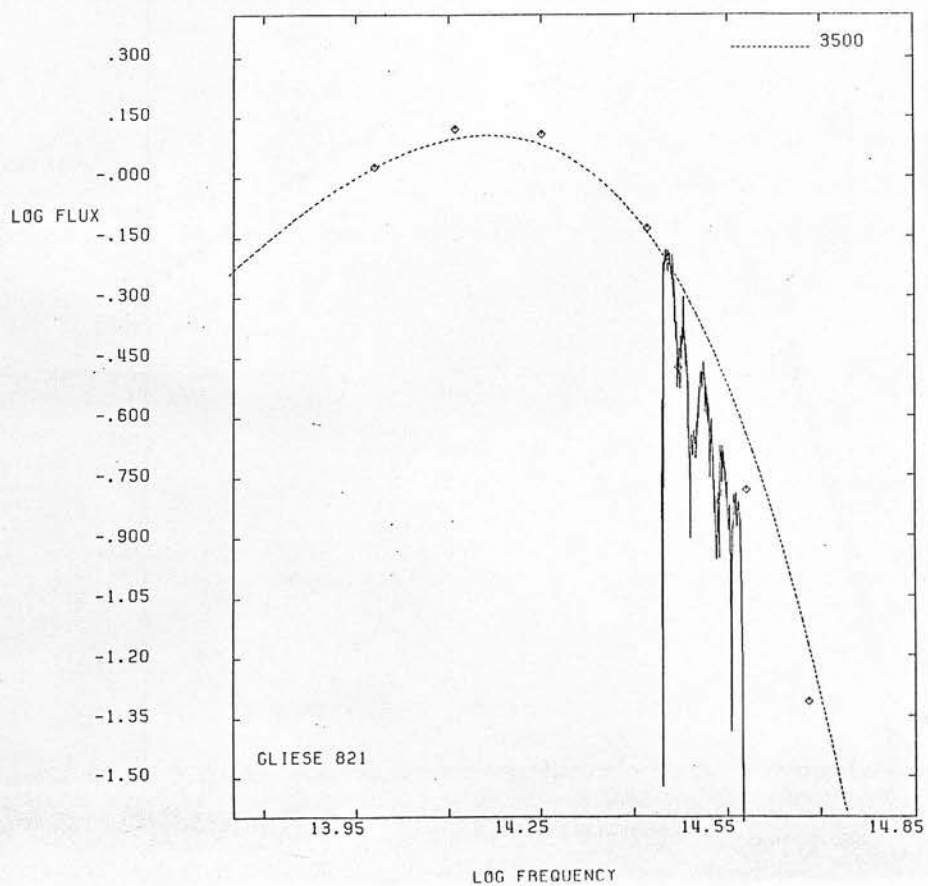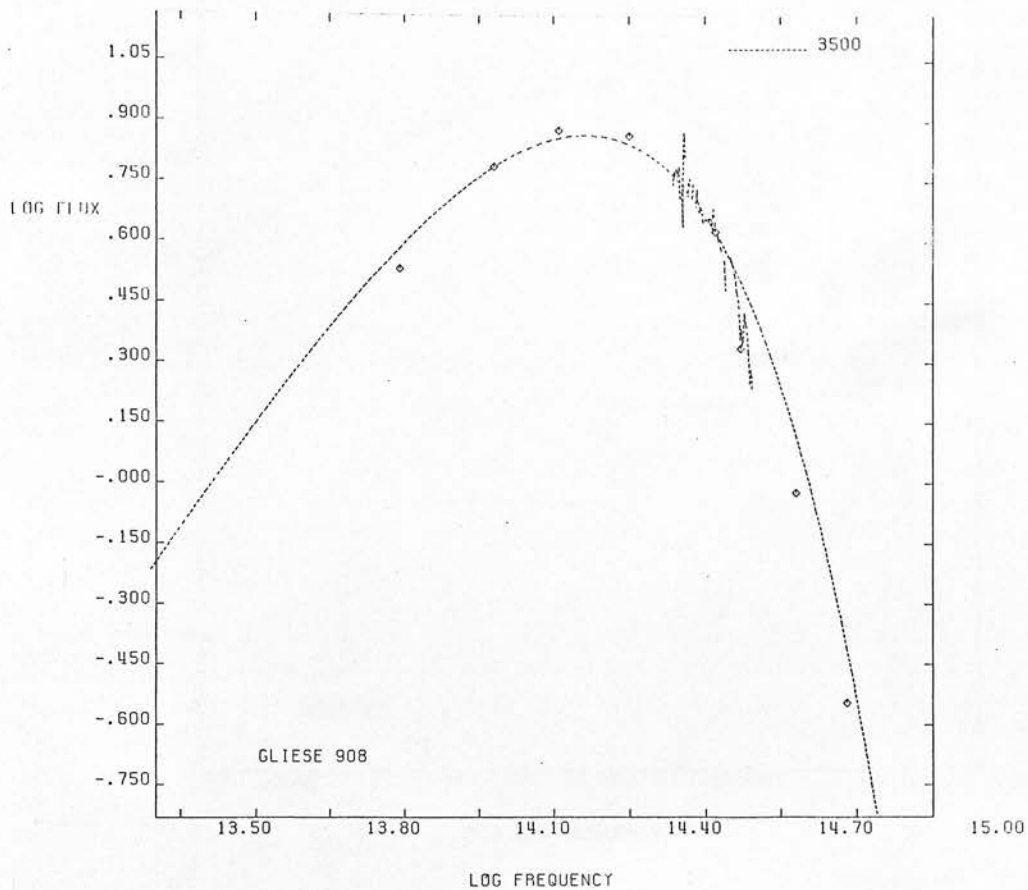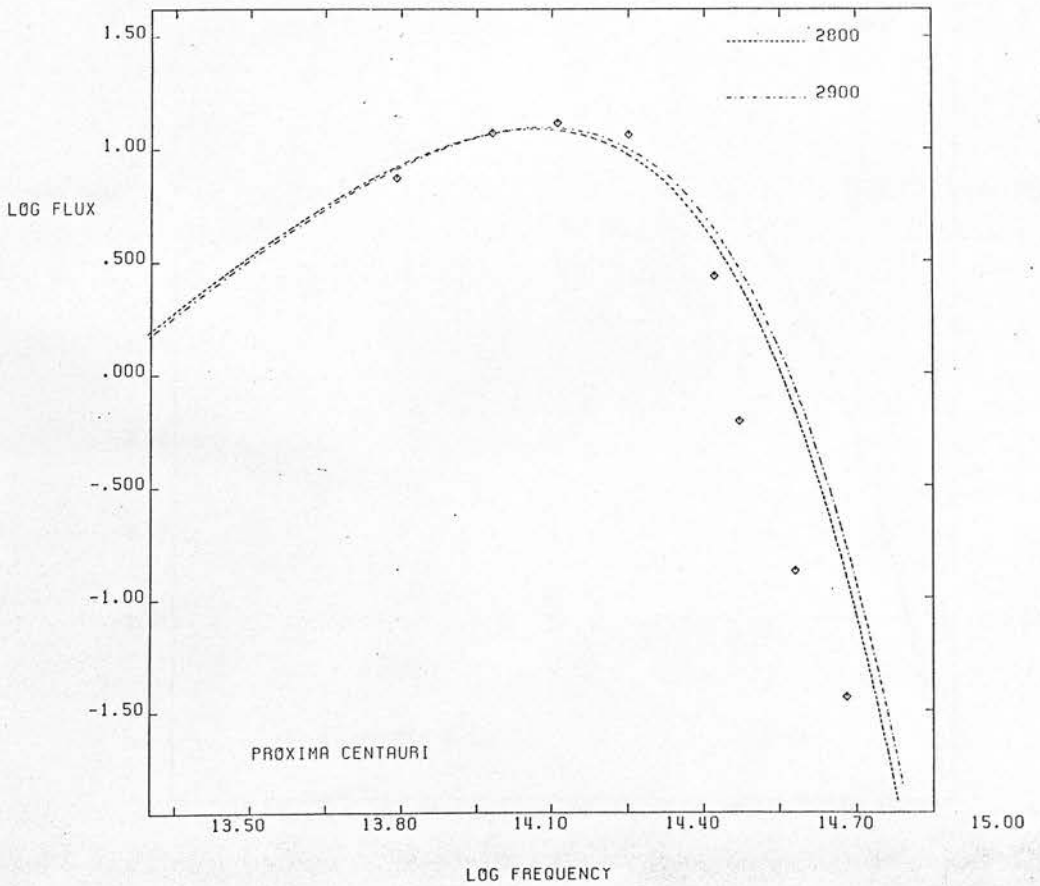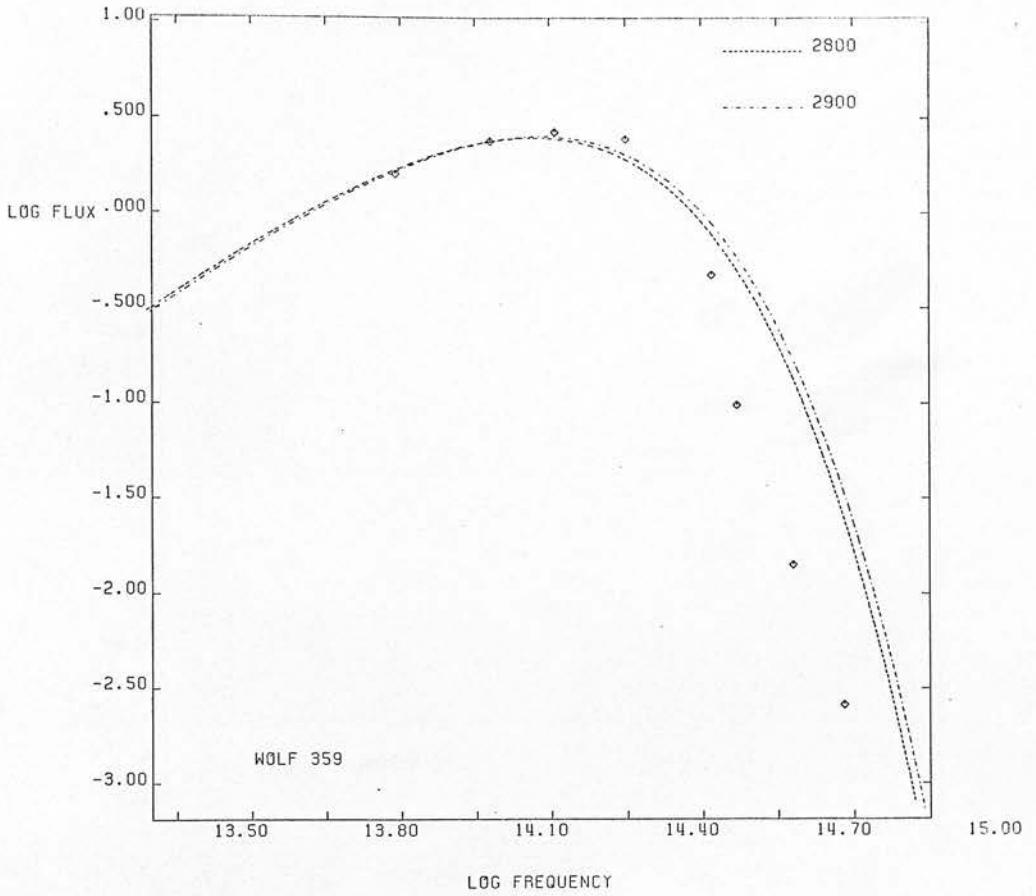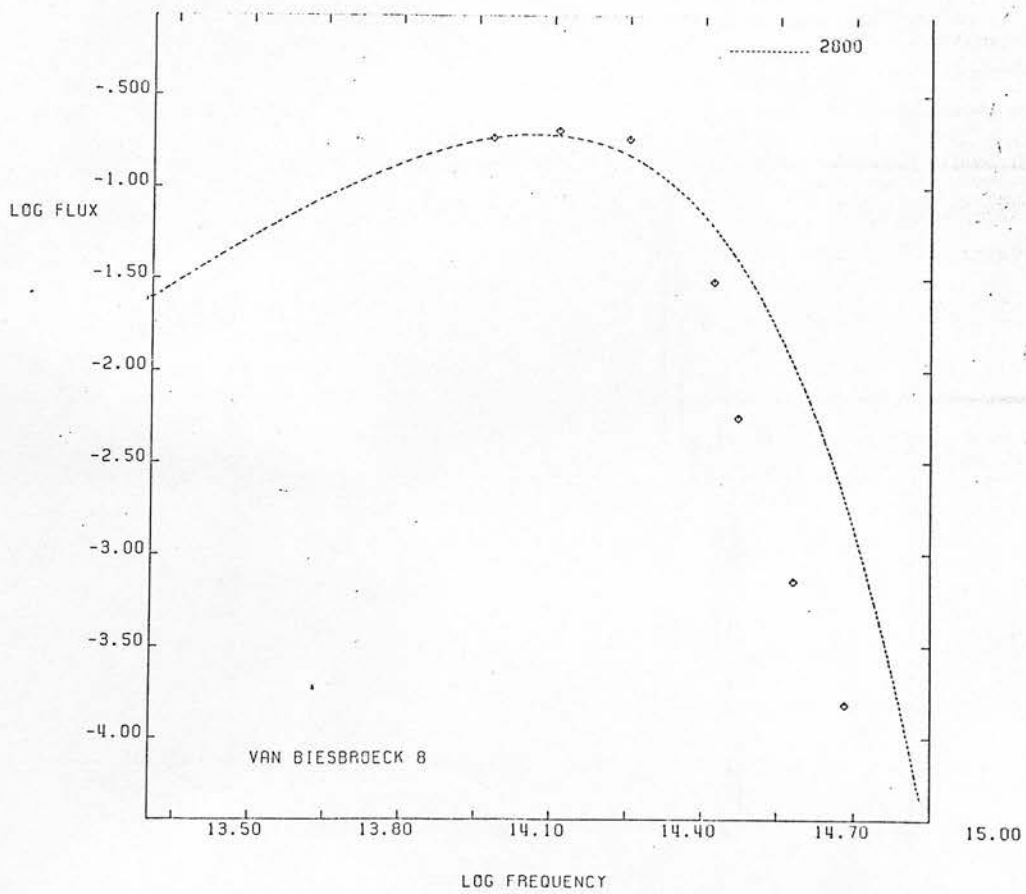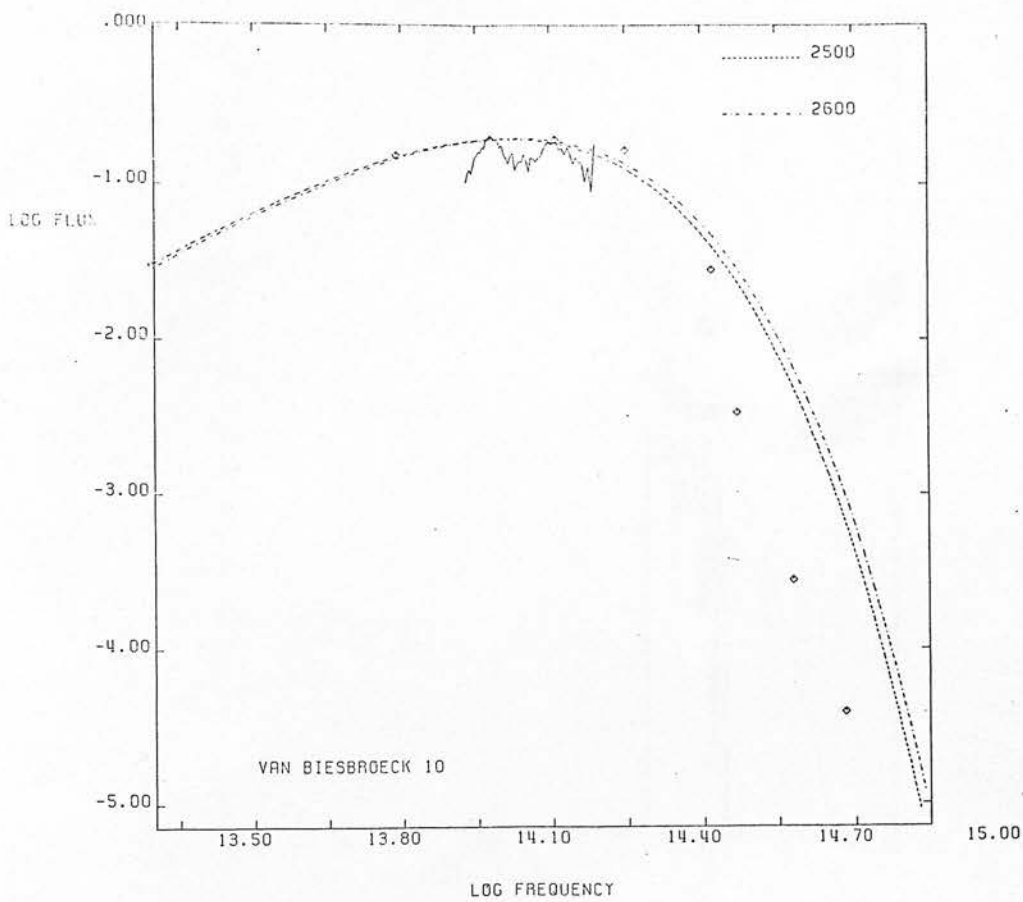
Figure 6.2   Variation with temperature of the apparent flux excess given
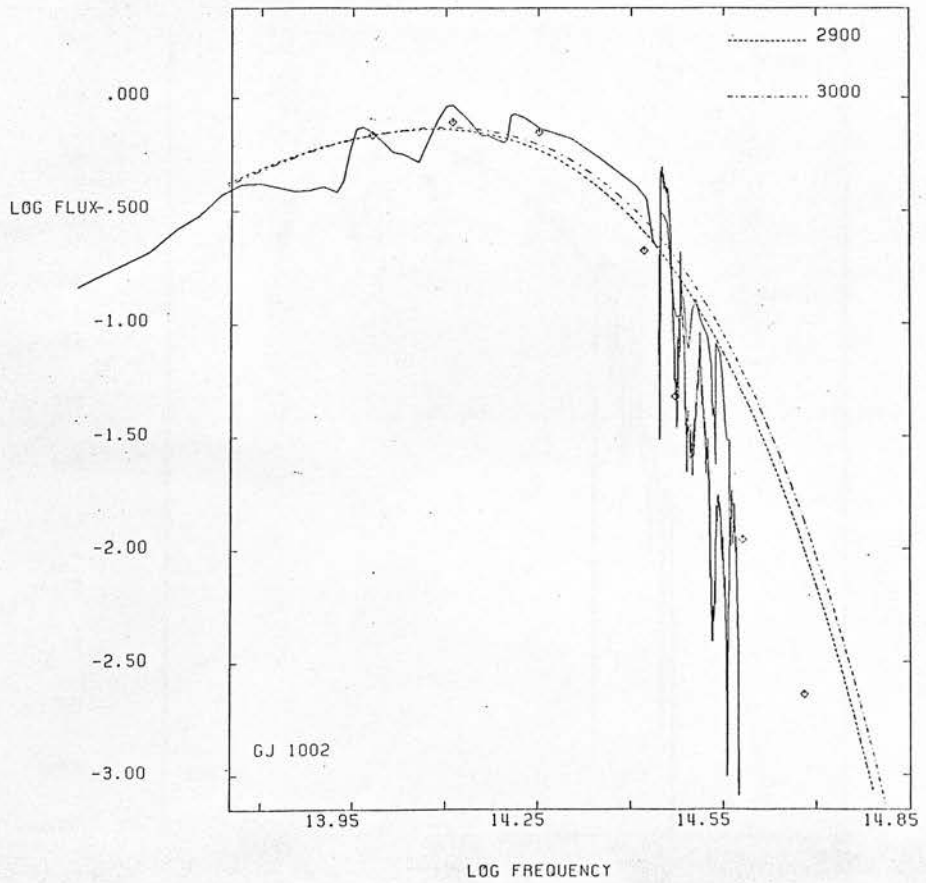by using only JHK, rather than spectrophotometric, fluxes.
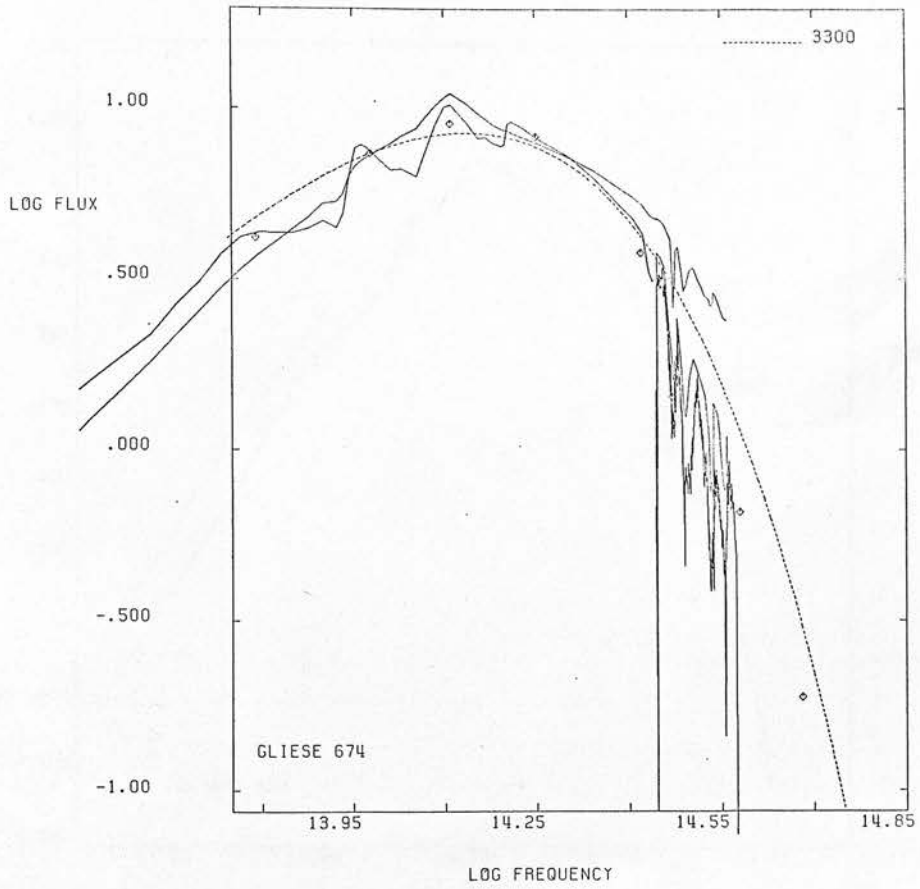
Figure 6.3   Representative blackbody fits. Mould models are also fitted
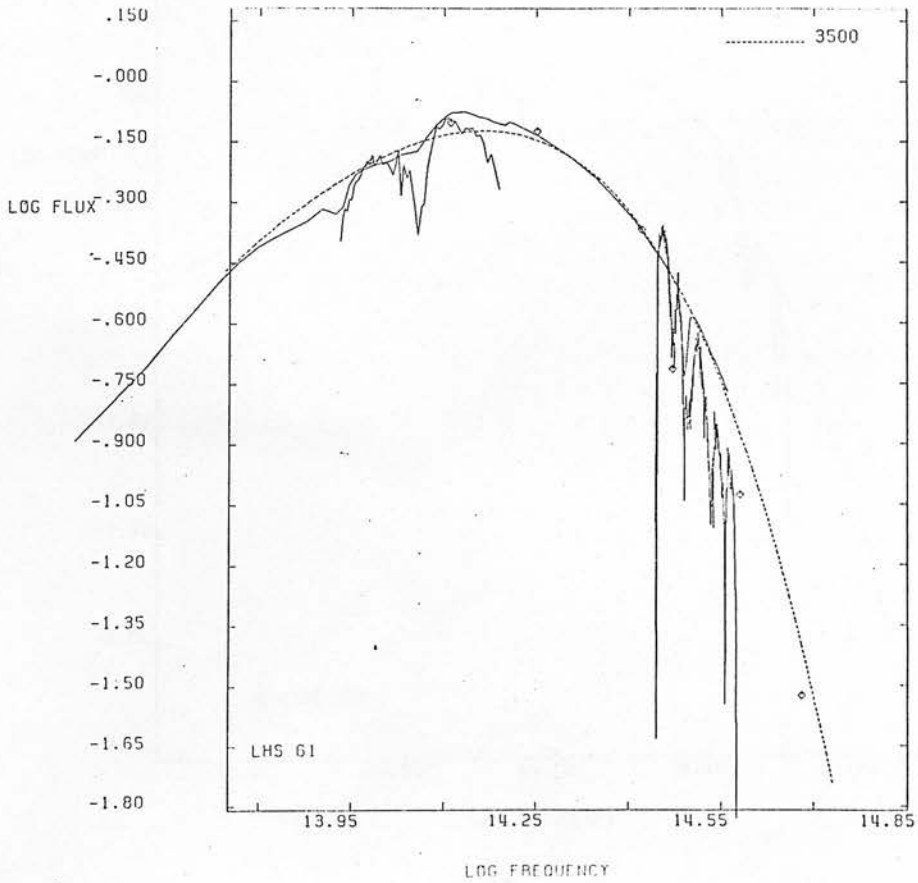   to some of the stars, as follows -
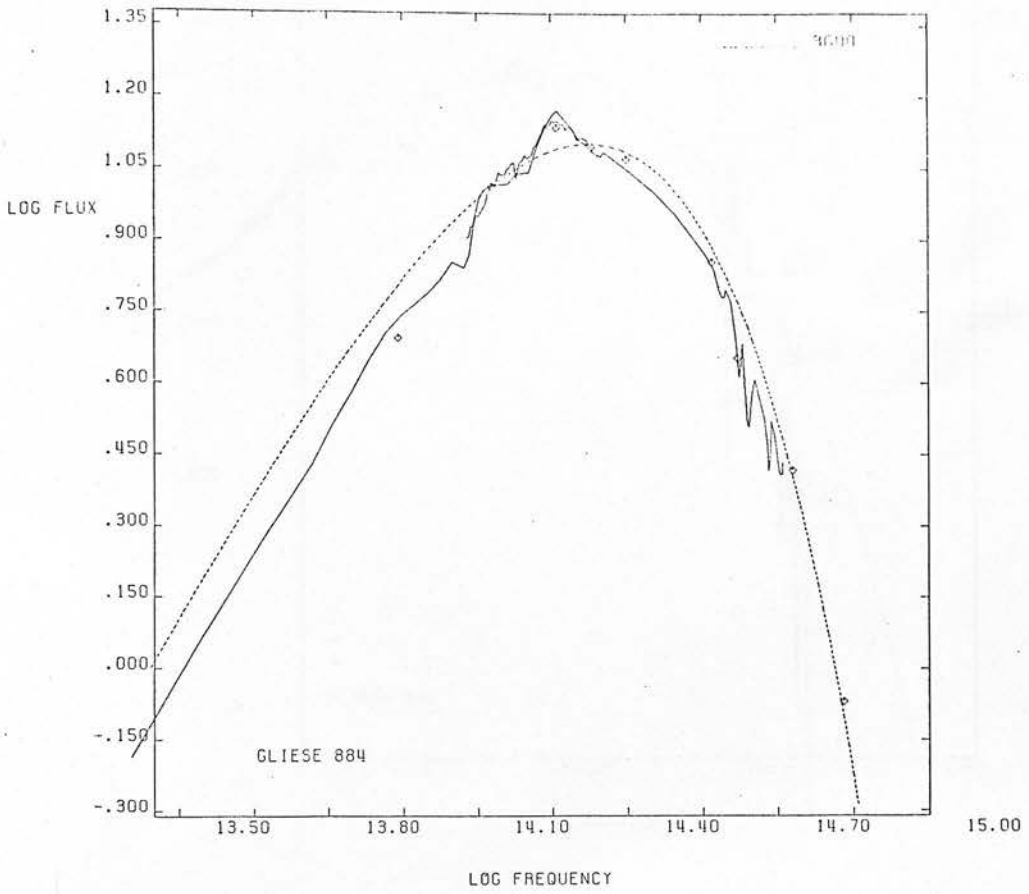   Gliese 674   4000K and 3250K old disk (OD) models
              GJ 1002   3000K OD
              LHS 61   3500K metals/100 (M/100)
              Gl 884   3750K OD
              Gl 866   3000K OD
              Gl 876   3250K and 3000K OD
              Gl 752a   3250K OD
              Gl 699   3250K M/5

GLIESE 908

GLIESE 821

WOLF 359

LOG FREQUENCY

PROXIMA CENTAURI

LOG FREQUENCY

VAN BIESBROECK 10

LOG FREQUENCY

VAN BIESBROECK 8

LOG FREQUENCY

LOG FLUX

GLIESE 674

LOG FREQUENCY

LOG FLUX

GJ 1002

LOG FREQUENCY

GLIESE 884

LOG FLUX

LOG FREQUENCY

3600

3500

LHS 61

LOG FLUX

LOG FREQUENCY

GLIESE 876

GLIESE 866

LOG FLUX

3300

GLIESE 752A

LOG FREQUENCY

LOG FLUX

3200

3300

BARNARD'S STAR

LOG FREQUENCY

RG 0050.5, -2722

RG 0049.5, -2857

Table 6.3

Star	M(bol)	Log(L/L$_\odot$)	Log(R/R$_\odot$)	T(eff)
RG0044.3,−2554	8.69	−1.608	−0.319	3300
RG0044.4,−2639	10.59	−2.368	−0.616	3000
RG0046.0,−2832	11.42	−2.700	−0.752	2900
RG0046.2,−2636	9.70	−2.012	−0.466	3100
RG0047.5,−3009	10.48	−2.324	−0.594	3000
RG0049.5,−2857	9.46	−1.916	−0.446	3200
RG0050.5,−2722	13.53	−3.544	−1.079	2600
RG0052.2,−2821	10.72	−2.420	−0.642	3000
RG0052.2,−2940	10.77	−2.440	−0.637	2950
RG0053.6,−2654	7.93	−1.304	−0.192	3400
RG0053.8,−2630	10.79	−2.448	−0.656	3000
RG0054.0,−2945	11.01	−2.536	−0.685	2950
RG0055.2,−2700	10.98	−2.524	−0.664	2900
RG0055.8,−2621	11.08	−2.564	−0.714	3000
RG0055.8,−2807	10.69	−2.408	−0.636	3000
RG0058.7,−2713	10.77	−2.440	−0.637	2950
RG0058.7,−2829	9.88	−2.084	−0.557	3300
RG0058.8,−2807	13.87	−3.680	−1.212	2800
RG0058.9,−2812	10.98	−2.524	−0.694	3000
RG0059.2,−2715	11.29	−2.648	−0.711	2850
RG0059.7,−2547	11.83	−2.864	−0.819	2850
RG0100.1,−2656	10.85	−2.472	−0.668	3000
RG0101.5,−2821	9.17	−1.800	−0.388	3200
RG0101.6,−2542	10.27	−2.240	−0.580	3100
RG0101.6,−2615	10.79	−2.448	−0.656	3000
RG0102.0,−2938	10.85	−2.472	−0.668	3000
RG0102.2,−2609	10.70	−2.412	−0.623	2950
RG0102.6,−2720	11.11	−2.576	−0.690	2900
LHS 61	8.50	−1.532	−0.332	3500
LHS 3602	9.69	−2.008	−0.519	3300
LHS 3839	9.91	−2.096	−0.508	3100
LP 826−500	9.93	−2.104	−0.512	3100
LP 826−261	8.20	−1.412	−0.246	3400
GL 1	8.75	−1.632	−0.369	3450
GJ 1002	12.56	−3.156	−0.995	2950
GL 79	7.47	−1.120	−0.126	3500
GL 83.1	11.05	−2.552	−0.736	3100
GL 87	8.59	−1.568	−0.324	3400
GL 191	9.53	−1.944	−0.550	3550
GL 205	7.61	−1.176	−0.116	3350
GL 213	10.12	−2.180	−0.578	3200
GL 273	9.64	−1.988	−0.482	3200
WOLF 359	11.92	−2.900	−0.837	2850
GL 551	11.59	−2.768	−0.771	2850
GL 595	9.99	−2.128	−0.592	3350
GL 631	6.50	−0.732	−0.110	4300
GL 643	10.43	−2.304	−0.653	3250
GL 644A	8.01	−1.336	−0.169	3250
VB 8	12.75	−3.232	−0.988	2800
GL 674	9.10	−1.772	−0.401	3300
GL 699	10.87	−2.480	−0.741	3250
GL 701	8.61	−1.576	−0.328	3400

GL 729	10.73	-2.424	-0.700	3200
GL 748	8.82	-1.660	-0.345	3300
GL 752A	8.35	-1.472	-0.251	3300
VB 10	12.88	-3.284	-0.949	2600
GL 821	9.23	-1.824	-0.478	3500
GL 831	9.80	-2.052	-0.472	3050
GL 866	10.80	-2.452	-0.628	2850
GL 876	9.36	-1.876	-0.398	3100
GL 884	7.51	-1.136	-0.158	3600
GL 908	8.72	-1.620	-0.376	3500

assess how these detailed effects balance out, so we have not.applied
corrections to the broadband-derived temperatures. In our view this is
unlikely to induce systematic errors of more than 50K even at the lowest
temperatures. Typical blackbody fits are illustrated in figure 6.3. Random
errors in effective temperature are nominally ± 50K (2.5 percent in total
flux).

The effective temperature scale derived can be tested using
photometry of the eclipsing binaries YY Geminorum (Veeder, 1974) and CM
Draconis (Lacy, 1977b). Probably through backwarming at K, our method
underestimates the effective temperature of the former, but to an extent
dependent on the (assumed) J magnitude. For 6.6 < J < 6.8 the best fit
temperature lies in the range 3500-3600 K - as compared with the 3770 ± 200
K determined from the measurement of the stellar radii by Kron (1952) and
by Leung and Schneider (1978). Similarly, for CM Draconis Lacy derived an
effective temperature of 3150 ± 100 K, as compared with the 3180 ± 30 K
(errors equivalent to changes of 2 percent in the total flux) that we
obtain from fitting to his photometry. These two stars can be used to set
limits on the degree of backwarming at K, with a flux excess (over
blackbody) of 12 percent giving agreement for YY Geminorum. Even a five
percent excess, however, raises the temperature derived for CM Draconis to
3250K, and we conclude that our fitting technique is reasonably reliable
for the cooler (T$_e$ < 3300 K) stars in our sample.

Comparing our results with previous studies (Table 6.4) there is
good agreement amongst the bolometric magnitudes, since the total flux is a
well defined quantity. However, while our temperature scale is in
relatively good agreement with Petterson's, Veeder's results are cooler by

Table 6.4

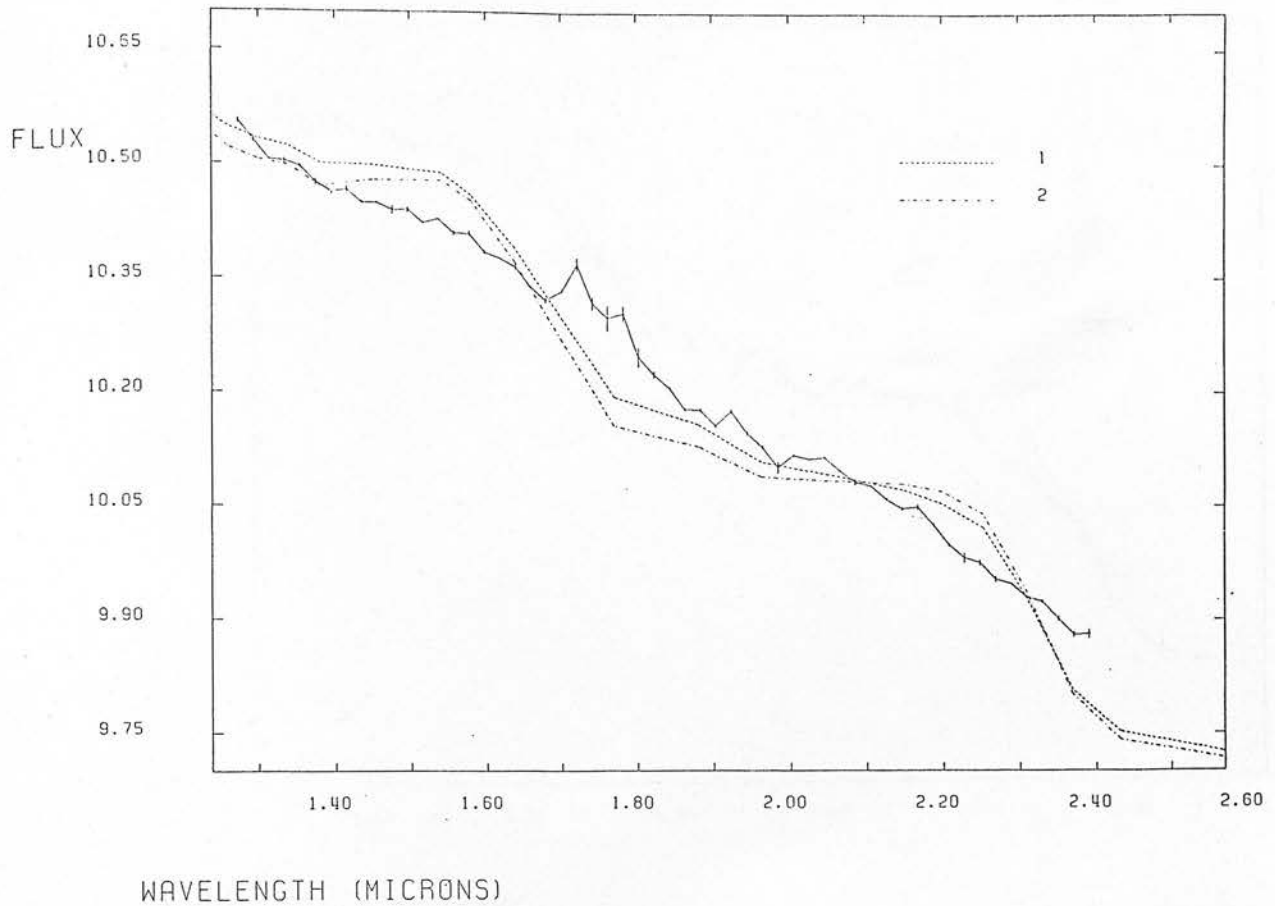| Star	This paper M_{bol}	T_e	Petterson M_{bol}	T_e	Veeder M_{bol}	T_e	GNB M_{bol}	T_e	Frogel et al M_{bol}	T_e
GJ 1002	12.55	2950			12.0	2700				
Gl 205	7.6	3350			7.6	3600				
Gl 213	10.1	3200			10.1					
Gl 273	9.65	3200			9.6					
Gl 406	11.9	2850	12.2	2800	12.2	2500	12.2	2500		
Gl 551	11.6	2850	11.6	3050	11.7	2750			11.66	2700
Gl 644A/B	8.7	3350	8.7	3400	8.7	3450	*			
Gl 699	10.9	3250			10.9	3250				
Gl 729	10.7	3200	10.7	3100	10.9	3000				
Gl 752A	8.35	3300			8.4					
VB 10	12.9	2600	13.15	2200			13.15	2250		
Gl 866	10.8	2850	10.65	3000	10.9	2750				
Gl 876	9.4	3100			9.4					
Gl 884	7.5	3600			7.4					
Gl 908	8.7	3500			8.7					

*   assuming equal components

Figure 6.4   CVF scans (in Log F_λ vs λ in microns) with Mould models
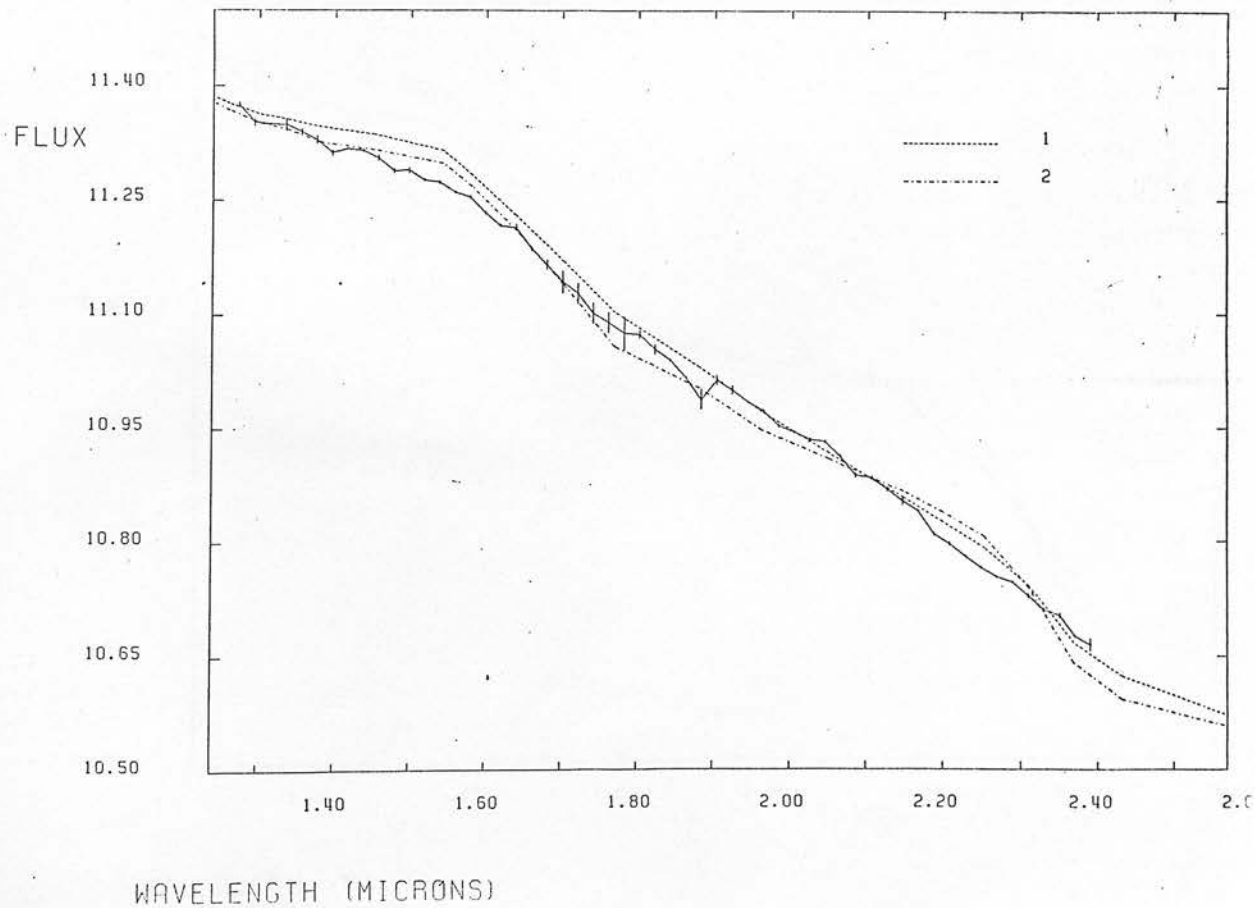   The models are –
              G1 701   1 – 3750K OD,   2 – 3500K OD
              G1 884   1 – 4000K OD,   2 – 3750K OD
              G1 866   Auman 3000K OD model
              G1 866   1 – 3250K OD   2 – 3000K OD
              G1 699   1 – 3250K OD,   2 – 3250K M/10
              G1 643   1 – 3250K OD,   2 – 3250K M/10
              VB 10   3000K OD model
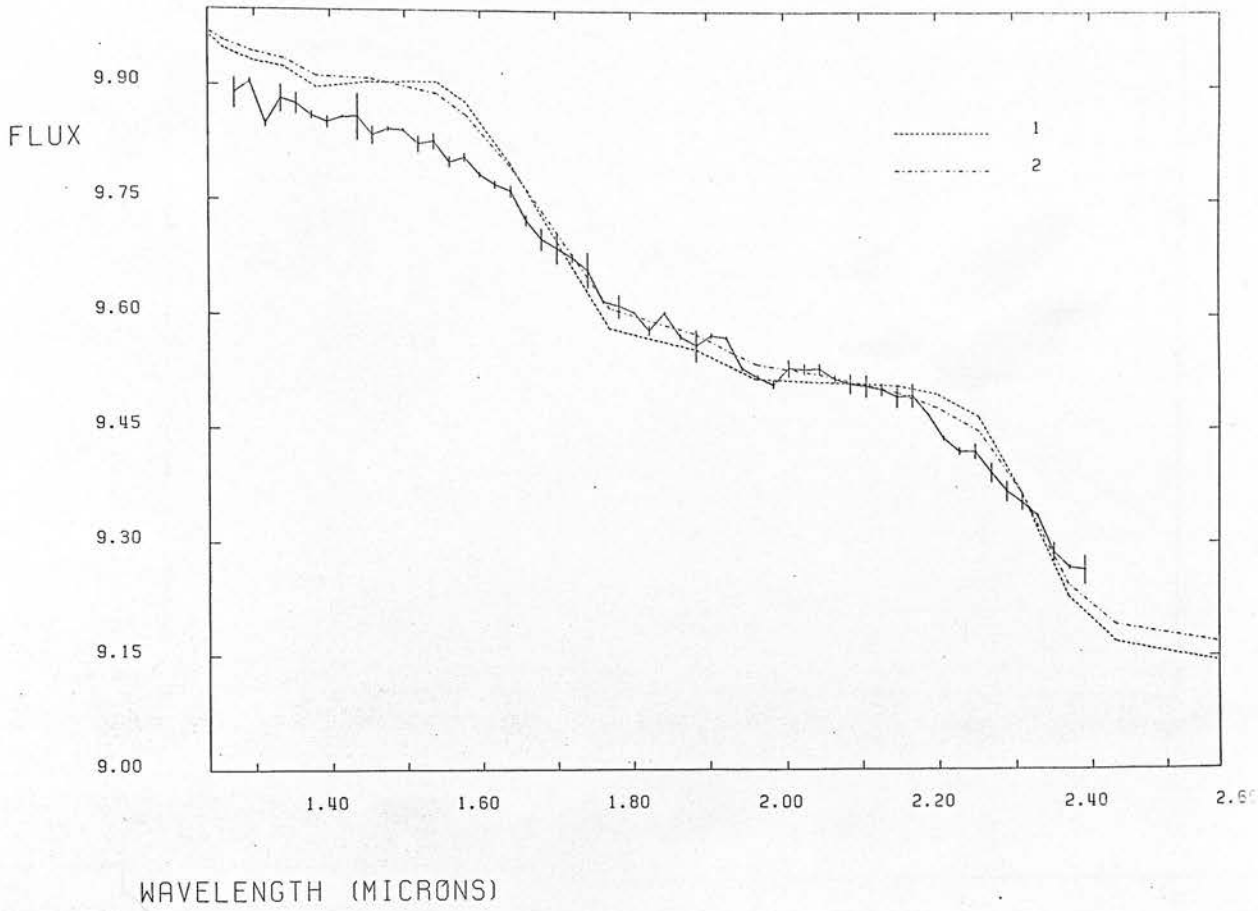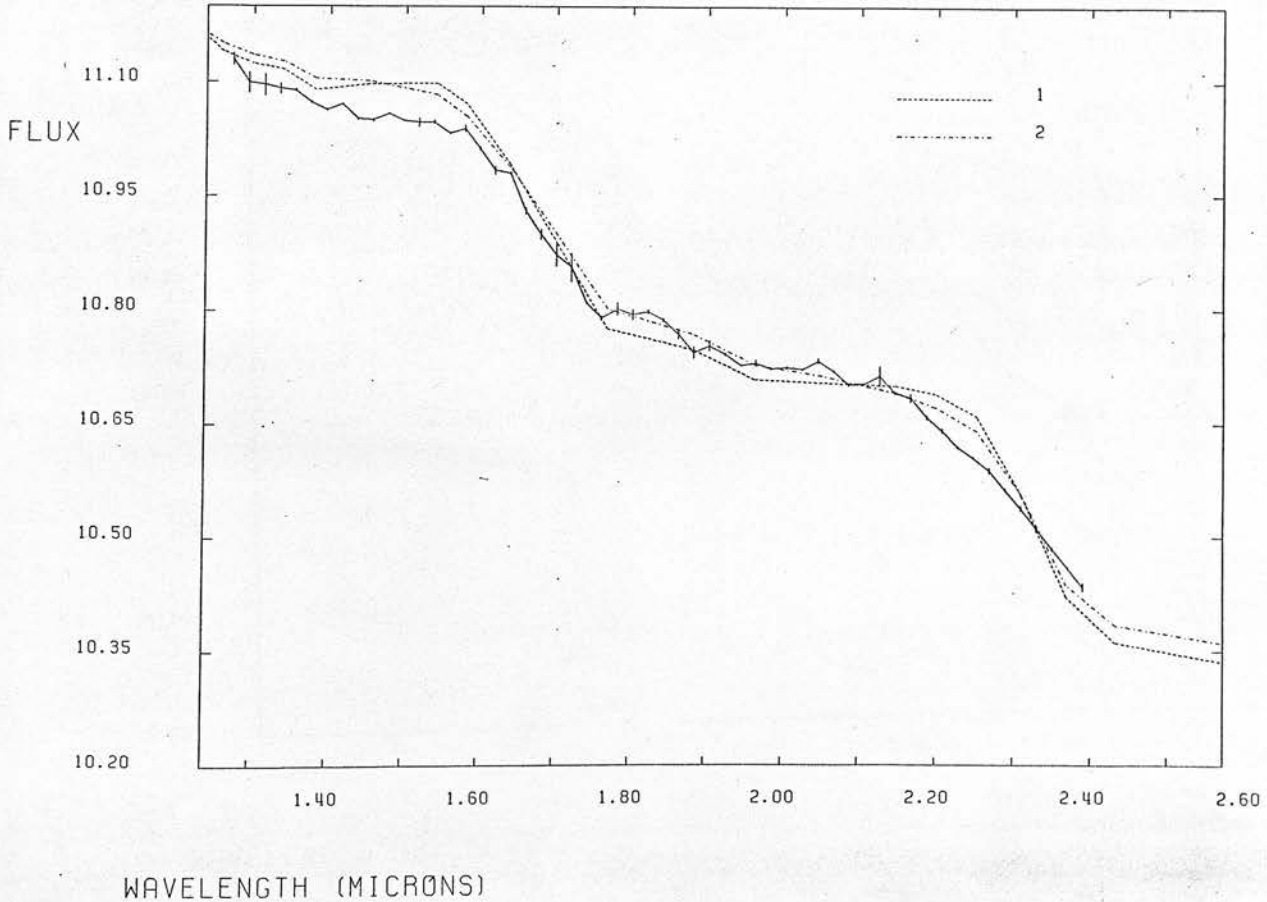   LHS 61   3500K M/100 model

GLIESE 701

FLUX

WAVELENGTH (MICRONS)

GLIESE 884

WAVELENGTH (MICRONS)

GLIESE 643

WAVELENGTH (MICRØNS)

BARNARD'S STAR

WAVELENGTH (MICRØNS)
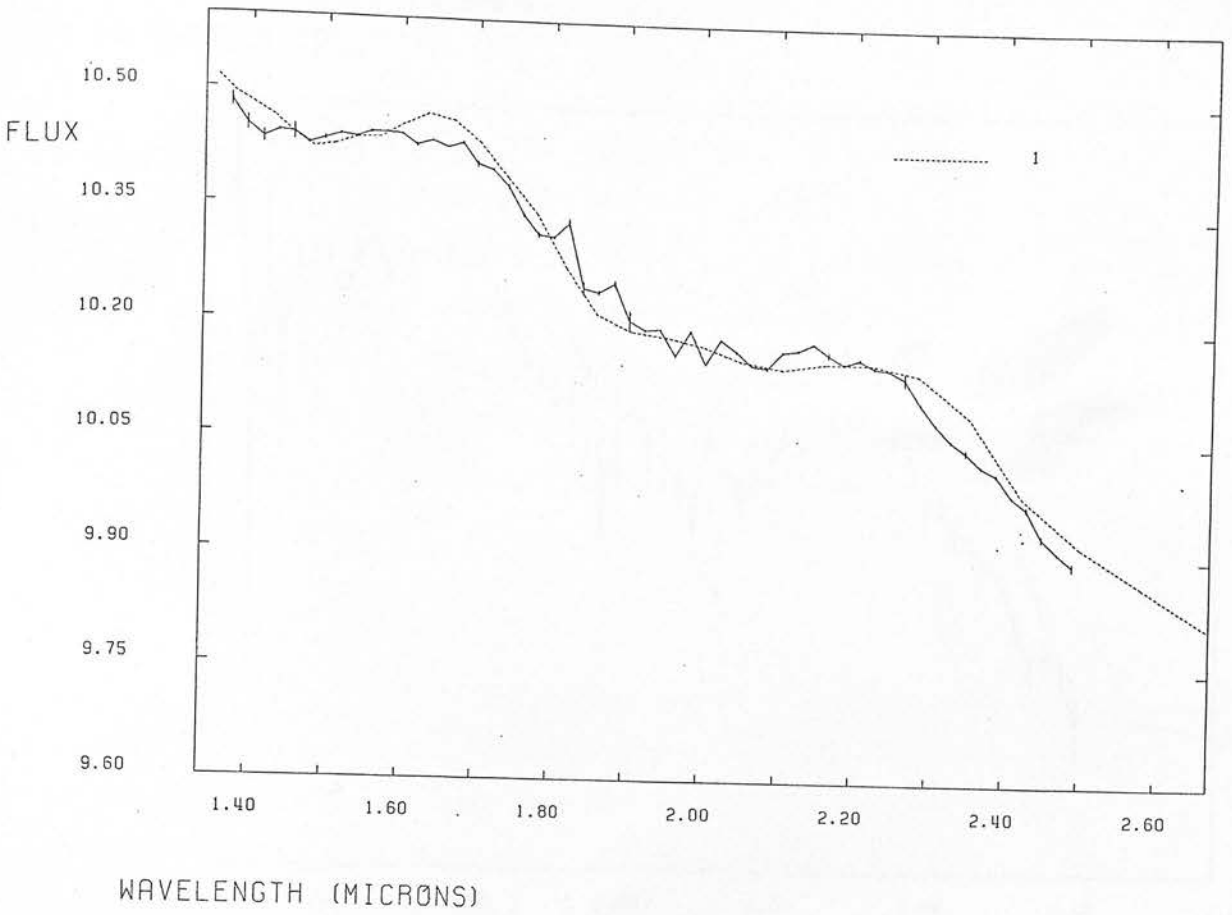
GLIESE 866

GLIESE 866

VAN BIESBROECK 10

WAVELENGTH (MICRONS)

LHS 61

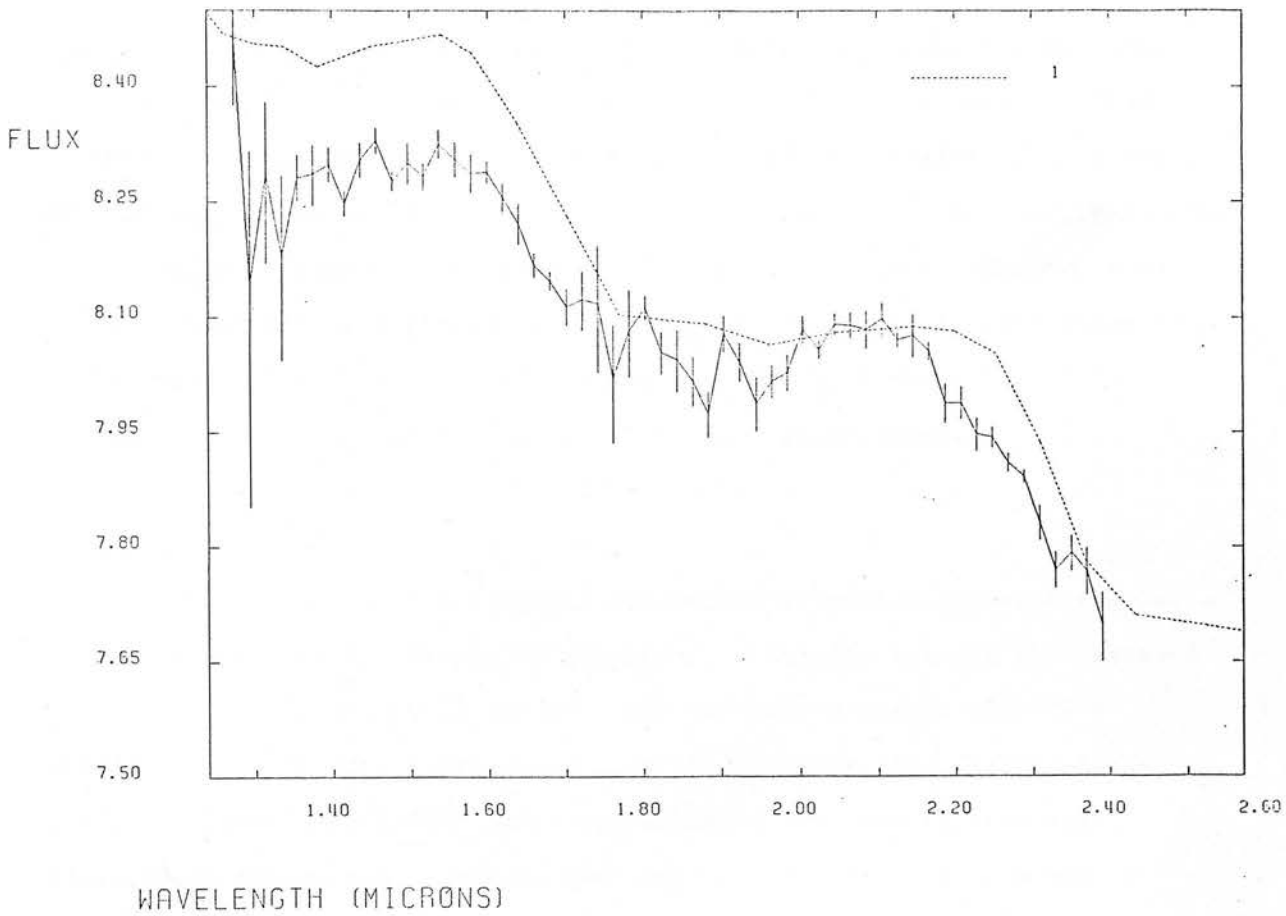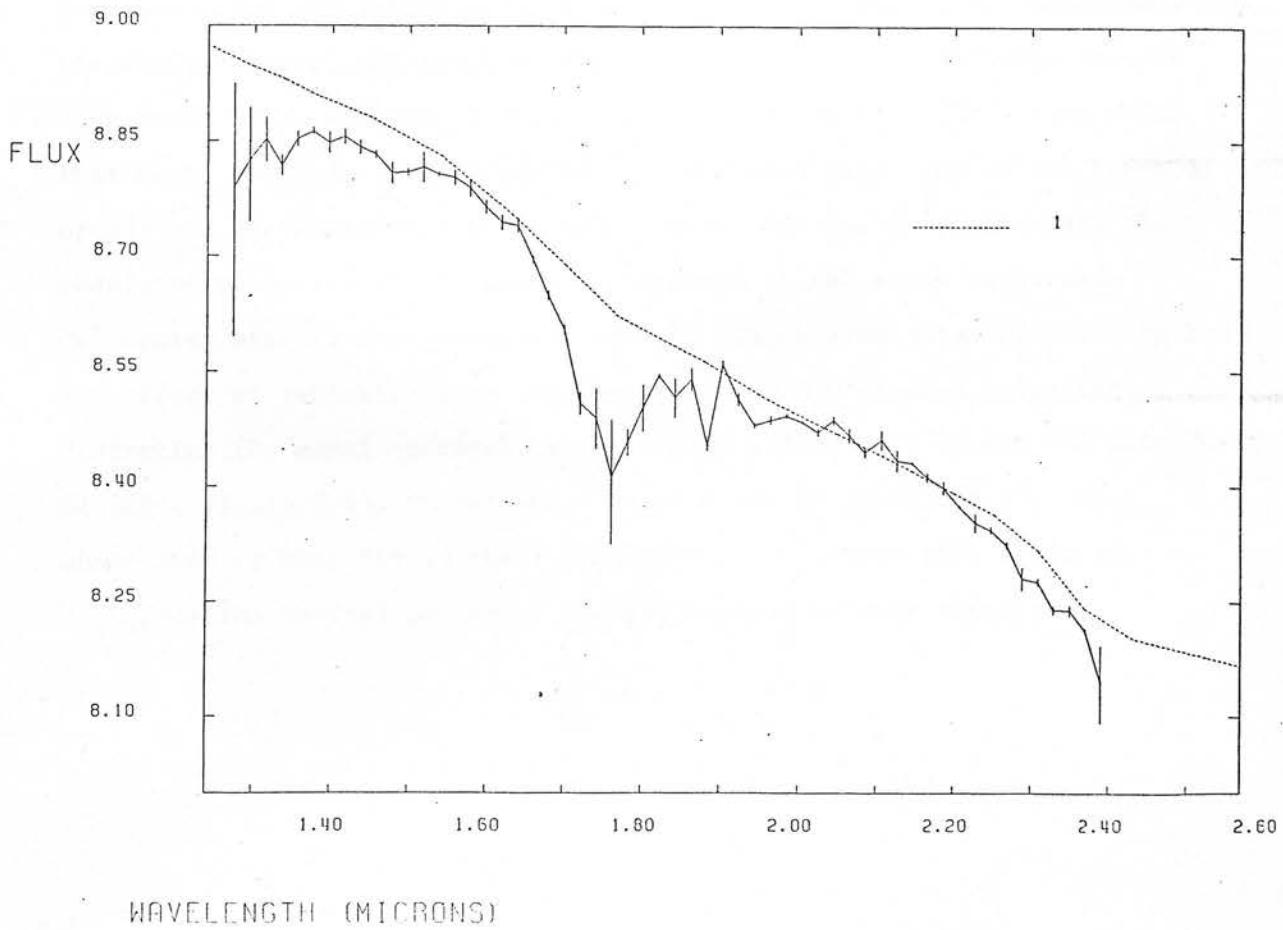WAVELENGTH (MICRONS)
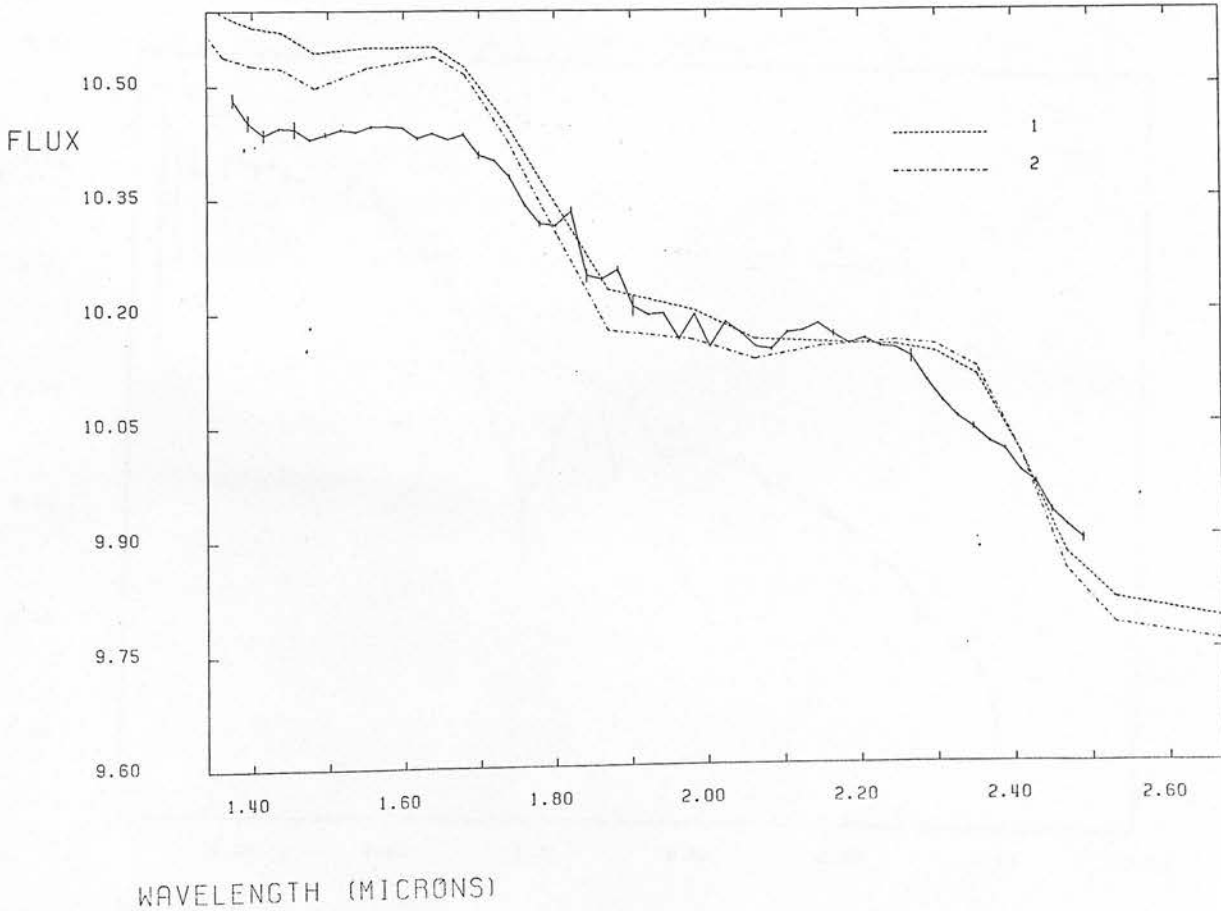
~200K for temperatures below 3100 K (his scale). This primarily reflects the effect of linear interpolation between I and H in the observed flux distribution. For example, applying our technique to UBVRIHKL photometry of GJ 1002 results in an effective temperature estimate of 2750K (cf. Veeder's quoted value of 2700 K). The lack of photometry at U in our observations makes no significant difference. The effect is most dramatically shown in GNB's results for VB10 and Wolf 359 (Gl 406) which, without 1.2 μ photometry, severely underestimate the stellar temperature.

Finally, Mould and Hyland determined effective temperatures for a number of stars in our sample by minimising residuals between the observed colours (R-I), (I-J), (H-K) and 1μΔ (the narrowband colour m(7540) − m(10235)) and colours synthesised from the emergent flux distributions predicted by Mould's (1976) model atmospheres. The temperatures are compared in figure 6.5, where we have included the results from our analysis of their photometry of stars not actually in our own sample. While the overall ranking of the stars is similar, MH deviate from our scale at both ends. For the hotter stars this undoubtedly reflects the inadequacy of blackbody fitting, and supports the contention that the technique breaks down near 3500K. However, Persson, Aaronson and Frogel (1977) have shown that Mould's models fail to predict the detailed behaviour of the infrared broad- and narrowband colours in the coolest dwarfs. In particular, the models overestimate the increase in strength of the steam bands with decreasing effective temperature, and the exagerrated water blanketting has the effect of redistributing the flux into the H_2O windows − further distorting the model spectrum. This is well illustrated by our CVF data for Gl 866 (figure 6.4). MH derived a temperature of 3000K but the water absorption is best fit by their 3250K model − although this fails to reproduce the optical spectrum. The discrepancy between model and
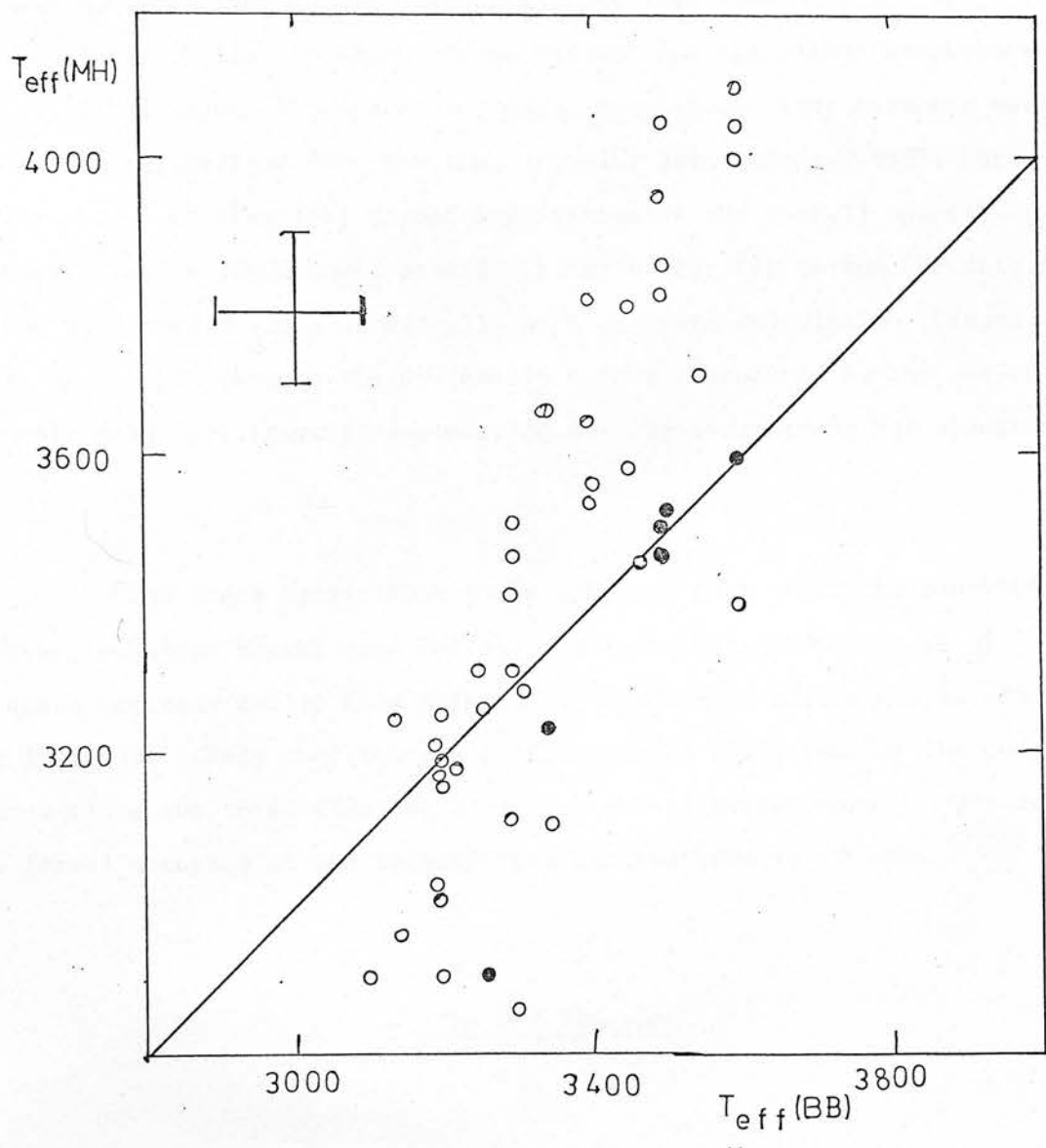
Figure 6.5   Comparison of MH temperature scale with that derived from our
             method of blackbody fitting.

observations at 2.4 μ is probably due to CO absorption - which is not included in Mould's calculations.

As an aside, the calculations for the Mould models incorporated TiO and H_2O opacities in the form of opacity distribution functions, with the H_2O data supplied by Auman. Auman himself has calculated atmospheres for a limited range of temperatures and compositions using harmonic mean H_2O opacities, derived from the same original data (Auman, 1969). Carbon (1974) has shown that this method underestimates the overall opacity. However, Auman's 3000K model provides a far better fit to the CVF data on Gl 866 than does Mould's numerically more accurate calculation (Figure 6.4), presumably through the systematic errors introduced by the use of the harmonic mean fortuitously compensating for the over-strong H_2O opacities.

From these comparisons it is apparent that while the blackbody fitting technique breaks down for stars hotter than ~3400K, it is of adequate accuracy cooler than this limit. Systematic biases may be present, but it is not likely that these are of more than 100K even for the coolest stars. Since the total flux can be determined to better than ± 5 percent, the formal accuracy of the temperatures derived here is ± 100K.

4   The H-R Diagram

Using the results of Section 3 we can construct an empirical $(Log(L/L_0) - Log(T_e))$ H-R Diagram for the lower main sequnce, and this is shown in figure 6.6 together with the hydrogen burning main sequence and
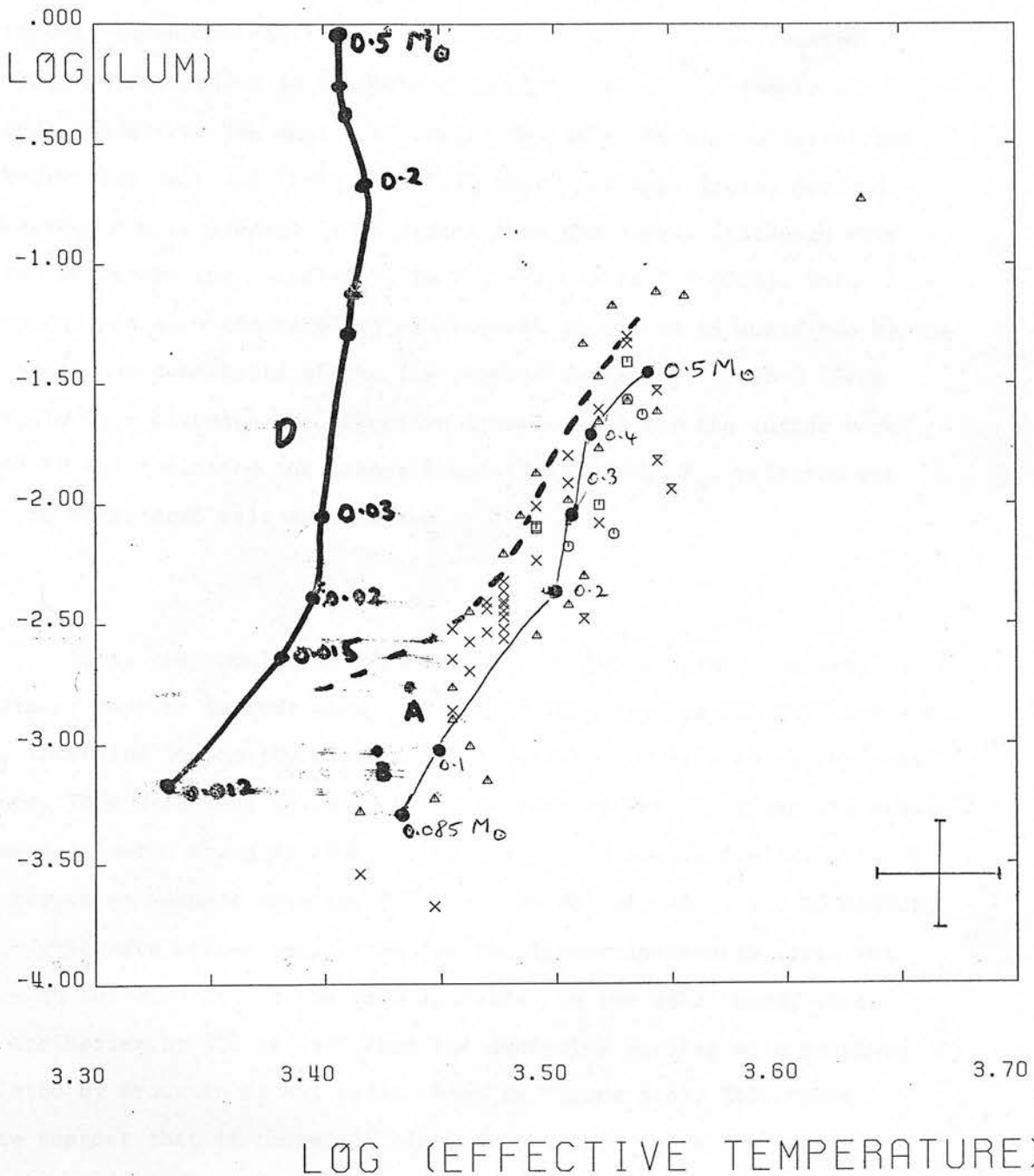
Figure 6.6   H-R diagram for stars in our sample. The stars are subdivided
into disk dwarfs ($\triangle$), disk subdwarfs (O), halo subdwarfs (X)
SGP stars (X), and Luyten proper motion stars ($\square$). The
points marked A and B are the components of the double star
L726-8. Also shown are the theoretical deuterium burning
main sequence (D) and the 10^8 and 10^9 year isochrones for
H-burning stars from Grossman et al (1974). Representative
masses (in solar units) along these tracks are marked.

the 10^8 year isochrone from the interior models calculated by Grossman, Hays and Graboske (1974). Theoretical models have also been calculated by Copeland, Jensen and Jorgensen (1970) and Hoxie (1970), but, as Petterson pointed out, these are not in as good agreement with the observations. Error bars corresponding to $\pm$ 100K and ± 0.4 in absolute bolometric magnitude are shown. The most substantial deviation between observations and theory lies near $\log (L/L_\odot) \sim -2.5$, where the empirically derived temperatures are on average $\sim$100K cooler than the models (although note that for SGP stars the uncertainty in $\log (L/L_\odot)$ is $\sim \pm 0.25$). This discrepancy was also commented on by Grossman et al and is supported by the position of the components of the low luminosity binary, L 726-8 (from Popper, 1980) – although the effective temperatures for the latter were derived by extrapolating the Barnes-Evans (1974) $(V-R)-F_v$ relation and cannot be considered well established.

As to the population structure in the H-R diagram, the most significant feature is that with the revised temperatures for Wolf 359 and VB 10, these low luminosity stars now lie (within the errors) on the main sequence. This statement holds even if the temperatures of these stars have been overestimated by up to 100K, as was suggested above. Similarly there is no reason to suspect that the SGP stars RG 0050.5, −2722 and RG 0058.8, −2807 – which are strong candidates for the lowest luminosity stars yet known – do not also lie on the main sequence. On the other hand, these stars are hotter by 300 to 400K than the deuterium burning main sequence calculated by Grossman et al. (also shown in Figure 6.6). Thus these results suggest that if there are black dwarfs then (with the possible exception of Jupiter) we have not yet found any examples.
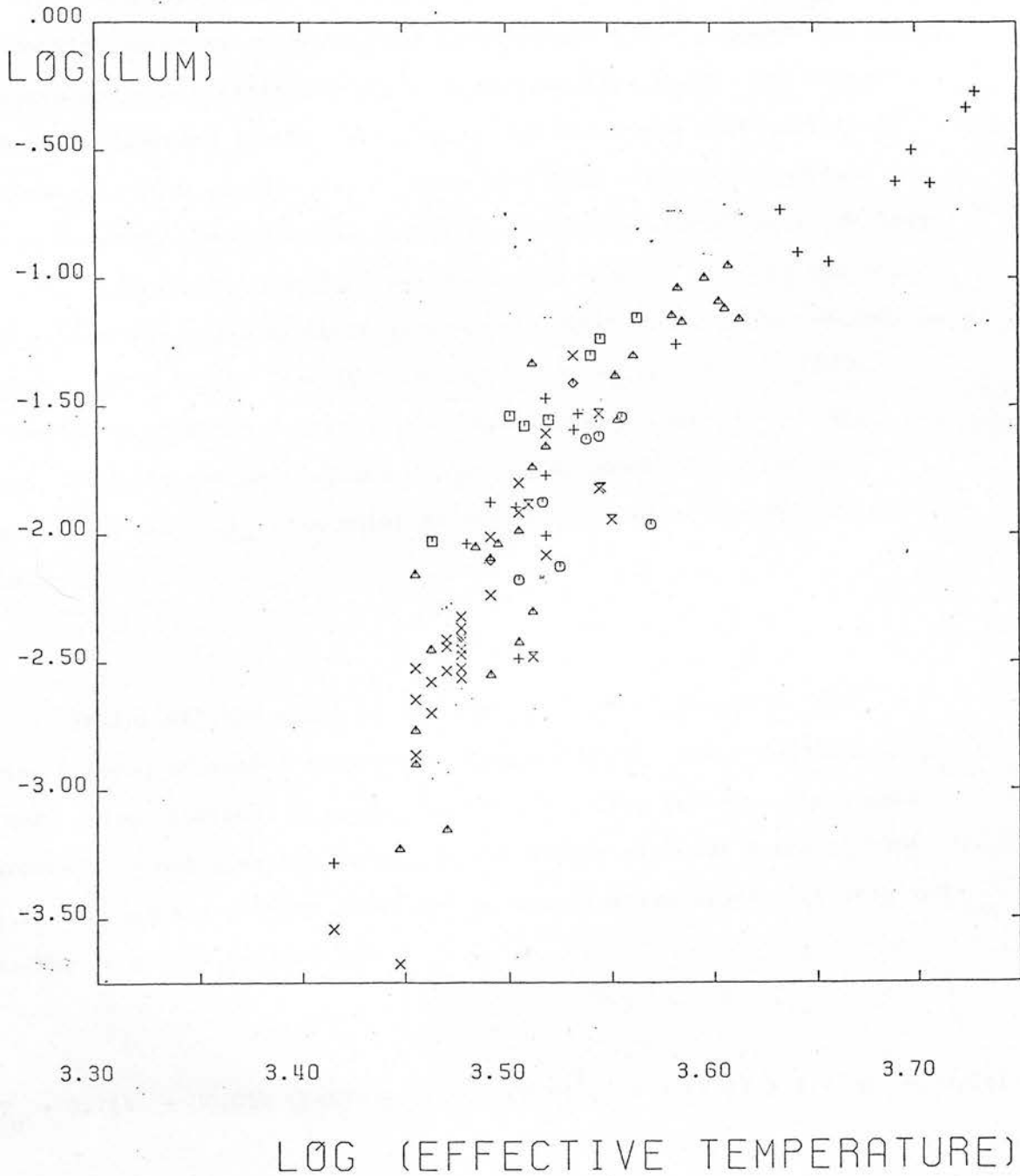
Figure 6.7   H-R diagram for the combination of our sample and those stars
              observed by Mould and Hyland. The coding is old disk (△),
              young disk (+), disk subdwarfs (0), halo subdwarf (X)
              "contracting " stars (□), SGP sample (X) and Luyten
              proper motion stars (*).

Our sample includes only six halo subdwarfs, but all of these lie at the high temperature edge of the main sequence, as expected given the lower overall opacities of metal poor atmospheres. There are also six young disk dwarfs and seven stars classed as disk subdwarfs by MH. The latter tend to be subluminous in the H-R diagram, but the young disk exhibit no group tendency. Both results are in agreement with with Mould & Hyland's findings. However, the situation regarding the "contracting" stars is less clear. These stars are identified in figure 6.7 - which combines our data with MH's results, adopting their temperature scale above 3600K, as well as including G and K dwarfs from the compilation of Perrin et al. (1977). While the MH "contracting" stars lie toward the upper edge of the main sequence, there is no clear evidence that these constitute a separate population. We return to this point in the discussion of JHK two-colour diagram.

Taking all the stars in our sample we have calculated the relation between effective temperature (on our scale) and the (V-K), (V-I) and (R-I) colour indices, with the latter two on the Kron-Cousins system. We purposely do not give the relations for either (B-V) or spectral type since in our opinion neither is suited to quantitative studies of very red stars. The relations derived are

$$\log T_e = 3.714 - 0.054 \, (V-K) + 0.0025 \, (V-K)^2, \quad 9 > (V-K) > 3, \quad \sigma = 0.011$$

$$\log T_e = 3.673 - 0.081 \, (V-I) + 0.007 \, (V-I)^2, \quad 6 > (V-I) > 2, \quad \sigma = 0.017$$

$$\log T_e = 3.675 - 0.173 \, (R-I) + 0.034 \, (R-I)^2, \quad 2.5 > (R-I) > 1, \quad \sigma = 0.021$$

The dispersions quoted are the r.m.s. deviations (in $\log(T_e)$) over the whole range of colour, and the actual scatter is appreciably larger for the coolest stars ($(V-I) > \sim 4$) Since there are only five halo subdwarfs in the whole sample, we have not attempted to subdivide the stars by stellar population. However, all five subdwarfs lie at the higher temperature edge of the H-R diagram, as expected given the lower overall opacities of metal poor atmospheres.

We can compare our temperature scale with Popper's (1980) tabulation of the Barnes-Evans $(V-R)_J - T_e$ relation over the limited range for which Bessell's (1979) $(V-R)_J$ to $(V-R)_C$ is valid (Table 6.5). Within the errors (the dispersion in the $(V-R)_C - \log(T_e)$ relation is ~ 0.027 in log (temperature)) there is reasonable agreement.

Using the bolometric magnitudes we have determined the bolometric corrections appropriate to this absolute magnitude range. We find

$$B.C. = 0.86 - 0.154 \, M_V - 0.01 \, M_V \quad 8 < M_V < 20, \quad \sigma_{BC} = 0.35$$

Furthermore, $(V-I)$ is closely related to the bolometric correction . We find

Table 6.5

$(V-R)_J$	$\log T_e$	$(V-R)_C$	$\log T_e$
1.4	3.571	0.79	3.565
1.5	3.556	0.85	3.555
1.6	3.542	0.91	3.549
1.7	3.528	0.97	3.533

$$B.C. = -1.31 \ (V-I) \ + 1.05 \qquad 1.5 < (V-I) < 5.5, \ \sigma_{BC} = 0.40$$

Veeder (1974) found that M_K was well correlated with M_{bol} for K and M dwarfs. This is confirmed by our results, which give

$$M_{bol} = 1.08 \ M_K \ + 2.05 \qquad 5 < M_K < 11, \ \sigma = 0.07 \ \text{in} \ M_{bol}$$

(cf. $M_{bol} = 1.12 \ M_K \ + 1.81$ found by Veeder).

On the other hand, the scatter in M_v is considerably larger.

$$M_{bol} = 0.86 \ + 0.85 \ M_v \ - 0.01 \ M_v^2 \ , \ 8 < M_v < 20, \ \sigma = 0.35 \ \text{in} \ M_{bol}$$

The observational errors in the broadband photometry (principally at J, H and K) imply formal uncertainties of ± 0.02 in M_{bol} - although this does not take into account the possible systematics introduced by, for example, the infrared steam absorption. However, assuming that M_{bol} is defined to this nominal accuracy, the residual dispersion is extremely small in the (M_{bol}, M_K) relation - implying less than 5 percent differential line blanketting/backwarming at K at a given luminosity. However, the equivalent spread is ± 70 percent on average in the V abnd, and increases to two magnitudes (i.e. a factor 6) at the faintest bolometric magnitudes - thus accounting for most of the dispersion in the visual mass-luminosity relation (Lacy, 1977a). This emphasises how much

more appropriate infrared indices are for red dwarfs stars.

Finally, we have used the results given in Table 6.3 to examine the effects of unrecognised duplicity on the position of stars in the (H-R) diagram. Taking VB 10, VB 8, Gl 866, GJ 1002, Gl 83.1, Gl 729, Gl 752A and Gl 701 as representative of their respective temperatures, we have synthesised joint broadband colours for the various combinations. (There is no evidence that any of the named calibrators are themselves in close binary systems). Obviously these binaries will have brighter total bolometric magnitudes - corresponding to a maximum increase of 0.28 in $\log(L/L_\odot)$ for equal components. However, the effective temperatures derived are little affected, with the maximum distortion for combinations where the temperature difference is 100K. In these cases the deduced temperature is cooler by ~75K. Given the uncertainties associated with the luminosities and temperatures determined above, neither effect would be discernible in figure 6.6.

5 The JHK Diagram

One of the main conclusions reached by Mould and Hyland was that the (J-H)-(H-K) two colour diagram provided clear population discrimination for lower main sequence stars. In particular they found that halo subdwarfs have bluer (J-H) colours at a given (H-K) than the disk main sequence. Our photometry includes only two halo stars not observed by Mould and Hyland (LHS 61 and Gl 821), but both lie beneath the JHK main sequence as do the Luyten proper motion stars LP 826-261 and LHS 3602 (Figure 6.8a). The latter has been classified as a young disk star by Rodgers and Eggen

Figure 6.8a   JHK diagram for stars within our sample. The coding is as in
               Figure 6.6 with the addition of AAO JHK standard stars (+)
               and funny faint red things (*).
        6.8b   JHK diagram for our sample plus the MH stars. The coding is
               as in figure 6.7 with the addition of the AAO JHK
               standards (*).

a)
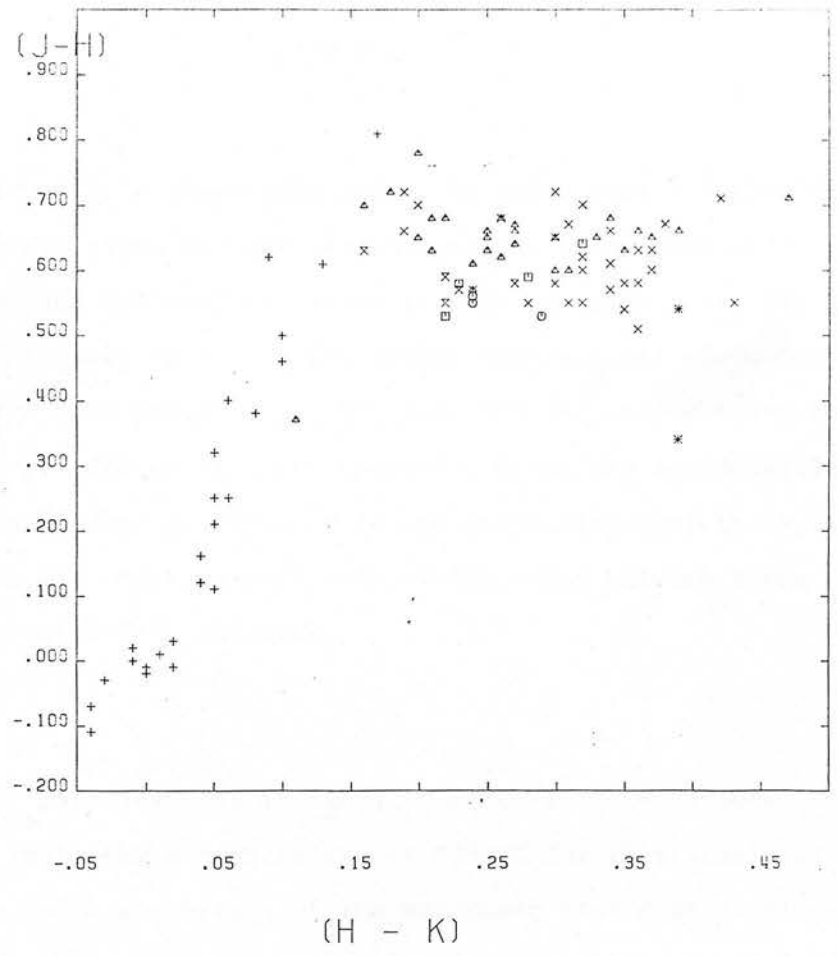
b)
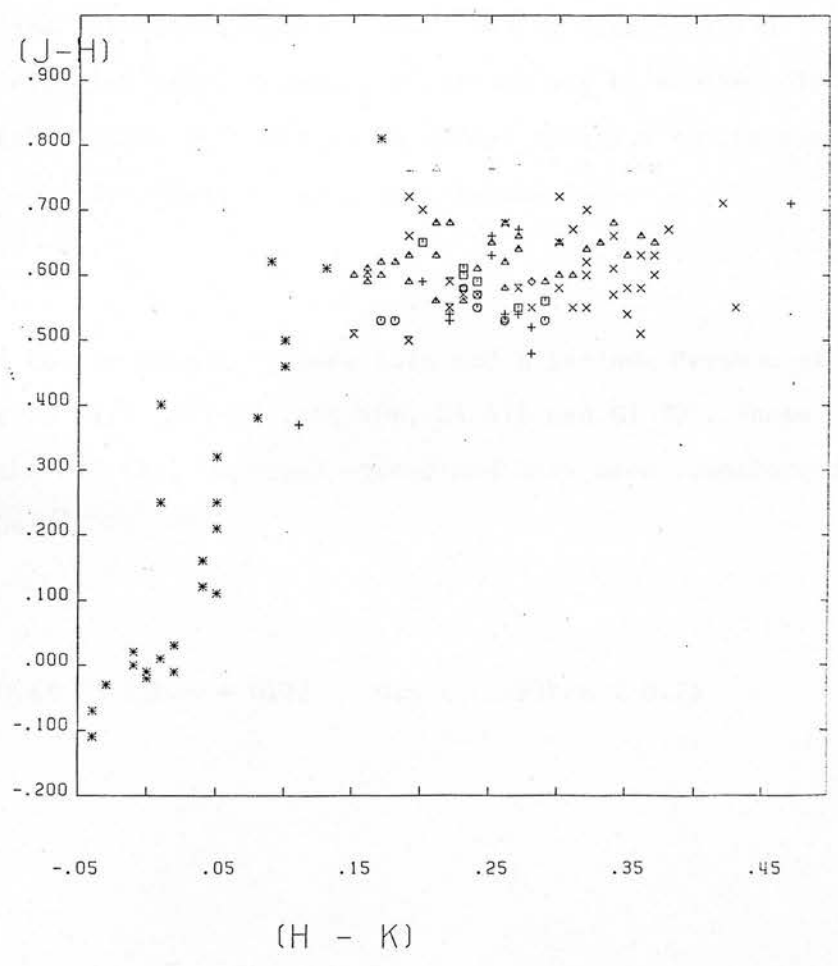
(1974) on the basis of it's space velocities. MH noted that a number of stars with similar disk-type motions lay amongst the halo stars and observations of CaH and TiO band strengths in some of these stars (Mould and McElroy, 1978) suggest that they are predominantly metal poor. Our observations of five such stars (Gl 1, 87, 213, 595 and 643) confirm their position at the lower edge of the main sequence. Given the age-metallicity relation for the disk (Twarog, 1980) it is not surprising that there should be late-type dwarfs with disk motions and metallicities between those normally associated with halo and disk.

One other parallax star is close by these stars - Gl 908. Blackbody fitting indicates a temperature of ~3500K for this star - as found for LHS 61 - and a comparison of the broadband flux distributions of these two stars shows them to be very similar (figure 6.2 - see also Gl 191). In particular the JHK flux distribution lies closer to the blackbody in these stars than in the disk stars of comparable (by our calibration) temperature - Gl 205 and 701 (3400K) and Gl 884 (3600K). Veeder (1974) classes Gl 908 as an old disk star, suggesting that it may be another disk subdwarf. However, with a space velocity of 75 km/sec relative to the sun (Gliese, 1969) it is equally likely to be a halo subdwarf.

In addition to our sample, figure 6.8a and b include Persson et al.'s observations of GJ 1111 (G51-15), Gl 406, Gl 411 and Gl 905. These observations are on the HCO (Mt. Hopkins) system and have been transformed onto the AAO system using

$$(J-H)_{aao} = 0.69 \ (J-H)_{hco} + 0.22 \qquad 0.5 < (J-H)_{hco} < 0.75$$

$$(H-K)aao = 1.08 \ (H-K)hco - 0.06 \qquad 0.15 < H-K)hco < 0.35$$

from ten stars in common. Both relations ahve r.m.s. dispersions of 0.02 magnitudes. Similarly, from 18 stars in common with MH we find

$$(J-H)aao = 0.915 \ (J-H)mssso \qquad \sigma = 0.015$$

$$(H-K)aao = (H-K)mssso \qquad \sigma = 0.015$$

in agreement with Hyland and Allen (1982).

Our JHK diagram includes substantially more low luminosity stars than were studied by MH, and these data confirm Persson et al.'s suggestion that (J-H) levels off beyond (H-K) = 0.25. Furthermore, there is substantial breadth to the main sequence, considerably more than could be explained by photometric errors. The stars towards the upper part of the sequence are those identified as members of the young stellar population by MH - and this subset would include about 20 percent of our SGP sample. However, these stars are taken from a volume-complete sample, drawn, moreover, at a mean height of about 80 parsecs above the Plane (i.e. one scale height for the young disk). This would imply an unreasonable local density of recently formed stars. Figure 6.8b adds our data to MH's JHK diagram, and it is clear that, while the "contracting" stars lay towards

the upper edge of MH's main sequence, they are firmly within the body of our more extensive dataset. A more likely explanation is that these stars are merely mildly metal rich counterparts of the disk subdwarfs (as Mould (1978) has suggested on the basis of FTS spectroscopy of GL 205) and that metallicity variations primarily account for the breadth of the main sequence.

On this basis, all save two of the SGP dwarfs are classified as disk population by their JHK colours. The exceptions are RG 0053.6, -2654 - which has the same infrared colours as Gl 908, although the optical photometry indicates stronger blanketting - and RG 0058.9, -2812 which lies in a position consistent with it being an extreme subdwarf . However, our observations suggest that it is a peculiar variable (amplitude 2 magnitudes at H) and further study of this object is planned.

Finally, three stars in our main sample have (H-K) redder than 0.40 - VB 10, RG0050.5 and RG0055.2. The former two also have red (J-H) colours. To the best of our knowledge only two other dwarfs this red are known - LHS 2397a (Bessell, priv. comm.) and LHS 132 (Gilmore, priv. comm.) and both of these stars are also comparatively red in (J-H) (see Appendix A), suggesting that this may be a characteristic of such extremely low temperature stars.

6 Conclusions

Applying a simple blackbody fitting technique to broadband

photometry and spectrophotometry we have defined a revised effective
temperature scale for M dwarfs. A comparison with other studies indicates
that this scale is accurate to better than ± 150K for disk dwarfs cooler
than ~3500K, and to somewhat higher temperatures for the less blanketted
metal poor stars. At the coolest temperatures (~2800K), infrared
spectrophotometry suggests that this calibration method may overestimate
temperatures through not allowing for stellar H_2O absorption. A more
accurate assessment of the size of this effect requires coverage of the
full spectral range - particularly 0.8 to 1.2 μ and where possible beyond
the K passband. Present observations suggest that this error is no larger
than 100K even in the stars of lowest luminosity.

The observational H-R diagram derived from these observations is
in good agreement with the stellar interior models calculated by Grossman
et al (1974), even making full allowance for the systematics noted above.
The particularly important feature of this result is that it places very
low luminosity stars such as Wolf 359, VB 10 and RG 0050.5 plausibly close
to the theoretical main sequence. Thus such stars can be interpreted as
old, low mass dwarfs, consistent with their old disk type motions, rather
than requiring them to be more exotic, black dwarfs, powered by deuterium
burning or gravitational collapse.

Comparing our observations with stellar atmospheres calculated by
Mould and Auman, we find that the H_2O ODFs used by the former substantially
overestimate the true opacity in these stars - confirming Persson et al's
results. It is probable that the better agreement with Auman's
calculations, which use the same basic H_2O data, is due to the compensating
underestimation of the total absorption which is a property of the harmonic

mean opacity. However, our infrared photometry confirms the broad halo-disk segregation found by Mould and Hyland, and the presence of disk subdwarf interlopers amongst the halo stars. Finally the number of stars from our volume limited sample which lie in the upper part of the disk JHK main sequence suggests that these stars, interpreted by Mould and Hyland as young stars still contracting onto the main sequence, are more likely to be metal rich dwarfs.

Appendix A

Infrared Photometry of Red Dwarfs

Star	V	V-R	V-I	J-H	H-K	K	
RG0044.3,−2554	14.44	1.01	2.24	0.72	0.19	10.12	
RG0044.4,−2639	20.96		4.05	0.68	0.26	14.24	
RG0046.0,−2832	19.97	1.98	3.43	0.67	0.31	13.57	
RG0046.2,−2636	20.74		4.02	0.57	0.34	14.37	
RG0047.5,−3009	20.94		3.96	0.58	0.35	14.35	
RG0049.5,−2857	19.33	1.61	3.32	0.55	0.28	13.73	
RG0050.5,−2722	21.50	3.22	4.84	0.71	0.42	12.56	
RG0052.2,−2821	20.25		3.37	0.62	0.32	14.16	
RG0052.2,−2940	21.50	1.81	4.28	0.60	0.37	14.49	
RG0053.6,−2654	21.50	1.50	3.54	0.57	0.24	16.06	
RG0053.8,−2630	20.51	1.90	3.79	0.55	0.31	13.97	
RG0054.0,−2945	22.10	2.81	4.89	0.58	0.36	14.41	
RG0055.2,−2700	21.50	0.80	3.25	0.57	0.43	15.45	
RG0055.8,−2621	20.12	1.56	3.52	0.54	0.35	13.74	
RG0055.8,−2807	20.40	1.50	3.20	0.70	0.32	14.49	
RG0058.7,−2713	20.38	1.89	3.54	0.66	0.34	14.11	
RG0058.7,−2829	15.10	1.21	2.60	0.66	0.19	10.31	
RG0058.8,−2807	20.42	0.50	2.69	0.61	0.34	13.84	
RG0058.9,−2812	20.02	1.60	3.20	0.51	0.36	14.00	
RG0059.2,−2715	20.30	1.66	3.48	0.67	0.38	13.91	
RG0059.7,−2547	19.40		3.52	0.63	0.36	12.74	
RG0100.1,−2656	19.14	1.45	3.30	0.65	0.30	13.07	
RG0101.5,−2821	16.13		3.21	0.70	0.20	10.73	
RG0101.6,−2542	20.15		3.47	0.55	0.32	14.11	
RG0101.6,−2615	20.19	1.37	3.30	0.60	0.32	14.14	
RG0102.0,−2938	20.70	1.85	3.71	0.58	0.30	14.22	
RG0102.2,−2609	20.16		3.41	0.72	0.30	14.07	
RG0102.6,−2720	20.06		3.64	0.63	0.37	13.57	
LHS 61	11.47	0.96	2.03	0.59	0.22	7.54	
LHS 3602	11.87	1.23	2.37	0.53	0.22	7.11	
LHS 3839	11.52	1.48	2.65	0.64	0.32	6.44	
LP 826−500	16.86		3.10	0.59	0.28	11.32	
LP 826−261	13.80	1.01	2.15	0.58	0.23	9.68	
GL 1	8.54	0.97	2.12	0.58	0.23	4.50	
GJ 1002	13.80	1.77	3.59	0.65	0.33	7.44	
GJ 1111	14.90	1.92	4.21				Bessell (priv. comm.)
LHS 2397a	R=17.4	R−I=2.3		0.80	0.46	10.75	" "
LHS 132	m(r)=18.1			0.69	0.43	10.13	
GL 79	8.88	0.91	1.81	0.72	0.18	5.21	
GL 83.1	12.27	1.79	3.09	0.64	0.27	6.72	
GL 87	10.02	1.02	1.87	0.56	0.24	6.07	
GL 191	8.85	1.01	1.95	0.55	0.22	5.05	
GL 205	7.96	0.98	2.08	0.78	0.20	3.86	
GL 213	11.60	1.57	2.84	0.53	0.29	6.36	
GL 273	9.86	1.16	2.69	0.62	0.26	4.85	
WOLF 359	13.53	2.28	4.20	0.63	0.35	6.09	
GL 551	11.11	1.85	3.67	0.66	0.36	4.36	
GL 595	11.85	1.01	2.52	0.55	0.24	7.24	
GL 631	5.76	0.45	0.86	0.37	0.11	3.84	

GL 643	11.77	1.33	2.74	0.61	0.24	6.83
GL 644A	9.02	1.10	2.45	0.65	0.25	4.38
VB 8	16.78	2.09	4.49	0.65	0.37	8.86
GL 674	9.36	1.03	2.29	0.63	0.25	4.86
GL 699	9.57	1.23	2.81	0.58	0.27	4.56
GL 701	9.43	1.11	1.97	0.65	0.20	5.39
GL 729	10.47	1.34	2.77	0.60	0.30	5.40
GL 748	11.11	1.26	2.60	0.63	0.21	6.30
GL 752A	9.13	1.17	2.35	0.66	0.25	4.68
VB 10	17.72	2.35	4.80	0.71	0.47	8.81
GL 821	10.87	0.95	2.03	0.57	0.23	6.97
GL 831	11.95	1.55	2.95	0.65	0.30	6.43
GL 866	12.18	1.35	3.60	0.68	0.34	5.60
GL 876	10.17	1.37	2.74	0.67	0.27	5.07
GL 884	7.86	0.77	1.48	0.70	0.16	4.50
GL 908	8.96	1.08	2.01	0.57	0.24	5.06

Appendix B

Atmospheric Absorption in the Infrared

Allen has presented CVF spectrophotometry of a G dwarf, observed from Siding Spring using the IRPS on the AAT (IRPS Handbook). Dividing the observed counts by a blackbody of ~6500K gives a measure of the relative atmospheric transparency over this wavelength range. Figure A1 shows the resultant curve, scaled so that the maximum transmission is 1.0, while figure A2 shows presents the corresponding plot from our UKIRT CVF observations. Since the respective dewars have different optics this does not represent a direct comparison of atmospheric transmission. The atmosphere, however, must make a substantial contribution. In any event, the different responses are worth bearing in mind, given that the two instruments are sometimes regarded as being on the same photometric system.

ATMOSPHERIC TRANSMISSION

FLUX
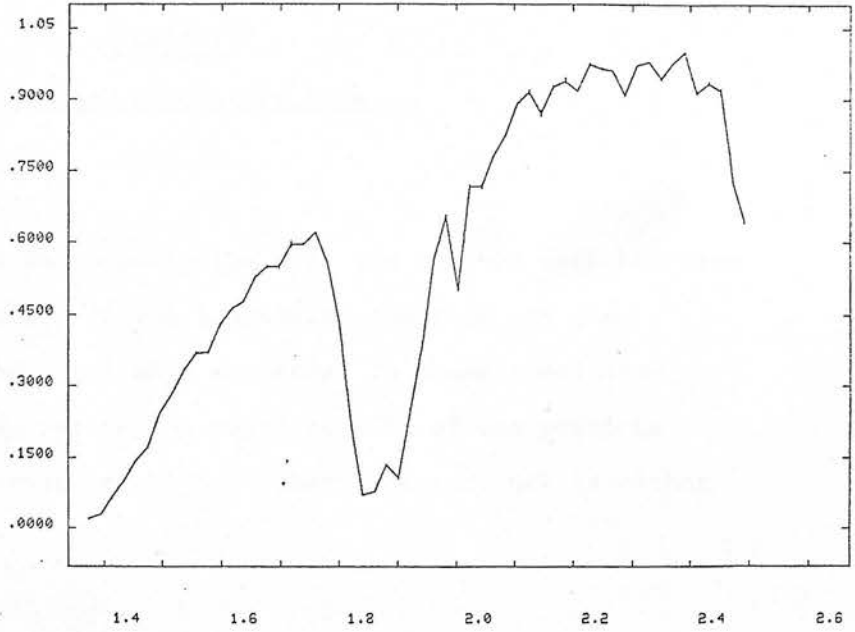
WAVELENGTH (MICRONS)

ATMOSPHERIC TRANSMISSION - AAT
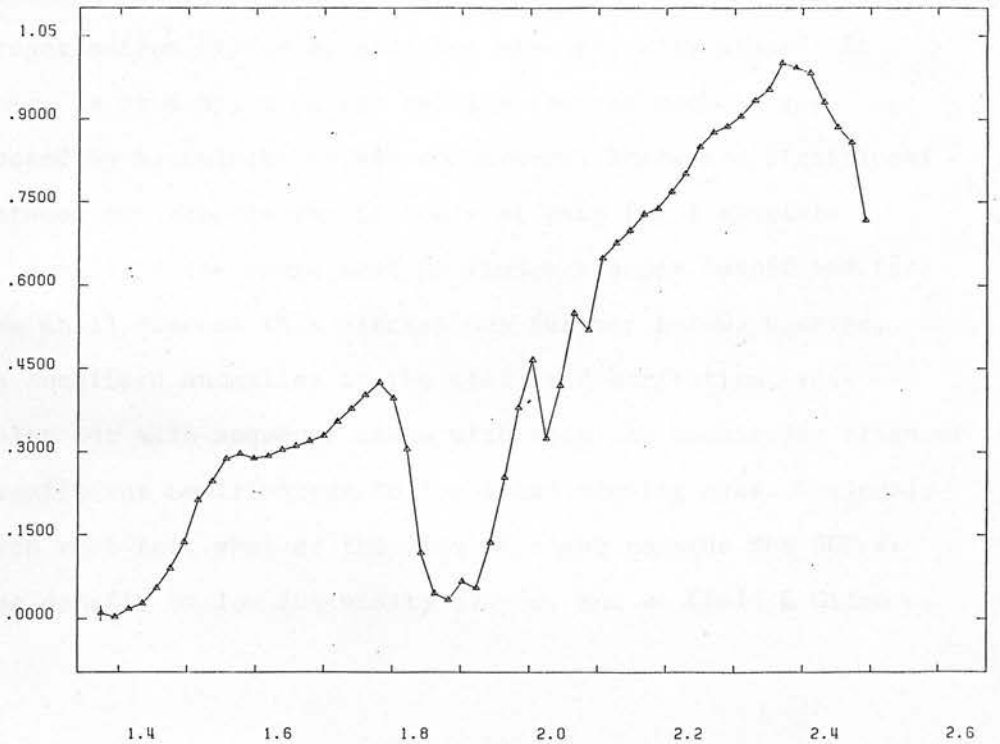
FLUX

WAVELENGTH (MICRONS)

Chapter 7

Summary and Future Work

As was stated at the outset, the main aim of this work has been an observational determination of the luminosity function and the population structure of the lower main sequence. In these concluding remarks we shall briefly summarise the major results of the previous chapters and outline the areas in which further research work is either prompted or required.

We have determined the local disk stellar luminosity function at faint absolute magnitudes by applying the method of photometric parallaxes to two kinematically unbiased samples of late type dwarfs - a sample of relatively bright (apparent magnitude) southern dwarfs and the fainter (both intrinsically and apparently) subset of stars within the SGP field. The results are in reasonably good agreement with the luminosity functions found by Luyten and Wielen - using stellar samples at least partially selected by proper motion criteria, and thus kinematically biased. In particular, there is no support in our results for the much larger densities proposed by Sanduleak and his co-workers. There are significant differences between our results and Luyten's at very faint absolute magnitudes ($M_V > +15$) in the sense that we find a steeper cutoff and far fewer stars. We shall discuss this discrepancy further below. However, barring severe localised anomalies in the stellar distribution, this effectively rules out main sequence stars with absolute magnitudes brighter than +19 as significant contributors to the local missing mass. Obviously further research must test whether the line of sight towards the SGP is atypical of the density of low luminosity dwarfs, and we (Reid & Gilmore,

in preparation) are currently extending this work to several other field. Preliminary results from one such area (at 22 hours, -18° 54′) are in broad agreement with the above conclusions.

Apart from anything else, this work illustrates the power of the automatic measuring machine/Schmidt plate combination once sufficient care has been taken in selecting appropriate passbands and accurately calibrating the photometry. Many projects require plate-to-plate differential photometry (either single or multi-colour) to study particular classes of objects. One of the major problems in the past has been identifying statistically complete samples of such objects from the ~100,000 real images on any one Schmidt plate. We have shown that by combining the traditional method of using several plates in any one passband with reliably calibrated COSMOS photometry, accuracies of better than 0.05 magnitudes are attainable. There are a number of calibration problems peculiar to COSMOS data. We have been able to adopt the technique of empirically correcting for these effects using external calibrations, and have therefore not carried out a detailed study of their cause. A more comprehensive discussion of the likely origin of some of these problems is given by Hewett (1982, Ph. D. thesis, in prep.).

We have concentrated on the use of V and I plates to identify the most extreme red objects — and the degree of success can be gauged by our detection of the first dwarf fainter than M_v = +19 found since van Biesbroeck discovered VB 10 in 1944. Similar methods can be applied to locate any subset of extreme-coloured objects — asymptotic giant branch stars or miras in the LMC (Mould & Reid, in preparation; Reid, Feast and Glass, in preparation); variables of all types (Hawkins, 1982); hot white

dwarfs (Wickramasinghe, Wegner and Reid, in preparation); ultraviolet excess extragalactic objects (Shanks, in prep.); high redshift galaxies (Hewett, Gilmore & Reid, in preparation); or OB subdwarfs (Gilmore & Reid, in preparation). Finally, besides identifying rare objects, the general star counts derived from such photometry provides an invaluable probe of Galactic Structure beyond the Solar Neighbourhood (see Paper III).

We have noted that all of the SGP dwarfs have photometric properties consistent with hydrogen burning main sequence stars. However, the interior models constructed by Grossman et al. (1974) show that the very low mass black dwarfs pass through a short-lived deuterium burning phase, when their surface temperatures and luminosities are virtually indistinguishable from main sequence stars. Assuming that these low mass "stars" follow the main sequence relation between bolometric and visual magnitude, Table 7.1 shows the percentage of the total population that would be visible now assuming a constant birthrate over the age of the disk ($\sim 5 \times 10^9$ years). Transforming these visibility fractions to number densities obviously requires present day observed densities - which do not yet exist. Upper limits can be set by arbitrarily assuming that 50% of the stars contributing to the luminosity function (ch. 4, Table 4.8) are really black dwarfs. This gives the overall mass densities shown in Table 7.1 - the corresponding "loss" in main sequence stars is less than 0.001 $M_\odot$.

However, the assumed present day density is definitely unrealistic at $M_V = +13.5$. A substantial number of stars of this luminosity are known. Most are found in binary or multiple systems, where there is no reason for assuming that the companion(s) is particularly young, and very few - probably less than 5 percent - have kinematics close to those

Table 7.1

M/M_0	Lifetime	% visible	M(bol)	M(v)	no. density	mass density
0.03	2.2×10^6	0.44	10.4	13.5	$1.08 / pc^3$	$0.032 \ M/pc^3$
0.02	3.6×10^6	0.72	11.3	15.0	0.37	0.007
0.015	4.3×10^6	0.86	12.1	17.0	0.29	0.004
0.012	7.5×10^7	1.5	13.2	19.0	0.67	0.008

expected for very young stars. Thus within the quoted magnitude range, at most ~0.02 $M_\odot$ per cubic parsec can be added by invoking black dwarfs and so a substantial contribution from massive Jupiters (0.001 to 0.01 $M_\odot$) is required if the full complement of "missing mass" is to be accounted for by such low mass fragments.

With a mass of 0.001 $M_\odot$, Jupiter (T_e ~ 135K) has an apparent magnitude of −7 at N (10μ), corresponding to an absolute magnitude of +25. This is about 17 magnitudes fainter than the current detection limits at this wavelength. At shorter wavelengths the source is fainter, with molecular absorptions adding to the decreased black body emission, while current detectors are less sensitive at longer wavelengths. Even with a 0.005 $M_\odot$ dwarf with a higher effective temperature of 200K the distance limit for detection is only ~0.04 parsecs or 8250 A.U. . Since the required number density is only 5 to 10 per cubic parsec, these planetary black dwarfs can be regarded as essentially indetectable.

Other suitably invisible components can also be postulated to account for the total local "missing mass". For example, taking 3 $M_\odot$ as the typical mass of a black hole remnant, the required number density is ~0.01 per cubic parsec − within the constraints set by background radiation at any wavelength (Carr, 1979). Similarly heavy leptons might be invoked, providing that they can be confined within a relatively thin disk. However, a more likely explanation for the apparent discrepancy may be that the local "missing mass" merely reflects insufficient knowledge of the local kinematics. Recent observations − in particular those of normal metallicity stars at high z-distances (e.g. Rodgers et al., 1981) − suggest that the kinematic assumptions implicit in the Oort dynamical mass calculation may

be inappropriate. For example, Perry (1969) was unable to derive a physically sensible force law using A stars at high z-distances, and suggested that this could indicate that these stars were not yet well mixed. Similarly, Hill et al. have shown that there are peculiarities in the density distribution of A and F stars near the Plane ($z < 200$ parsecs) with neither distribution a pure exponential (as would be expected in a well-mixed population). Although the F-star density law can be approximated to $z = 500$ parsecs by an exponential of scale height ~125 parsecs, the space density is constant within 40 parsecs of the Plane. The A-star population, however, requires two exponentials - scale heights 90 and 170 parsecs. Fianlly, van der Kruit and Searle (1981a,b) have shown that by excluding stars close to the Plane ($z < 400$ pc.) a mass density of 0.08 $M_\odot$ /pc^3 follows from Oort's K_z analysis. In short, substantially better understanding of the kinematics of the local stellar populations is needed before definite conclusions can be reached as to whether there is any local "missing mass" at all, never mind what it's constituents might be.

As we mentioned above, our photometrically derived luminosity functions agree well with Luyten's kinematically determined function to M_v ~ +14. Fainter than this Luyten's quoted number densities are systematically substantially higher. This is consistent with the inclusion of distant, high velocity halo stars in the proper moion surveys. We have demonstrated that the method of mean absolute magnitudes employed by Luyten assigns these stars intrinsic luminosities that are too faint because it implicitly assumes that all stars are drawn from a single kinematic population. Using Monte Carlo simulations of the local stellar population structure we have shown how these subdwarfs probably comprise the bulk of the faint ($V > 17$) proper motion stars and thus prop up the faint tail of the luminosity function. Furthermore, our investigation has illustrated how

sensitive a population discriminant the reduced proper motion diagram is. Again this is an area where automated measuring machines can be put to good use, especially with the growing availability of the UK Schmidt JR equatorial survey - covering a region of the sky surveyed from Palomar in the early 1950s. With this baseline a proper motion of 0".05 per year corresponds to a movement of 20 microns which, given the positional accuracy of COSMOS, is a five sigma motion. In addition, since many galaxies are measured, the proper motions can be set on an absolute scale. We are undertaking a pilot study of eight fields to further assess the possibilities of this line of research (Hewett & Reid, in preparation). In particular, this approach offers the prospect of obtaining substantial information on the halo star luminosity function - which our preliminary study (chapter 5) indicated may differ in shape from that of the disk - as well as on the status of the intermediate population II.

One area of study on which this research has direct bearing is, of course, star formation - both on the determination of generalised mechanisms and on the history of star formation over the lifetime of the Galaxy. As we briefly outlined in chapter 2, most star formation mechanisms predict smooth, exponentially increasing number densities to the H-burning limit. Figure 7.1 shows the observationally determined mass function, peaking at $M \sim 0.2 \, M_\odot$ and including the K dwarf deficit which most other determinations (including that by Miller and Scalo (1979)) have ignored. It must be strongly emphasised that a single Salpeter-type function (and even a combination of up to three power laws) does not represent the real world at all well.

The existence of a peak in the field star mass function implies
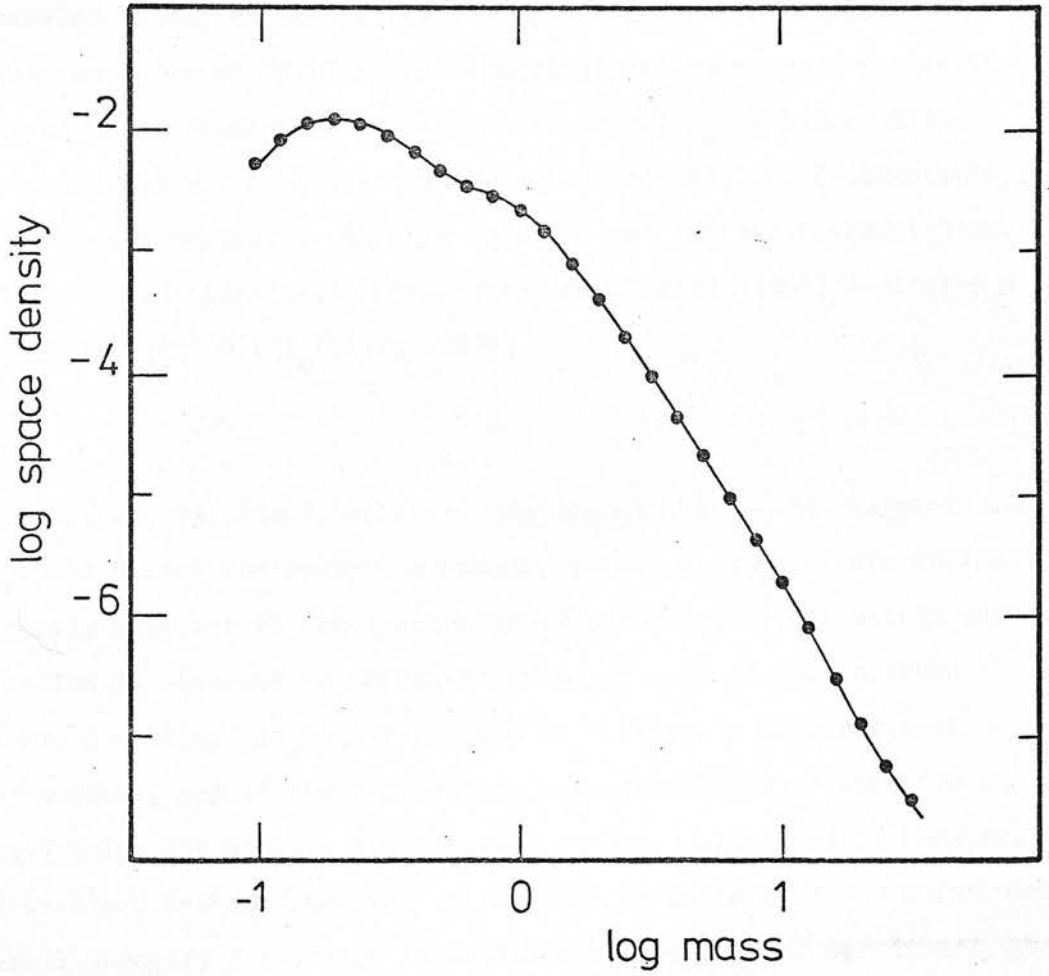
Figure 7.1   The Stellar Mass Function.

a preferred fragment size during the period of star formation. Miller and Scalo have reviewed the initial mass functions predicted by different star formation mechanisms and conclude that most are unable to produce the observed flattening at low masses. However several do predict masses close to the observed value. While opacity limited fragmentation produces a minimum fragment size of ~0.01 $M_\odot$ in spherical collapse, more realistic spheroidal collapse suggests a limiting mass of 0.1 $M_\odot$. Indeed Silk (1977) suggests 0.2 $M_\odot$ as a critical mass for protostellar fragmentation, with larger masses subject to dynamic collapse and further fragmentation. Similarly, magnetic flux-limited fragmentation (Mestel, 1965) indicates a lower mass limit of ~ 0.1 $M_\odot$ (Silk, 1979).

Larson (1981,1982), however, has argued that these fragmentation processes, calculated for near-homogeneous, quiescent clouds, are unlikely to be directly relevant to the inhomogeneous molecular clouds within which star formation is observed to occur. He proposes that if the observed internal cloud motions can be interpreted as a hierachy of supersonic turbulent motions, and if the correlation between velocity dispersion and size (mass) holds for density enhancements within a single cloud complex, then the smallest sub-condensation (protostar) is defined at the point when the internal velocity dispersion is equivalent to the sound speed, and the fragment is no longer pressure supported. This predicts a lower mass limit of ~0.25 $M_\odot$, although the one sigma limits on this value are large (0.05 to 1.0 $M_\odot$).

These mechanisms deal with the initial structure of the mass function of protostellar fragments, but it is a reasonable expectation that accretion, mass loss and coalescence of fragments, as well as interactions

with the ambient medium, will substantially modify this distribution.
Pumphrey and Scalo (preprint) have extensively discussed these processes,
using numerical simulations to investigate their effects on various initial
mass spectra. Not surprisingly, the results show that collisions enhance
the number of large mass objects at the expense of the smallest fragments,
although the actual shape of the final distribution is strongly dependent
on many factors, including the initial mass spectrum, the collisional
cross-section and the evolution time. Qualitatively, however, such
coalescence processes give plausible explanations for the shape of the
observed function.

A further point is that there is no direct observational evidence
for a single dominant mechanism of star formation. Indeed the shape of the
observed mass spectrum, once the K dwarf deficit is included, is suggestive
of two, overlapping broadly Gaussian distributions - possibly reflecting
star formation in open clusters (higher masses) and looser associations
(low mass stars). The fact that the proportion of low mass stars varies
from open cluster to open cluster may reflect the extent to which the
second process could take place, given the initial conditions. Miller and
Scalo (1979) and Scalo (1979) have extensively reviewed this topic, as well
as discussing the evidence for variations in the initial mass function over
the lifetime of the disk. Given the metallicities and kinematics of the
halo and intermediate populations, both are probably older than the oldest
disk stars - but neither has an observationally well determined luminosity
function at faint magnitudes. Detailed quantitative analysis requires
better knowledge of the kinematics of the two populations and a
considerable larger observational sample. The proper motion star survey
outlined above will be particularly fruitful in this respect.

Finally, we have considered the evolutionary status of the very low luminosity red dwarfs, using our broad band photometry and spectrophotometry to study the spectral energy distribution and applying blackbody fitting techniques to derive a new effective temperature scale. A comparison of our results with the few available external checks on this scale suggests that the method breaks down for disk dwarfs hotter than ~3400K and may overestimate the temperatures of the coolest stars (~2700 K) by up to 110K. Even so, the significant feature of this revised scale is that it brings the observational low luminosity main sequence into agreement with the theoretical models of Grossman et al (1974). On this result there is no reason for postulating that these stars are other than hydrogen burning main sequence dwarfs, and hence there is no observational evidence for the presence of numerous very low mass black dwarfs as a solution to the local missing mass.

Substantial research remains to be done in this particular field, however. Observations at wavelengths longer than 3 microns - where the flux distribution is likely to be more representative of the pure Planck curve - would produce a more reliable temperature scale, while CVF spectrophotometry can provide a measure of the steam absorption in these cool stars. This is especially important given the current lack of atmosphere models. Further theoretical studies will require more accurate molecular opacities. It is possible that these are provided by Sharp's recent work (1982), and we intend to modify the model atmosphere programme MARCS (Gustafsson, Bell, Eriksson and Nordlund, 1975) to incorporate this data in the near future.

Bibliography

Ake, T.B. and Greenstein, J.L.   1980   Astrophys.J. <u>240</u>, 859

Arnett, W.D.   1978   Astrophys. J. <u>219</u>, 1008

Auman, J.R.   1969   Astrophys. J. <u>157</u>, 799

Bahcall, J.N., Schmidt, M. and Soneira, R.M.   1982   Astrophys. J., in press

Bahcall, J.N. and Soneira, R.M.   1980   Astrophys. J. Suppl. <u>44</u>, 73

Barnes, T.G. and Evans, D.S.   1976   Mon. Not. R. astr. Soc. <u>174</u>, 489

Batten, A.M.   1973   Binary and Multiple Systems of Stars, (Pergamon Press, Oxf

Becker, W.   1980   Astr. Astrophys. <u>87</u>, 80

van den Bergh, S.   1975   Astrophys. J. <u>201</u>, 585

Bessell, M.S.   1979   Publ. astr. Soc. Pacif. <u>91</u>, 589

Bessell, M.S. and Wickramasinghe, D.T.   1979   Astrophys. J. <u>227</u>, 232

Biermann, P.   1975   I.A.U. Symposium No. 69, ed. A. Hayli
        Dynamics of Stellar Systems, p.321 (D. Reidel, Dordrecht-Holland)

van Biesbroeck, G.   1944   Astr. J. <u>51</u>, 61
                        1966   Astr. J. <u>66</u>, 528

Blaauw, A. and Garmany, C.D.   1976   Proc. 3rd European Astronomical
                        Meeting, ed. E.K. Kharadze

Blaauw, A. and Schmidt, M.   1965   eds. Galactic Structure,
                (Univ. of Chicago Press, Chicago)

Bopp, B.W., Gehrz, R.D. and Hackwell, J.A.   1974   Publ. astr. Soc.
                        Pacif. <u>86</u>, 989

Burstein, D.   1979   Astrophys. J. <u>234</u>, 829

Buser, R. and Kurucz, R.L.   1978   Astr. Astrophys. <u>70</u>, 555

Butler, D., Kinman, T.D. and Kraft, R.P.   1979   Astr. J. <u>84</u>, 993

Caldwell, J.A.R. and Ostriker, J.P.   1981   Astrophys. J. <u>251</u>, 61

Camm, G.L.   1950   Mon. Not. R. astr. Soc. <u>110</u>, 305
                1952   Mon. Not. R. astr. Soc. <u>112</u>, 155

Cannon, R.D.   1974   Mon. Not. R. astr. Soc. <u>167</u>, 551

Carbon, D.F.   1974   Astrophys. J. <u>187</u>, 135

Carbon, D.F., Gingerich, O.J. and Latham, D.W.   1969

        Low Luminosity Stars, p. 435 (ed. S.S. Kumar; Gordon & Breach, london)

Carney, B.W.   1979a   Astrophys. J. 233, 211

                1979b   Astrophys. J. 233, 877

                1979c   Astr. J. 84, 515

Carr, B.J.   1979   Mon. Not. R. astr. Soc. 189, 123

Chiu, L.-T. G.   1980a   Astr. J. 85, 812

                1980b   Astrophys. J. Suppl. 44, 31

Clayton, M.L. and Feast, M.W.   1969   Mon. Not. R. astr. Soc. 146, 411

Cochran, A.L.   1980   University of Texas Publ. in Astronomy, No. 16

Copeland, H., Jensen, J.O. and Jorgensen, H.E.   1970

            Astr. Astrophys. 5, 12

da Costa, G.A.   1982   Astr. J. 87, 990

Couch, W.J. and Newell, E.B.   1980   Proc. Astr. Soc. Aust. 4, 85

Cousins, A.W.J.   1980   S.A.A.O. Circulars 1, 166

Cousins, A.W.J., Lake, R. and Stoy, R.H.   1966   R. Obs. Bull. 121

Cousins, A.W.J. and Stoy, R.H.   1963   R. Obs. Bull. 64

Crawford, D.W., Mavridis, L.N. and Stromgren, B.   1979

        Abh. der Hamburger Sternmarte 10, 82

Delhaye, J.   1965   Galactic Structure, ch. 4, (eds. Blaauw & Schmidt;

                Univ. of Chicago Press, Chicago)

Dixon. M.E.   1970   Mon. Not. R. astr. Soc. 150, 195

Dyer, E.R.   1954   Astr. J. 59, 221

Eggen, O.J.   1964   R. Obs. Bull. 84

                1973   Astrophys. J. 182, 821

                1974   Publ. astr. Soc. Pacif. 86, 697

                1975   Publ. astr. Soc. Pacif. 87, 107

                1976a   Astrophys. J. 204, 101

                1976b   Astrophys. J. Supp. 30, 351

                1979a   Astrophys. J. 229, 158

1979b   Astrophys. J. <u>230</u>, 786

Eggen, O.J., Lynden-Bell, D. and Sandage, A.   1962   Astrophys. J. <u>136</u>, 748

Eriksson, P-I.W.   1978   Uppsala Astr. Obs. Report no. 11

Faber, S.M., Burstein, D., Tinsley, B.M. and King, I.R.   1976
Astr. J. <u>81</u>, 45

Feast, M.W.   1963   Mon. Not. R. astr. Soc. <u>125</u>, 367

Fenkart, R.P.   1977   Astr. Astrophys. <u>56</u>, 91

1980   Astr. Astrophys. <u>91</u>, 352

Fowler, W.A. and Hoyle, F.   1960   Ann. Phys. <u>10</u>, 283

Frogel, J.A., Kleinmann, D.E., Kunkel, W., Ney, E.P. and Strecker, D.W.
1972   Publ. astr. Soc. Pacif. <u>84</u>, 581

Giclas, H.L., Burnham, R. and Thomas, N.C.   1972   Lowell Obs. Bull, 158

Gilmore. G.   1981   Mon. Not. R. astr. Soc. <u>195</u>, 183

Gilmore. G. and Reid, N.   1982   Mon. Not. R. astr. Soc., in press
(Paper III)

Glass, I.S.   1974   Mon. Not. astr. Soc. South Africa <u>33</u>, 53

Gliese, W.   1956   Z. Astrophys. <u>39</u>, 1

1969   Veroff. Astr. Rechen-Institut, Heidelberg, Nr. 22

1971   Veroff. Astr. Rechen-Institut, Heidelberg, Nr. 24

1972a   Astr. Astrophys. <u>21</u>, 431

1972b   Q. Jl R. astr. Soc. <u>13</u>, 138

1981   Astr. Astrophys. Suppl. Ser. <u>44</u>, 131

Gliese, W. and Jahreiss, H.   1979   Astr. Astrophys. Suppl. Ser. <u>38</u>, 423

1980   Astr. Astrophys. <u>85</u>, 350

Graboske, H.C. and Grossman, A.S.   1971   Astrophys. J. <u>170</u>, 363

Green, R.F.   1980   Astrophys. J. <u>238</u>, 685

Greenstein, J.L., Neugebauer, G. and Becklin, E.E.   1970
Astrophys. J. <u>161</u>, 519

Grossman, A.S., Hays, D. and Graboske, H.C.   1974   Astr. Astrophys. <u>30</u>, 95

Gunn, J.E., Knapp, G.R. and Tremaine, S.D.   1979   Astr. J. <u>84</u>, 1181

Gustafsson, B., Bell, R.A., Eriksson, K. and Nordlund, A.   1975
        Astr. Astrophys. 42, 407

Harrington, R.S. and Dahn, C.C.   1980   Astr. J. 85, 454

Harris, D.L.   1961   The Solar System Vol. III, p. 272
        (ed. G. Kuiper & B.M. Middlehurst; Univ. of Chicago Press)

Hartwick, F.D.A.   1970   Astrophys. J. 161, 845

                    1977   Astrophys. J. 214, 778

Hawkins, M.R.S.   1981   Nature 293, 196

Hayes, D.S. and Latham, D.W.   1975   Astrophys. J. 197, 593

Heintz, W.D.   1969   Jl R. astr. Soc. Can. 63, 275

van Herk, G.   1965   Bull. astr. inst. Netherlands 18, 71

Herschel, W.   1785   Phil. Trans. 75, 213

Hill, G., Hilditch, R.W. and Barnes, J.V.   1979

                            Mon. Not. R. astr. Soc. 186, 813

House, F. and Kilkenny, D.   1980   Astr. Astrophys. 81, 251

Hoxie, D.J.   1970   Astrophys. J. 161, 1083

Hyland, A.R. and Allen, D.A.   1982   Mon. Not. R. astr. Soc. 199, 943

Iben, I.   1967   A. Rev. Astr. Astrophys. 5, 571

Jarvis, J.F. and Tyson, J.A.   1981   Astr. J. 86, 476

Jenkins, R.   1980   Dimbleby Lectures, The Listener

Jennens, P.A.   1975   Mon. Not. R. astr. Soc. 172, 695

Joeveer, M. and Einasto, J.   1977   Highlights of Astronomy 4 II, 33

Johnson, H.L.   1966   A. Rev. Astr. Astrophys. 4, 193

Jones, D.H.P.   1962   Royal Obs. Bull. No. 52

                1972   Astrophys. J. 178, 467

                1976   R. Obs. Bull. 182, p. 1

Jones, E.M.   1972   Astrophys. J. 173, 671

Joy, A.H.   1947   Astrophys. J. 105, 96

van de Kamp, P.   1971   A. Rev. Astr. Astrophys. 9, 103

Kapteyn, J.C.   1914   Astrophys. J. 40, 43

Kinman, T.D.   1959   Mon. Not. R. astr. Soc. 119, 559

Koo, D.C. and Kron, R.G.   1975   Publ. astr. Soc. Pacif. 87, 885

Krisciunas, K.   1977   Astr. J. 82, 195

Kron, G.E.   1952   Astrophys. J. 115, 301

          1958   Publ. astr. Soc. Pacif. 70, 102

Kron, G.E., Gascoigne, S.C.B. and White, H.S.   1957   Astr. J. 62, 205

Kron, R.G.   1978   Ph. D. thesis, Univ. of California, Berkeley

          1980   Astrophys. J. Supp. 43, 305

van der Kruit, P.C. and Searle, L.   1981   Astr. Astrophys. 95, 105

          1981b   Astr. Astrophys. 95, 116

Kumar, S.S.   1969   Low Luminosity Stars, p.255,

          ed. S.S. Kumar, Leander McCormick Observatories

Lacy, C.H.   1977a   Astrophys. J. Supp. 34, 479

          1977b   Astrophys. J. 218, 444

Lang, K.R.   1974   Astrophysical Formulae, Springer-Verlag, Berlin

Larson, R.B.   1981   Mon. Not. R. astr. Soc. 194, 809

          1982   Mon. Not. R. astr. Soc. 200, 159

Leung, K.-C. and Schneider, D.P.   1978   Astr. J. 83, 618

Liebert, J.   1980   White Dwarfs and Variable Degenerate Stars,

          I.A.U. Colloquium 53, p. 146 (ed. H.M. van Horn and V. Weidemann)

Lutz, T.E.   1978   Modern Astrometry, IAU Colloquium 48, p. 7

          (ed. F.V. Prochazka & R.H. Tucker)

Lutz, T.E., Hanson, R.B., Marcus, A.H. and Nicholson, W.L.   1981

          Mon. Not. R. astr. Soc. 197, 393

Lutz, T.E. and Kelker, D.H.   1973   Publ. astr. Soc. Pacif. 85, 573

Luyten, W.J.   1925   Astrophys. J. 62, 8

          1938a   Publ. Astr. Obs. Minnesota 2, No. 7

          1938b   Publ. Astr. Obs. Minnesota 2, No. 9

          1941   Annals New York Acad. Sci. 42, 201

          1963a   Bruce Proper Motion Survey, The General Catalogue Vol. I

University of Minnesota, Minneapolis, Minnesota

1963b   Proper Motion Survey with the 48-inch Schmidt Telescope,
Part I, University of Minnesota, Minneapolis, Minnesota

1968   Mon. Not. R. astr. Soc. <u>139</u>, 221

1974   Highlights of Astronomy <u>3</u>, 389

1977a   Highlights of Astronomy <u>4</u> II, 89

1977b   Proper Motion Survey with the 48-inch Schmidt, LI

1980   The LHS Catalogue, 2nd ed., University of Minnesota
Minneapolis, Minnesota

1981   The NLTT Catalogue, University of Minnesota, Minneapolis

Luyten, W.J. and La Bonte, A.   1973   The South Galactic Pole
Publ. Univ. Minnesota, Minneapolis, Minnesota

MacGillivray, H.T., Martin, R., Pratt, N.M., Reddish, V.C., Seddon, H.
Alexander, L.W.G., Walker, G.S. and Williams, P.R.   1976
Mon. Not. R. astr. Soc. <u>176</u>, 265

McCuskey, S.W.   1956   Astrophys. J. <u>123</u>, 458

1966   Vistas in astronomy <u>7</u>, 141

Malmquist, K.G.   1936   Stockholm Obs. Medd., No. 26

Menzies, J.W., Banfield, R.M. and Laing, J.D.   1980   S.A.A.O. Circulars <u>1</u>, 14

Mestel, L.   1965   Qu. Jl R. astr. Soc. <u>6</u>, 265

Miller, G.E. and Scalo, J.M.   1979   Astrophys. J. Suppl. <u>41</u>, 513

Mould, J.R.   1976   Astr. Astrophys. <u>48</u>, 443

1978   Astrophys. J. <u>226</u>, 923

Mould, J.R. and Hyland, A.R.   1976   Astrophys. J. <u>208</u>, 399

Mould, J.R. and McElroy, D.B.   1978   Astrophys. J. <u>220</u>, 935

Murray, C.A. and Corben, P.M.   1979   Mon. Not. R. astr. Soc. <u>187</u>, 723

Murray, C.A. and Sanduleak, N.   1972   Mon. Not. R. astr. Soc. <u>157</u>, 273

Notni, L.   1956   Mitteilungen Jena Obs., No. 26

Oke, J.B.   1973   Astrophys. J. Supp. <u>27</u>, 21

Oke, J.B. and Schild, R.E.   1970   Astrophys. J. <u>161</u>, 1015

Oort, J.H.   1932   Bull. astr. inst. Netherlands 6, 249

               1960   Bull. astr. inst. Netherlands 15, 45

               1965   Galactic Structure, ch. 21, ed. Blaauw & Schmidt,
                         University of Chicago Press, Chicago

Oort, J.H. and Plaut, L.   1975   Astr. Astrophys. 41, 71

Osvalds, V. and Risley, A.M.   1961   Publ. Leander McCormick Obs. 11, pt. 21

Parenago, P.P.   1951   Pub. Sternberg Inst. 20, 26

Perrin, M.-N., Hejlesen,P.M., Cayrel de Strobel, G. and Cayrel, R.

               1977   Astr. Astrophys. 54, 779

Perry, C.L.   1969   Astr. J. 74, 139

Persson, S.E., Aaronson, M. and Frogel, J.A.   1977   Astr. J. 82, 729

Pesch, P.   1972   Astrophys. J. 177, 519

Pesch, P. and Dahn, C.C.   1982   Astr. J. 87, 122

Pesch, P. and Sanduleak, N.   1978   Astr. J. 83, 1090

Peterson, B.A., Ellis, R.S., Kibblewhite, E.J., Bridgeland, M.T., Hooley, T.,
       and Horne, D.   1979   Astrophys. J. Lett. 233, L109

Petterson,B.R.   1980   Astr. Astrophys. 82, 53

Pickering, E.C.   1891   Ann. astr. Obs. Harvard 26, p. xiv

Popper, D.M.   1980   A. Rev. Astr. Astrophys. 18, 115

Probst, R.G. and O'Connell, R.W.   1981   Astrophys. J. Lett. 252, L69

Rees, M.   1976   Mon. Not. R. astr. Soc. 176, 483

Reid, I.N.   1982   Mon. Not. R. astr. Soc. 201, 58 (Paper I)

Reid, I.N. and Gilmore, G.F.   1981   Mon. Not. R. astr. Soc. 196, 15p

               1982   Mon. Not. R. astr. Soc. 201, 73 (Paper II)

van Rhijn, P.J.   1925   Pub. Kapteyn astr. Lab. Gron., No. 38

               1936   Pub. Kapteyn astr. Lab. Gron., No. 47

Richstone, D.O. and Graham, F.G.   1981   Astrophys. J. 248, 516

Rodgers, A.W., Harding, P. and Sadler, E.   1981   Astrophys. J. 244, 912

Rodgers, A.W. and Eggen, O.J.   1974   Publ. astr. Soc. Pacif. 86, 742

Sandage, A.   1969   Astrophys. J. 158, 1115

                    1981   Astr. J. <u>86</u>, 1643

Sanduleak, N.   1965   Ph. D. thesis, Case Western Reserve University
                    1976   Astr. J. <u>81</u>, 350

Scalo, J.M.   1979   Protostars and Planets, p. 265
            (ed. T. Gehrels, Univ. of Arizona press, Tucson, Arizona)

Schild, R.E., Peterson, D.M. and Oke, J.B.   1971   Astrophys. J. <u>166</u>, 95

Schilt, J.   1954   Astr. J. <u>59</u>, 55

Schlesinger, F. and Jenkins, L.F.   1940   Catalogue of Bright Stars (2nd ed.)
            Yale University Observatory, New Haven

Schmidt, M.   1975a   I.A.U. Symposium No. 69, ed. A. Hayli, p. 325
        Dynamics of Stellar Systems, p. 325 (D. Reidel, Dordrecht-Holland)
                    1975b   Astrophys. J. <u>202</u>, 22

Schwarzschild, K.   1907   Gottingen Nachr. 1907, p. 614

von Seeliger, H.   1898   Abh. der K. Bayer, Akad. d. Wiss. II,
                    Kl. 19, 564 (Munich)

Sharp, C.   1982   Ph. D. thesis, University of St. Andrews

Silk, J.   1977   Astrophys. J. <u>214</u>, 152
            1979   Protostars and Planets, p. 172 (ed. T. Gehrels;
            University of Arizona Press, Tucson, Arizona)

Sion, E.M. and Liebert, J.   1977   Astrophys. J. <u>213</u>, 468

Smethells, W.   1974   Ph. D. thesis, Case Western Reserve University

Spitzer, L. and Schwarzschild, M.   1951   Astrophys. J. <u>114</u>, 385

Staller, R.F.A.   1975   Astr. Astrophys. <u>42</u>, 155

Staller, R.F.A. and Bochem-Becks, A. Ch. Th.   1979   in Ph. D. thesis (Staller
            University of Amsterdam

Staller, R.F.A. and de Jong, T.   1980   in Ph. D. thesis (Staller),
            University of Amsterdam

Staller, R.F.A., The, P.S. and Bochem-Becks, A. Ch. Th.   1982
                    Publ. astr. Soc. Pacif, <u>93</u>, 728

Starikova, G.A.   1960   Astr. Zh. <u>37</u>, 476; Soviet Astr. <u>4</u>, 451

Stevenson, D.J.   1978   Proc. astr. Soc. Australia $\underline{3}$, 227

Strand, K.Aa., Harrington, R.S. and Dahn, C.C.   1974   New Problems in
        Astrometry, IAU Symposium 61, p. 159, ed W. Gliese, C.A. Murray
        & R. H. Tucker,   D. Reidel, Dordrecht

Stromgren, B.   1964   Astrophys. Norvegica. $\underline{9}$, 334

                1976   ESO Messenger No. 7, p. 12

Taam, R.E., Kraft, R.P. and Suntzeff, N.   1976   Astrophys. J. $\underline{207}$, 201

Tarter, J.G.   1975   Ph. D. thesis, University of California, Berkeley

The, P.S. and Staller, R.F.A.   1974   Astr. Astrophys. $\underline{36}$, 155

                1979   in Staller, R. , Ph. D. thesis, University of Amsterdam

Toomre, A.   1964   Astrophys. J. $\underline{139}$, 1217

Trumpler, R.J. and Weaver, D.F.   1953   Statistical Astronomy,
                University of California Press, Berkeley

Tsuji, T.   1969   Low Luminosity Stars, p. 457 (ed. S.S. Kumar;
                (Gordon & Breach, London))

Turon-Lacarrieu, C.   1971   Astr. Astrophys. $\underline{14}$, 95

Twarog, B.   1980   Astrophys. J. $\underline{242}$, 242

Tyson, J.A. and Jarvis, J.F.   1979   Astrophys. J. Lett. $\underline{230}$, L153

Upgren, A.R.   1962   Astr. J. $\underline{67}$, 37

                1963   Astr. J. $\underline{68}$, 475

                1977   Vistas in Astronomy $\underline{21}$, 241

                1978   Astr. J. $\underline{83}$, 626

Upgren, A.R. and Armandroff, T.E.   1981   Astr. J. $\underline{86}$, 1898

Upgren, A.R., Gatewood, G.D., Lutz, T.E. and Ianna,P.A.   1978
                Bull. Amer. astr. Soc. $\underline{10}$, 649

Upgren, A.R., Grossenbacher, R., Penhallow, W.S., MacConnell, D.J.
        and Frye, R.L.   1972   Astr. J. $\underline{77}$, 486

Upgren A.R. and Lutz, T.E.   1979   Dudley Obs. Rept. no. 14, p. 235

Upgren, A.R. and Weis, E.W.   1975   Astrophys. J. $\underline{197}$, L53

Veeder, G.   1974   Astr. J. $\underline{79}$, 1056

Wanner, J.F.   1964   Ph. D. thesis, Harvard University (unpublished)

          1972   Mon. Not. R. astr. Soc. 155, 463

Ward, M., Allen, D.A., Wilson, A.S., Smith, M.G. and Wright, A.E.

          1982   Mon. Not. R. astr. Soc. 199, 953

Warren, P.R.   1976   Mon. Not. R. astr. Soc. 176, 667

Weistrop, D.   1972a   Astr. J. 77, 366

          1972b   Astr. J. 77, 849

          1974   Astr. J. 79, 954

          1976   Astrophys. J. 204, 113

          1977   Astrophys. J. 215, 845

          1980   Astr. J. 85, 738

Wielen, R.   1974   Highlights of Astronomy 3, 395

          ed. G. Contopoulos, (D. Reidel Dordrecht-Holland)

Wood, P.R. and Cahn, J.H.   1977   Astrophys. J. 211, 499

Woolley, R. v.d.r.   1962   Vistas in Astronomy 3, 3

          1978   Mon. Not. R. astr. Soc. 184, 311

Woolley, R. v.d.r., Pocock, S.B., Epps, E.A. and Flinn, R.   1971   R. Obs. Bul

Woolley, R. v.d.r. and Stewart, J.M.   1967

          Mon. Not. R. astr. Soc. 136, 329

Acknowledgements

A star of very low luminosity

I. Neill Reid *Department of Astronomy, University of Edinburgh, Blackford Hill, Edinburgh EH9 3HJ*

Gerard Gilmore *Royal Observatory, Blackford Hill, Edinburgh EH9 3HJ*

Summary. The method of photometric parallax ($M_V/V-I$ relation) has been applied to a UK Schmidt Telescope field towards the South Galactic Pole to derive a kinematically unbiased luminosity function for low mass stars. We present here the discovery of one such star, RG0050–2722, which has an absolute magnitude $M_V \approx +19$, and is 25 ± 6 pc from the Sun. This is only the second star known to have $M_V \geqslant +18$.

Introduction

Studies of the low luminosity main sequence are of considerable importance in determining the stellar mass density in the solar neighbourhood, the stellar initial mass function, and the evolutionary status of very low mass ($M \lesssim 0.2 M_\odot$) stars. All currently known very low luminosity ($M_V \gtrsim +16$) stars were initially identified in proper motion surveys, with subsequent absolute magnitude calibration by direct trigonometric parallax measurement (e.g. Wolf 359 – Kuiper 1942; G51-15 – Dahn *et al.* 1972), or by searching stars of known proper motion for faint red companions (e.g. VB8, VB10 – van Biesbrock 1944, 1961). However, in principle, such stars can also be discovered by purely photometric techniques.

We are currently engaged in a study of the stellar distribution towards the South Galactic Pole using UK Schmidt Telescope plates measured on the COSMOS facility at the Royal Observatory, Edinburgh. We are using the absolute magnitude sensitive $(V-I)_{KC}$ colour index, calibrated by stars of accurately known parallax (see, e.g. Strand, Harrington & Dahn 1974), to determine photometric parallaxes for a complete sample of all stars with $(V-I)_{KC} \geqslant 2.5$ ($M_V \gtrsim 11.5$) and $I \leqslant 19$, independent of the star's space velocity. Thus our sample includes all stars within 25 pc of the Sun with $M_V \leqslant +21$, and within 1 kpc for $M_V = +11.5$. We are also carrying out near infrared (JHK) photometry of the visually reddest stars to provide luminosity and population classification. We discuss here one of these stars, RG 0050–2722, whose position in the $J-H/H-K$ diagram shows it to be a nearby dwarf with an absolute magnitude comparable to that of VB10, ($M_V \sim +19$, Greenstein, Neugebauer & Becklin 1970) the star of lowest known luminosity.

Observations

Our photometry of the star RG 0050–2722 and four other late M dwarfs is presented in Table 1. R and I magnitudes are from UK Schmidt Telescope plates (one R and four I), which have been calibrated against some 1800 photographic and photoelectric magnitudes. RG 0050–2722 is not visible on the SRC $'J'$ sky survey, which has a limiting magnitude near $B = 23$, and is also fainter than $V \sim 21.5$. This sets a lower limit of 6 mag to the $B-I$ colour. Individual magnitudes are on the Kron-Cousins system, and preclude variability greater than ~ 0.4 mag. Near infrared JHK photometry was also obtained on 1980 October 26, with the IRPS system on the AAT. These magnitudes are accurate to ± 0.02.

From COSMOS measures of five UKST plates, we have derived a limit on the proper motion of RG 0050–2722. First, using Turner's six plate constant method, and a grid of 76 SAO stars, the equatorial coordinates were computed from the measured positions on one R and on one I plate. The derived positions agree to ± 0.2 arcsecs at RA $= 00^h\,50^m\,28^s.4$ Dec $= -27°\,22'\,17''$ (equinox 1950.0, epoch 1978). This internal agreement compares with the rms residuals of ~ 1.0 arcsec in each coordinate of the SAO grid standards.

A more precise limit was derived by comparing the measures of our four deep I plates, which have a time baseline of four years. In this case a linear (six plate constant) transformation was used to map all stars within a $1° \times 1°$ area centred on RG 0050–2722 (approximately 1100) on to the coordinate system of our earliest plate. We then derive a proper motion of 0.08 ± 0.13 arcsec yr^{-1} in RA, and 0.08 ± 0.11 arcsec yr^{-1} in Dec. Thus the annual total proper motion is 0.11 ± 0.17 arcsec, which is consistent with zero in both coordinates. The individual values are presented in Table 2, and the significance of this limit is discussed further below.

Discussion

Absolute magnitudes may be derived for stars of known luminosity class from the absolute magnitude–colour relations (photometric parallax). We have obtained visual (SAAO) and

Table 1. Photometric data for RG 0050–2722, and four M dwarfs. The JHK data for Gl 551 are from Mould & Hyland (1976), corrected to the AAT I/R system, (which is not identical to that in use at SAAO), and all other data are our own.

Star	$B-V$	V	$R-I$	I	$J-H$	$H-K$	K	M_V
Gl 551	1.90	11.22	1.66	7.31	0.66	0.36	4.36	15.62
G 158-27	1.85	13.76	1.53	10.50	0.65	0.33	7.44	16.11
G 51-15	2.06	14.81	1.85	10.78	0.66	0.42	7.32	17.0
VB8	1.94	16.77	2.10	12.26	0.68	0.39	8.81	17.8
RG 0050–2722			2.6	16.65	0.74	0.44	12.50	
				(± 0.1)			($\pm .02$)	

Table 2. Measured positions for RG 0050–2722 relative to a grid of 1100 nearby stars. No corrections for either magnitude or colour dependent effects have been applied. The X- and Y- axes are approximately aligned with RA and Dec respectively, and 1.0 μm is equivalent to 0.07 arcsec.

Plates	Baseline (yr)	Residuals All stars (means)		RG 0050–2722	
		X (μm)	Y (μm)	X (μm)	Y (μm)
I3635–I4338	0.75	3.6	4.0	$+3.0$	$+1.7$
I3635–I6427	3.0	3.3	3.7	-2.5	$+6.2$
I3635–I6523	3.1	5.0	4.3	-4.5	$+0.5$

Plate 1. A finding chart for RG 0050–2722. The scale bars which indicate the object are each 1 armin in length, and the orientation is marked. This is reproduced from an *I* plate taken with the UK Schmidt Telescope, and is reproduced by permission.

Table 3. Determinations of the absolute magnitude of RG 0050–2722 by photometric parallax.

Colour relation	Colour	M_V	M_K	$m-M$
$V-K$	> 8	> 18	> 10	< 2.5
$I-J$	3.0 ± 0.2	20.5 ± 1	13	− 0.5
$H-K$	0.44 ± 0.03	19.0 ± 0.5	10.5 ± 0.5	2.0 ± 0.5
$R-I$	2.6 ± 0.3	19.5 ± 1	10.8 ± 0.5	2.0 ± 0.5

infrared (UKIRT, AAT) photometry of a large sample of stars of accurately known parallax, and therefore absolute magnitude, to calibrate these relations in our photometric system. The details of this calibration will be discussed elsewhere. We have four estimates of the absolute magnitude of RG 0050–2722 from these relations which are presented in Table 3.

The results show that derived absolute magnitudes are in excellent agreement, except those derived from a mixture of visual and infrared colours. This discrepancy is illustrated in Fig. 1, where we show the spectral energy distributions derived from our observations of G1 551 (M_V = 15.6; Proxima Cen), VB8 (M_V = 17.8) and RG 0050–2722. Also shown are blackbody curves fitted only to the infrared fluxes, the derived temperatures being 3125 K (G1 551), 2750 K (VB8) and 2625 K (RG 0050–2722). The uncertainties in the temperatures are ~ ± 100 K. The visual flux of RG 0050–2722 is seen to be depressed by a factor of 3 below the blackbody line relative to the depression of the other two dwarfs.

We can exclude a systematic error in colour as the cause of this anomaly. Photoelectric photometry on our brighter very red stars was carried out at the same time as our observations of the late type parallax stars, which include G1 551 and VB8. The differential colour terms between our photographic and photoelectric colour systems are 0.00 ± 0.03 mag per magnitude to a limit of $V-I \leqslant 2.6$, and $R-I \leqslant 1.3$. While it is possible that large colour dependent scale errors may exist for still redder stars we think this unlikely both because none of our other red stars shows a similar deficiency, and both I and R magnitudes would have to be in error by a full magnitude.

A possible explanation is suggested by the large $J-H$ colour. Mould & Hyland (1976) identify early M stars with values of $J-H$ near 0.7 as young stars with low surface gravity,
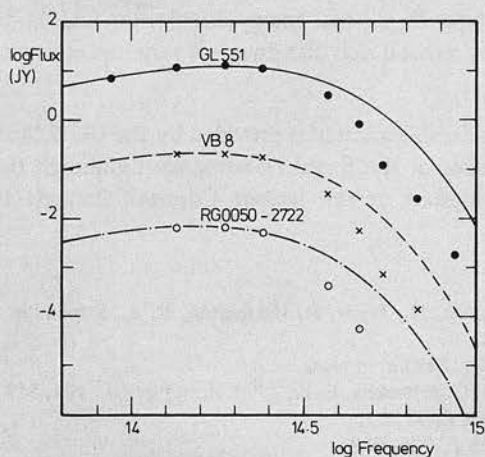

Figure 1. Spectral energy distributions for three late-type dwarfs. G1 551 (Proxima Cen, M_V = + 15.6; solid points), VB8 (M_V = 17.8, crosses) and RG 0050–2722 (M_V ~ + 19, open circles). The curves are blackbody fits to the infrared data only, and have temperatures 3125, 2750 and 2625 K respectively. The increasing depression of the visual flux below the blackbody line with decreasing temperature is evident.

which are still contracting to the main sequence. One such star, G1 205, was later also shown to be metal rich by a factor of order 3 (Mould 1978). It is likely that RG 0050–2722 is similarly a very low luminosity metal rich dwarf. The high metallicity is not expected to affect significantly the J passband, which suffers comparatively slight line blocking. However, the α- and γ-systems of TiO provide extensive blanketing in the R and I passbands. It is also possible that extreme blanketing shortward of 1 μm could lead to significant backwarming at longer wavelengths. We are currently carrying out a programme of near infrared spectroscopy to test this possibility.

It is interesting to compare our results with the work of Greenstein *et al.* (1970) on VB10. In analysing their photometry $(BVIHKL)$ they derived an effective temperature estimate by equalizing the areas under a blanketing-corrected blackbody curve, and their observed flux distribution. By following the same technique with our results for RG 0050–2722, we derive a temperature of approximately 2250 K. This is in agreement with the value derived for VB10 by Greenstein *et al.* and supports our derived absolute magnitude.

Assuming that the short wavelength $(R$ and $I)$ flux deficiency is due to line blanketing, the derived absolute magnitude is $M_V = +19 \pm 1$, $M_K = 10.5 \pm 0.5$. The predicted B magnitude is then 24, consistent with our non-detection on the sky survey, and further proof of the importance of R and I band photometry in the study of intrinsically faint stars. The consequent distance of RG 0050–2722 is 25 ± 6 pc, for a distance modulus of 2 ± 0.5 mag Using our derived limit on the total proper motion of 0.11 ± 0.17 arcsec yr^{-1}, we derive a space velocity of 13 ± 23 km s^{-1}, consistent with disc motions.

Conclusion

The technique of photometric parallax is being applied to a complete sample of stars with $I \leqslant 19$ towards the South Galactic Cap. Infrared (JHK) photometry of the resulting sample of very red stars allows luminosity and population classification, and the derivation of a kinematically unbiased stellar luminosity function. The use of I magnitudes allows us to sample much deeper into the luminosity function than earlier studies, and has already led to the discovery of RG 0044–2958, an M supergiant at a distance of 2.5 Mpc (Gilmore & Reid 1981), and RG 0050–2722 (this paper). This is the first star of very low luminosity to be discovered by purely photometric criteria, has an absolute V magnitude $M_V = 19 \pm 1$, and lies at a distance of 25 ± 6 pc. Its spectral energy distribution and limits on its proper motion are consistent with it being a metal rich disc dwarf of very low mass and luminosity.

Acknowledgment

References

Dahn, C. C., Behall, A., Guetter, H., Priser, J., Harrington, R. S., Strand, K. Aa. & Riddle, R., 1972. *Astrophys. J.*, **174**, L87.
Gilmore, G. & Reid, I. N., 1981. *Nature*, in press.
Greenstein, J. L., Neugebauer, G. & Becklin, E. E., 1970. *Astrophys. J.*, **161**, 519.
Kuiper, G. P., 1942. *Astrophys. J.*, **95**, 201.
Mould, J. R., 1978. *Astrophys. J.*, **226**, 923.
Mould, J. R. & Hyland, A. R., 1976. *Astrophys. J.*, **208**, 393.
Strand, K. Aa., Harrington, R. S. & Dahn, C. C., 1974. In *New Problems in Astrometry. IAU Symp. 61*, p. 159, eds Gliese, W., Murray, C. A. & Tucker, R., D. Reidel, Dordrecht.
van Biesbrock, G., 1944. *Astr. J.*, **51**, 61.
van Biesbrock, G., 1961. *Astr. J.*, **66**, 528.